



Royal Netherlands  
Meteorological Institute  
*Ministry of Infrastructure and the  
Environment*

# KNMI'14: Climate Change scenarios for the 21st Century – A Netherlands perspective

Bart van den Hurk, Peter Siegmund, Albert Klein Tank (Eds)

De Bilt, 2014 | KNMI scientific report WR 2014-01



## **KNMI'14: Climate Change scenarios for the 21st Century – A Netherlands perspective**

Version 26 May 2014

### **KNMI WR 2014-01**

Bart van den Hurk, Peter Siegmund, Albert Klein Tank (Eds)  
Jisk Attema, Alexander Bakker, Jules Beersma, Janette Bessembinder, Reinout Boers, Theo Brandsma,  
Henk van den Brink, Sybren Drijfhout, Henk Eskes, Rein Haarsma, Wilco Hazeleger, Rudmer Jilderda,  
Caroline Katsman, Geert Lenderink, Jessica Loriaux, Erik van Meijgaard, Twan van Noije,  
Geert Jan van Oldenborgh, Frank Selten, Pier Siebesma, Andreas Sterl, Hylke de Vries,  
Michiel van Weele, Renske de Winter, Gerd-Jan van Zadelhoff

This report documents and motivates the KNMI'14 climate change scenarios. It has an intermediate status, implying that the current content of the document can be considered to be final, but that additional components on applications and spin-off issues and requested additional background information may be added at a later stage.

This report should be cited as:

KNMI (2014): KNMI'14: *Climate Change scenarios for the 21st Century – A Netherlands perspective*; by Bart van den Hurk, Peter Siegmund, Albert Klein Tank (Eds), Jisk Attema, Alexander Bakker, Jules Beersma, Janette Bessembinder, Reinout Boers, Theo Brandsma, Henk van den Brink, Sybren Drijfhout, Henk Eskes, Rein Haarsma, Wilco Hazeleger, Rudmer Jilderda, Caroline Katsman, Geert Lenderink, Jessica Loriaux, Erik van Meijgaard, Twan van Noije, Geert Jan van Oldenborgh, Frank Selten, Pier Siebesma, Andreas Sterl, Hylke de Vries, Michiel van Weele, Renske de Winter and Gerd-Jan van Zadelhoff. Scientific Report WR2014-01, KNMI, De Bilt, The Netherlands. [www.climatescenarios.nl](http://www.climatescenarios.nl)

## Contents

1.	Scope of the climate change scenarios .....	4
1.1	Drivers of change.....	4
1.1.1	Climate variability .....	4
1.1.2	The recent findings on regional climate change.....	4
1.1.3	Scenarios for a Delta region.....	5
1.1.4	A new set of climate change scenarios.....	6
1.2	Imagining the future.....	6
1.2.1	Criteria for useful climate scenarios .....	7
1.2.2	From user requests to the new climate scenarios.....	11
2.	General structure of KNMI'14 .....	12
2.1	Natural and forced regional climate variability .....	12
2.2	Spanning a likelihood range .....	14
2.2.1	The global temperature increase and chosen time horizons: the G and W scenarios .....	15
2.2.2	Regional deviations from the global mean picture: the L and H subscripts .....	16
2.3	The scenario construction procedure.....	17
2.3.1	Selection of model samples .....	18
2.3.2	Scenarios for 2030 .....	20
2.4	Observations, climate normals and estimates of natural variability.....	20
2.4.1	Station observations used for KNMI'14 .....	20
2.4.2	Normal periods and natural variability of 30-year averages .....	21
2.5	Temporal and spatial variability .....	23
2.5.1	Scenario periods and time scales.....	23
2.5.2	Spatial variability.....	24
2.6	Models used .....	24
2.6.1	Evaluation of modelled trends in (extreme) precipitation and temperature.....	25
2.7	KNMI'14 scenarios and RCPs .....	26
2.7.1	Assessment of the RCPs.....	26
2.7.2	Consistency of KNMI'14 global temperature projections with CMIP5 .....	27
3.	Observed trends and scenarios per variable .....	30
3.1	Temperature and precipitation .....	30
3.1.1	Observed temperature and precipitation trends .....	30
3.1.2	The resampling methodology and its results.....	32
3.1.3	Downscaling with the Regional Climate Model .....	36
3.1.4	Seasonal and monthly temperature and precipitation response .....	38
3.1.5	Time series transformation.....	39
3.1.6	Small scale precipitation extremes .....	43
3.1.7	Climate change signals in the Rhine basin.....	47
3.2	Sea level rise.....	48
3.2.1	Introduction.....	48
3.2.2	Processes included in the scenarios .....	49
3.2.3	Regionalization .....	50
3.2.4	Implementation and uncertainties .....	51
3.2.5	Scenarios for the 21st century.....	53
3.2.6	Conclusion and discussion .....	58
3.3	Extreme wind.....	59
3.3.1	Introduction: scope and model quality assessment. ....	59
3.3.2	Observations - past changes .....	60
3.3.3	Projections for the future .....	62
3.3.4	Construction of the wind scenarios .....	69
3.3.5	Conclusions .....	69
3.4	Relative humidity, solar radiation, evaporation and drought .....	69
3.4.1	Observed trends .....	69
3.4.2	Seasonal and monthly responses .....	70
3.5	Extreme weather .....	71

3.5.1	Hail and Thunderstorms.....	72
3.5.2	Visibility.....	75
3.5.3	Summary of changes in extreme weather.....	78
4.	The KNMI'14 scenarios table: key figures.....	80
5.	Guidance for use.....	87
5.1	Difference with earlier scenarios.....	87
5.2	Scenarios in neighbouring countries.....	88
Acknowledgements.....		92
References.....		92
6.	Annexes.....	99
6.1	List of GCMs.....	99
6.2	Appendix to the KNMI'14 sea-level scenarios.....	100
6.3	Meteorological scenarios translated to changes in air pollution levels.....	101

## 1. Scope of the climate change scenarios

### 1.1 Drivers of change

#### 1.1.1 Climate variability

Climate, defined as the “average weather including its statistical distribution”, varies spatially and is variable at all time scales. The origin of these variations varies strongly, ranging from fluctuations in the solar radiance, the Earth-Sun geometry, volcanic disturbances of the atmospheric aerosol load, internal interactions between the physical and biogeochemical components of the system, and – since fairly recently in the history of the planet – anthropogenic influences on the atmospheric composition and land cover.

The variability of the system poses limitations to the predictability of the climate state. Internal variations of the climate system beyond monthly time scales apart from the contribution from the positive multidecadal surface temperature trend that is currently eminent (Oldenborgh et al. 2012) and oceanic variability (Hazeleger et al. 2013), are difficult to predict and at time scales of 30 – 100 years useful predictions are basically impossible. Not only because of the large contribution of the natural variability, also because the external forcing related to human activity is considered to be unpredictable. Any attempt to make climate predictions at a relatively small spatial scale such as the Netherlands or even Western Europe for multiple decades ahead cannot be expected to lead to skilful results. However, helpful images of possible future states of the regional climate can be made, after formulating a number of driving assumptions and applying projection tools that can be expected to give a realistic response to these external forcings. These conditional foresights can be identified as “scenarios”.

In the Netherlands a strong tradition in constructing climate change scenarios has developed over the past decades (Können 2001; Van den Hurk et al. 2007). Frequent updates of these scenarios are desirable, as both scientific insights and user requirements develop over time.

In this report the construction of a new set of climate change scenarios for the Netherlands is described. It discusses the design criteria, the underlying assumptions, the technical procedure to construct them, and the final result and additional products. First, we will briefly review the recent scientific findings that give an incentive to the update of the Dutch climate change scenarios, followed by a description of the setting in which they are applied, and changes in the requirements that have developed over time.

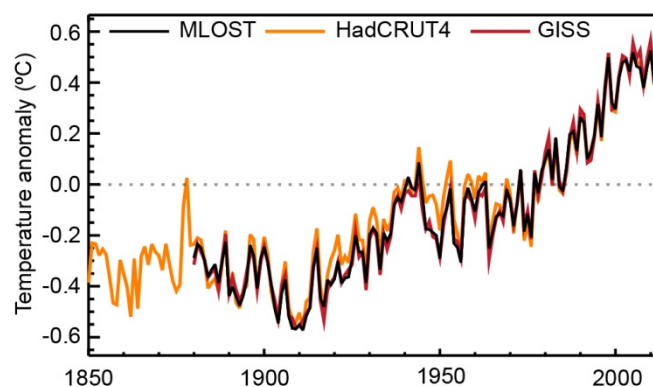


Figure 1.1 Global mean temperature anomaly relative to the mean temperature in 1961-1990 for three datasets. (Source: IPCC (2013), fig. 2.19).

#### 1.1.2 The recent findings on regional climate change

Not only climate is variable, also the knowledge about climate is rapidly developing. Recently, the Intergovernmental Panel on Climate Change (IPCC) released the Working Group I contribution to the 5<sup>th</sup> IPCC Assessment report (AR5; IPCC, 2013). These periodic assessment reports provide an overview of the state-of-the-art knowledge about observed climate variability and change, its representation in models and future projections. In separate reports the IPCC assesses the impacts of climate change (Working Group report II) and mitigation options (Working Group III).

The main conclusions from the previous IPCC Working Group I report have proven to be robust, including the findings that are relevant for the Netherlands. However, a few important new insights can be deduced from this new IPCC report and various regional studies:

- The global mean temperature continues to rise, but the increase since 1998 is clearly lower than in the period between 1950 and 1998 (see Figure 1.1). This decline is partially attributed to a reduction in the climate forcing (reduced solar activity; more volcanic aerosols) and partially to natural variability of the complex climate system.
- The sea level projections in the Summary for Policy Makers of the AR5 report display a range that is larger than in the 4<sup>th</sup> report, AR4 (IPCC, 2007). Contribution of melting ice caps and glaciers and terrestrial water extraction are now included in the estimations. Explicit regional effects, such as changes in gravitational pull by ice mass changes, are also included in this assessment. For the end of the 21<sup>st</sup> century (2081 – 2100) the global sea level is likely to be 26 – 82 cm higher than in the reference period (1986 – 2005). It is notable that for the first time the AR5 report assigns a likelihood to these estimates which was not possible in the past, indicating the increased understanding of sea level changes.
- The lower estimate of the range of the equilibrium climate sensitivity (the surface temperature reached after doubling the CO<sub>2</sub>-concentration after bringing the system into equilibrium) is reduced from 2°C in AR4 to 1.5°C in AR5, while the upper estimate of 4.5°C is not changed. This is due to utilization or reprocessing of observations of the ocean heat content, and the longer record of available surface temperature data (see Figure 1.1).
- The observed temperature increase in Western Europe (including the Netherlands) during the last 50 years is about twice the increase in the global mean (see also Van Oldenborgh et al. 2009). This is partly due to changes in the circulation statistics (wind direction), and partly due to increased solar insolation. In addition a reduction in the number of cold days and an increase in number of warm days in Western Europe is observed.
- Precipitation in the Netherlands has increased by 26% between 1910 and 2013 (Buishand et al. 2013). Also the intensity of extreme showers during the summer has increased, particularly in the coastal areas.
- The projected global mean temperature increase at the end of the 21<sup>st</sup> century is different from AR4: 0.3 – 4.8°C in AR5, compared to 1.1 – 6.4°C in AR4. This is largely due to a change in the emission scenario approach, that reduced the spread by prescribing the imposed radiative forcing instead of CO<sub>2</sub>-emissions (leading to different socio-economic storylines) and by reduced spread in the model projections.

### 1.1.3 Scenarios for a Delta region

The Netherlands are shaped by its adaptation to climate variability. It has a long history in coping with variable water levels, from sea, rivers and inland hydrology. Dutch authorities are aware that climate is not stationary.

However, the recent decade has seen a paradigm shift in the national attitude towards adapting to climate variability. Where traditionally adaptation measures were designed and implemented in response to past climatic events that have had a high society impact, the modern ambition is to shape the Dutch Delta while anticipating to possible future conditions ([www.deltacommissaris.nl](http://www.deltacommissaris.nl)), that may differ systematically from today's conditions due to an anthropogenic effect on climate and socio-economic changes. This implies that for instance the design discharge of the major rivers Rhine and Meuse (discharge volume that is used as reference for the design of flood mitigation measures) should not only be quantified for current climate and socio-economic conditions, but should take foreseeable changes in discharge statistics and land use practices into account.

The approach followed in the Dutch Delta Program clearly illustrates this orientation on future conditions, which are governed by a combination of natural and human induced changes. The design and evaluation of measures aiming at a robust Delta infrastructure are guided by the so-called Delta Scenarios (Bruggeman et al. 2013) in which key indicators of both future climate and socio-economic conditions are quantified. These Deltascenarios are based on a selection (and modification) of the previous set of KNMI climate change scenarios (KNMI'06). Apart from the design of the Dutch delta, future climate conditions also play a role in decisions related to sewage design, city planning, nature conservation, health and others.

#### 1.1.4 A new set of climate change scenarios

The previous generation of KNMI climate change scenarios (KNMI'06, Van den Hurk e.a. 2007) were constructed in response to a strong request from multiple stakeholders in the Dutch society, particularly in the water management sector who used the earlier WB21 scenarios (Können 2001). They were developed from observations, regional model projections coordinated at a European level through the PRUDENCE project (Christensen and Christensen 2007), and global projections from the 3<sup>rd</sup> Coupled Model Intercomparison Project CMIP3 (Meehl et al. 2007), which provided significant input to AR4. The scenarios covered two dimensions in which considerable uncertainty exist about future developments: the global temperature increase, and the response of the regional atmospheric circulation to this increase. This 2 × 2 scenario matrix does not include a “middle” scenario, and allowed to span a range of climate conditions that appeared to be relevant to a broad collection of interested stakeholders. Features such as enhanced summer drying, sea level rise, increased extreme precipitation (both in showers and in multiday amounts), and moderately extreme wind speeds were quantified that allowed many types of impact assessment (see section 5).

Yet, both the scientific insights and the user requirements have changed over time. In preparation of AR5 a 5<sup>th</sup> Coupled Model Intercomparison Project (CMIP5, (Taylor et al. 2011) was executed and made available. Prolonged observational time series and refined modelling tools have changed the scientific insights (see Section 1.1.2).

Since 2004/2005 more effort is invested in tailoring climate information for various user groups and societal sectors, whose information need is very diverse. The publication of the KNMI'06 climate change scenarios resulted in many requests for additional information and guidance of these scenarios and their implications for society stakeholders. The experience with the user requests and their use of the available climate information were documented (Bessembinder et al. 2011b) and cross-checked in two user consultation workshops and a climate scenario user working group. In the user requirements surveys new types of information are requested, among others:

- more climate variables
- more information on natural (year-to-year) variability
- information on the relation between scenarios and observed trends
- scenarios for 2030
- more regional detail in the climate change information
- sub-daily (hourly) extreme conditions
- probabilistic assessment of the various scenarios
- visual illustration of the manifestation of climate change and its possible impacts
- time series associated with the scenarios.

Given these changes in scientific insights and enhanced detail in the user requests a new set of climate change scenarios, **KNMI'14**, has been constructed, that is described in detail in this report. The general structure of the KNMI'14 scenarios and the choice of the steering variables for the scenario matrix is similar to the approach taken in KNMI'06, and the details of this structure and the tools used are presented in Chapter 2. The methodological procedures for the set of variables are described in Chapter 3, followed by a summary of scenario values in Chapter 4. Further guidance on the relationship between these scenarios and on-going scientific and policy activities in our neighbourhood are discussed in Chapter 5. But first we will further elaborate on the concept of climate change scenarios, and the justification of the methodological procedures (largely based on interpreting model projections) to create them.

## 1.2 Imagining the future

The practice of generating an outlook for future climate conditions has grown substantially during the past decades. The ever increasing number of referenced publications in the periodic IPCC reports is just a partial illustration of this growth. Many institutions, both governmental and non-governmental, adopt some kind of foresighting procedure to assess risks or opportunities of current or planned policies against changing environmental conditions. The purposes and methodologies of these foresighting activities vary widely. Berkhout et al. (2013) discuss the existence of different frames of reference with which climate assessments are approached. A contrast between “top-down” and “bottom-up” perspectives generally exists, where “top-down” refers to a perspective and methodology where global climate change induced by anthropogenic radiative forcings serves as a starting point and a cascade through downscaling and impact assessment is followed in order to map local consequences of this climate perturbation. “Bottom-up” takes the vulnerability

or resilience of a specific area or societal sector as a starting point and uses outlooks of a mixture of drivers (of which climate is only one specimen) to make adequate assessments (see also Hulme and Dessai 2008). The previous set of KNMI climate scenarios referred to as KNMI'06 (Van den Hurk et al. 2007) were intended to bridge a gap between the “top-down” and “bottom-up” paradigm, by following an essentially top-down approach for making large-scale climate change assessments for the Netherlands and surrounding, and responding to “bottom-up” formulated user needs by providing specific quantities and tailored scenarios (Van den Hurk et al. 2013).

Whatever approach is taken to create climate foresights, it is of importance that a methodology is chosen that meets the requested purpose. And since climate change assessments serve different purposes, different requirements need to be specified for the chosen tools. Climate change assessments that are used as input to a targeted (quantitative) decision making process (such as representative weather time series used for e.g. sewage design) are different from applications where a qualitative picture of the possible changes is used to illustrate the context in which such a decision process is taken (such as the justification of the “grand design” of the Dutch Delta area). In general, these different assessment procedures will use predictions, projections or scenarios differently.

IPCC (2013b) uses the term “climate *projection*” to refer to a simulated response of the climate system to an imposed forcing derived from a scenario of future emission or concentration of greenhouse gases and aerosols (a possible future situation under assumption of a forcing scenario), while a “climate *prediction*” (or climate forecast) is an estimate of the actual evolution of the climate in the future. A projection that is exposed to an external forcing whose probability is not explicitly assessed is in essence a sensitivity study, a tool to explore the “space of options” (e.g. von Storch et al. 2008) or a “conditional prediction” (Giorgi 2005). Bray and von Storch (2009) tested the agreement among scientists that a prediction is to be interpreted as “the most probable outcome”, while a projection is a “possible future situation”. 20 to 30% of the respondents did not comply with these associations.

Climate simulations are governed by their initial state, the assumed external forcing throughout the simulation, and internal (natural) variability (Hawkins and Sutton, 2009). An initialized prediction is exposed to an intrinsic level of uncertainty, due to the chaotic nature of the climate system, imperfect models and limited ability to generate realistic initial states. So climate predictions, analogous to weather forecasts, are essentially probabilistic: they provide statements about the likelihood of a given condition to occur.

Climate *scenarios* are defined by IPCC (2013b) as “a plausible and often simplified representation of the future climate, based on an internally consistent set of climatological relationships that has been constructed for explicit use in investigating the potential consequences of anthropogenic climate change, often serving as input to impact models. Climate projections often serve as the raw material for constructing climate scenarios, but climate scenarios usually require additional information such as the observed current climate. A climate change scenario is the difference between a climate scenario and the current climate.” Similarly, Von Storch (2008) describes climate scenarios as possible, plausible, and internally consistent, but not necessarily probable, developments.

This definition is somewhat imprecise concerning the dependence on the underlying assumed forcing. Relying on climate projections (being conditional forecasts given an assumed forcing pathway), also a climate scenario depends on the chosen emission pathway. Each scenario is one alternative image of how the future can unfold. A set of scenarios can be constructed that *together* provide a plausible description of how the future may develop (Komen, 2013). But as for projections: when quantitative probabilities are not given to the key driving forces of the scenarios, they cannot be considered to be probabilistic forecasts of the future.

In essence, any projection can be interpreted as a scenario. Each member from the conditional ensemble of predictions that is made to generate a probabilistic conditional forecast is a different scenario, a “what if” condition. A climate projection is a scenario, conditioned on the validity of the model and boundary conditions chosen to make the projection. Also a (future) snapshot of a short episode of (extreme) weather in a small domain extracted from a global model projection is a scenario, appropriate for the very specific conditions and assumptions used to select the snapshot (Hazeleger 2012). The definition of climate scenarios should not be confined to the outcome of global climate models driven by a given greenhouse gas emission or concentration scenario.

### 1.2.1 Criteria for useful climate scenarios

The important question to answer is: what are the criteria that need to be satisfied to consider climate scenarios to be useful? In the KNMI'06 project the criteria for useful climate scenarios were *plausibility*, *internal consistence* and *relevance*. Plausibility and internal consistence imply that the scenarios are physically

consistent and well understood, and are supported by quantitative evidence obtained from models and observations. Relevance (or salience) is ensured by generating climate change variables that are considered useful by a large group of users. In KNMI'06, where water management was a dominant scope, it led to the derivation of quantitative changes in 10-day precipitation sums (relevant for major river discharge regime assessments), 1/10 year daily precipitation sums and a set of sea level rise scenarios that included a wider range of uncertainties than considered by the 4<sup>th</sup> IPCC Assessment report (see also Van den Hurk et al. 2013; Enserink et al. 2013).

However, given their role in a decision making process (either in sketching the decision context, or by providing quantitative predictions) scenarios are usually interpreted differently by different users, depending on their frame of reference. Here “frame of reference” describes the actual decision context including its physical and non-physical boundary conditions, but also the personal and social characteristics that play a role in the decision making process (perception of risk, experience in dealing with uncertainty, sense of urgency or priority) (Berkhout et al. 2013). As different users have different frames of reference, the interpretation of scenarios is subjective. The concept “plausibility” depends on the perception by the user. An evolution of the climate that is perceived as “plausible” (or possible, likely) by one user can simultaneously be framed as “not certain” or even “unlikely” by another.

Tang and Dessai (2012) evaluated the usability of the UK Climate Impacts Program (UKCP09; McKenzie-Hedger et al. 2006) scenarios using a mixed set of methodologies involving both constructors and users of the scenarios. Their selection of criteria reflects the level of usefulness as experienced by the user: *credibility*, *salience* and *legitimacy* were explored. Credibility points at scientific soundness, which excludes scenarios that are either very unlikely or physically implausible. The KNMI'06 criteria plausibility and internal consistency can be considered to contribute to credibility. Salience implies that the scenarios are fulfilling the user's needs and are consistent with their frame of reference. In the KNMI'06 set the criterion relevance is closely related to this interpretation. Legitimacy is a criterion that was not addressed explicitly before in KNMI'06. It expresses the degree to which the scenarios were constructed in a transparent way and consider different views and values (Cash et al. 2003).

The KNMI'14 scenarios are designed to provide a scientific set of plausible, consistent and relevant future climate conditions, to be used as a reference framework for a multitude of society impact assessments of different scope and origin. However, the degree to which KNMI'14 meets the criteria cannot be solely judged from their design. A user survey as applied by Tang and Dessai (2012) is beneficial to demonstrate their usefulness and credibility. One can also elaborate on the degree to which the followed methodology contributed to meeting these criteria. We will follow the latter approach and discuss the three criteria used in KNMI'06 and the new criterion legitimacy in the context of the KNMI'14 scenario framework.

### **Plausibility and internal consistency**

The criterion *plausibility* has two different elements. The first is that the resulting scenarios comply with theoretical and observation based understanding of the relevant physical mechanisms that affect climate and its variability. The criterion *internal consistency* used in KNMI'06 is in fact inherent to this element of the plausibility criterion: a scenario that fails to reproduce internally consistent physical quantities will not be plausible, as apparently relationships that are based on physical evidence are violated. The second element of the plausibility criterion refers to the expectation that a given scenario will become true. In brief, the first element refers to the quality of the (model or other) tools used to construct the scenarios, while the second refers to the realism of the boundary conditions that drive them.

Information derived from models (and observations) is always imperfect, but assists in the physical understanding of the regional response and the conditions that govern this response. Climate models are not designed uniquely as forecasting tools. Their purpose is also to improve the understanding of the behaviour of complex systems (Orrell and McSharry, 2009; cited by Enserink et al. 2013). A climate model may thus be seen as a collection of insights, cast in the form of a sample of numerical equations, with which mutual dependencies between processes and variables can be studied.

Lack of model skill in replicating observed variations and trends in (regional) climate patterns (Van Haren et al. 2013; Min et al. 2013) do pose a challenge to the plausibility (and usefulness) of regional climate scenarios based on model output. Given the complexity of the climate system and the models used to describe this system, an objective estimate of the level of skill that one can expect is difficult to give, and varies widely with chosen metrics, scale, process and scope. In addition, model skill to represent future climate conditions can by definition not be assessed. Smith (2002) argues that we should agree on the fact that the understandability (and predictability) of complex systems is limited and that these limits are impossible to locate (see also Komen, 2013). However, a pragmatic solution is to continue the process of model

improvement by frequent confrontation with observations and following sound reasoning and physical laws, make use of new scientific evidence (observational or theoretical), and remain aware of the inherent uncertainty that is associated with using imperfect models.

Another pragmatic solution is to generate an *ensemble* of scenarios that both reflect the major sources of uncertainty (including future forcings and limited model skill) and together span a range of future conditions that can be argued to be plausible. It is not straightforward to reformulate this collection of scenarios in terms of a probability range (Enserink et al. 2013). There is no formal justification for treating the ensemble of models as a reflection of the true collection of possible future directions in which the complex system can develop. Every ensemble of models, or in fact, ensemble of scenarios, is by definition an ensemble of opportunity (Sanderson and Knutti 2012).

The quality of the underlying narratives that lead to different boundary conditions to drive the climate model projections is not easily established. Again, a range of forcing scenarios is often used to express the inherent uncertainty. Although also this range is to be considered an ensemble of opportunity, it should reflect conflicting scientific insights on for instance the increase of the world's population, and the way the socio-economic activity affects the climate system.

In order to span a *plausible* range of future conditions, KNMI'14 is based on a set of paradigms and concepts:

- It utilizes the comprehensive climate assessment from (IPCC 2013b), both by putting the observed trends and variations in regional climate patterns in a global context, and by using the global model projection archive CMIP5 as a basic resource of the scenario range (Van den Hurk et al. 2014). The KNMI'14 scenarios span a large fraction of the range of future climate conditions projected by CMIP5. Worldwide the IPCC assessments and the associated Global Climate Model (GCM) projections are considered as a benchmark of the current state of climate science. Many authors of KNMI'14 have contributed in various ways to the IPCC assessment, which ensures that experience and information from our part of the world is integrated in AR5.
- Observed climate characteristics in the Netherlands are an important driver for the construction of the regional climate change scenarios. This particularly applies to observations of local sea level rise, spatial patterns of trends in (extreme) precipitation and temperature, and observed variability of these quantities at decadal time scales. Also, the scenario changes for future climate have been evaluated against recent trends in the observations.
- The scenarios have been constructed largely by means of simulations with "in house" models. Apart from analysing the CMIP5 archive, simulations with the global model EC-Earth (Hazeleger et al. 2012) and RACMO2 (Van Meijgaard et al. 2008) were generated and selected in order to span a large range of the response generated by the CMIP5 projections. Although it confines the range of produced scenarios to the limits imposed by the EC-Earth and RACMO2 models (which is in some aspects smaller than the CMIP5 range), it introduces a higher level of understanding of the physical rationale behind the projections. Relevant systematic biases in these models are documented and processed in the scenarios.
- In KNMI'14 internal consistence is imposed by deriving quantities that are physically related from a similar set of climate simulations, grouped in samples reflecting the assumed large scale steering variables for each scenario. This grouping of ensemble simulations from a single regional climate model, driven by a single global climate model ensured that coherent patterns of temperature, precipitation, winds, evaporation, radiation and other derived quantities could be compiled for each scenario. In KNMI06 many variables were derived by some form of scaling or statistical downscaling, which challenged this requirement of internal consistence.

### Relevance

The depicted scenarios should obviously fit in the frame of reference of the user. Climate scenarios generating very exotic conditions for a certain area, dealing with quantities or processes that are not relevant nor familiar to the user, or that deviate strongly from scenarios released only relatively recently will not be very useful.

An extensive stakeholder interaction has taken place during the formulation of the KNMI'14 scenarios (see section 1.1.4). This process was clearly supported by the extensive experience that users have gained with the KNMI'06 scenarios, allowing them to formulate a much clearer set of additional needs and requirements. A general set of climate scenarios, such as KNMI'06 or KNMI'14, cannot ensure salience to all users of these scenarios, as many climate indicators become relevant at different spatial or temporal scales for different users. Relevance is therefore often increased by application of further tailoring the scenarios to the users' needs. Yet the stakeholder consultation did enhance the *relevance* of the KNMI'14 scenarios:

- Variables are selected for which a wider community showed interest. A large number of requests collected after KNMI'06 are incorporated in KNMI'14, including more spatial detail, information about natural variability, and new variables.
- The basic conceptual framework of the scenarios does not deviate significantly from KNMI'06. Also the selected main global steering variables are similar (but not identical) to the choices made in KNMI'06. This increases the tenability of the scenarios as a multi-year outlook, accommodating long-term adaptation programmes like the Deltaprogramme. The introduction of new insights are put in the context of the previous set of scenarios.
- The scenarios are based on understandable and generally accepted principles. Although climate science (both the physical and socio-economic disciplines) is complex and not transparent to a large group of users, the underlying concepts (greenhouse gas processes, economic development, regional climate variability) are understandable and well documented in the literature (and IPCC reports).
- KNMI'14 consists of a set of generic scenarios, designed as a framework in which application specific and tailor-made climate change information can be produced. The KNMI'14 method was designed to make this tailoring process easier than before, by generating an internally consistent set of explicit model simulations for each scenario. As such they provide a reference to which a broad set of sector- or area-specific climate assessments can be related and compared.
- A strong link between the climate research and several impact/adaptation research institutes allowed a more rapid transfer of relevant information after the release of the KNMI'14 climate change scenarios.
- The presentation of the scenarios serves a wide range of applications, and varies from a glossy brochure, a website with visual interpretations, and fact sheets to convey the general concepts and results on one hand, to a practical tool to generate detailed time series of climate variables on the other.

Further improvement of the salience of KNMI'14 can be obtained by putting the scenarios in the context of natural variability or weather phenomena that are familiar to the users. Some of this natural variability is explicitly included in the time series generation tool (section 3.1.5).

### **Legitimacy**

*Legitimacy* reflects the need that the scenarios are produced transparently, and reflect different views and values. The transparency is achieved when a clear indication of the level of understanding (and lacks thereof) of the governing mechanisms, the quality of the models, the origin and plausibility of the driving forces is supplied. And different views and values must be embedded in the chosen forcing pathways and the (regional) climate response to these.

The scenarios are constructed following a scientific methodology, that implies the use of well documented scientific findings such as reflected in the IPCC assessments, participate in the international scientific arena, publish studies in the peer-reviewed literature, and actively develop, operate, and evaluate the modelling tools (see plausibility criterion above). A formal assessment of the quality of the methodologies and assumptions, as for instance proposed by Klopogge et al (2005) and applied by Tang and Dessai (2012) for UKCP09, is not (yet) carried out. In this quality assessment a systematic analysis of the underlying assumptions, the weak components in the analysis chain, and the potential value-ladenness should be applied. However, the elements that contribute to the legitimacy of KNMI'14 are:

- The scenarios are not framed as quantitative probabilistic forecasts of the future climate of the Netherlands, but rather depict a range of possible future climate conditions that is considered plausible and relevant to explore when anticipating changes in global and regional climate and non-climate conditions. Different socio-economic pathways are followed, reflecting different views on the future evolution of the global economy and social structure. A general scenario of “no change compared to present day conditions” could have been included, reflecting the view that climate is not affected significantly by human interference. Although for some variables the projected change in any scenario is indeed very small given the large natural variability and/or uncertainty, a general “no change” scenario is not added because (a) observations, models and theoretical understanding make such a scenario very unlikely and would be at odds with the criterion “plausibility”, (b) natural climate variability is explored and utilized explicitly, resulting in notably different climate conditions even under a similar (or small) anthropogenic climate forcing, and (c) it does not provide any new information compared to the available observational documentation of the climate in our region.
- The methodology is not the only one that could have been followed (e.g. simple energy balance models or complex Bayesian statistics) but is documented well, and at different levels: this scientific report,

peer-reviewed literature and fact sheets and brochures for the general public are produced. This contributes to the transparency of the product chain.

- Systematic biases in models and shortcomings in observations are not ignored but explicitly addressed, partly via publications in the peer-reviewed scientific literature.
- An extensive user survey has provided a platform for addressing different perspectives and interpretations of the role of climate change in different sectors of society. Regular workshops and newsletters informed the potential users about the construction process in an early stage, and allowed an inventory of specific needs and desires.

### 1.2.2 From user requests to the new climate scenarios

Climate change scenarios can serve different purposes. A general function is that the physical insights they provide may enrich the mental frame of a decision maker or planner. In other words: the physical and non-physical narratives on which they are based can provide insights and “set the scene” for any future outlook activity. A set of specific climate change scenarios can serve as a reference framework for a collection of assessments, to enhance consistency and comparability. And finally, a more practical application of climate scenarios is to provide quantitative information (“hard numbers”) for specific sectoral or regional assessments.

The different applications of the scenarios require different levels of detail. KNMI'14 is designed to provide a general scenario framework, in which a limited selection of possible future global temperature pathways is selected, but that also provides quantitative information on the regional response to these pathways. However, for many applications the information provided by KNMI'14 will still be too general and coarse grained, and additional tailoring of the scenarios is needed. As noted by Van den Hurk et al. (2013), the KNMI'06 scenarios as well as the scenarios described here bridge a gap between a top down oriented climate assessment framework that uses the global projections of future climate as starting point, and the bottom up vulnerability assessments that are guided by the relevant range of local meteorological drivers.

Compared to KNMI'06, the general framework provided by KNMI'14 is updated by accommodating specific user requests. A persistent request from scenario users is a quantitative estimate of the likelihood of any scenario provided. This has been accommodated by discussing the likelihood that a given scenario is within the bandwidth of projections for a given Representative Concentration Pathway (RCP) provided by the CMIP5 model ensemble (Section 2.7). However, even this set of CMIP5 projections cannot be considered a quantitative likelihood estimate, as they are highly conditional on the chosen emission pathway and the quality of the modelling tools used to generate the projections. Quantitative likelihood estimates easily lead to confusion about the difference between scenarios and predictions (see also Section 1.2). Enserink et al. (2013) criticised the framing of the sea level rise scenarios (Katsman et al. 2011) produced after the release of KNMI'06 as a likely scenario in order to generate policy support for the Dutch Delta Programme. The level of quantitative detail provided here is limited to the statement that the KNMI'14 scenarios are presented as a plausible range of future climate conditions, spanning the range of the majority of the CMIP5 projections used for the scenarios. The real climate evolution may well evolve well outside this range, certainly when smaller spatial and temporal scales are considered. Detailed future weather projections (Hazeleger 2012) give a more vivid and realistic expression of possible future conditions, but this enhanced realism aims at improving their conceivability, not their predictability (Smith 2002).

## 2. General structure of KNMI'14

### 2.1 Natural and forced regional climate variability

The KNMI'14 climate change scenarios are designed to give a quantitative visualisation of a range of climate conditions to which our country and its surroundings are presumably exposed in the coming century. Changes relative to the current climate can be expected from forced climate change related to prolonged greenhouse gas and aerosol emissions and land use change, and natural variability at multiyear time scales. The amplitude of natural variations becomes smaller for longer averaging periods, but even for 30 year averages – the usual period to define a climate – variations occur just by chance. Natural variations are larger for precipitation than for temperature, larger for extremes than for the mean, and larger for the climate of the Netherlands than for the global climate.

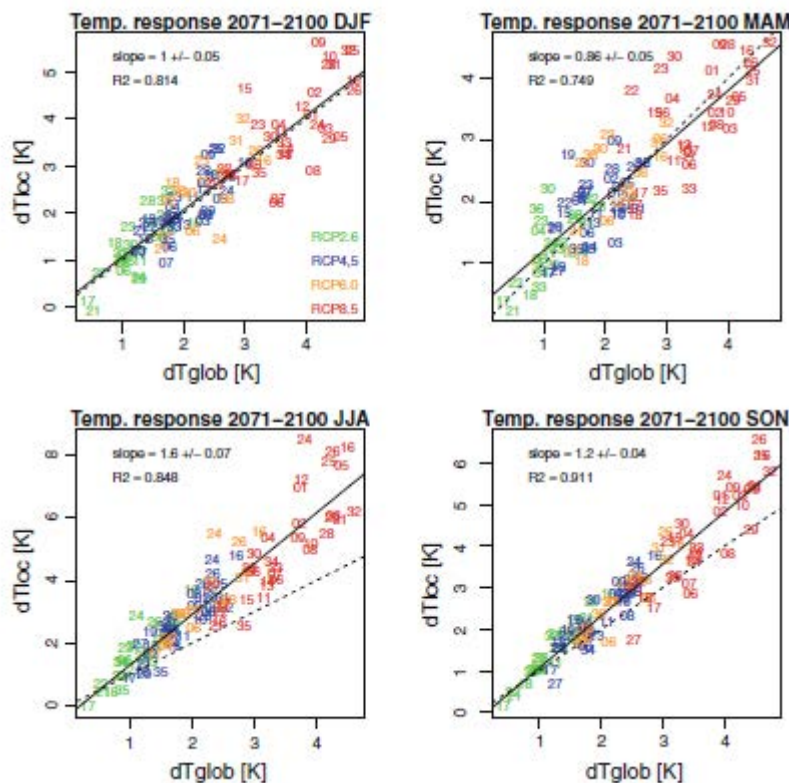


Figure 2.1: Temperature response in the Rhine basin per GCM/RCP combination in 2071-2100 relative to 1976-2005 as function of  $\Delta T_{glob}$  over the same period. Numbers refer to the GCM system, color code refers to the RCP. Also shown is the best linear fit (solid lines) and the 1:1 slope (dotted lines) (source: (Van den Hurk et al. 2014).

Future projections of the global and regional climate, such as the model results generated in the context of the CMIP5 model ensemble (Taylor et al. 2011), reflect the spatial and temporal patterns of the variable climate. A systematic survey of the CMIP5 model results for Western Europe was carried out by Van den Hurk et al. (2014). For this analysis a total number of 245 GCM projections (between 1950 and 2100) was used distributed over four greenhouse gas scenarios (Representative Concentration Pathways, RCP (Van Vuuren et al. 2011) and 37 modelling systems. The seasonal mean temperature response ( $\Delta T_{loc}$ ) in a region roughly encompassing the Rhine basin ( $6^{\circ} - 9^{\circ}\text{E}$ ,  $47^{\circ} - 52^{\circ}\text{N}$ ) is strongly correlated to the global mean temperature increase  $\Delta T_{glob}$ , with 75 – 92% of the variance in  $\Delta T_{loc}$  explained by variations in  $\Delta T_{glob}$  (Figure 2.1). It is clear that the regional temperature increase is stronger than the global mean temperature increase in the summer (JJA) and autumn (SON) seasons, while for winter (DJF) and spring (MAM) the local response is similar or slightly smaller than the global mean. This is related to systematic seasonal patterns in the atmospheric circulation and regional feedbacks, bringing warmer than average air into the domain in the summer and autumn.

Figure 2.1 also shows that a comparison of GCM projections driven by a similar greenhouse forcing scenario reveal considerable spread, being a combination of systematic differences in model formulations and their response to a given forcing, and of natural climate variability simulated by the GCMs. Not only the global mean temperature response varies per RCP, also the link to the regional temperature response is not uniform across the ensemble.

The distinct spatial patterns of global warming exhibited by the GCM projections are associated with systematic alterations of the Mean Sea Level Pressure (MSLP) distribution. However, within an ensemble of climate model simulations, natural variability and systematic spread in the modelled regional response generate a large variability in the projected changes in MSLP, leading to a large variability in the regional temperature and wind response. The relationship between local temperature/precipitation response and regional MSLP response is shown in Figure 2.2, using the spread displayed in the large GCM/RCP ensemble. For temperature, models with a strong tendency for low pressure systems in Southern Europe tend to produce high temperature responses in the Rhine area in JJA (related to the warm Easterlies; (Haarsma et al. 2009). Anomalous wet conditions in DJF are related to low pressure systems at higher latitudes, while cyclonic conditions close to the Rhine area likewise lead to advection of warm moist air in summer. The different responses between models have been explained by (Haarsma et al. 2013a) and are related to different heating patterns in the subtropics, the associated meridional sea surface temperature gradient and the subsequent response of the meridional circulation.

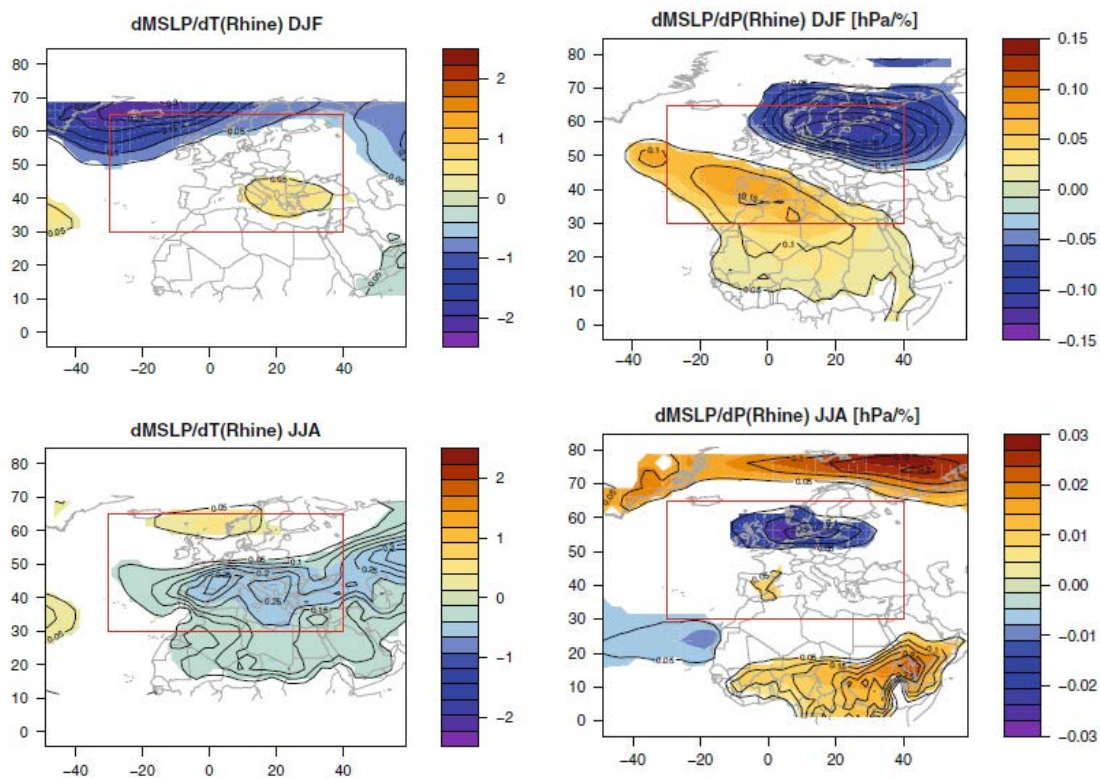


Figure 2.2: Left panels: Normalized MSLP response pattern [hPa/K] related to the normalized Rhine basin temperature response  $T_{loc}$  [K/K] for DJF (top) and JJA (bottom), derived from linear regression across the sample of GCM/RCP combinations. Areas where the fraction of explained variance of the regression between  $T_{loc}$  and MSLP (indicated by contour lines)  $< 0.05$  are blanked. Right panels show the same for the precipitation-related MSLP response (source: (Van den Hurk et al. 2014).

However, the patterns shown above are governed by both forced and natural variability across the GCM ensemble. To illustrate the role of natural variability, Figure 2.3 shows the future changes in summer precipitation in the Netherlands derived from eight projections of the EC-Earth model (Hazeleger et al. 2012) downscaled with the regional climate model RACMO2 (Van Meijgaard et al. 2008) exposed to the RCP8.5 greenhouse forcing scenario. The average shows a gradual decrease in summer precipitation, a general feature depicted in the scenarios. The individual model calculations behave differently. By chance precipitation is sometimes higher and sometimes lower than the average. Consequently, natural variations can mask forced climate change, and lead to trends temporarily opposing the scenario signal. For example, three of the eight

calculations in Figure 2.3 show temporary precipitation increases until about 2050, due to long term natural variations in the climate, followed by strong decreases thereafter. Likewise, observed trends over the recent history may deviate from the long term mean that is captured by the climate change scenarios.

The discussion above illustrates the need to consider a combination of sources of uncertainty (or model spread) when making assessments of the future climate conditions at a regional level:

- the future evolution of anthropogenic forcings is uncertain, introducing the need to consider a range of forcing scenarios (RCPs)
- the modelled response to a given forcing depends on the model-specific formulation and may contain model-specific systematic biases, making consideration of a range of climate models necessary
- natural variability at various time and spatial scales introduces temporal or local deviations from the anticipated mean climate signal, making it necessary to use multiple realizations of individual modelling systems, and making statements of individual model quality based on their agreement with available observations inherently difficult.

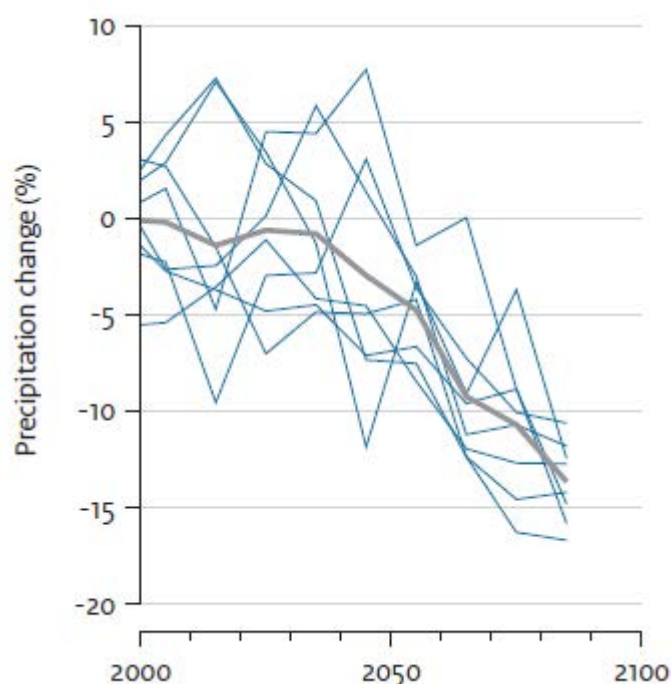


Figure 2.3: Future changes in summer (JJA) precipitation (30 yr averages relative to 1981-2010) in The Netherlands according to eight RACMO2 projections exposed to the RCP8.5 forcing scenario (blue lines). The grey line indicates the long-term average decrease.

## 2.2 Spanning a likelihood range

Local expressions of changes in climate variables may thus be linked to a combination of a global mean climate forcing and a regional expression induced by local feedbacks and circulation responses. In KNMI'06 the effect of these two factors was explicitly expressed by setting up a two-axis scenario framework: one axis depicting different values of the projected global mean temperature increase (resulting from uncertainties in emission scenarios and climate sensitivity), and one axis expressing the response to an (uncertain) regional circulation response. The main motivation for including this regional circulation response was the inherent contribution to the uncertainty of, particularly, precipitation and temperature variables: a strong increase in frequency of westerlies in DJF leads to relatively warm and wet winter conditions, while dry and warm summer conditions are associated with anomalously frequent easterlies. However, the limited set of available model projections enforced the use of simple statistical techniques leading to a loss of spatial information and enhanced physically inconsistency (Lenderink et al. 2007).

Based on the user comments to KNMI'06 (Section 1.2.2) we maintain the two-axis scenario framework, but intend to improve on the ability to generate coherent climate characteristics across a range of desired variables, and spatial and temporal scales.

### 2.2.1 The global temperature increase and chosen time horizons: the G and W scenarios

In KNMI'06 the chosen reference period was 1976 – 2005, with 1990 as a central marker year. Scenarios were constructed for 2050 (2036 – 2065) and 2100, which was obtained by generally doubling the scenario values for 2050.

In KNMI'14, the global mean temperature increase used as driver for the scenarios is derived from the range of values generated by the CMIP5 model ensemble (Taylor et al. 2011) encompassing the period 1951 – 2100. In CMIP5 a total of roughly 35 GCM systems is used to generate projections of future climate driven by emission and concentration scenarios (RCPs; Van Vuuren et al. 2011). Figure 2.4 shows the projected global mean temperature increase relative to 1981-2010 ( $\Delta T_{glob}$ ) for two RCPs. Scenarios are derived by exploring the temperature response generated for targeted time horizons, rather than by linear extrapolation from the 2050 scenarios as was applied in KNMI'06. Table 2.1 shows the selected global mean temperature change values and the time horizons chosen for KNMI'14. The considerations for this choice were:

- every scenario period covers 30 years expressing a climatological mean
- the reference period is synchronized with the latest climatological reference period of 30 years
- the desire for a near-term (2030) scenario was clearly expressed by users in response to KNMI'06
- and end-of-century scenario generated from GCM model output does not allow analyses beyond 2100 due to lack of available model output.

A low global mean temperature increase is used to construct the group of so-called “G” (from “Gematigd” or “moderate”) scenarios, while stronger temperature increases are identified with “W” (of “Warm”).

*Table 2.1: Scenario time horizons and corresponding global mean temperature values*

Label	Period	Global mean temperature response (°C)
Reference	1981 – 2010	0
2030	2016 – 2045	0.9
2050	2036 – 2065	1 – 2
2085	2081 – 2100	1.5 – 3.5

Figure 2.4 clearly illustrates that the different emission scenarios become increasingly distinguishable as time proceeds. Unlike around 2050 and 2085, differences in calculated global temperature increase around 2030 cannot be linked to differences in emission scenario, and also model spread is relatively small. Therefore, the KNMI'14 scenario for 2030 does not distinguish between different values for global temperature rise. The 2030 scenario is not defined from the CMIP5 spread, but derived from ensemble projections from a single model (EC-Earth) (see section 2.3.2).

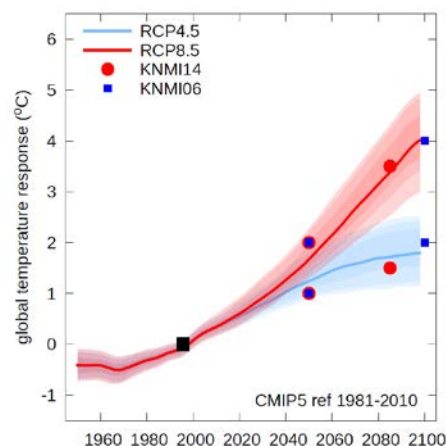


*Figure 2.4: Global temperature change ( $\Delta T_{glob}$ ) according to CMIP5 climate projections for two RCPs. The solid coloured lines represent the ensemble mean 30 year averaged temperature increase for all model projections used for the indicated RCP, while the surrounding lighter shading indicates the 50%, 80% and 90% distributions around the mean. The dots and squares indicate the global temperature rise selected for the KNMI climate scenarios for the Netherlands.*

## 2.2.2 Regional deviations from the global mean picture: the L and H subscripts

Regional deviations from the global mean changes result from systematic advection of air masses from remote areas, specific regional surface conditions (for instance presence of oceans and land-ocean gradients) and processes and feedbacks that are specific to the region of interest. This also applies to the response to climate forcings: the regional change deviates strongly from the global mean values, as the role of natural variability, local anomalies in the mean climate, advection and circulation, and local processes affected in the climate response all differ greatly from the global mean picture.

In KNMI'06 an uncertainty in the regional deviations from the global mean response was expressed by analysing the regional consequences of an uncertain response in the regional atmospheric circulation, in combination with uncertainty in local feedbacks (Lenderink et al. 2007). Strong increases in the frequency of westerly winds in winter lead to stronger precipitation increases, more wet days and less cold nights, while enhanced easterlies in summer resulted in dryer and warmer conditions. Annual maximum daily mean wind speed was not clearly linked to assumed changes in the atmospheric circulation, but an uncertain range in response was distributed over the 4 scenarios. For sea level no connection with atmospheric circulation was (and is) implemented.

In the current scenarios we have followed a similar rationale but a different technical approach. Again uncertainty in regional responses are treated as a second driver for spanning a scenario range. In KNMI'06 this was done by expressing all responses explicitly as a function of the circulation steering variable (called  $G_{west}$ ) by a statistical regression technique, which was derived for each scenario separately – a procedure which led to a loss of spatial resolution and physical consistency. In the new scenarios there is no explicit circulation steering variable, but the main focus is on representing the spread in precipitation response. The regional responses are computed directly from samples of high resolution model simulations that satisfy the requirement to span 60 – 80% of the simulated CMIP5 spread for a set of temperature and precipitation characteristics. With this procedure spatial detail is retained and physical consistency is not significantly affected. Also the response of monthly extremes (dry/warm/wet/cold months) in comparison with CMIP5 was explicitly evaluated.

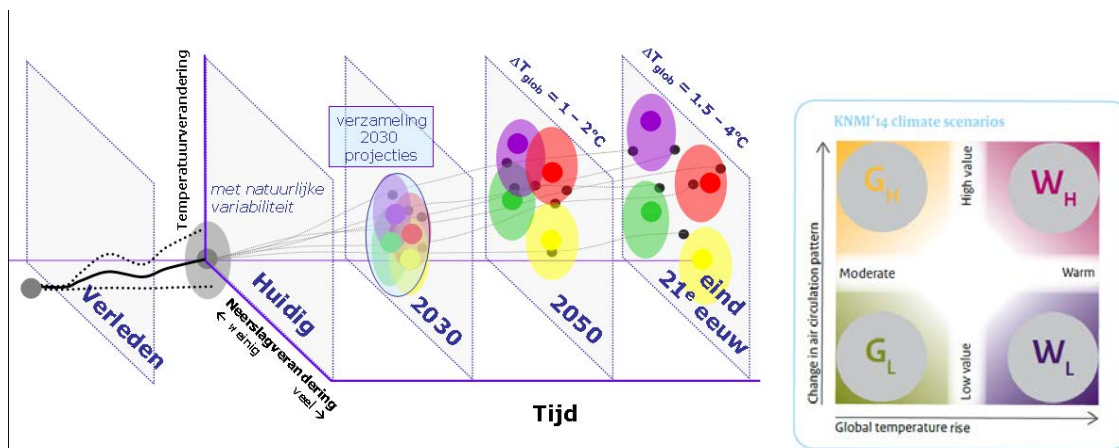


Figure 2.5: Conceptual overview of the construction of the KNMI'14 scenarios. The horizontal axis denotes time, where a transition from past to present and future is visualized. On the vertical axis the temperature change relative to a reference climate is depicted, while on an imaginary depth axis the difference between a low or high precipitation response is shown, with higher responses further away from the virtual “zero change” plane. Observed and projected time series are depicted in thin grey lines, where the values at given climatological time intervals are shown as black “bullet holes”. The uncertainty in the observed and projected response results from a combination of natural variability and systematic uncertainty in the modelled climate response, where the latter is captured by different representative color symbol, and where natural variability is indicated by a pale coloured uncertainty range around that symbol. For the time period around 2030 the systematic difference between the individual scenarios is overwhelmed by natural variability, and thus only a single scenario is constructed. Note that also the observations are associated with natural variability: observed trends should be considered as a single realization of a possible range of values. The right panel shows the scenario icon.

Basically the model projections with EC-Earth/RACMO are stratified in two different pools, one representing a strong response (labelled with subscript “H”) with wetter winters and drier summers, and one with a relatively weak response (labelled with subscript “L”) with smaller changes in precipitation in both

seasons. The response of other variables except sea level rise (temperature, wind speed, evaporation) are derived from these two pools, thus ensuring a consistent set of variables grouped together in each scenario.

A graphical representation of the construction of the KNMI'14 scenarios is given in Figure 2.5, where the combination of a low/high temperature and low/high precipitation response is grouped into 4 discrete scenarios. A 2D version of this diagram used for communication purposes is provided in Figure ... Each scenario is representative for a 30 year climatological period. The significance of the difference between the scenarios varies for the different variables and projection periods, and is related to the natural variability of the 30 year climatological value of the variable concerned. The role of natural variability will be further discussed in the next section.

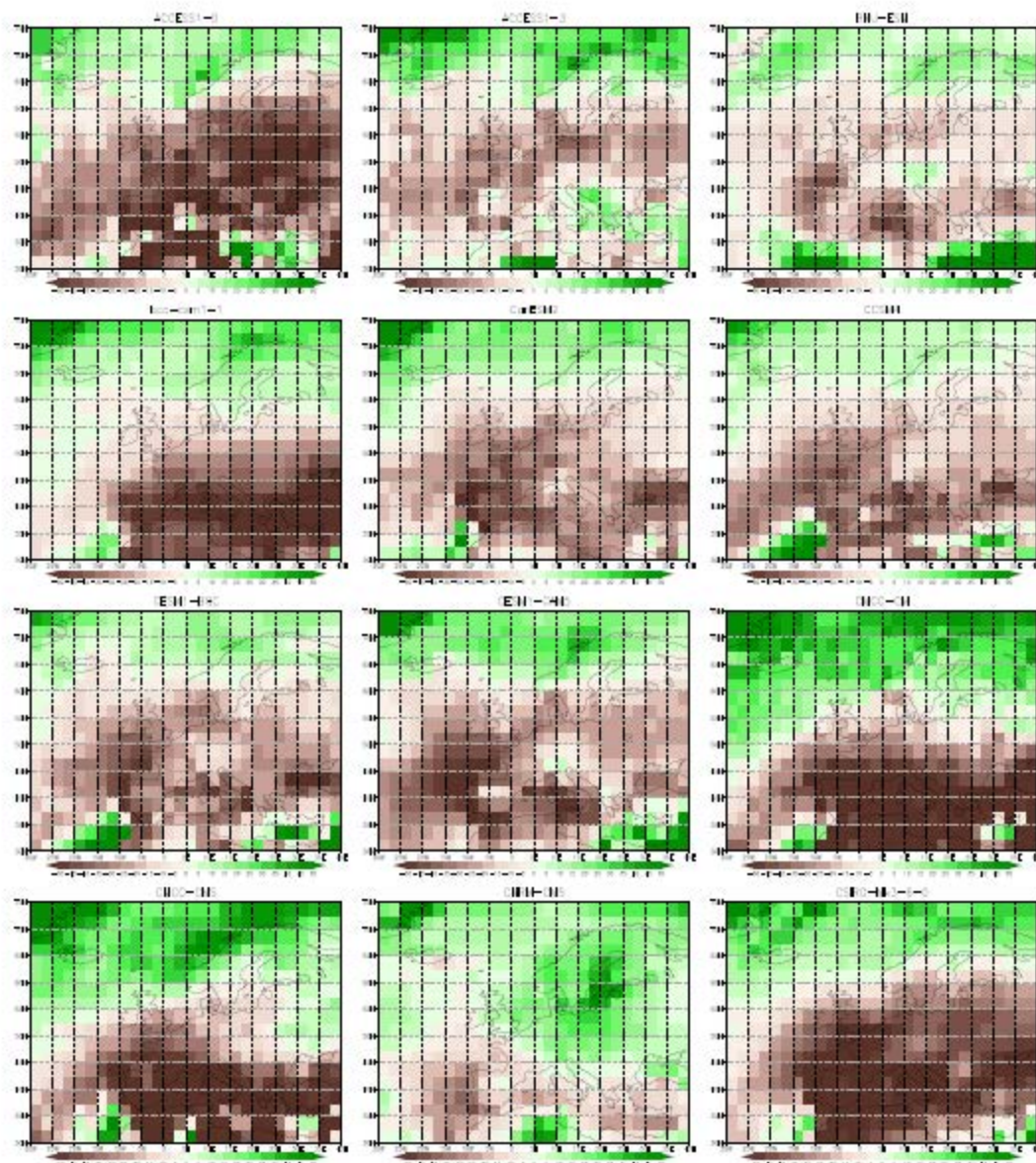


Figure 2.6: Sample of projections of precipitation change in JJA (%; 2071 – 2100 relative to 1981 – 2010) from a subset of CMIP5 models driven with the RCP8.5 emission scenario.

### 2.3 The scenario construction procedure

For different sets of variables different procedures have been followed to construct the scenarios. The temperature, precipitation, evaporation and radiation indices are obtained from a multistep procedure, where a selection of samples from an ensemble of RACMO2 simulations is grouped into a number of subsets corresponding to the scenarios and target periods (section 2.3.1). From these subsets a number of response characteristics are derived (such as the seasonal mean temperature change, or the change in a given precipitation percentile, detailed in section 3.1.4. Further downscaling to local climate change indicators is

applied using a time series transformation process (section 3.1.5). A special case of the scenario construction applies to the near term horizon 2030, as described in section 2.3.2. For the thermal expansion component of sea level and for extreme wind speed information is mainly retrieved from the ensemble of CMIP5 model output, and these procedures are described in detail in section 3.2 and 3.3, respectively.

Chapter 4 presents a summary of the results in tables. A guidance table 4.4 provides a summary of the methodology followed for each variable and quantity.

### 2.3.1 Selection of model samples

Compared to the time KNMI'06 was produced, a much larger set of global climate projections is available for KNMI'14. Figure 2.6 illustrates this model data set for the European domain, by showing the seasonal mean precipitation change in summer from a subset of CMIP5 models. This example clearly demonstrates the large difference in spatial response patterns, resulting from inherent uncertainty in climate response and the role of natural variability at decadal time scales.

However, similar to the KNMI'06 project, the available set of regional climate model (RCM) projections, necessary to improve the temporal and spatial structure of the GCM projections, is still fairly sparse. The ENSEMBLES project (Van der Linden and Mitchell 2009) resulted in a large set of RCM projections, but driven by a limited set of GCMs. A follow-up regional downscaling project is currently ongoing (CORDEX; Giorgi et al. 2009) but results for the European area are not widely available yet.

The incentive to produce internally consistent and spatially and temporally explicit pictures of climate change (Section 1.1.4) calls for using a different procedure than the fairly pragmatic selection and scaling method (Lenderink et al. 2007) that was followed before. Another relevant notion is that natural variability leads to a large range of projected regional precipitation responses for a given atmospheric forcing (Figure 2.7). Projections generated with a single model and single radiative forcing already span a portion of the spread in climate response values depicted by the CMIP5 ensemble.

These notions lead to a simulation strategy in which a single set of climate models is used to create 4 different scenarios that together span a large fraction of the spread in regional response displayed in the CMIP5 ensemble. We use a group of 8 EC-Earth simulations driven with the RCP8.5 forcing scenario, and downscaled with the RACMO2 regional climate model (for technical details see section 2.6). For each scenario appropriate time intervals are selected from the 8 GCM-RCM time series, that comply with a set of criteria that coincide with the specification of the chosen scenario. The group of selected time intervals are used to construct a time series of RCM fields for each scenario, from which the relevant climate variables are deduced. In order to preserve the temporal correlation structure in these time series, the time interval are chosen to cover 5 consecutive seasonal cycles each.

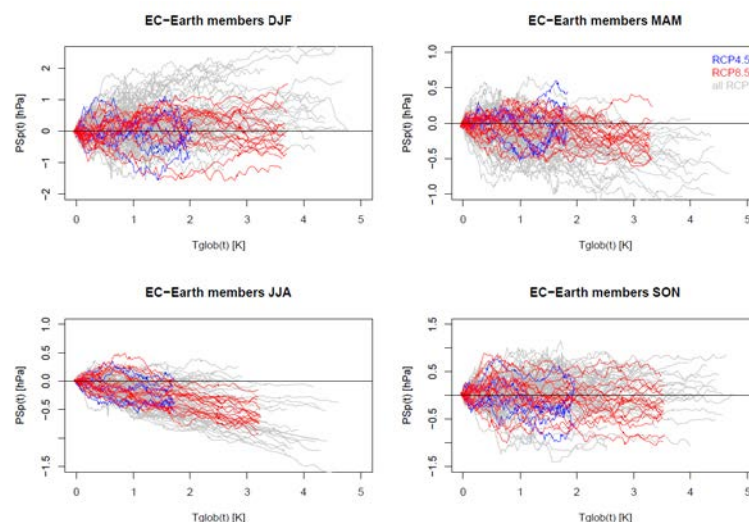


Figure 2.7: Illustration of the contribution of natural variability to projected regional precipitation response. Shown are 30-year mean time filtered seasonal response in  $T_{glob}$  versus the precipitation response in The Netherlands, derived from an ensemble of EC-Earth simulations driven by two RCPs (in colour). The grey lines depict results from all CMIP5 models and all RCPs as analysed by (Van den Hurk et al. 2014)

The selection of the time intervals per scenario is based on a group of criteria, that together create a sample that matches the desired properties for each scenario. These criteria concern the assumed global

temperature increase, and the regional precipitation and temperature response. A summary of these criteria used to select the time slices per scenario, and the scenario labels are listed in Table 2.2. After selection on intervals with a given  $\Delta T_{glob}$ , a selection of samples matching a given precipitation response in winter is applied. For the scenarios with “low” changes in the precipitation climate ( $G_L$  and  $W_L$ ) a winter precipitation change of 4% per degree global warming is chosen. This is higher than the various estimates of the global mean precipitation increase (1 – 3%/°C) and more representative for the Western European climate. For “high” precipitation change scenarios ( $G_H$  and  $W_H$ ) a winter precipitation change of 8%/°C is selected, corresponding to increased advection of mild and moist air (Van den Hurk et al. 2013b). Further criteria (detailed in section 3.1.2) select precipitation and temperature responses in winter and summer, as noted in the CMIP5 ensemble.

Table 2.2: Summary of the criteria used to select the GCM-RCM time slots for each scenario

Time period	Scenario	$\Delta T_{glob}$ (°C)	First selection of $\Delta P_{DJF}$ (%/°C)	Further criteria
2050 (2046 – 2075)	$G_L$	1	+4	Wet spring and dry summer in reference period, reverse in future Cold and wet summer in reference period, warm and dry in future
	$G_H$	1	+8	Wet spring and dry summer in reference period, reverse in future Cold and wet summer in reference period, warm and dry in future
	$W_L$	2	+4	Wet spring and dry summer in reference period, reverse in future Cold and wet summer in reference period, warm and dry in future
	$W_H$	2	+8	Wet spring and dry summer in reference period, reverse in future Cold and wet summer in reference period, warm and dry in future
2085 (2066 – 2095)	$G_L$	1.5	+4	Wet spring and dry summer in reference period, reverse in future Cold and wet summer in reference period, warm and dry in future
	$G_H$	1.5	+8	Wet spring and dry summer in reference period, reverse in future Cold and wet summer in reference period, warm and dry in future
	$W_L$	3.5*	+4	Wet spring and dry summer in reference period, reverse in future Cold and wet summer in reference period, warm and dry in future
	$W_H$	3.5*	+8	Wet spring and dry summer in reference period, reverse in future Cold and wet summer in reference period, warm and dry in future

\* obtained by selecting intervals with  $\Delta T_{glob} = +3$  °C, and extrapolating the results to  $\Delta T_{glob} = +3.5$  °C

The procedure to construct sets of time slices that comply with a number of scenario criteria has a number of clear advantages:

- all variables (except sea level rise) are derived from a similar set of RCM projections, ensuring internal consistence between variables across spatial temporal scales as represented in the RCM model formulation
- apart from the tabulated scenario values (section 0), fields of variables are available for analysing spatial and temporal structures in the climate change signal, and for selecting relevant and/or representative episodes that can be analysed as cases of “Future Weather”.

A number of disadvantages are present as well:

- for a number of crucial variables the range span by the chosen GCM-RCM combination is not covering the desired fraction of the CMIP5 range, because our method is based on a single model configuration
- variables linked to processes poorly resolved in the available GCM-RCM suite are not captured well in the scenarios. Additional scaling or post-processing is required, for instance with respect to precipitation extremes
- the multidecadal natural variability may be disrupted by combining time slices that in the continuous model simulations did not occur in the same chronological order.

Similar to KNMI'06 the procedure is not free of expert judgement. Also, the scenario values are largely based on results generated with an imperfect model configuration that cannot be validated or corrected in all aspects, including the correlation between variables that may be crucial.

Technical details of the selection method, the climate indicators retrieved from the selected samples, and the cross-validation with the CMIP5 models is presented in section 3.1.2.

### 2.3.2 Scenarios for 2030

In response to the request for quantitative climate information at shorter (decadal) time scales a set of scenarios has been produced for the time era around 2030. The request both reflects a need to be useful for many stakeholder decision processes that have a shorter than half century time scale, and to provide quantitative information on patterns of trends and natural variability. A formal scenario approach as described above does not lead to very discriminating scenarios concerning global temperature change, given the low signal that is visible at this time scale (Figure 2.4).

Therefore a different procedure is followed to construct the 2030 scenarios. Instead of sampling time intervals from the RCM ensemble, the 8 ensemble projections are grouped and their response in the 2016-2045 time interval is averaged and presented in conjunction with the scenario variables for 2050 and 2085 (Chapter 4). These numbers are thus taken from a single model system only. Although the climate sensitivity of the chosen modelling system EC-Earth is close to the CMIP5 ensemble mean (Hazeleger et al. 2012), the averaged scenario values do not adequately represent the (small) range of values produced by CMIP5. Therefore a transient comparison to the scenarios for 2050 and 2085 is not straightforward.

However, the main intention of these scenarios is not to generate a “best guess” estimate for changes in regional climate variables during the next decades. Their aim is to present a set of different realizations of the climate in the near future, thus illustrating the role of natural variability in the regional spatial and temporal gradients. For a number of quantities, considerably different response values can be seen in the individual samples, as will be further illustrated in section 3.1.

## 2.4 Observations, climate normals and estimates of natural variability

### 2.4.1 Station observations used for KNMI'14

Station observations have been used to determine the climate normals and the natural variability of the 30-year time scales that are given in the scenario tables presented in chapter 4. In this section it is described which stations are used for each variable and what period these station observations cover. For several variables (including temperature, relative humidity, solar radiation and evaporation) a single station was used that is considered to be representative of the Netherlands. For the variables already mentioned this station is De Bilt (lying centrally in the Netherlands) and for wind this station is Den Helder (lying at the Dutch coast north of Amsterdam). For sea level and fog a small number of stations is used and for precipitation 102 or 240 stations are used to account for the large spatial variability of precipitation. Below the station data are summarized (see also Table 4.4).

#### **Sea level**

This is the only variable for which KNMI is not the source of the data. The sea level observations are so-called PSMSL data (see [www.psmsl.org](http://www.psmsl.org)). Sea level observations were used for 6 stations along the Dutch coast: Delfzijl, Den Helder, Harlingen, Hoek van Holland, IJmuiden and Vlissingen for the period 1901 – 2012. In these sea level observations tidal effects were already filtered out.

#### **Temperature**

De Bilt, 1901 – 2013 (includes daily average, daily minimum and daily maximum temperatures).

#### **Precipitation**

For mean amount, number of wet days ( $\geq 0.1$ mm), number of days  $\geq 10$  or 20 mm 102 homogenized station series for the period 1910 – 2013, and for the once in 10 year precipitation (10-day in winter and 1-day in summer) 240 homogenized precipitation stations (1981 – 2010). The homogenization of these series is described in Buishand et al., 2013. For hourly intensity, hourly precipitation observations were used from station De Bilt for the period 1906 – 2013.

#### **Wind**

Station Den Helder; wind direction for the period 1906 – 2012, wind speed for the period 1981 – 2012. For wind speed use is made of the so-called potential wind. The potential wind speed is corrected for differences and (historical) changes in the surface roughness (see [www.knmi.nl/klimatologie/onderzoeksgegevens/potentiele\\_wind/uitleg.html](http://www.knmi.nl/klimatologie/onderzoeksgegevens/potentiele_wind/uitleg.html)).

**Relative humidity**

Station De Bilt for the period 1951 – 2013.

**Solar radiation and evaporation**

Station De Bilt for the period 1958 -2013.

Solar radiation refers to global radiation, or more precisely the incoming solar radiation. Evaporation is not measured directly but calculated from daily solar radiation and daily temperature according to the Makkink formula for potential evaporation (see De Bruin (1981) and CHO, 1988). This is also known in the Netherlands as the Makkink evaporation which is operationally calculated by KNMI from 1987 onwards. Later it was also calculated for the period 1958 – 1986 i.e. from the year that the solar radiation measurements became available.

**Drought; precipitation deficit**

For station De Bilt for the period 1951 -2010.

The precipitation deficit is calculated from the (Makkink) evaporation and precipitation. It is calculated on a daily basis for the period 1 April to 30 September. In contrast to the solar radiation and the evaporation the used time series of the precipitation deficit already starts in 1951. This was possible due to the availability of Makkink evaporation estimates based on sunshine duration rather than on solar radiation for the years 1951 to 1957 (see Beersma and Buishand 2002).

**Fog**

Fog observations from 5 stations (Beek, De Bilt, De Kooy, Eelde and Vlissingen) for the period 1956 -2010 were used. The visual fog measurements ended in 2002.

**2.4.2 Normal periods and natural variability of 30-year averages****Normal periods**

Climate normals are calculated from the observations for two 30-year normal periods: 1951 – 1980 and 1981 – 2010. The latter normal period also serves as the reference for the scenario changes presented in chapter 4. Depending on the specific variable these normals represent averages, frequencies or other statistics based on these 30-year periods.

For the rate of change of sea level along the Dutch coast the normals are obtained from 30-year regressions for the normal periods. The 'normals' of the once in 10 year precipitation (10-day in winter and 1-day in summer) are obtained from GEV distributions fitted to the 30-year time series of each of 240 precipitation stations. The normal values (presented in chapter 4) are averages of the 10-year precipitation from all 240 fitted distributions. For each station the location and scale parameter of the GEV distribution are estimated using Maximum Likelihood. The shape parameter  $\kappa$  is fixed according to  $\kappa = -0.090 + 0.017D$ , with  $D$  the duration of precipitation in days (see Smits et al., 2004). So, for 1-day and 10-day precipitation  $\kappa$  is respectively -0.073 and 0.080. A negative shape parameter implies a long-tailed distribution.

For the once in 10 year precipitation deficit normal, the 2003 precipitation deficit Beersma et al (2004) of ~230 mm for De Bilt is used.

Due to observations starting after 1951 (solar radiation) or ending before 2010 (fog) some normals that are presented for "1951 – 1980" or "1981 – 2010" do therefore not fully correspond to the years 1951 – 1980 or 1981 – 2010 respectively. The solar radiation and evaporation normals for 1951 – 1980 are therefore calculated for the years 1958 – 1980. Likewise, since the fog measurements start in 1956 the 1951 – 1980 fog normal is calculated for the years 1956 – 1980. Further, the visual observations of fog stop in 2002 and combining these with an instrumentally based alternative leads to an inhomogeneous fog series. For the 1981 – 2010 fog normal therefore the 1971 – 2000 fog normal was used instead.

The 1981 – 2010 normals serve as the reference for the scenario change values for the climates around 2030, 2050 and 2085 (presented in Chapter 4). The difference between the 1981 – 2010 and 1951 – 1980 normals gives a first indication of climate change in the recent decades. However, differences are not necessarily anthropogenic in nature, they can also be the result of natural variability of the 30-year time scale.

**Natural variability estimates**

In addition to the normals, estimates of the natural variability of the 30-year time scale of the normals are given. This natural variability of the 30-year time scale (from now on simply denoted as natural variability) is determined from the observations as described in section 2.4.1. In this report it is assumed that the natural

variability in the future scenarios is to the first order the same as for the historical climate (as obtained from the observational series). This natural variability estimate can be used to put the scenario change values with respect to the 1981 – 2010 normal period as well as differences between the two normal periods into perspective. It is calculated in such a way that the effects of systematic trends are eliminated. The natural variability estimate represents a 90% range. The range is assumed to be symmetric, the lower limit corresponds to the 5% quantile and the upper limit to the 95% quantile of the normal value. This means that there is a 10% probability that the 'real climate' deviates more from the reference normal than indicated by the natural variability range. The same holds for the future scenarios; these are uncertain as well and there is a 10% probability that a future scenario value deviates more from the presented scenario value for a specific scenario than indicated by the natural variability range. Both the current climate (represented by the normals) and the future climate (represented by the scenarios presented in Chapter 4) are thus uncertain due to natural variability. As a result, and again assuming that the natural variability is the same both for the current and the future climate, scenario values significantly deviate from the current climate if they are outside  $\sqrt{2}$  times the natural variability range. This factor  $\sqrt{2}$ , which comes from the fact that the natural variability range applies to both the future and the current (i.e. the reference) climate, is also used for the shaded areas in Figures 4, 8, 14, 21, 22 and 23 in KNMI (2014).

Below the details are given on how the natural variability range is calculated. Use is made of a number of statistical concepts:

- The 90% range (corresponding with the range used by IPCC) equals  $\pm 1.645$  times the standard deviation (assuming a Normal distribution).
- The standard deviation of a 30-year mean is  $\sqrt{30}$  smaller than the standard deviation of a series of annual values if there is no serial correlation in that series.
- To eliminate the (undesired) effect of a systematic trend in the annual series on the standard deviation the standard deviation is calculated from the successive difference series rather than from the original series. If there is no serial correlation then this standard deviation is  $\sqrt{2}$  larger than the standard deviation from the original series.
- With (significant) serial correlation a correction factor for the standard deviation (obtained from the successive difference series) of  $\sqrt{(1+r)/(1-r)}$  is needed in which  $r$  represents the lag 1 serial correlation.
- As a rule of thumb (and given the length of the observational series) serial correlation is considered to be significantly different from zero if  $r$  is larger than 0.2 and for larger values of  $r$  the standard deviation should be corrected for the serial correlation.
- To reduce the uncertainty of the standard deviations used for the natural variability ranges, they are calculated from as long as possible annual series. (Just as the estimation of a mean is uncertain and this uncertainty, which is often denoted with the standard error, depends on the length of the series this also holds for the uncertainty in the estimate of the standard deviation. The longer the series the smaller the uncertainty.) In many cases this is longer than just the 30 years used for the 1981 – 2010 normal or the 60 years when adding the 1951 – 1980 and the 1981 – 2010 normal periods. For each variable the exact period from which the standard deviation is calculated is given in section 2.4.1.
- In case for a variable more than one station is used, the natural variability is first calculated for each station individually and thereafter the natural variability is averaged. For all variables the natural variability is thus an estimate of local variability and not the variability of a spatial average (which is generally smaller).

For almost all variables the lag 1 serial correlation of the (detrended) annual series is considerably smaller than 0.2 and correction of the standard deviation used for the natural variability estimate is therefore not needed. However for the detrended annual series of the sea level along the Dutch coast  $r$  is on average 0.26 and the standard deviation and thus the natural variability range are corrected for. Further, for the annual average temperature and the minimum temperature in summer  $r$  is very close to 0.2. For these two temperature variables correction of the standard deviation could be questioned. Since these are the only two temperature variables (of many more considered in the scenario tables in Chapter 4 for which a correction would be desirable it was chosen (based on uniformity of the estimation of the natural variability of all temperature related variables) not to correct the natural variability ranges for these two variables. Would they have been corrected, however, the ranges for the natural variability for the annual average temperature and the (daily) minimum temperature in summer would respectively be  $\pm 0.21$  and  $\pm 0.25$  °C rather than the uncorrected  $\pm 0.16$  and  $\pm 0.18$  °C presented in the scenario tables in Chapter 4 and in KNMI (2014).

There are three exceptions on the calculation of the natural variability as described above. First, for the rate of change of sea level the standard deviation of the 30-year mean is calculated from all overlapping 30-year regressions in the 1901 – 2012 series for each of the 6 stations. The standard deviations are averaged over the 6 stations. The natural variability range, finally, is again obtained as  $\pm 1.645$  times this standard deviation. Second, for precipitation also values for the 1 in 10-year precipitation are given for both normal periods. These values are obtained from GEV fits to the precipitation observations (for details see 'Normal periods' in this subsection). The natural variability range of the once in 10-year precipitation is obtained from the expected Fisher information (see e.g. Prescott en Walden, 1980) averaged over both normal periods. Third, the natural variability for the 'mean highest precipitation deficit during the growing season' was calculated from the original series rather than the successive difference series separately for the 1951 – 1980 series and the 1981 – 2010 series and then averaged.

## 2.5 Temporal and spatial variability

### 2.5.1 Scenario periods and time scales

IPCC defines climate in a narrow sense as the average weather, or more rigorously, as the statistical description in terms of the mean and variability of relevant quantities over a period of time ranging from months to thousands or millions of years. The classical period for averaging these variables is 30 years, as defined by the World Meteorological Organization. The relevant quantities are most often surface variables such as temperature, precipitation and wind. Climate in a wider sense is the state, including a statistical description, of the climate system (IPCC 2013c). Climate change at a given location thus not only concerns the change of a seasonal mean weather variable, but also its characteristics of temporal variability. Natural variability occurs at all time scales (Figure 2.8), and these temporal characteristics will vary differently for different time scales.

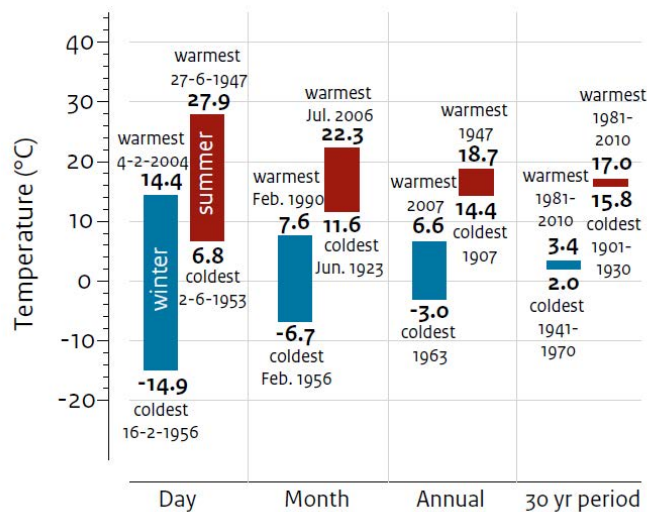


Figure 2.8: Observed temperature variations in De Bilt (the Netherlands) since 1901 averaged over different time scales for winter (blue) and summer (orange). For shorter time scales (left in graph) these variations are primarily due to synoptic ("weather") variability, on longer times scale (right) these are due to natural variations of the climate system and a climate change signal over the century.

The KNMI'14 scenarios have been constructed for the time horizons 2030, 2050 and 2085 (section 2.2.1), where the labels identify a 30 year ("climatological") time range centred around these years. For all variables except sea level rise the climate change signal varies over the seasons. The natural variability of each quantity over 30 year periods (how much a quantity varies from one 30-year period to another due to the natural variations) is given as a scenario quantity and is assumed not to vary over the scenario horizon. It is calculated from the observational records and climate model output. Interannual variability of (seasonal) variables is much larger and usually exceeds the mean climate change signal (see Figure 2.8 for an illustration). For seasonal mean temperature and precipitation a change in the interannual variability is included as a scenario quantity, calculated as discussed in section 3.1.2.

Changes in extremes are given for various time scales of interest. For temperature the annually coldest and warmest day correspond to the public perception by referring to a quantity that is experienced every year,

and therefore is easily remembered and put in the context of routine operations. It is not specifically relevant for many safety standards or analyses of resilience, for which longer return times are often more salient. Precipitation related quantities exceeded once per 10 years are given for 10-day precipitation sums in winter (for analyses of the discharge behaviour of the large rivers), (sub)daily precipitation sums in summer (for local flooding and sewage design measures) and growing season precipitation deficits (for agricultural resilience analysis).

### 2.5.2 Spatial variability

Another request echoed frequently after the release of KNMI'06 is information about spatial gradients in the climate change signal. These gradients particularly apply to sea level rise (where North Sea changes are different from global mean values), gradients across the Netherlands related to coastal precipitation in summer (Attema and Lenderink 2014), different precipitation and temperature patterns for the Rhine basin (te Linde et al. 2010), and distinguished climate effects in urban areas. The methodology of deriving spatially explicit sea level information is given in section 3.2.

The construction of climate response fields as described in section 2.3 retains the basic spatial patterns of this climate response, at least, as far as they are reproduced by the RCM. As an illustration Figure 2.9 shows the mean JJA precipitation response in 2036 – 2065 (relative to 1981 – 2010) for the original RACMO2 simulations and selected for  $W_L$  and  $W_H$  according to the criteria listed in Table 2.2. The tendency to reduce summertime precipitation clearly shows a spatial structure, with a strong response in the south-western sector of the domain shown, related to the systematic influence of the Azores high pressure area. The selection procedure mutes the drying trends in  $W_L$  and intensifies them in  $W_H$ , but in each sample a pronounced difference in the spatial gradient between e.g. the Netherlands and the upstream Rhine catchment area exists, with a lower response in the Rhine basin. The method thus allows to generate spatially varying climate change information

However, not all relevant spatial structures are well captured by the model and the selection procedure. For instance, a clear gradient of extreme precipitation in the coastal area is not evident from the ensemble simulations. Also small scale features such as anomalous climate conditions in urban areas are not explicitly resolved. Therefore the ability to make firm statements on spatially varying climate change signals is limited. This will be further elaborated in the relevant sections in Chapter 3.

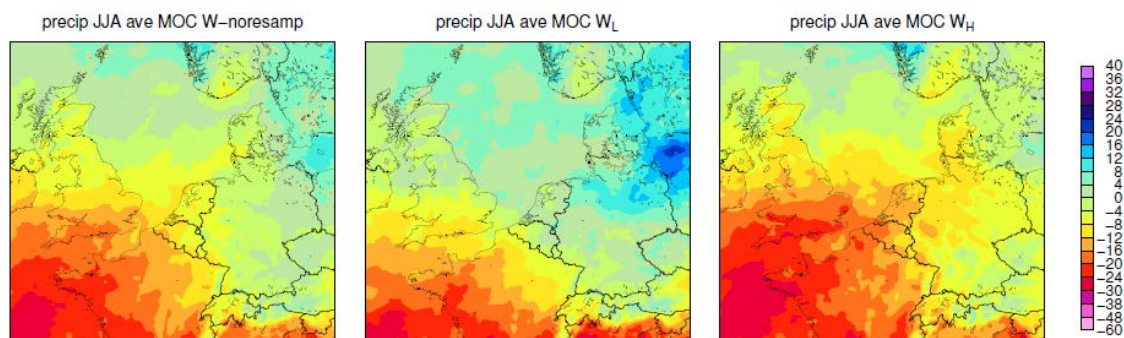


Figure 2.9: Seasonal mean precipitation response in summer in 2050 (relative to 1995) averaged from the 8 RACMO2 simulations (left), and resulting from the conditional selection of time slices according to the  $W_L$  and  $W_H$  scenarios (middle and right panel, respectively).

## 2.6 Models used

A large amount of information on the climate response to the anthropogenic forcing is derived from the results of the 5<sup>th</sup> Coupled Model Intercomparison Project CMIP5 (Taylor et al. 2011). This coordinated global climate modelling effort has provided significant input to the IPCC 5<sup>th</sup> Assessment report (AR5) and its climate atlas ([http://climexp.knmi.nl/plot\\_atlas\\_form.py](http://climexp.knmi.nl/plot_atlas_form.py)), and maps the climate response to 4 different Representative Concentration Pathways (RCPs). In these RCPs, transient changes in the concentration of atmospheric greenhouse gases, aerosol and land cover are prescribed (Van Vuuren et al. 2011). Most of the CMIP5 model data were accessed from the CMIP5 data portal ([cmip-pcmdi.llnl.gov/cmip5/data\\_portal.html](http://cmip-pcmdi.llnl.gov/cmip5/data_portal.html)) and uploaded in the Climate Explorer of KNMI ([climexp.knmi.nl](http://climexp.knmi.nl)). For some modelling systems data were directly obtained from the modelling team. Within the climate explorer, all GCM data were interpolated to the same  $2.5 \times 2.5^\circ$  grid, their file structure and storage conventions were homogenized, and synchronized to the same monthly time

axis covering the 1950-2099 period. Table 2.3 lists the number of GCMs and projections used for many parts of the scenario analysis. A detailed list of participating GCMs is given in Annex 6.1.

Also the EC-Earth model (Hazeleger et al. 2012) participated to the CMIP5 project, making available 8 projections for each of the RCPs 4.5 and 8.5. In addition, KNMI and other EC-Earth members executed another set of 8 projections for the RCP8.5 scenario, using the same model version and enlarging the ensemble size for this configuration.

The 8 EC-Earth members running the RCP8.5 scenario that have been submitted to CMIP5 have been further downscaled using the regional climate model RACMO2 (Van Meijgaard et al. 2008). This model has been set-up at a grid spacing of roughly 10km. Generally daily outputs have been retrieved from these experiments, and used for analysing regional climate responses, and stratified along the lines as explained in section 2.3.

Since this procedure aims at reconstructing a reasonable part of the CMIP5 climate response, the climate response of the EC-Earth/RACMO2 combination *relative* to this CMIP5 range of responses is of great interest. The global mean equilibrium climate sensitivity of EC-Earth represents the CMIP5 mean value fairly well, and also the transient climate sensitivity of EC-Earth is representative for the CMIP5 ensemble. However, this “moderate” climate sensitivity, in combination with its relatively cool and wet reference climate, does not enable EC-Earth to reproduce the entire range of seasonal mean European temperature and precipitation change projected by the CMIP5 ensemble. Particularly the extremely hot and dry summer conditions in central and southern Europe found in some CMIP5 models are not simulated in any of the EC-Earth/RACMO2 members. To explore this deficiency further a set of additional EC-Earth experiments and CMIP5 model analyses have been performed, and discussed in the next section. Also discussed is an analysis of the ability of the used models to reproduce the observed trends in extreme temperature and precipitation features in Europe.

### 2.6.1 Evaluation of modelled trends in (extreme) precipitation and temperature

An analysis of the ability of regional climate models to reproduce observed 20<sup>th</sup> century trends in Western-European precipitation is carried out by Van Haren et al. (2013). The seasonal mean precipitation showed pronounced trends in large European areas. Precipitation in winter increased in major parts of Northwestern Europe, while a reduction was seen in Southern Europe, particularly in the second half of the 20<sup>th</sup> century. During summer an increase was observed along the Western European coastal zone (Figure 2.10 top panels).

Many regional climate models (RCMs) underestimate these observed trends, when driven by global climate model projections forced by observed greenhouse gas emission and aerosol scenarios (Figure 2.10 middle row). This underestimation is inherited from the driving GCMs. RCMs driven by observed atmospheric circulation and sea surface temperature (SST) are much better capable of reproducing the observed trends (bottom row).

A statistical decomposition of two major factors affecting the observed trends (that is, atmospheric circulation and trends in SST) shows that the atmospheric circulation changes dominate the contribution to the trends in winter precipitation. A higher frequency of strong westerlies increased winter precipitation at high latitudes, accompanied by a reduction in Southern Europe. This is not directly related to the North Atlantic Oscillation (NAO), but can be diagnosed by a continental surface pressure gradient between the Mediterranean and Scandinavia. (Summertime) changes in precipitation along the European West coast is predominantly related to trends in SST. The origin of the trends in these large scale drivers is still uncertain, and so is the expected future continuation of these trends.

A similar result is found for trends in extreme hot days by Min et al. (2013). The RCMs, when forced by GCM boundary conditions tend to underestimate the observed trends in hottest day of the year.

The combination of global and regional climate models enables the downscaling of the large scale features simulated by the GCMs. However, the RCMs cannot resolve systematic discrepancies in trends of the large scale phenomena simulated by the GCMs. For this reason, the construction of the KNMI'14 scenarios is not based on a direct utilization of the available GCM/RCM model output. The applied procedure takes uncertainty in future atmospheric circulation responses (an evident source of the mismatch shown in Figure 2.10) explicitly into account. However, a systematic bias in the trends in all GCMs involved in the scenario construction is possible, which would affect the overall range in responses projected in these scenarios. A formal estimate of the likelihood and sign of such a systematic bias is yet impossible to make.

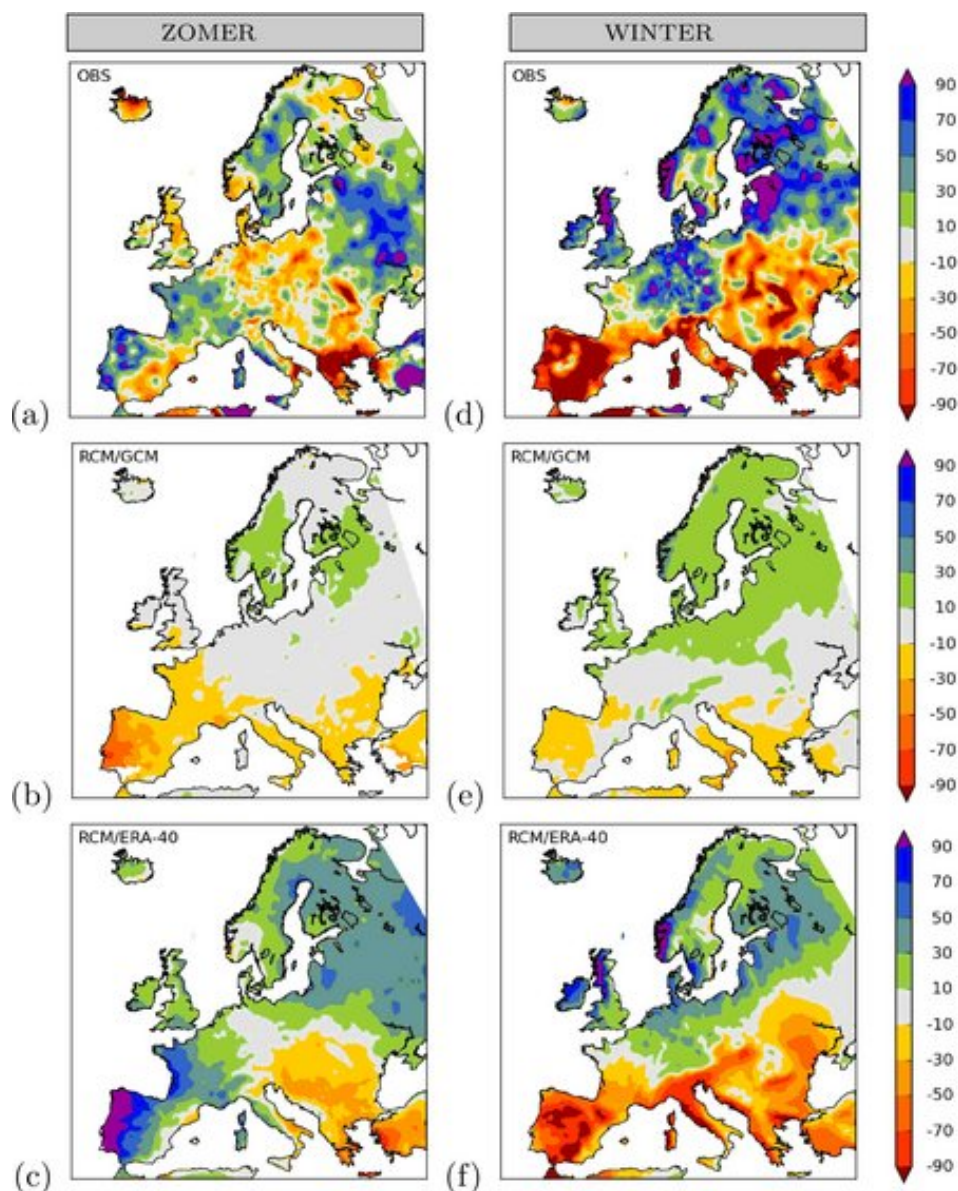


Figure 2.10: Observed (1961-2000) and modelled precipitation trends in Europe (in %/century) for (left) summer and (right) winter. Top panels show observed trend, second row display mean results from an ensemble of RCMs driven by a collection of global climate models, and bottom row represents RCM results driven by observed large scale circulation and SST.

## 2.7 KNMI'14 scenarios and RCPs

### 2.7.1 Assessment of the RCPs

The Representative Concentration Pathways (RCPs) that have been used for the CMIP5 climate simulations provide plausible descriptions of how the future may evolve with respect to a range of variables including socio-economic change, technological change, energy and land use. Together these descriptions provide the basis for the forcings used in the CMIP5 climate simulations. Through integrated assessment modelling (e.g. Van Vuuren et al. 2011) the RCPs provide the time evolution (pathway) of the emissions and concentrations of greenhouse gases and air pollutants, as well as of land use from 2000 up to the year 2100 and beyond.

Each of the RCPs is identified by a total radiative forcing in the year 2100. For example, RCP4.5 implies a radiative forcing of  $4.5 \text{ Wm}^{-2}$  in 2100 compared to 1750. Together the RCPs span the range of 2.6 to  $8.5 \text{ Wm}^{-2}$ , where the lowest RCP2.6 is an ambitious mitigation scenario, RCP4.5 and RCP6.0 provide stabilization scenarios in terms of greenhouse gas concentrations, and RCP8.5 is a scenario with continued growth in greenhouse gas emissions and concentrations up to 2100.

### CO<sub>2</sub> and other long-lived gases

The RCPs have the same starting point in the year 2000 with an observed global-mean CO<sub>2</sub> concentration of 369 ppm (part per million) and an “effective” CO<sub>2,eq</sub> concentration of 416 ppm. CO<sub>2,eq</sub> is a measure to include in one quantity CO<sub>2</sub> and other long-lived greenhouse gases, with for each gas the contribution weighted with its global warming potential (IPCC 2013b). The projected greenhouse gas concentrations start to deviate from each other especially in the second half of the 21<sup>st</sup> century (Van Vuuren et al. 2011). For CO<sub>2</sub>, the RCPs follow almost the same path over the period 2000-2012 for which we have observations to compare the RCP projections with. The CO<sub>2</sub> growth rate in recent years was nearly 2 ppm (0.5%) per year. Since 2000 the globally averaged CO<sub>2</sub> concentration in the RCPs was projected to increase with 24 to 25 ppm. The actual observed increase of 24 ppm in the background CO<sub>2</sub> concentrations closely followed the projection.

The RCP projected increase in the globally averaged concentration of methane (CH<sub>4</sub>) was between 23 and 48 ppb (ppb = parts per billion). The actual observed increase was 36 ppb, i.e. in the middle of the range provided by the projections for this short time period. The CH<sub>4</sub> growth rate was nearly 3 ppb (0.17%) per year. The range in the RCPs for the CH<sub>4</sub> concentrations up to 2100 is large and reflect the large uncertainty in the evolution of future CH<sub>4</sub> emissions. At present contributions to anthropogenic CH<sub>4</sub> emissions are divided over fossil energy use, agricultural activities, waste management and some minor sources. The natural sources of methane do not show important trends over the last decades (Kirschke et al. 2013).

N<sub>2</sub>O concentrations increased since 2000, as projected, with about 0.8 ppb per year. N<sub>2</sub>O concentrations, which are mainly related to agricultural activities, are projected to further increase gradually in all four RCP scenarios. During the 21<sup>st</sup> century the contribution to climate forcing of the non-CO<sub>2</sub> gases is projected to decrease relative to CO<sub>2</sub>. Following the regulations in the Montreal Protocol the contribution of the ozone-depleting F-gases has already started to gradually decline and will become marginal by the end of the century.

### Short-lived climate forcers (SLCFs)

Among the greenhouse gases tropospheric ozone ranks third in its contribution to climate forcing, after CO<sub>2</sub> and CH<sub>4</sub>, but before N<sub>2</sub>O and the F-gases, and together with aerosols, contributes significantly to the total radiative forcing. Both ozone and aerosols are short lived in the atmosphere. Aerosols exert both positive (e.g. black carbon) and negative (e.g. sulphate) radiative forcings. The projected trends in tropospheric ozone and aerosol vary per region and critically depend on the assumed implementation of regional air quality policies. Both ozone and many aerosol components are not directly emitted but chemically formed in the atmosphere. Aerosols are largely controlled by emissions of precursors including a.o. sulphurdioxide (SO<sub>2</sub>), nitrogen oxides (NO<sub>x</sub> = NO + NO<sub>2</sub>), ammonia (NH<sub>3</sub>) and volatile organic compounds (VOCs). Ozone formation is favoured by emissions of NO<sub>x</sub> and VOCs. Satellite observations of NO<sub>2</sub> show large positive trends over many regions of the world, especially over China and the globally averaged increase of 7% in NO<sub>2</sub> has increased tropospheric ozone and aerosol nitrate production over the last decade. Satellite observations of the total amount of aerosols over the oceans over the 10-year period 2000-2009 show in their global-mean hardly any trend (Zhang and Reid 2010). For this time period an increase in the amount of aerosols is observed over (a.o.) China and India and a decrease over Europe and the United States.

The RCPs assume rapid implementation of stringent air quality policies. This might indeed be unavoidable for health reasons in many regions that currently suffer from high levels of air pollution (see Annex 6.3). Required clean technologies to significantly reduce pollution levels are available and future implementations largely depend on political choices and other societal factors. All RCPs project a decrease in global ozone and aerosol precursor emissions after the year 2000. This global decrease is however not supported by the observations over the period 2000 to 2012. For the KNMI'14 scenarios scientific uncertainties in the radiative forcing by SLCFs are less important, mostly because of the dominant and increasing role of CO<sub>2</sub> emissions in the plausible range of radiative forcings up to 2100.

## 2.7.2 Consistency of KNMI'14 global temperature projections with CMIP5

Figure 2.4 is based on a total of 245 CMIP5 model simulations from 36 GCM systems (Table 2.3). These were used for a probabilistic assessment of the KNMI'14 scenarios. The consistence of each of the KNMI'14 scenarios with the RCPs is defined by adopting the ensemble of projections per RCP as a probabilistic estimate, without weighting any projection: all members from all GCMs are assumed to be equally probable. Using this assumption a frequency distribution of modelled  $\Delta T_{glob}$  in any future episode is then interpreted as a probability distribution for this quantity. Such a distribution of can be constructed. Here we constructed probability distributions for the 30 year mean  $\Delta T_{glob}$  centred around 2030, 2050 and 2085. The position of the

$\Delta T_{glob}$ -values from the KNMI'14 scenarios in this probability distribution is used to qualify the likelihood of this temperature to be higher, similar or lower than the estimate derived from the CMIP5 ensemble. Likelihood classes are similar to the definitions used by the IPCC assessment reports: values in the extreme 1% of the distribution are qualified as “certainly below or above” the RCP-value, while values in the extreme 10% of the range are labelled “very likely below or above”. Values in the extreme 33% are “likely below or above”, while values within the 33-66% of the range are identified as “likely within range”.

Table 2.3: Number of GCMs and ensemble projection members per RCP

Scenario	Nr of GCMs	Total nr of projections
RCP2.6	24	50
RCP4.5	36	83
RCP6.0	16	33
RCP8.5	34	79
<b>Total</b>		<b>245</b>

Figure 2.11 shows the result for the annual mean globally averaged temperature increase relative to the 1981-2010 mean. For the near term scenario (2030) the assumed value of  $\Delta T_{glob}$  (0.92K) generally falls within the 10-90% of the projected range for every RCP, but the different RCPs do not diverge strongly in this time horizon (see also Figure 2.4). However, for 2050 and more so for 2085 it can be seen that the KNMI'14  $G_L$  and  $G_H$  scenarios are clearly not compatible with RCP8.5 (too cold), while  $W_L$  and  $W_H$  can not be considered representative for any of the RCP2.6, RCP4.5 or RCP6.0 scenarios. The scarcity of categories “probably within range” also indicates that the KNMI'14 scenarios tend to be situated at the edge of the overall CMIP5 range, and should generally thus be considered as fairly unlikely given any of the RCP scenarios, at least, according to the definition of likelihood that can be deduced from this simple comparison.

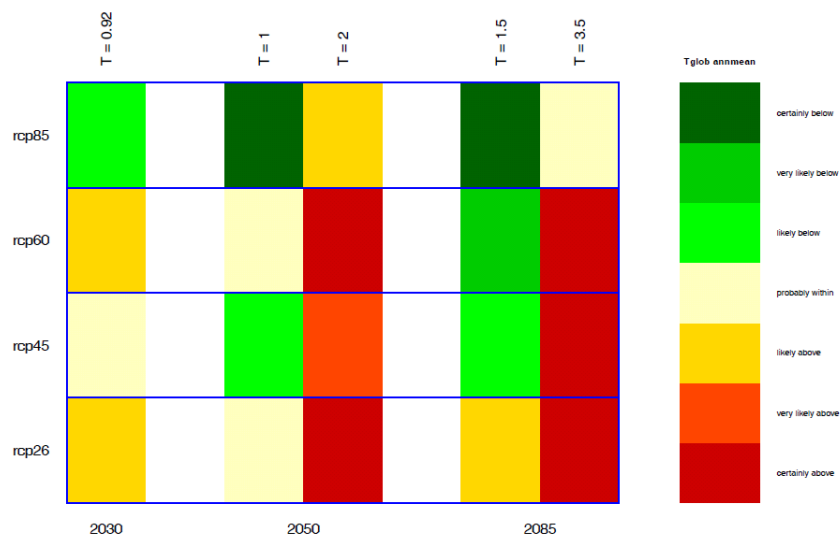


Figure 2.11: Probability of the value of  $\Delta T_{glob}$  assumed in any of the KNMI'14 scenarios to be consistent with the projected temperature range per RCP. The colour coding refers to the position of the KNMI'14 value relative to the distribution of the CMIP5 range: green colours denote KNMI'14 temperature to be positioned in the lower part of the CMIP5 range, while orange and red colours denote values in the high end of the range. Further explanation: see text.

A similar exercise is carried out using the seasonal mean temperature and precipitation response for the Netherlands. From the CMIP5 ensemble these seasonal mean values were extracted from a single gridpoint centred around (6.25°E, 51.25°N), and from these values a similar probability distribution is compiled per RCP as discussed above.

For the winter season the temperature distribution follows the match observed in the  $\Delta T_{glob}$  comparison roughly similar (Figure 2.12), but for summer the KNMI'14 scenarios tend to display generally lower seasonal mean temperatures than the majority of the CMIP5 projections. This will be discussed in more detail in Section 3.1. The generally pale colors shown for precipitation (lower panels in the Figure) reflect the large spread in the CMIP5 ensemble compared to the values generated in the KNMI'14 scenarios.

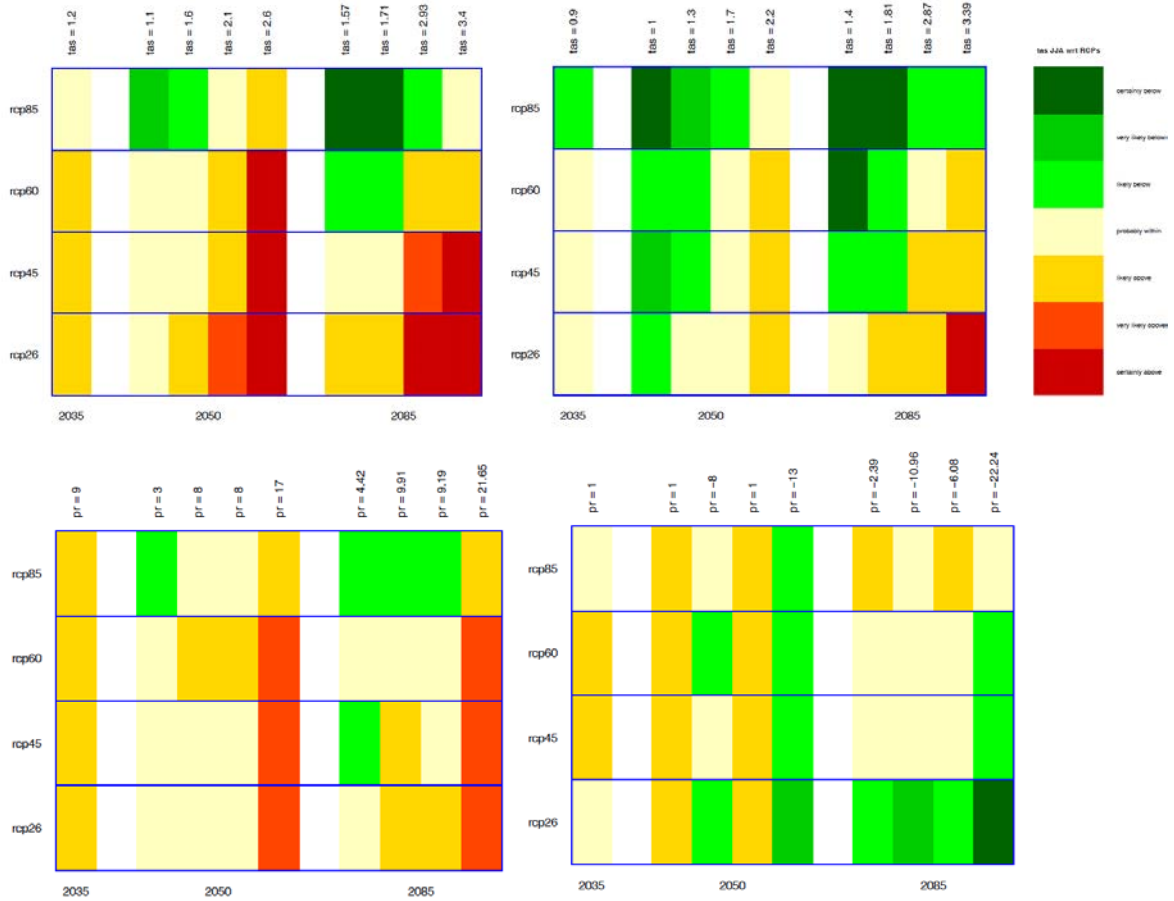


Figure 2.12: As Figure 2.11, for the seasonal temperature (top row) and precipitation (bottom row) response in DJF (left) and JJA (right). For 2050 and 2085 four scenarios are shown:  $G_L$ ,  $G_H$ ,  $W_L$  and  $W_H$  respectively.

### 3. Observed trends and scenarios per variable

In this section we describe the derivation of the observed trend values of temperature, precipitation, fog, global radiation and evaporation. First the choice of the trend lines, linear versus non-linear, is discussed. Thereafter we present the trend lines and values for each of the variables.

#### Linear versus non-linear trends

The non-linearity of the trend lines has been assessed by comparing for each variable a non-linear LOESS model (Cleveland and Devlin 1988) with a linear model based on ordinary least squares regression. In each case the dependent variable was the annual value of the variable of interest and the independent variable the time (year).

LOESS performs locally weighted polynomial regression. At each point in the data set a low-degree polynomial is fitted to a subset of the data, with explanatory variable values near the point whose response is being estimated. The polynomial is fitted using weighted least squares, giving more weight to points near the point whose response is being estimated and less weight to points further away. The value of the regression function for the point is then obtained by evaluating the local polynomial using the explanatory variable values for that data point. The LOESS fit is complete after regression function values have been computed for each of the data points.

The F-test has been used to compare the models and test the significance of the non-linear model. It appeared that only for temperature a non-linear model is significantly better than the linear model.

### 3.1 Temperature and precipitation

#### 3.1.1 Observed temperature and precipitation trends

The globally averaged surface air temperature data show a warming of about 0.9 °C over the period 1880–2012. A reduced temperature trend is observed over the past 15 years, primarily due to natural variations of the ocean circulation. However, sea level, energy storage in the oceans, glaciers and snow cover have continued to indicate warming in this period (IPCC 2013b).

The Netherlands has also become warmer. Figure 3.1 shows the non-linear trend line for the **annual mean temperatures** of De Bilt. The underlying daily values have recently been standardized (Brandsma et al. 2013). The homogenized version of the De Bilt temperatures have not been used because these apply only to monthly values, while KNMI'14 uses also indices of daily values. The differences in annual mean trends for both series are, however, negligible. The LOESS curve in the figure uses a span of 0.5, a polynomial of degree 1 (locally-linear fitting), and assumes a gaussian distribution of the errors. The span of 0.5 means that for each year the fit uses 50% of the nearest neighbors. We found that a span of 0.5 complies well with a running 30–years average.

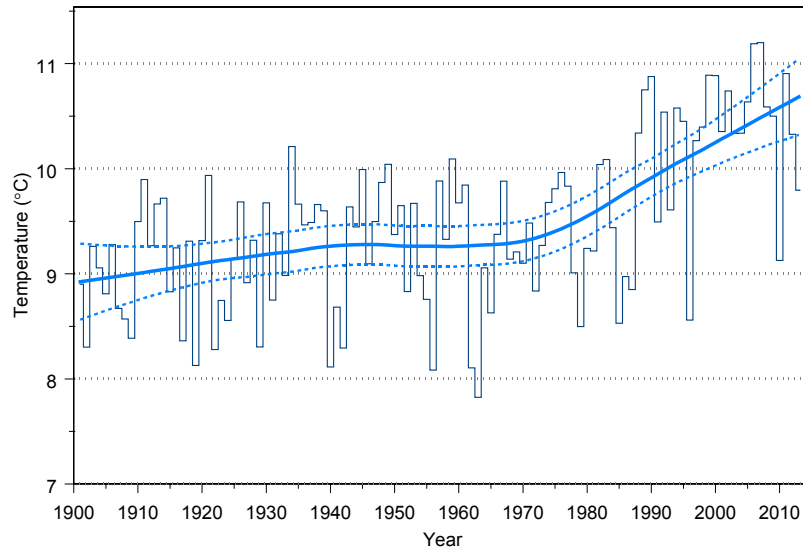


Figure 3.1: Annual mean temperature De Bilt 1901-2013. The bold smooth line represents a LOESS smoother, the dashed lines give the 2x pointwise standard error band of the smooth.

The figure clearly shows the non-linearity of the trend with most of the increase in the second half of the 20th century. The values on the trend line in 1901, 1951 and 2013 are 8.9, 9.3 and 10.7°C, respectively. This implies that the total temperature increase between 1901 and 2013 equals 1.8°C and that 1.4°C of this increase is in the 1951-2013 period.

The increase since 1951 is about twice the global increase averaged over all land and oceans. The warming was similar for our neighbouring countries. Land masses generally warm faster than the oceans. In winter (December, January, February) more frequent westerly winds have led to milder temperatures. In summer (June, July, August), an increase in solar radiation (see section 3.4) has contributed to the additional warming. This increase in solar radiation is due mainly to a reduction in air pollution.

Averaged over the mid-latitude land areas of the Northern Hemisphere, precipitation has increased since 1901. There is medium confidence of a human-induced contribution to these precipitation changes since 1950. The amount of water vapour in the atmosphere has increased globally since the 1970s. This is consistent with the observed warming, because warm air can contain more moisture (IPCC 2013b).

The **annual mean precipitation** is calculated from 102 stations in the Netherlands that have long-term time series (starting in 1910). These series have recently been homogenized (Buishand et al. 2013). For each series we calculated monthly sums. The monthly sums are then averaged over the 102 stations and then used to calculate the annual mean sums for the Netherlands.

Figure 3.2 shows the linear trend line for the annual mean precipitation in the Netherlands. The values on the trend line in 1910, 1951 and 2013 are 689.5, 760.6 and 868.1 mm, respectively. The total increase between 1910 and 2013 equals 178.6 mm (25.9%).

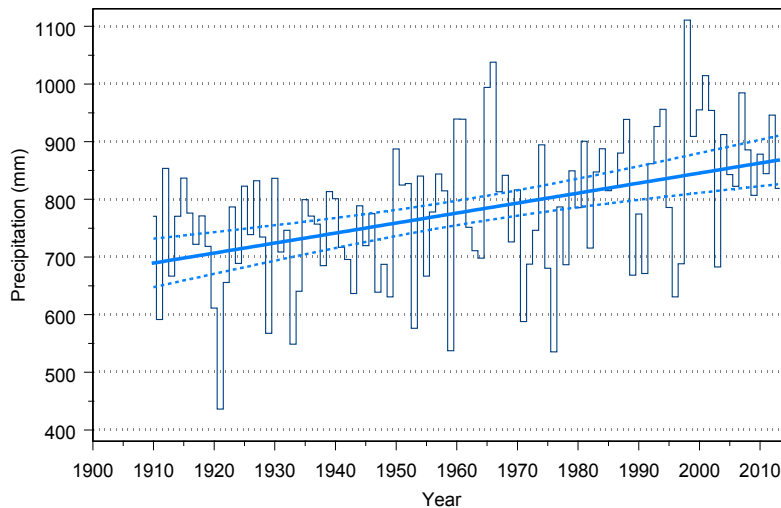


Figure 3.2: Annual precipitation in the Netherlands 1910-2013 (mean of 102 stations). The straight line represent a linear regression fit. The dashed lines give the 95% confidence bands.

All seasons except summer have become wetter. The number of days per year with at least 10 mm precipitation in winter and the number of days with at least 20 mm precipitation in summer increased (Figure 3.3). On average, these thresholds of moderate extremes are exceeded several times a year at any given location in the Netherlands. The largest increase of these moderate extremes is observed in the coastal regions. The total number of days with precipitation above 0.1 mm, known as ‘wet days’, does not exhibit a trend. Because of the temperature increase also the amount of water vapour in the atmosphere has increased significantly since 1950. This trend partly explains the observed increase in mean precipitation amount. The effect on precipitation extremes is even greater. Observations show that the hourly intensity of the most extreme showers increases by about 12% per degree of warming.

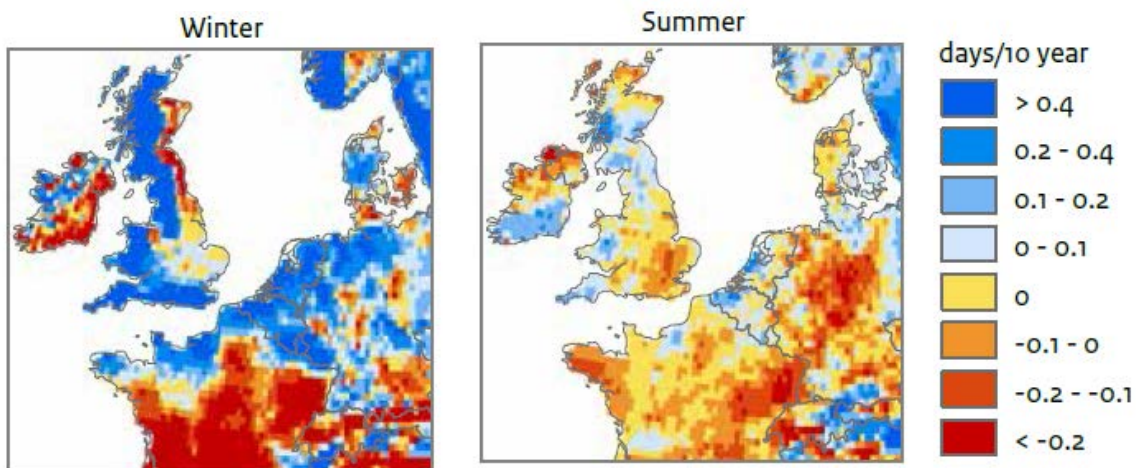


Figure 3.3: Observed trends in the number of winter days per year with at least 10 mm precipitation (left) and summer days per year with at least 20 mm precipitation (right) between 1951 and 2013. Source: [www.ecad.eu](http://www.ecad.eu).

### 3.1.2 The resampling methodology and its results

A method based on selection and resampling of model data has been used to represent most of the spread contained in the CMIP5 ensemble. This method will be described below. From the resampled model data obtained changes in a large number of variables and statistics can be derived, including temperature and precipitation. These statistics will form the basis of the scenarios (except for sea level rise).

The representation of the signal and spread contained in CMIP5 model integrations is the main purpose of the procedure. However due to the coarse resolution of the global climate model simulations, and the

limited data availability, it is obvious that not all aspects of CMIP5 can be reproduced or are useful to consider. In KNMI'06 we evaluated the scenarios against the mean seasonal changes of temperature and precipitation. Here, we evaluate against seasonal mean temperature and precipitation, and in addition to changes in moderate extremes of month mean precipitation and temperature. By considering these change in “cold, warm, dry, and wet” we evaluate the scenarios on more user relevant quantities, which is reflected for instance in changes in inter-annual variability. This cross evaluation is performed for the changes at a point in the south east of the Netherlands (6.25 °E, 51.25 °N), and all CMIP5 integrations are interpolated to this location. This location is chosen in the Netherlands, but as far as possible from the North Sea in order to avoid capturing the changes over sea instead of over land.

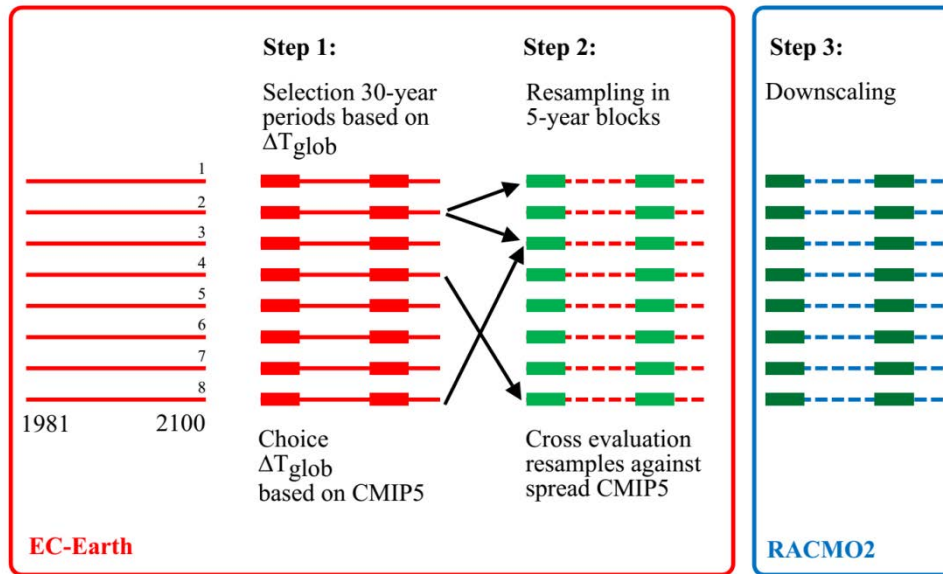


Figure 3.4: Overview of the method to construct the scenario's (see text for details).

A schematic over of the method is given in Figure 3.4. We only give a brief overview of the method here. The basis material of the scenarios are formed by an ensemble of 8 integrations with EC-Earth, and embedded 8 simulations with the regional climate model RACMO. These runs start in 1950 and end in 2100, but we here will only consider the data after 1981. Thirty years after initialization the 8 different members have diverged considerably, also in the slowly varying parts of the climate systems like the oceans. In the first step of the scenario construction, we select 30-year time periods based on the global mean temperature rise. The reference time period is 1981-2010. For the scenarios for 2050, the selected values for the global temperature rise are 1 and 2 °C, and the corresponding future time periods are 2031-2060 and 2046-2075. In this step it is effectively assumed that the climate change response for the Netherlands is a function of the global temperature rise, neglecting the influence of time or time lag. In the second step the actual resampling is done use the aforementioned selected periods. Resampling is done both for the control periods as well as for the future time periods.

The procedure of resampling is rather complex, and is done in several sub-steps. The essential part is that the final samples that are used for the scenarios contain the characteristics of the changes in CMIP5, giving a good representation of the signal as well as the spread. This will be evaluated in the next section, but first we described the steps below. The evaluation and the development of the selection procedure has been developed iteratively. What is described is the final outcome.

Resampling is done based on 5-year periods, constructing 30 years climate from 5 years samples of the EC-Earth ensemble (and in the downscaling step of 5 years from the RACMO2 ensemble). By taking long block periods of 5 years we guarantee that much of variations on longer time scales, such as the inter-annual variability, are retained. Thus, a 30-year climate is constructed from six 5 years periods, chosen from the 8 ensemble members. In resampling, the calendar is respected, so we do not mix results for one 5 years period with another one. In total, for each 30-year period, there are  $8^6$  (~2.6 10<sup>5</sup>) re-combinations or samples. From these samples we sub-select 8 samples based on the following procedure.

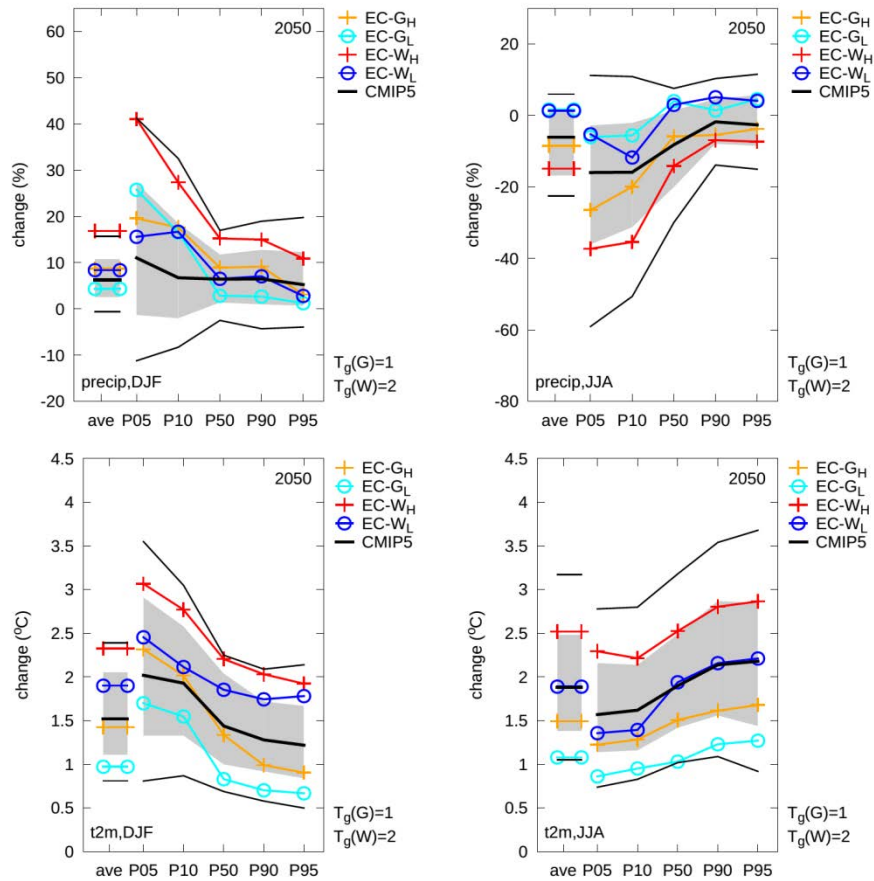


Figure 3.5: Precipitation (%) and temperature (°C) changes in 2050 (MOC) from the Ec-Earth based scenarios in comparison with CMIP5. The different scenarios are given by EC-X, with X the scenario label. The central 50% CMIP5 range is given by grey shaded area, whereas the 80% range is given by the two outer black lines.

The first criterion of resampling is the change in winter precipitation. One type of scenarios, the “L” family, has an assumed change in mean winter precipitation of 4% per degree rise in global mean temperature. The “H” scenarios assumes a dependency of 8% per degree. These dependencies are reasonably close to the dependency from the Clausius-Clapeyron relation, of 7% per degree, which governs the saturation specific humidity as a function of temperature. It turns out that many samples are very close to these prescribed dependencies, which is a reflection of the large natural variability in winter. The 1000 samples closest to the assumed dependencies are chosen, and within these samples we sub-select approximately 50 samples based on the seasonal mean changes in summer and winter temperature, and changes in summer precipitation. The selection is such that the “H” scenarios have a relatively large change in temperature both in summer as in winter, and a (relatively) strong decrease in summer precipitation. The “L” scenarios have relatively low temperature changes and a moderate change in summer precipitation. Finally, from these ~50 samples we sub-select 8 samples based on the objective of retaining as much different model data as possible. We do not allow a block of 5-year model data to re-occur more than 3 times. (We note that in the first setup of the selection procedure we omitted the last step, and this resulted in some 5 year periods reoccurring 4 times or more).

The final results of the procedure, by selection based on  $\Delta T_{\text{glob}}$  and subsequent resampling, are shown in Figure 3.5 and Figure 3.6 for winter and summer, and compared to the spread in CMIP5. Two outer lines are also shown, representing 80% of the CMIP5 range that is used as a target for our scenarios, and implying that more extreme model results are generated by 20% of the CMIP5 simulations. The intention to cover the 80% CMIP5 range is rather ambitious considering that we only develop 4 scenarios and we evaluate the spread for a range in statistics. Our minimum requirement is that at least the central 50% range (between the 25<sup>th</sup> and 75<sup>th</sup> percentiles) is represented. In additions to the seasonal mean changes, we also compare the 5,10, 90 and 95<sup>th</sup> percentiles of monthly mean changes (within a season). These represent warm, cold, wet and dry months.

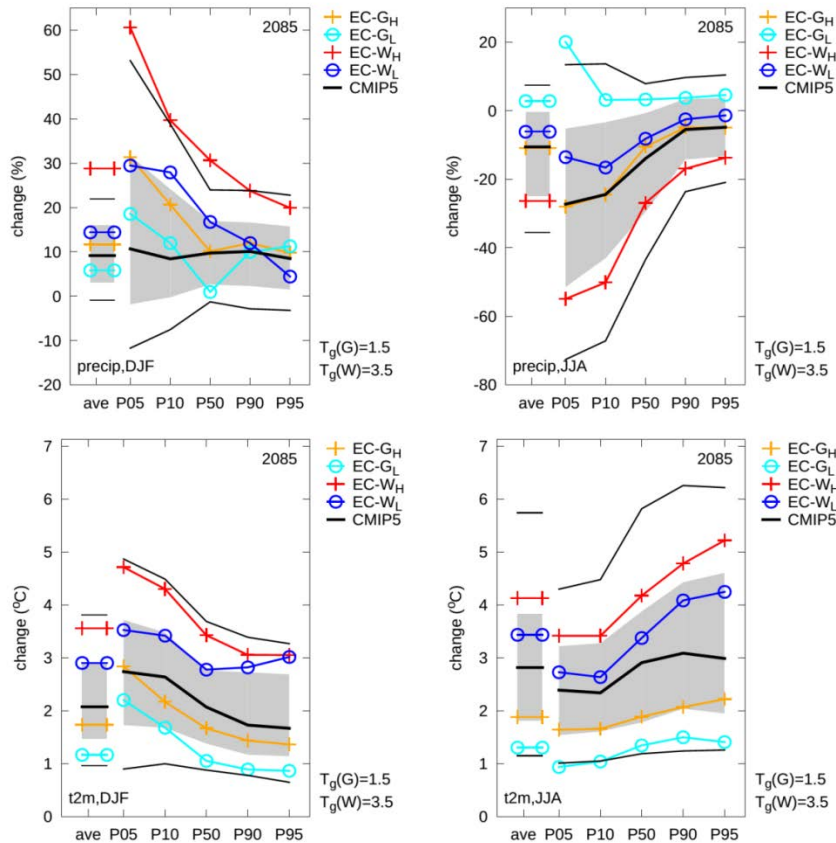


Figure 3.6: As Figure 3.5 for the scenarios for 2085.

The CMIP5 range in winter temperatures is well covered by the scenarios. For seasonal mean temperatures the 80% range in CMIP5 spans 0.8 °C to 2.4 °C, whereas the resampling covers between 1.0 °C and 2.4 °C. For the different percentiles of monthly mean temperatures the upper bound in CMIP5 is covered well with the  $W_H$  scenario (red line), but the cool outliers of CMIP5 are not captured similarly well, in particular for cold months, given by the 5<sup>th</sup> and 10<sup>th</sup> percentiles (P05 and P10).

For summer temperature, the lower bound of CMIP5 is covered by the  $G_L$  scenario. However, the warmer  $W_H$  scenarios only cover the upper bound of the central range. For instance, the seasonal mean temperature change in the  $W_H$  scenario is 2.5 °C, whereas the upper bound from CMIP5 is 3.2 °C.

For precipitation, results of the resampling typically cover a smaller fraction of the CMIP5 range. In particular, winter appears to be difficult to represent. While the range in mean winter precipitation change is reasonable captured – a scenario range between +4 and +17%, and a CMIP5 80% range between +0% and +16% – the distribution over dry and wet months is not covered that well. In the scenarios increases in dry month precipitation (P05 and P10) are too strong whereas changes in wet months (P90 and P95) are underestimated. This behavior is already present in the unsampled model data (ENS-EC) and the re-samples inherit much of this behavior. Inspection of the spatial fields of precipitation changes shows that there is a relatively small area with relatively high values (20 – 25%) of the change in P05 and P10 near the Netherlands, which also exists in ENS-EC.

Mean summer precipitation covers the central CMIP5 range with changes between almost zero and -15%. The characteristic CMIP5 broadening of the range for relatively dry months is also represented with the scenarios. Precipitation decreases by almost 40% in the driest months in the  $W_H$  scenario.

For the end of this century (2085) results are very similar for most characteristics (Figure 3.6). In summer, the scenarios cover a slightly higher fraction of the CMIP5 range than for 2050, both for temperature and precipitation changes. Results for winter temperature are very similar. Winter mean precipitation change in the  $W_H$  scenario of +28% is now above the CMIP5 upper bound. We note, however, that it is with the full envelope of the CMIP5 results, driven by all RCPs. Analysis of the CMIP5 model results driven by RCP8.5 show that approximately 10% of the models have a mean winter time precipitation increase of approximately 30% or more, while for RCP6.0 this is 5% of the models. Part of the high response is due to the strong increase during relatively dry months, which for winter is considered not very relevant when extreme precipitation is of

primary interest. The scenario increase during wet months (P90 and P95), which is particularly relevant for flooding during winter, is within the upper bound of CMIP5.

Finally, spatial pattern of the changes in the  $G_L$  and  $W_H$  scenarios and CMIP5 are shown in for summer precipitation. For CMIP5, model integrations were taken that were used to produce the CMIP5 atlas (IPCC 2013a). The 25<sup>th</sup> and 75<sup>th</sup> percentiles of the changes in seasonal mean temperature and precipitation are considered, thus reflecting the central 50% range in CMIP5, and matching the  $W_H$  and  $G_L$  scenario, respectively, for the Netherlands (Figure 3.7). The spatial patterns of changes are broadly similar, but the scenarios display a more pronounced spatial gradient. For the statistics shown here smoothing of the spatial structures is stronger in CMIP5 than in the resampled scenarios due to the smaller sampling size of the scenarios (8 members) versus the CMIP5 ensemble (~100 members).

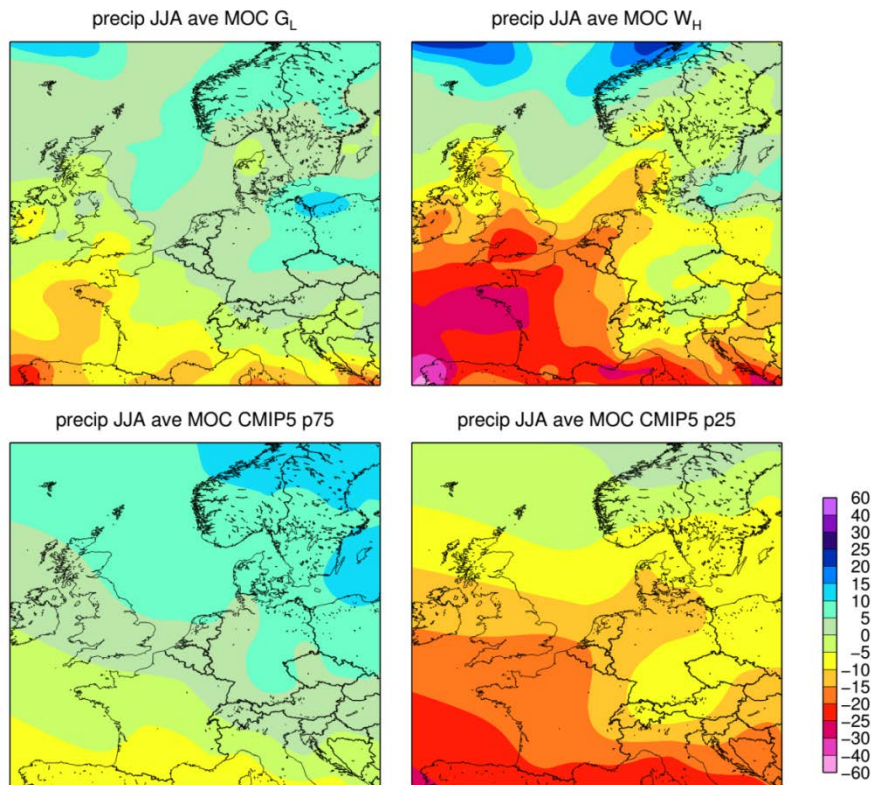


Figure 3.7: Comparison of precipitation change of two scenarios  $G_L$  (left) and  $W_H$  (right; upper panels) to the 75th (left) and 25th (right) percentile of the response in the CMIP5 ensemble (based on the RCP4.5, RCP6 and RCP8.5; lower panels).

### 3.1.3 Downscaling with the Regional Climate Model

So far, we discussed relatively coarse resolution results produced by EC-Earth, in comparison with CMIP5, and developed our resampling method based on that. Our motivation is that the spread in CMIP5 should be compared to results from a GCM, not a high resolution RCM that could display systematic differences with the GCM due to better resolving land-sea borders and the topography.

Downscaling with RACMO2 has been done in a straightforward manner. As said, we employ RACMO2 on a relatively small domain of  $212 \times 216$  longitude-latitude grid points at 11 km resolution centered on the Netherlands. The small domain of RACMO ensures that the large scale circulation statistics provided by EC-Earth are very well reproduced in RACMO2. Also, RACMO2 shares large part of the physics with EC-Earth as both are based on a cycle of the ECMWF physics package. The resampling of RACMO2 results has been done using the resamples chosen in the selection procedure with EC-Earth, using exactly the same 5-year blocks for each scenario.

This procedure leads to very similar response in the RACMO2 re-samples as obtained with EC-Earth. Considering the relatively small domain and the very similar physics this is not entirely unexpected. Figure 3.8 shows the results from RACMO2 for the southeastern part of the Netherlands (roughly south of  $51^\circ\text{N}$  and east of  $5.2^\circ\text{E}$ ), which can be compared to the GCM results shown in Figure 3.6. There are two aspects for which RACMO2 clearly modifies the response of EC-Earth. The RACMO2 results predict slightly higher values of future

summer time precipitation (or less drying) in the  $G_H$  and  $W_H$  scenarios. For instance, in the  $W_H$  scenario for 2085 the mean precipitation response is -21% in RACMO2 versus -26% in EC-Earth.

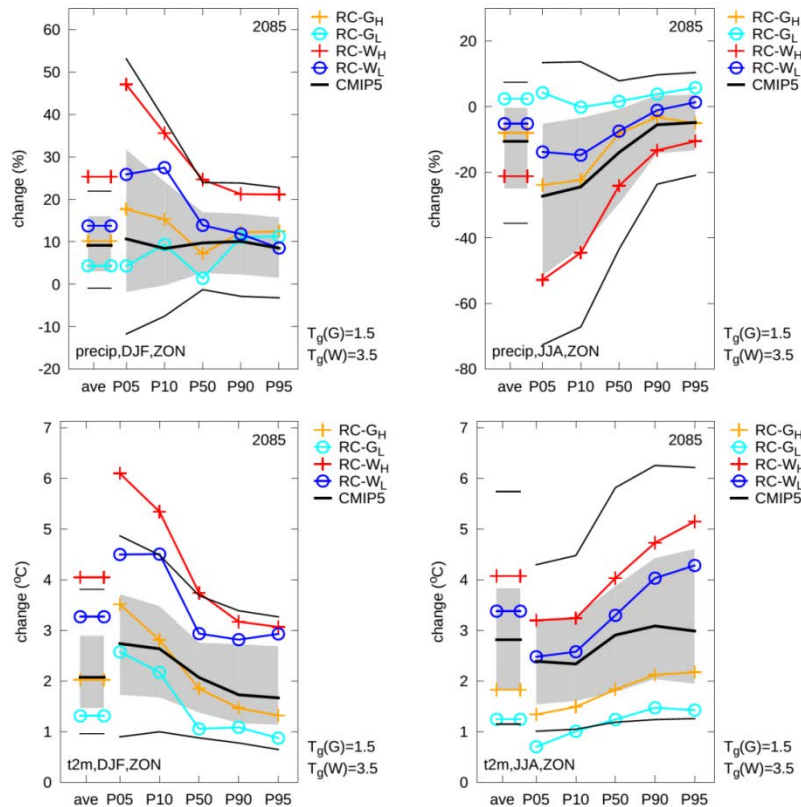


Figure 3.8: As Figure 3.6 for the RACMO2 simulations. Shown are the averages for an area (labeled ZON, see Figure 3.9) in the southeastern part of the Netherlands.

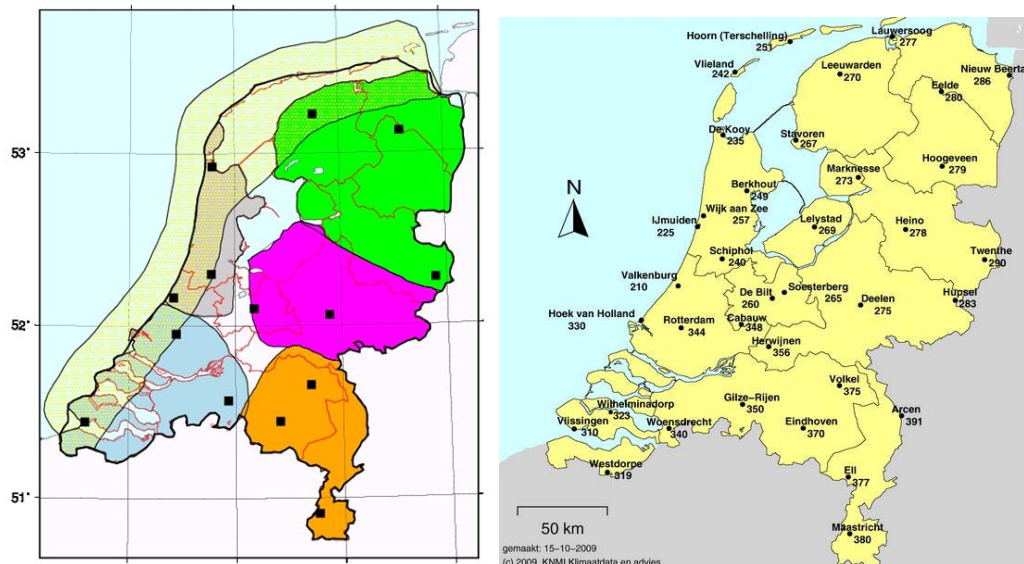


Figure 3.9: Left: Identification of regions for which different temperature change assessments were carried out. Color coding of regions: yellow/light green: NZK; green: NON; purple: MON; orange: ZON; light blue: ZWN and grey: NWN. The Netherlands as a whole: NLD. Right: Automatic meteorological stations in the Netherlands. Den Helder and De Kooy refer to the same station.

However, the most outspoken difference is the temperature response for cold months in winter, with changes in the 5<sup>th</sup> and 10<sup>th</sup> percentile that are approximately 1°C higher in the RACMO2 simulations in  $W_H$  and  $W_L$ . This is the result of resolving the land-sea contrast much better in RACMO2, possibly enhanced by a more

advanced boundary layer scheme in RACMO2 based on turbulent kinetic energy which resolves the temperature stratification of the lowest levels of the atmosphere better under cold conditions (Lenderink and Holtslag 2004; Baas et al. 2008; Van Meijgaard et al. 2012).

### 3.1.4 Seasonal and monthly temperature and precipitation response

From the resampled output of RACMO2 we derived average changes for the Netherlands, as well as averages over a number of sub-regions within the Netherlands (Figure 3.9). Seasonal mean changes are computed as well as the changes for the different months of the year. Monthly changes are filtered with a digital 1-2-1 filter to smooth out noise from month-to-month. This filtering affects the seasonal means computed from the monthly values, creating a small inconsistency with the seasonal means that are directly computed. Therefore, we re-adjusted the monthly value by adding or subtracting a constant for each month within a season, so that the mean over the season is the same as the mean before filtering. In general, this is a small correction.

Figure 3.10 presents mean temperature and precipitation increase for winter and summer according to the scenarios. Both the mean temperature and mean precipitation will increase in future in all four scenarios except for summer precipitation. Model calculations disagree about the sign of change in mean precipitation in summer, and this is reflected in the scenarios.

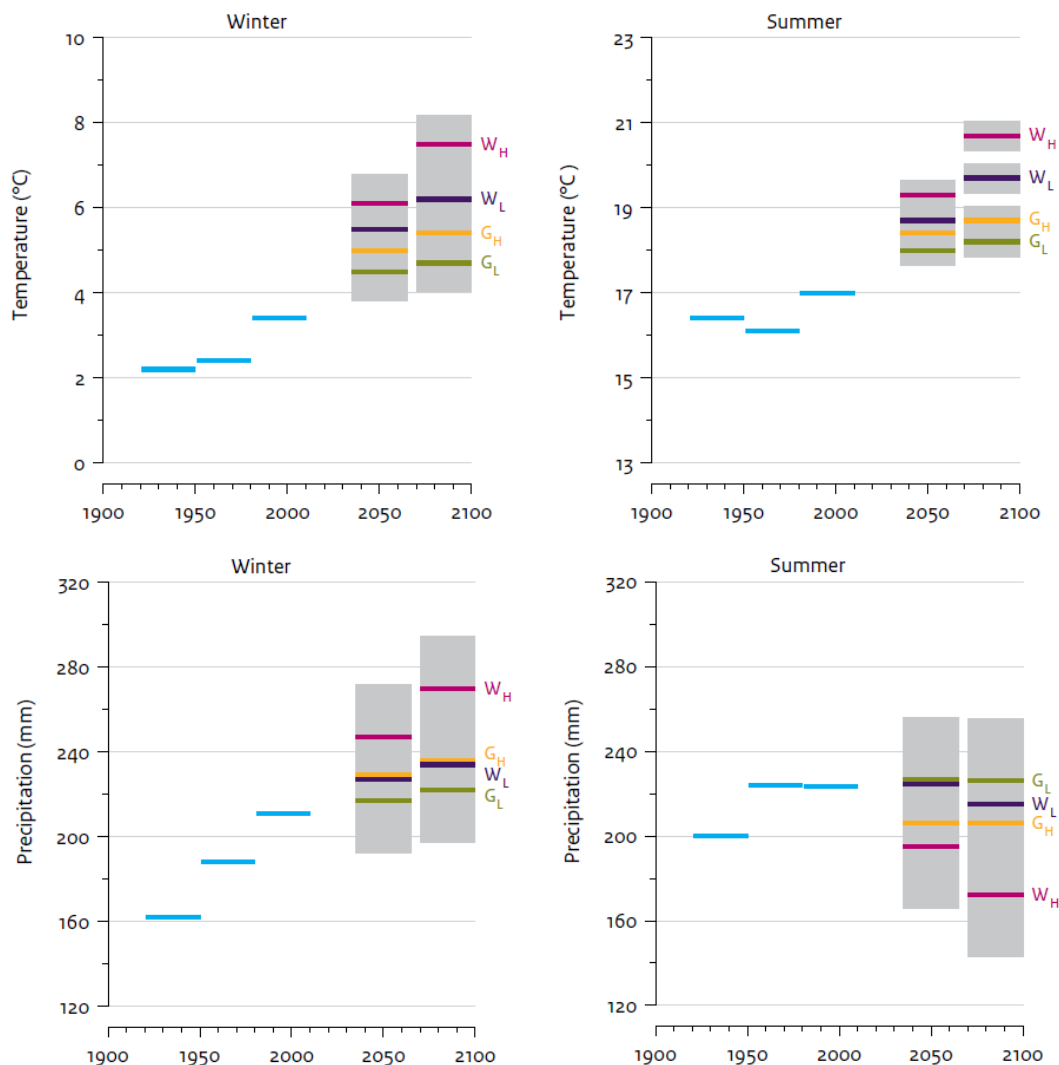


Figure 3.10: Winter and summer temperature (top) and precipitation (bottom) in De Bilt (Netherlands). Observations (three 30-year averages, in blue), KNMI'14 scenarios (2050 and 2085, in four colours) and natural variations for 30-year averages (in grey) are shown

Figure 3.11 to Figure 3.14 give the mean seasonal cycle of the changes in three percentiles of daily temperature, mean precipitation, wet-day frequency and relative humidity for the 4 scenarios and the two time periods. In general, the change in the 5<sup>th</sup> percentile of daily mean temperature are largest for the winter months, with changes up to 6 °C for the W<sub>H</sub> scenario in 2085. The changes are largest for the areas in the eastern part of the Netherlands, ZON, MON and NON, with changes approximately one degree than the western part of the Netherlands. Changes in these cold days are relative small in summer.

For the 95<sup>th</sup> percentiles, the warm days, the situation is different and the changes are largest in summer and for the south-eastern part of the Netherlands (ZON).

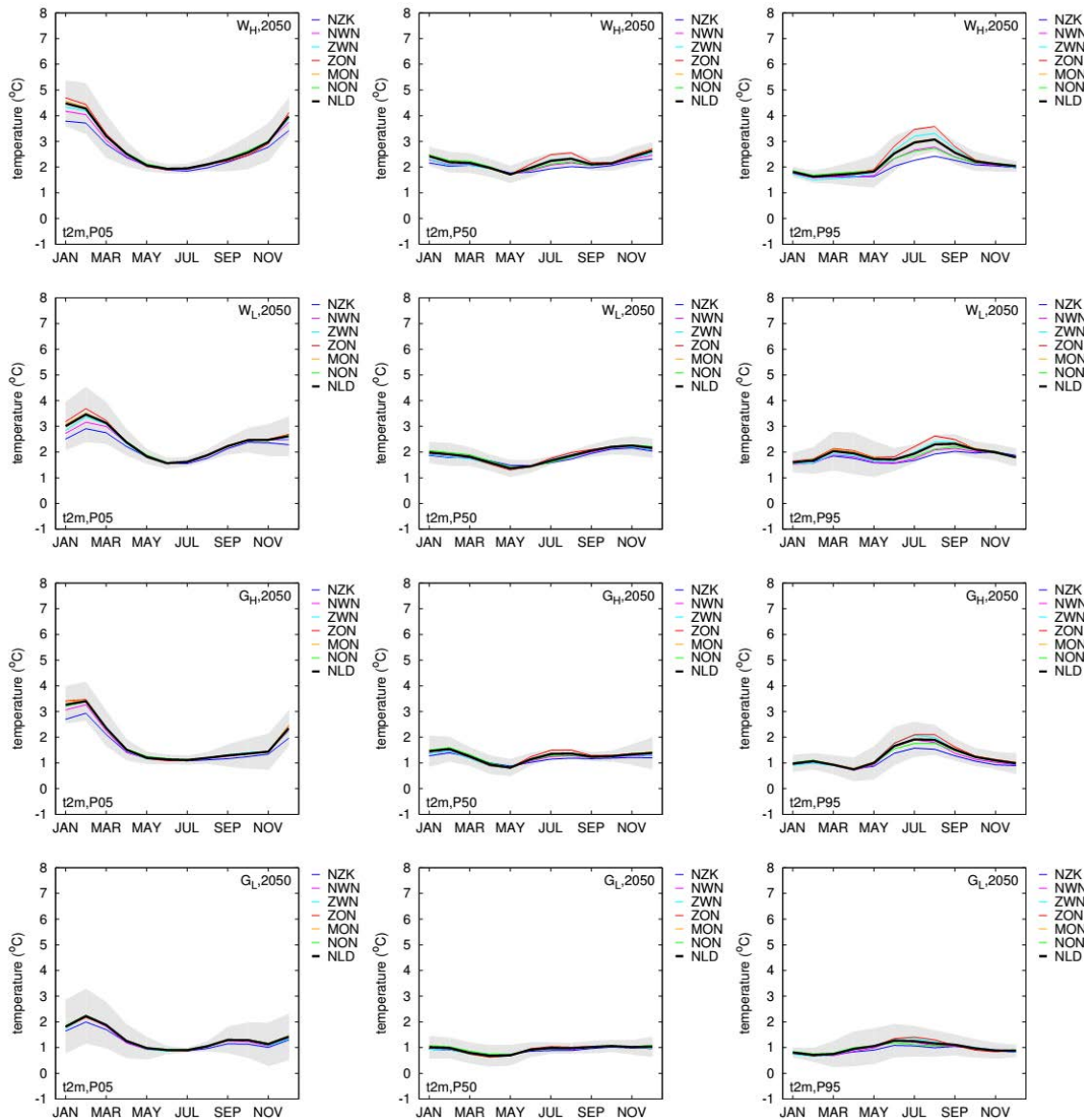


Figure 3.11: Yearly cycle of changes in 5<sup>th</sup> (left column), 50<sup>th</sup> (middle), and 95<sup>th</sup> (right) percentile of daily mean temperature for the four scenarios for 2050, from top to bottom, W<sub>H</sub>, W<sub>L</sub>, G<sub>H</sub> and G<sub>L</sub>. The grey band is the standard deviation between the 8 members of the RACMO2 simulations (before resampling).

### 3.1.5 Time series transformation

Similar to the KNMI'06 approach (Van den Hurk et al. 2006), additional information on climate indices such as extreme precipitation or temperature, evaporation and interannual variability is derived using statistical downscaling of the (resampled) regional climate model output described in section 2.3.1. This downscaling makes use of homogenised time series of 102 precipitation stations (240 stations for the once in ten year precipitation results) distributed over the Netherlands (Brandsma et al., 2014; section 2.4.1) and for all other

variables of local observations at De Bilt, on which a transformation is applied based on the modelled responses. This so-called time series transformation tool (Bakker and Bessembinder 2012) is made available to users via a website interface, and proved to be a valuable tool for generating localized time series of temperature and precipitation (Bessembinder et al. 2011a). A reference data set (generally based on observations) needs to be provided as input, and a transformation is applied that brings this data set into the context of one of the climate scenarios and desired time horizon. From this transformed time series, also climate indices such as changes of the coldest/warmest winter day, wet day frequency or extreme precipitation are derived.

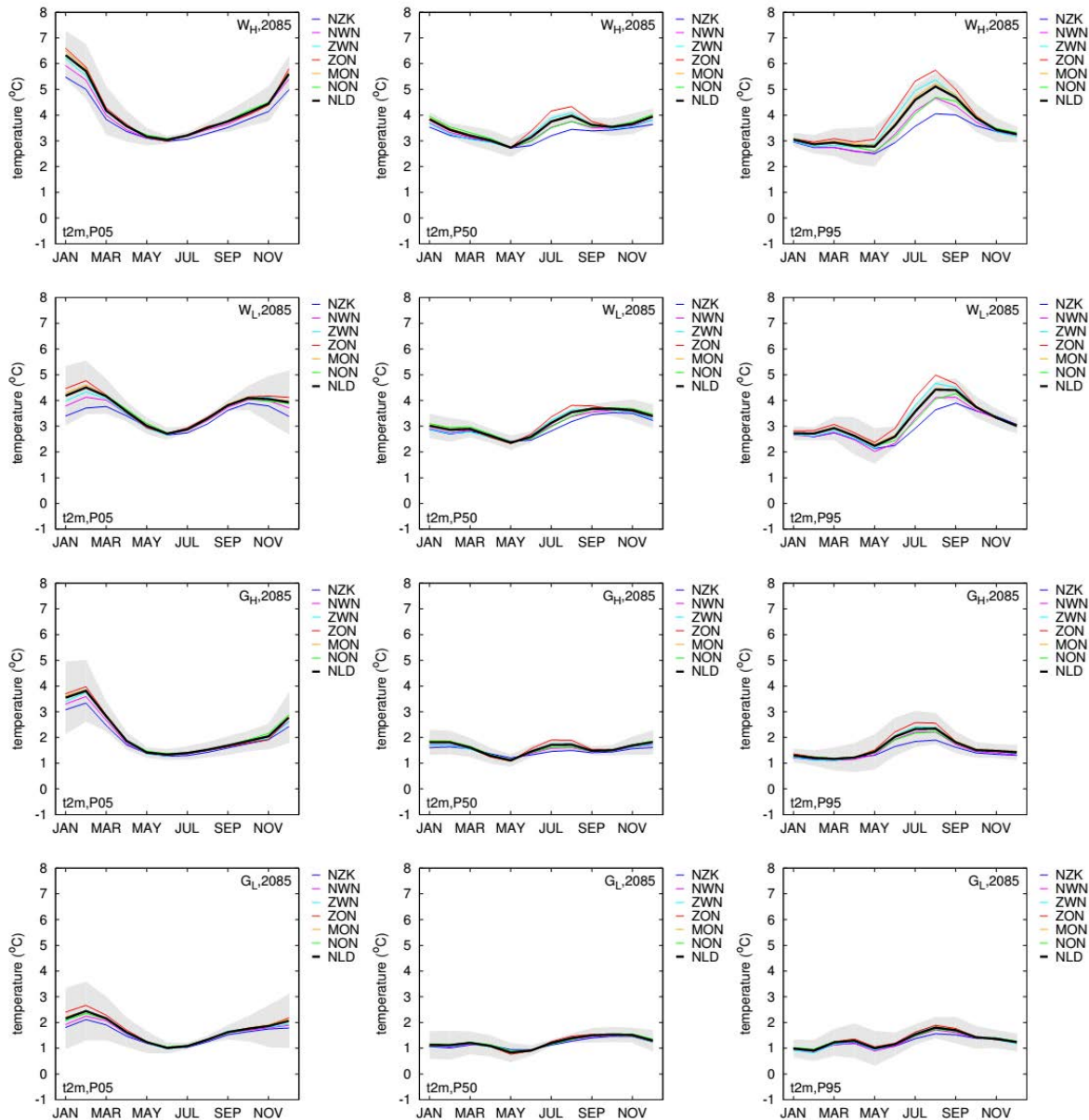


Figure 3.12: As Figure 3.11, but for 2085.

For daily mean, minimum and maximum **temperature**, a linear quantile scaling is applied to transform a reference time series into a time series representative for the specific climate scenario. From the RCM output changes in median and 5<sup>th</sup>, 10<sup>th</sup>, 90<sup>th</sup> and 95<sup>th</sup> percentile values are derived for every calendar month for mean, min and max temperature separately (see section 3.1.4 for details). Similar percentiles are derived from the reference (observed) time series  $T^c$ , and a quantile-based interpolation is applied between the indicated percentile values to generate a future time series  $T^f$ :

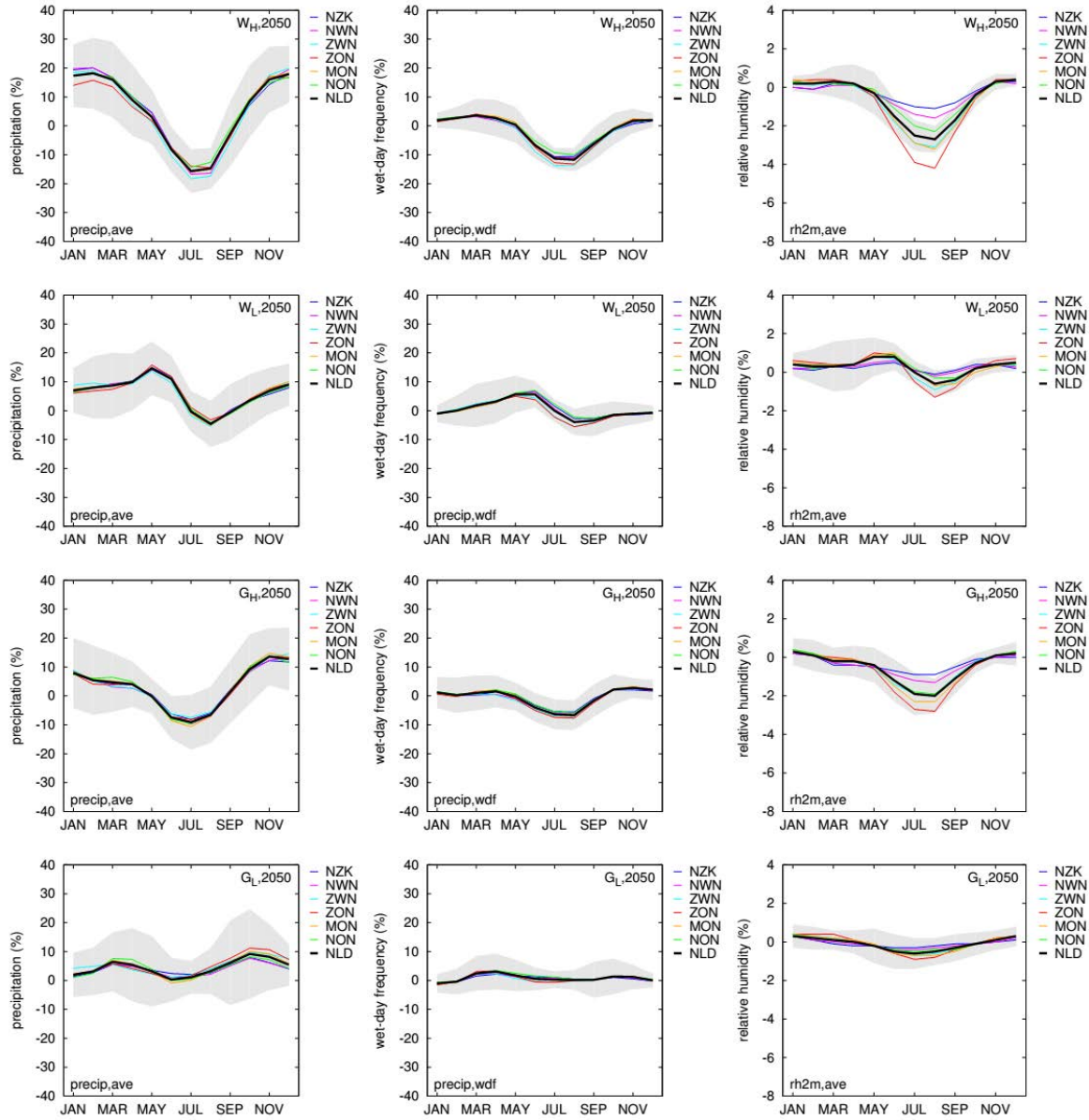


Figure 3.13. Yearly cycle of changes in mean precipitation (left column), wet-day frequency (middle), and relative humidity (right) for the four scenarios for 2050, from top to bottom,  $W_H$ ,  $W_L$ ,  $G_H$  and  $G_L$ .

$$T^f = aT^c + b \quad (3.1)$$

where  $a$  and  $b$  are scaling factors depending on the position in the probability distribution function. For  $a$  these piece-wise linear interpolation coefficients read

$$a = \begin{cases} \frac{T_{95}^f - T_{90}^f}{T_{95}^c - T_{90}^c} & T_c > T_{90} \\ \frac{T_{90}^f - T_{50}^f}{T_{90}^c - T_{50}^c} & T_{50} < T_c < T_{90} \\ \frac{T_{50}^f - T_{10}^f}{T_{50}^c - T_{10}^c} & T_{10} < T_c < T_{50} \\ \frac{T_{10}^f - T_5^f}{T_{10}^c - T_5^c} & T_c < T_{10} \end{cases} \quad (3.2)$$

and a similar approach is used to define  $b$ .

For **precipitation** a two-step transformation procedure is applied. It involves the relative changes in the wet-day frequency (defined as days with >0.1 mm precipitation), the mean wet-day amount and the 99%-quantile of the wet-day amounts derived from the RCM output.

In the first step of the transformation the observed *wet-day frequency*  $W^c$  is changed into a future value  $W^f$ , according to the relative change  $\Delta W$  projected by the RCM ensemble. For  $\Delta W < 0$ , a number of wet days are “dried” or “removed” by setting the precipitation amount to zero. For every month, a sample of target precipitation amounts is defined of which the sample size equals the number of days to dry. Amounts are uniformly extracted from the empirical probability density function (PDF) of the reference precipitation amounts. In this way, the change of the PDF due to ‘wet-day removal’ is minimized. Subsequently, from low to high precipitation, precipitation amounts are selected for drying that as closely as possible resemble the target amounts. The only additional criterion is that the day before *or* after should be already dry. For, the transformation tool for KNMI'06 (Bakker and Bessembinder 2012), this procedure was applied per calendar month. For KNMI'14, first all target values for all months are set and then all wet days are dried from low to high.

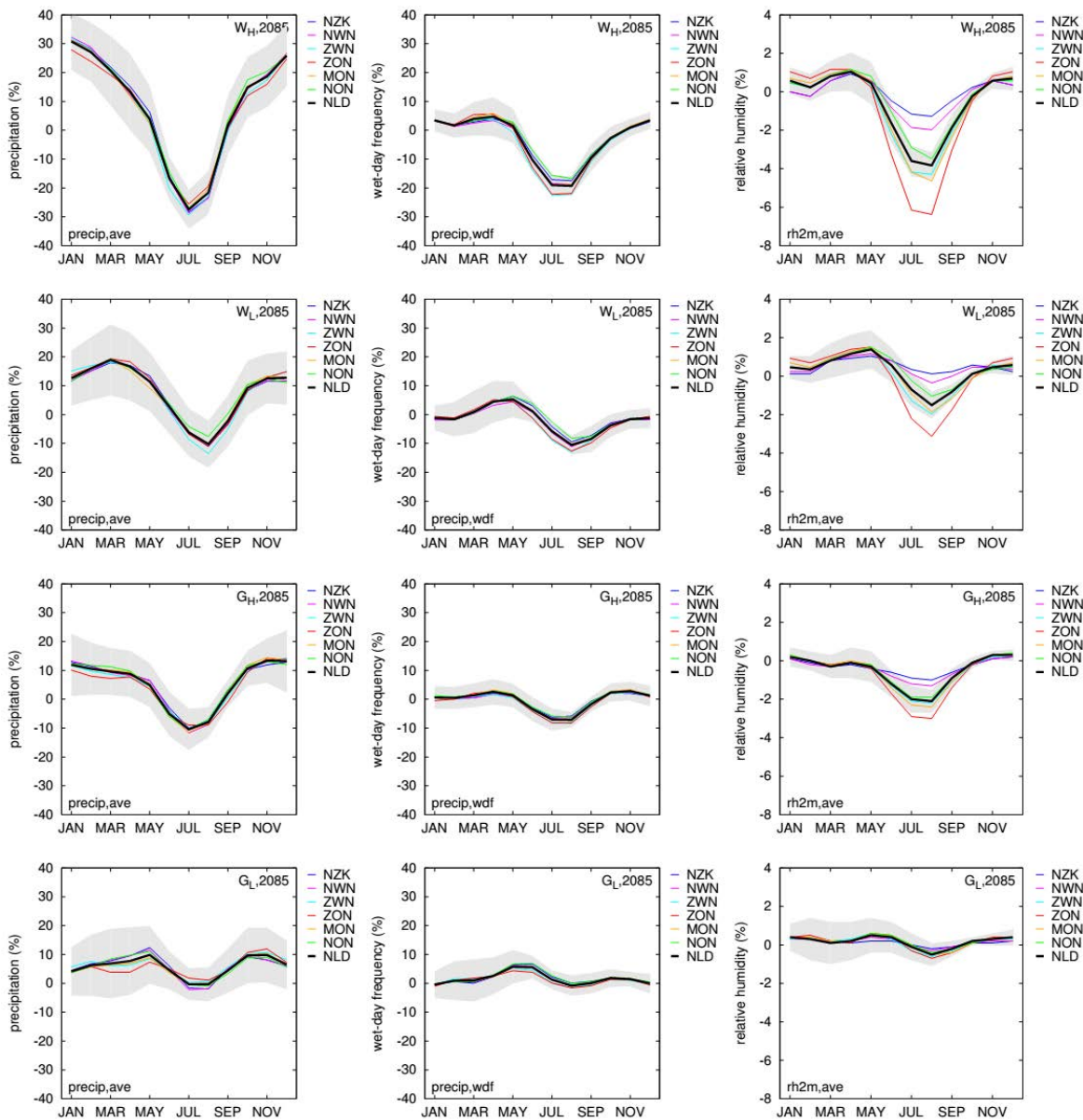


Figure 3.14. As Figure 3.13, but for 2085.

In the case that  $\Delta W > 0$ , a sample of target precipitation amounts is defined similarly as for the “wet-day removal procedure”. The selection of dry days to be ‘wetted’ is based on the number of preceding wet days. Therefore, a wet day counter is increased by  $|\Delta W|$  with each wet day in the chronological order. The first dry day after the counter exceeds unity is turned into a wet day (and the counter is decreased by 1). This procedure automatically ensures that every new wet day succeeds an already existing wet day (no isolated wet days are created). This ensures a better maintenance of the temporal correlation. Note that the procedure allows “wetting” of two or more succeeding days if the preceding wet period is long enough (because the counter is not reset to zero, but decreased by 1 after wetting a dry day). The target amounts are assigned according to the amounts of the preceding wet day amount. So, the lowest target amount is assigned to the day with the lowest amount at the preceding day.

In the second step, the precipitation amounts on wet days are adjusted by a quantile scaling technique that uses a power-law transformation function (with units in mm/day):

$$P^f = \begin{cases} P^{c*} & P^{c*} < 0.1 \\ \max\left(0.1, a(P^{c*})^b\right) & 0.1 \leq P^{c*} \leq P_{99}^c \\ (1 + \Delta P_{99}) & P^{c*} > P_{99}^c \end{cases} \quad (3.3)$$

where  $P^{c*}$  is the reference precipitation adjusted for the scenario/time horizon specific wet day frequency, and  $P^f$  is the desired future precipitation value.  $a$  and  $b$  are transfer coefficients calculated from the median and 99-percentile precipitation changes derived from the RCM model output, following Leander and Buishand (2007).

The chosen procedure resembles the KNMI'06 approach greatly. Main (technical) differences are the choice of a precipitation threshold of 0.1 mm/day instead of 0.05 mm/day (3.3), and the use of an estimated calendar month specific 99-percentile precipitation change based on the 90-percentile changes derived from the model output.

### 3.1.6 Small scale precipitation extremes

Like any climate model, RACMO2 does not resolve convective processes in the atmosphere, despite its very high resolution (for a climate model) of 11 km. Convective clouds – the typical thunderclouds with strong vertical motions caused by vertical instability of the atmosphere – are responsible for many precipitation extremes, in particular in the summer season. On large scales – for instance multi-day extremes on a Rhine catchment scale – large scale systems like frontal zones associated by low pressure system are primarily responsible for extremes. However, on local scales convective clouds are the main player. The fact that RACMO2 (as well as any other climate model) does not resolve these convective processes, but uses a simple statistical approximation called a parameterization, is therefore of major concern. Thus, it is generally realized that changes in local precipitation extremes are highly uncertain and cannot be determined solely from (regional or global) climate model output.

For these reasons we take a different approach here. Instead of using the regional climate model output directly, we use relatively simple scaling arguments based on the increase in moisture content of the atmosphere. The increase in moisture content of the atmosphere is the primary reason for the expected increase in precipitation extremes. This increase can be measured by the dew point temperature. Each degree rise in dew point temperature will lead to an increase in moisture content near the surface of 6-7 %. If the relative humidity does not change, a one degree rise in temperature will result in a one degree rise in dew point.

Increases in dew point temperature are reasonable robust in the regional climate model integrations. In particular, if we consider the change in dew point temperature on days with rain a very uniform response in summer is obtained across western Europe (see Figure 3.15). Compared to the global temperature rise of 3 °C derived from comparing 2066-2095 with 1981-2010, the rise in dew point temperature conditioned on rainy days lags about 0.5 °C.

Besides RACMO2 results the scenarios take into account two additional information sources: i) based on observed relations, and ii) based on short simulations with a mesoscale atmospheric model. The latter model, Harmonie, uses a resolution of 2.5 km and a dynamical core in which the largest convective motions are resolved (and not parameterized like in RACMO2). The model, however, is computationally far too expensive to be used in long climate model simulation, noting that we have simulated > 1200 years with RACMO2 for the construction of the climate scenarios and that in terms of computational costs we can run Harmonie only for a season or a few years at most.

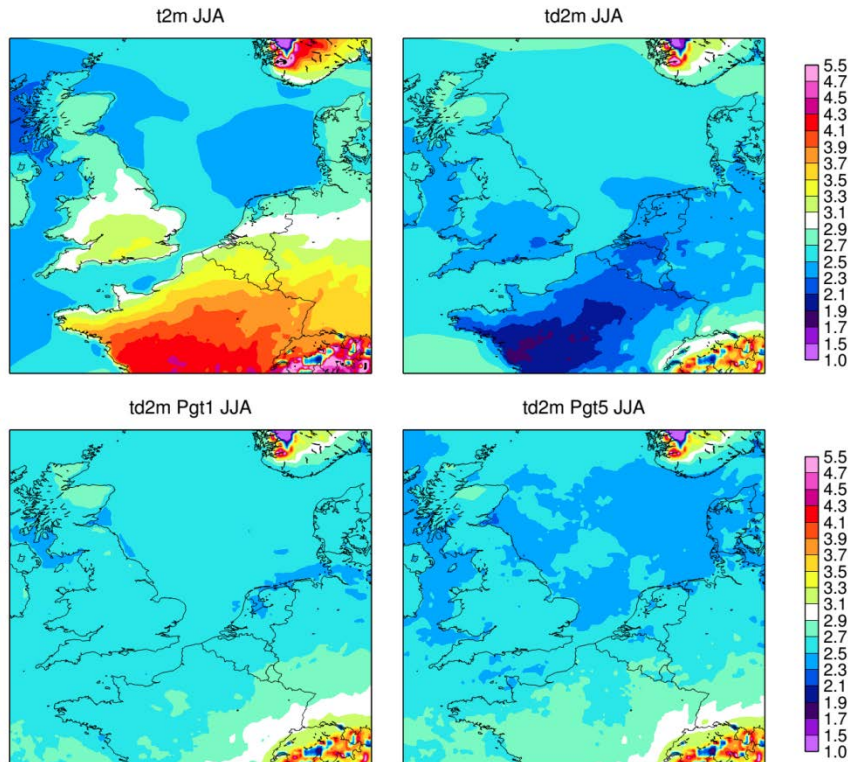


Figure 3.15: Changes in temperature (*t2m*), dew point temperature (*td2m*), dew point temperature on days with >1 mm (*Pgt1*) and days with >5 mm (*Pgt5*) of rain. Results are derived from RACMO2, by comparing 2066-2095 with 1981-2010, before the resampling. The global temperature rise is 3 C, and changes of the size are shaded white.

Analyses of the 90<sup>th</sup>, 99<sup>th</sup> and the 99.9<sup>th</sup> percentiles of the precipitation intensity for high-temporal resolution data for 27 stations in the Netherlands as a function of near surface dewpoint temperature for different time intervals are shown in Figure 3.16 (Loriaux et al. 2013). These results show that the frequency of the high percentile precipitation intensities for the 10 minute interval increases with around 14% per Kelvin over the whole range of observed dewpoint temperatures, which is around twice the value one would expect on the basis of the Clausius-Clayperon (CC) relation. For reference, Figure 3.17 shows this 2 times CC-scaling as dashed lines and the CC-scaling as dotted lines. For longer time intervals the rate of increase of precipitation intensity decreases to values of around 7% per Kelvin (CC-scaling) when daily intervals are used.

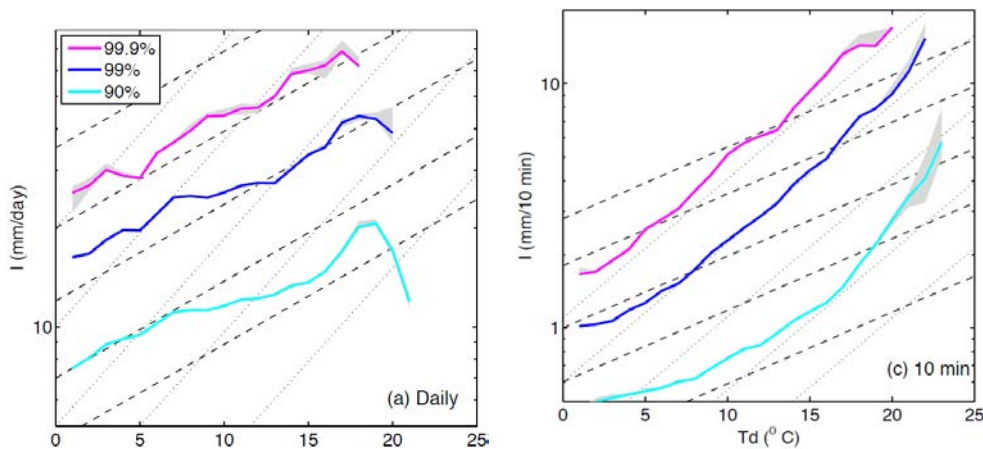


Figure 3.16: Observed precipitation intensity for the 90<sup>th</sup>, 99<sup>th</sup> and 99.9<sup>th</sup> percentiles with respect to dewpoint temperature (*Td*) at daily (left panel) and 10 minute resolution (right panel) (from: Loriaux et al. 2013).

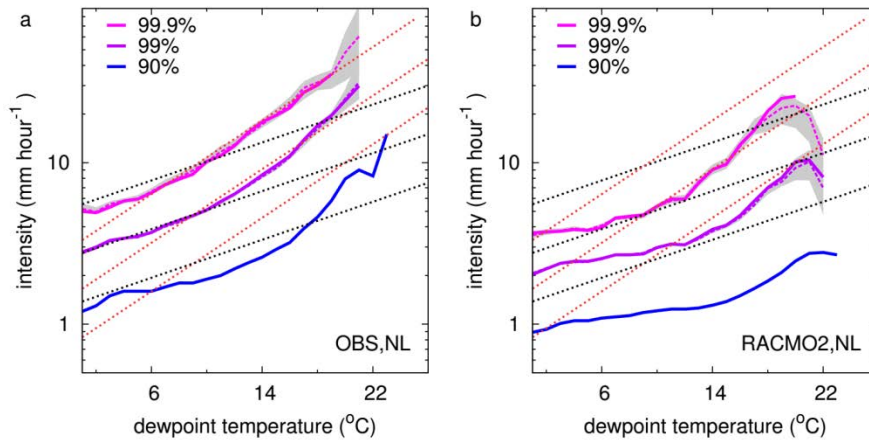


Figure 3.17: Dependency of hourly precipitation extremes on dewpoint temperature derived from 26 stations in the Netherlands; left: observations, right: a model simulation for present-day climate with RACMO2. Dewpoint temperatures are taken 4 hours before the event. Shown are results for the 90, 99 and 99.9th percentile of wet events. Solid line: raw data, stippled lines: estimated from a GPD fit, including uncertainty estimates (grey shading). Red and black linear lines show (exponential) dependencies of 7 and 14 % per degree.

In order to explore the physical basis of the 2CC scaling for the high temporal (10 minutes) intervals a conceptual simple convective updraft model has been studied (Loriaux et al. 2013). Radiosonde profiles for extreme precipitation conditions were used to construct a typical vertical profile for temperature and humidity. These profiles were perturbed with various temperature perturbations uniformly with height while keeping the relative humidity constant as to mimic simple but realistic future climate conditions. The change in precipitation intensity in this updraft model shows an increase of around 10% per Kelvin, again significantly beyond the CC-scaling of 7% per Kelvin. A break-up of the underlying mechanisms shows that a 7% percent increase per Kelvin can be understood from thermo-dynamical considerations, i.e. the availability of moisture that increases with temperature as Clausius-Clayperon. An additional increase is due to intensified vertical motions that enhances the local moisture convergence and adds an extra 3% increase. The underlying reason of this increase of the vertical motion is due to an increase of the destabilisation of the atmosphere as expressed by an increase of CAPE. In turn, the increase of CAPE is a result of the assumed uniform warming of the troposphere.

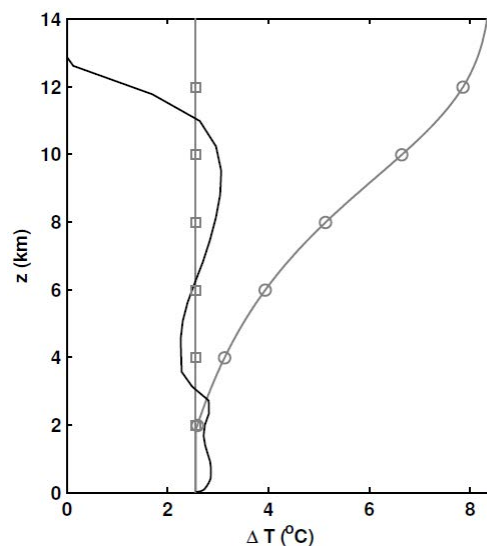


Figure 3.18: (solid line) RACMO temperature difference between future (2046-2075) and present (1981-2010) climate derived from the 1000 profiles with the highest CAPE. For reference a uniform vertical profile (grey squares) and the moist adiabatic profile (grey circles) are shown as well.

The validity of this uniform warming has been evaluated with data of an eight member downscaling of RACMO driven by EC-Earth according to the RCP8.5 Greenhouse gas scenario (see Figure 3.18). The profile of

the temperature increase based on 1000 profiles with the highest summertime (JJA) CAPE values shows that the assumption of a uniform warming in the case of extreme events is justifiable. For reference also a temperature perturbation profile for the case that the perturbation follows the moist adiabat is shown, which is a situation that is expected to be more common in the tropics. In that case the associated change in CAPE will be close to zero and as a result a precipitation intensity scaling beyond CC would not be expected.

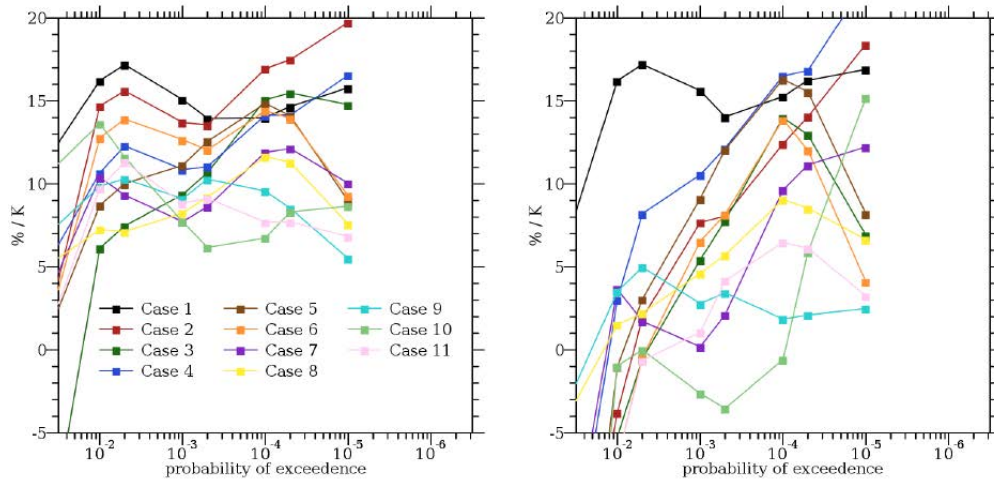


Figure 3.19: Scaling of precipitation rates in percent per Kelvin based on 11 different cases as simulated by HARMONIE for uniform warming (left panel) and for realistic warming profiles based on RACMO results (right panel).

Further evidence has been obtained by simulations with the high resolution non-hydrostatic model HARMONIE for 11 separate days over the Netherlands characterized by intense precipitation. These runs were perturbed with a uniform +2K and -2K scenario while keeping the relative humidity constant. A third perturbation was performed based on changes in the atmospheric profiles of RACMO future climate runs based on a selection of the 1000 profiles with the highest CAPE for each summer month (Attema et al. 2014). For all these runs the change per Kelvin warming of the probability of exceedance for precipitation intensity has been determined (see Figure 3.19). On average the results show an increase of 9~11 %/K depending on the type of perturbation although large differences can be observed from case to case.

The time series transformation tool uses the change in 99<sup>th</sup> percentile conditioned on wet events,  $\Delta P99_w$ . This is the same quantity that has been issued for the previous set of scenarios (Lenderink et al. 2007). We note that for unconditional precipitation extremes, the influence of changes in the number of wet-events has to be accounted for. The number of wet-events is affected by circulation changes (see Lenderink et al. 2007 and the values of the number of wet days are given in the previous section (Figure 3.13 and Figure 3.14). However, we note that in practice the change in events with very long return periods will be close to the change in  $\Delta P99_w$ .

Percentage changes in  $\Delta P99_w$  are computed by

$$\Delta P99_w = 100[(1 + \alpha/100)^{\Delta T_{dew*}} - 1] \quad (3.4)$$

with  $\alpha$  the percentage changes that are chosen based on the previous results and  $\Delta T_{dew*}$  the change in dew point temperature on days with 1 mm or more rain. For each season an upper and lower limit is chosen. Values of  $\alpha$  are also different between daily and hourly precipitation extremes, and the different seasons, and are given in the second column of Table 3.1.

In winter, we take for daily extremes values of  $\alpha$  of 4 to 9 % per degree, centered around the prediction based on the Clausius-Clapeyron relation of 7 % per degree. The upper boundary is slightly higher than based on the RACMO simulations (third column of Table 3.1). Some preliminary results with Harmonie for a case in November also indicated a larger sensitivity than those based on RACMO2. Additional analysis of vertical profiles of the atmosphere in RACMO2 revealed substantial increases of approximately 15 % per degree in values of the Convective Available Potential Energy (CAPE). For the same reason the upper estimate of changes in hourly extremes is set to 11 % per degree; the lower estimate follows the average RACMO prediction of 5 % per degree.

In summer daily precipitation extremes are assumed to change according to 2 and 12 % per degree. The lower range is based on RACMO2 results, the upper range on Harmonie results. Changes in hourly extremes are between 7% and 14 % per degree. The upper boundary is based on the observed relations, and is supported by Harmonie results as well. The lower boundary is larger than the RACMO2 results for the Netherlands, giving on average 3 % per degree. However, we feel that RACMO2 results do underestimate potential changes, for instance as based on Figure 3.17, where it is shown that RACMO2 does underestimate the dependency of hourly precipitation extremes on dew point temperature for high dew point temperatures. We also note that RACMO2, as well as other climate models, appear to be too sensitive to a projected decreases in relative humidity (Hohenegger et al. 2009; Lenderink and van Meijgaard 2010). Therefore, we rely for hourly extremes more on the results of Harmonie and the observed relations.

*Table 3.1: Scaling constants used for daily and hourly precipitation extremes (P99w) in % per degree for summer and winter (first column), in comparison with results from RACMO, Harmonie, and observations. The last column provides additional information, provided when the  $\alpha$  range does not correspond to the range given by RACMO2 and Harmonie (indicated by bold, italic numbers in second column).*

	Scenario range (% °C <sup>-1</sup> )	RACMO2 (% °C <sup>-1</sup> )	Harmonie (% °C <sup>-1</sup> )	Obs. (% °C <sup>-1</sup> )	Additional information/ Expert judgment
DJF daily	4-9	4-8	-	~7	possible effect North Sea <sup>1</sup>
DJF hourly	<b>5-11</b>	4-8	-	~7	high increases in CAPE <sup>2</sup> >7 % observations sub-hourly <sup>3</sup>
JJA daily	2-12	2-5	7-12	~7	
JJA hourly	<b>7-14</b>	3-7	7-14	10-14	RACMO limitations

Although the chosen values of  $\alpha$  as given in Table 3.1 are of course to some extent subjective, we think it gives a balanced overview of information from observations and models. In general, we take the full range taken from the RACMO2 as well as the Harmonie results to be leading for daily extremes. For winter, no Harmonie results are available, and we take a 1 % per degree higher upper boundary in winter primarily to account for possible influences of the North Sea on convective precipitation in the Netherlands.

In conclusion, based on observations, simulations, conceptual models and physical principles it can be expected that the frequency of extreme precipitation will increase with dew point temperature with 9~14 %/K for the short term convective events. These numbers are combined with the changes in the near surface dew point temperature for the four different KNMI'14 scenarios.

### 3.1.7 Climate change signals in the Rhine basin

Of prime interest for the Netherlands is the climate change signal depicted in the Rhine/Meuse basins. Discharge characteristics of these major rivers governs the safety and freshwater policies in a major portion of the Netherlands. The KNMI'14 scenarios have been constructed in order to span the modelled climate response from CMIP5 for *The Netherlands area*, not necessarily coinciding with a similar fraction of the CMIP5 range in other neighbouring areas such as the Rhine and Meuse catchments.

Figure 3.20 illustrates the summer (JJA) precipitation response from a fraction of the CMIP5 ensemble (those models driven by RCP4.5, RCP6.0 and RCP8.5), shown for different percentiles in the distribution of the >100 member ensemble. Also shown is the precipitation response for the resampled set of EC-Earth and RACMO2 simulations that are used to construct the  $W_H$  scenario (see Table 2.2). A first order comparison of the  $W_H$  scenarios with the CMIP5 results shows that for the Netherlands the chosen scenario is exceeded (that is, drier projections) by roughly 17% of the CMIP5 ensemble, which is considered to be acceptable, given the suspected dry bias in some of the driest CMIP5 models (not shown). However, for the Rhine basin the  $W_H$  results are closer to the median of the CMIP5 ensemble, and the dry part of the CMIP5 range is obviously not covered in this scenario.

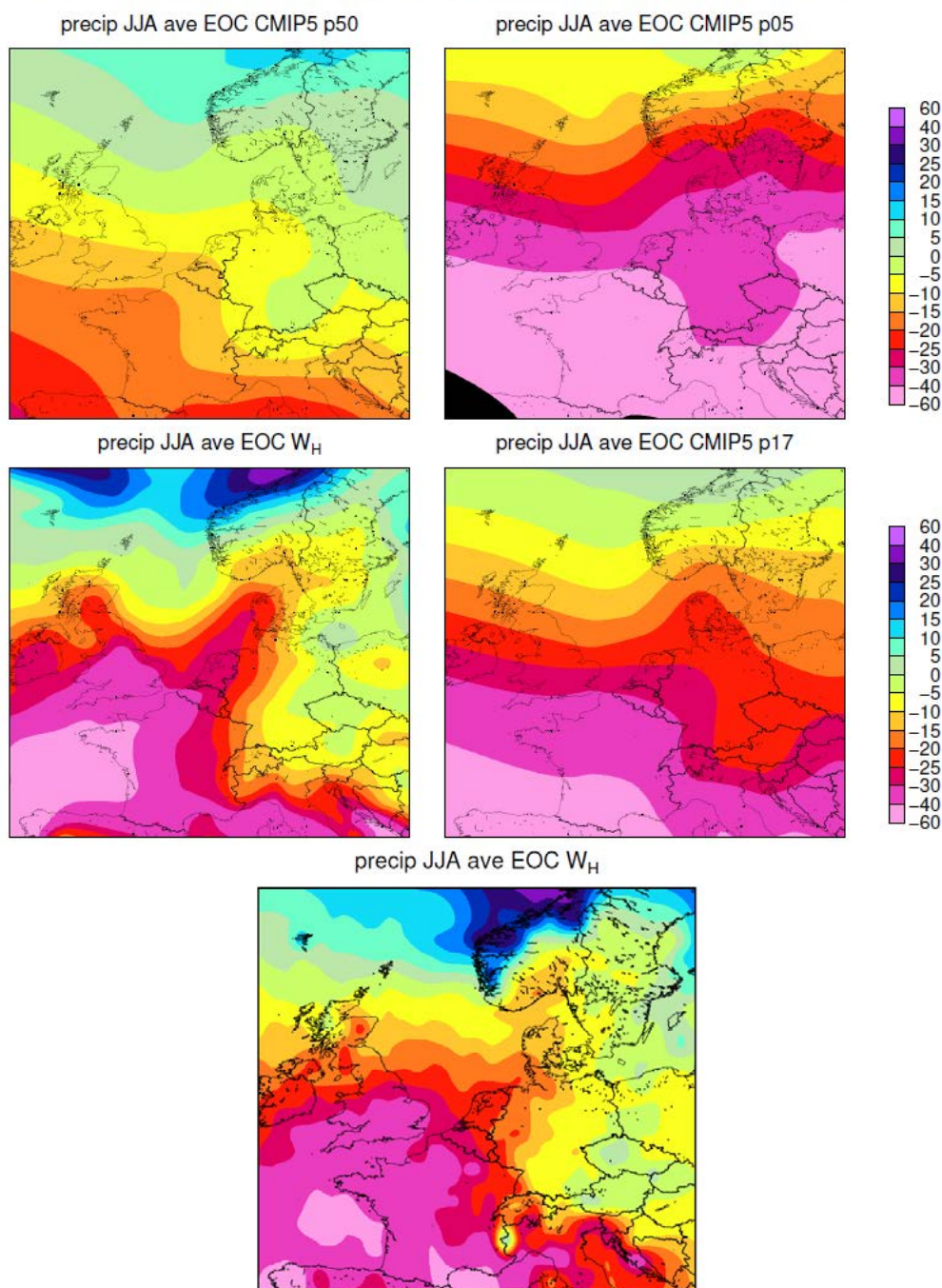


Figure 3.20: Projections of change in JJA precipitation in 2085 as simulated by selections of GCMs (top 4 panels) and the RACMO2 ensemble (bottom panel). Top row left is the median of all CMIP5 model results corresponding to the RCP4.5, RCP6.0 and RCP8.5 scenario, while the upper right panel shows the 5% quantile (5% of the CMIP5 ensemble shows precipitation responses drier than shown). Second row left is the resampled EC\_Earth result, where the resampling was conditioned on the  $W_H$  scenario. Right of this is the 17% quantile of the CMIP5 ensemble, indicating that the resampled result is exceeded by 17%. Lowest panel is the resampling result of the 2085  $W_H$  set based on the RACMO2 ensemble.

## 3.2 Sea level rise

### 3.2.1 Introduction

KNMI develops climate scenarios for the Netherlands as a consistent set of climate variables for particular time-horizons (also called sight years). As in the previously issued KNMI scenarios the primary axis for spanning

model ranges is global temperature change,  $dT_{\text{glob}}$ . Two distinct time paths are chosen for  $dT_{\text{glob}}$ , corresponding to a moderately warming scenario (G, 2050 +1°C, 2085 +1.5°C), and a warm scenario (W, 2050 +2°C, 2085 +3.5°C; see Table 2.1). For 2100 the G-scenario assumes  $dT_{\text{glob}} = +1.6^\circ\text{C}$ , whereas the W-scenario uses  $dT_{\text{glob}} = +4.0^\circ\text{C}$  in 2100. For years falling in between the eight years we use a linear interpolation. For the atmospheric variables, circulation/precipitation change is used as a second steering variable to distinguish between the scenarios. However, since local sea-level change is determined by a wide range of global and regional processes, circulation/precipitation change is not useful for spanning the projected range of sea-level change. For this reason only one steering variable was considered for sea level in KNMI'06. For the KNMI'14 scenarios the same approach is used: for each temperature scenario, we compute sea-level rise and a likely range. Because the G-scenario leads to systematically lower sea-level rise than the W-scenario, the sea-level rise scenarios will be referred to as the “Low” and “High” sea-level scenario. The key results rounded to 5cm precision are given in Table 3.2.

*Table 3.2: KNMI'14 Sea-level scenario ranges for Global and North Sea (with respect to 1995, the central year of the reference period 1985-2005). The values in this table are taken from the 5-95% ranges of Table 3.3 after rounding to 5cm precision.*

KNMI'14 scenario	Low (2050)	Low (2085)	High (2050)	High (2085)
$dT_{\text{glob}}$	+1.0°C	+1.5°C	+2.0°C	+3.5°C
Global mean	15 to 30 cm	30 to 60 cm	20 to 35 cm	45 to 75 cm
North Sea	15 to 30 cm	25 to 60 cm	20 to 40 cm	45 to 80 cm

The sea level scenarios in KNMI'14 are derived from a thorough analysis of the CMIP5 model archive, complemented by a detailed analysis of the various processes, their uncertainty and their relative contribution to the overall sea level rise scenarios. The final result is a sea level rise value for both global mean and the North Sea area, for two values of the assumed global temperature increase, and for two time horizons. For each scenario and time horizon, an upper and a lower value is given, corresponding to a 5 – 95% uncertainty range of the sea level rise estimated from model simulations. Apart from the resulting sea level, an estimate of the rate of sea level is given in the accompanying brochure for the various scenarios. A review of the processes involved is given first, followed by a discussion of the statistical uncertainty combination and the final results. More details are provided in Annex 6.2.

### 3.2.2 Processes included in the scenarios

Many different physical processes contribute to global and regional sea-level change (Church et al. 2010). Primary contributors to present-day sea level change are the expansion of the ocean due to warming and the reduction of the amount of water stored on land, mostly in the form of ice and snow (Church and White 2011; Church et al. 2011; IPCC 2013c). Changes in the earth surface elevation, however, are ignored. These changes may follow from glacial isostatic adjustment (the response of the earth crust to past glacial cycles) and other processes (e.g. drying of peat, sinking due to heavy building). Not taking into account the changes in the earth surface elevation implies that the KNMI sea-level scenarios are scenarios of absolute sea-level changes.

The following processes are taken into account:

1. *Oceans*: Changes associated with ocean expansion as a result of changes in ocean temperature and salinity, as well as (associated) changes in the ocean circulation (i.e., dynamics). Coupled Atmosphere-Ocean General Circulation Models (AOGCMs) are used to examine this term. To calculate the ocean thermal expansion and the resulting sea-level change, requires knowledge of the three-dimensional temperature and salinity structure of the ocean. The ocean has a large heat capacity, and during warming climatic periods enormous amounts of heat are absorbed. These are ventilated into the deep ocean, only to be gradually released during cooler climatic periods. For this reason the ocean stores a considerable amount of heat of the past climate, and its response to global warming is generally non-linear. Ocean circulation changes, such as the response of the Meridional Overturning Circulation (MOC), the ocean gyres, introduce yet more complexity to the problem, related to density changes resulting from changes in temperature and salinity. Together, these processes yield a specific pattern of sea level change that varies in time and space.

2. *Glaciers and ice-caps (GIC)*: Changes in surface mass balance and dynamics of the glaciers and small ice-caps. In this term are included the glaciers on Greenland and Antarctica not connected to the main ice sheets. These glaciers and small ice-caps are treated separately from the largest ice-sheets on Earth (see below). Glaciers and small ice-caps respond more quickly than the Ice Sheets to climate change and global temperature increase, so their short-term influence on the global and regional sea-level change is expected to

be considerable despite their limited total volume which is estimated to be equivalent to between 31 and 53 cm of global sea level. These numbers are based on a number of recent glacier inventories also used in AR5 (Arendt et al. 2012; Huss and Farinotti 2012; Marzeion et al. 2012; Radić et al. 2014; Grinsted 2013). Important parameters that influence local glacier volume and are the regional climate (temperature and precipitation), the orientation and altitude. Despite these subtleties, the total contribution from all glaciers together can be parameterized approximately in terms of global mean temperature change (Van de Wal and Wild 2001; Slangen and van de Wal 2011). For the KNMI-scenarios such parameterizations are used. The required global temperatures are obtained from the same AOGCMs that also provided the ocean expansion fields.

3. *Ice sheets*: Changes of the largest ice-sheets on Earth, those of Greenland (GIS) and Antarctica (AIS). The Antarctic Ice Sheet contains by far the most ice, and if it would melt completely would raise global mean sea level by more than 60m. The GIS contains approximately an equivalent of 7m of global sea level and is thus much smaller than AIS. Some studies prefer to subdivide the AIS into a Western part (WAIS) and an Eastern part (EAIS). In this subdivision the EAIS outweighs GIS and WAIS by a factor 10, but is generally considered to be the least sensitive to changes in the climate on centennial timescale. Studies are less certain about WAIS and potentially large changes cannot be ruled out. For the KNMI scenarios, we consider the combined changes in the western and eastern part of AIS. The contributions from the ice sheets are subdivided into mass-balance changes and rapid-dynamical changes as explained below.

- *Surface mass balance changes* (SMB; i.e. SMB-AIS and SMB-GIS): Changes in SMB reflect changes in the balance between snowfall and summer melt of snow and ice resulting in liquid run-off from the ice sheet. High resolution regional climate models forced by AOGCMS are used to estimate the contribution from these processes and to find suitable parameterisations of SMB in terms of global mean temperature change (e.g. Fettweis et al. 2013).
- *Rapid dynamical changes* (denoted DYN-AIS and DYN-GIS): Rapid dynamical changes comprise changes driven by iceberg calving and basal melt of tidewater glaciers by warmer ocean water leading to an ice dynamical adjustment of the ice sheet. Although melt of ice shelves does not contribute to sea-level rise per se, it is associated with ice flow from grounded glaciers to the floating ice shelves which does contribute to sea-level rise. Extrapolation of recent observations, together with expert opinions are used to determine scenarios. There is however considerable spread in these changes, which is reflected in the relatively large uncertainty bands.

4. *Landwater changes*: Changes in water storage on land. This term is quite general and includes changes in the amount of water stored in the form of lakes and rivers, wetlands, as well as the snowpack at high altitudes and latitudes. Contributions attributable more directly to human activity such as groundwater mining, dam building, and increased runoff due to land-use changes, are also included.

5. *Atmospheric pressure loading*: Atmospheric pressure changes are an important source of short-term local sea level variability, because for each mbar of pressure drop, local sea level increases 1 cm (this is referred to as the inverse barometer effect). In a warming climate, the moisture content of the atmosphere will increase, yielding a sea level drop. In the global mean this term appears small, but locally it can be a substantial contributor to sea level change (Slangen et al. 2014). The term is computed from the pressure and moisture fields of the AOGCMs.

The contributions from each of these terms are given in Table 3.3.

### 3.2.3 Regionalization

Regional sea-level estimates are obtained from the global estimates by taking into account the fact that the meltwater from for example the glaciers will not distribute evenly over the oceans due to the elastic deformation of the solid Earth and gravitational and rotational changes induced by the accompanying change in mass distribution (the so-called self-gravitation effect) (Milne et al. 2009; Katsman et al. 2011). As a result, a shrinking land ice mass yields a distinct pattern of local sea level rise referred to as its fingerprint (e.g., Mitrović et al. 2001). The gravitational, elastic and rotational effects can be incorporated in the scenario for sea level rise by multiplying each of the global mean contributions from ice melt from glaciers and ice sheets by their respective relative fingerprint ratios (the fraction of the melt water that actually ends up at a certain location; Katsman et al. 2011; Slangen et al. 2012). The fingerprints for the KNMI'14 scenarios (Figure 3.21 and Figure 3.22) are taken from Slangen and et al. (2014). The GIC-fingerprint in the Netherlands decreases from about 75% of the global mean at the beginning of the 21<sup>st</sup> century, to about 70% near the end due to the changes in the geographical locations. Figure 3.21 (left) shows the GIC-fingerprint field for the North East Atlantic region. Also for the ice sheet contributions, regional estimates are obtained from the global estimates by taking into account the self-gravitation effect. For Greenland the contribution reaching the Netherlands is small compared

to the global mean, less than 20% (Figure 3.22, top row). As one can see, however, there is a strong gradient over the North East Atlantic of the fingerprints associated with the Greenland ice sheet due to its proximity. The geographical boxes used in the scenarios are also shown. Since the North-Sea scenarios are designed to be suitable for the Netherlands, we will use the fingerprint values close to the coast. With 110-120% the Antarctic contribution reaching the North Sea exceeds the global mean (Figure 3.22, bottom row).

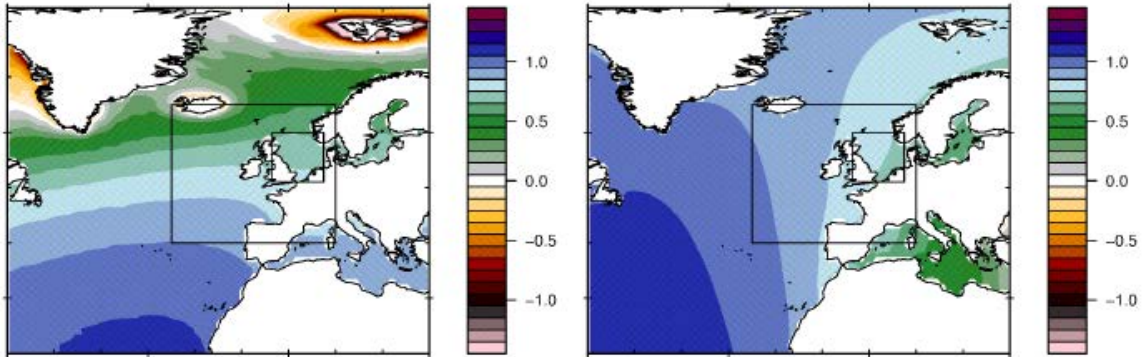


Figure 3.21: Fingerprint fields for (left) Glaciers and small ice caps; (right) Landwater changes. The fields change slowly over time, and the mean value is shown. The two subdomains "North East Atlantic" and "North Sea" are indicated by the black boxes.

Finally, also for the land water term the self-gravitation effect is accounted for in the regional contribution. The land water-fingerprint in the Netherlands is about 75% of the global mean contribution from the Antarctic ice sheet (Figure 3.21, right).

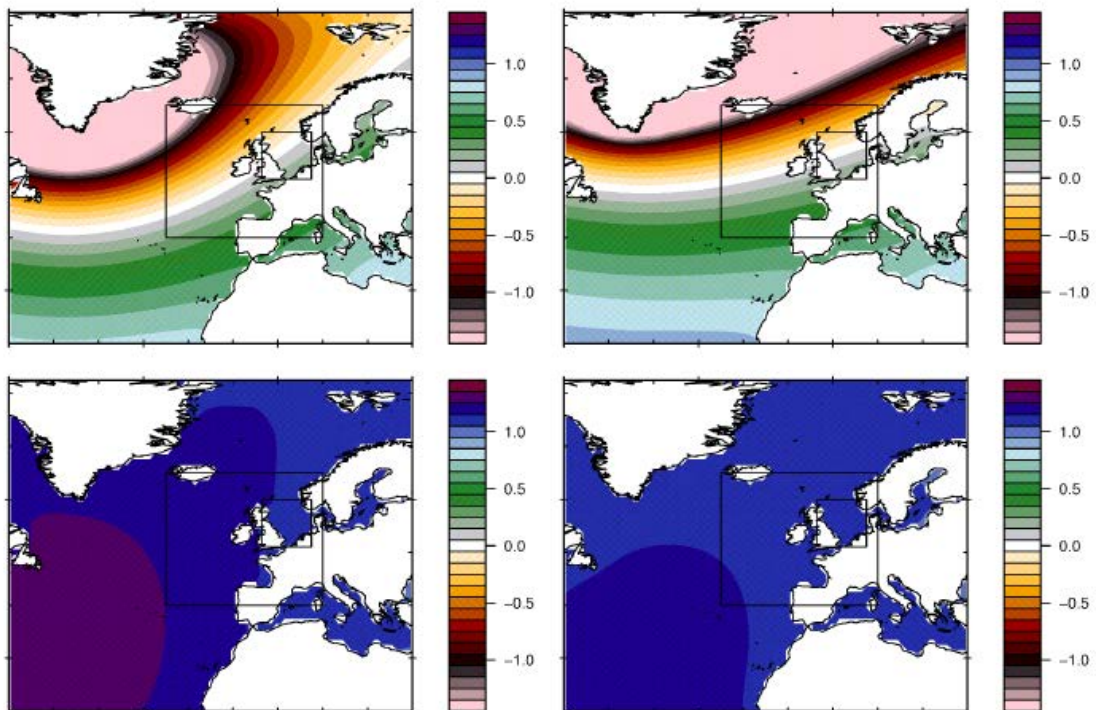


Figure 3.22: Fingerprint fields for (top) DYN-GIS and SMB-GIS and (bottom) DYN-AIS and SMB-AIS. The two subregions "North East Atlantic" and "North Sea" are indicated by the black boxes. The values show fractional change of sea level compared to the global mean change.

### 3.2.4 Implementation and uncertainties

To implement the above-mentioned processes into the scenarios, it has been decided to closely follow chapter 13 of IPCC AR5 (IPCC 2013d), unless there are good reasons for deviating. In fact, only for the rapid dynamical changes of the Antarctic Ice Sheet (DYN-AIS) KNMI has a higher upper-bound than that given by IPCC AR5. The

reason for this is that this contribution is expected to be skewed towards higher values by experts (Bamber and Aspinall 2013). In KNMI'14 this skewness is explicitly taken into account making use of the extreme high-end scenario for DYN-AIS formulated in Katsman et al. (2011). Possible changes in the Antarctic Ice Sheet have a relatively strong effect at Northern mid-latitudes such as the North Sea area.

All processes manifest themselves as a superposition of a slowly varying (trend)-signal and faster fluctuating (random) components. The fast fluctuations (mostly natural variability, see below) imply that the exact future state cannot be predicted at long lead times. However, in most cases even the slowly-varying (trend) signal itself is subject to considerable uncertainty. The KNMI sea-level scenarios aim to describe just this slowly varying component (i.e., the climate). Quite generally, uncertainties in the future climate state come into existence for three main reasons:

- [N] Natural variability. Fluctuations of the climate-variable over the time-scales considered, assuming a stationary climate. Fluctuations of this type over the typical windows of 30 years are relatively small for global-mean sea level. On shorter time- and spatial scales however, variations can be considerable. For example, the North Sea as a whole features decadal fluctuations of the order of 10 cm (see Figure 3.26 explained in a later section).
- [E] Ensemble spread. Different models give different results. In the present discussion, also external forcing variations are included in this term (sometimes referred to as scenario-uncertainty).
- [M] Model uncertainty, associated with incomplete physics descriptions, methodological inaccuracies and shortcomings, or otherwise.

*Table 3.3: Process contributions for global and regional sea-level change with respect to 1995 (1986-2005). Indicated is the 5-95% range. The ranges do not include natural variability on time-scales smaller than 30 years. The contribution termed "Oceans" involves ocean expansion due to thermo- and halosteric changes, as well as the dynamic changes.*

<b>GLOBAL</b>	Low (2050)	Low (2085)	High (2050)	High (2085)
Oceans	07 to 11 cm	12 to 21 cm	09 to 14 cm	19 to 29 cm
Glaciers	03 to 08 cm	06 to 15 cm	05 to 10 cm	10 to 19 cm
AIS-dyn	00 to 09 cm	00 to 22 cm	00 to 09 cm	00 to 22 cm
GIS-dyn	01 to 03 cm	02 to 06 cm	01 to 03 cm	02 to 06 cm
AIS-smb	-1 to 00 cm	-4 to 00 cm	-2 to -1 cm	-6 to -2 cm
GIS-smb	00 to 02 cm	-1 to 07 cm	01 to 03 cm	04 to 11 cm
Landwater	01 to 04 cm	00 to 09 cm	01 to 04 cm	00 to 09 cm
Inv.barom	00 to 00 cm			
<b>Total</b>	<b>17 to 29 cm</b>	<b>30 to 60 cm</b>	<b>22 to 34 cm</b>	<b>44 to 75 cm</b>

<b>NORTHATL</b>	Low (2050)	Low (2085)	High (2050)	High (2085)
Oceans	07 to 17 cm	12 to 30 cm	12 to 22 cm	25 to 43 cm
Glaciers	02 to 05 cm	04 to 10 cm	04 to 07 cm	07 to 13 cm
AIS-dyn	01 to 11 cm	00 to 26 cm	01 to 11 cm	00 to 26 cm
GIS-dyn	-1 to 00 cm	-2 to -1 cm	-1 to 00 cm	-2 to -1 cm
AIS-smb	-2 to 00 cm	-4 to 00 cm	-2 to -1 cm	-6 to -2 cm
GIS-smb	00 to 00 cm	-1 to 00 cm	-1 to 00 cm	-2 to -1 cm
Landwater	01 to 03 cm	00 to 08 cm	01 to 03 cm	00 to 08 cm
Inv.barom	-1 to 00 cm	-1 to 00 cm	-1 to 00 cm	-1 to 01 cm
<b>Total</b>	<b>13 to 29 cm</b>	<b>20 to 56 cm</b>	<b>19 to 35 cm</b>	<b>35 to 70 cm</b>

<b>NORTHSEA</b>	Low (2050)	Low (2085)	High (2050)	High (2085)
Oceans	07 to 20 cm	13 to 34 cm	14 to 27 cm	29 to 50 cm
Glaciers	02 to 05 cm	04 to 10 cm	04 to 07 cm	07 to 13 cm
AIS-dyn	01 to 11 cm	00 to 26 cm	01 to 11 cm	00 to 26 cm
GIS-dyn	00 to 00 cm	00 to 01 cm	00 to 00 cm	00 to 01 cm
AIS-smb	-2 to 00 cm	-4 to 00 cm	-2 to -1 cm	-6 to -2 cm
GIS-smb	00 to 00 cm	00 to 01 cm	00 to 00 cm	00 to 02 cm
Landwater	00 to 03 cm	00 to 07 cm	00 to 03 cm	00 to 07 cm
Inv.barom	-1 to 00 cm	-1 to 01 cm	-1 to 01 cm	-1 to 01 cm
<b>Total</b>	<b>14 to 32 cm</b>	<b>25 to 62 cm</b>	<b>22 to 40 cm</b>	<b>43 to 80 cm</b>

A consequence of the above sources of variability is that each process at a given lead time results in a whole distribution of possible outcomes. And because not all processes can be modelled simultaneously in a fully interacting way by a single global climate model or earth system model, we have an incomplete knowledge of possible covariances and correlations between the individual terms. Therefore, to obtain an estimate of the total sea-level change, certain assumptions have to be made. In making these assumptions about the relations between different terms, we follow IPCC AR5. In determining estimates from the different process contributions, the correlations between global temperature and the ocean thermal expansion fields are retained. The different contributions are subsequently combined using a sampling method, and the likely range is determined as the difference between a high and a low percentile of the distribution. Estimates and ranges for the individual processes are determined from their distributions. Thus, the range of the total sea level change is not equal to the sum of the individual ranges. However, a reasonable approximation for obtaining the total contribution is explained below. The central estimate (median, P50) of the total sea-level change can be approximated by the sum of the individual central estimates:

$$m_{tot} \approx \sum_i m_i(t) \quad (3.5)$$

where  $m_i(t)$  is the median from process  $i$  in period  $t$ , and the sum runs over all contributing processes. Similarly, the likely range of the total sea level change can be approximated from the percentiles of the contributing processes

$$q_{tot}(t) \approx m_{tot}(t) + \text{sgn}(\alpha_q) \sqrt{\sum_i [q_i(t) - m_i(t)]^2} \quad (3.6)$$

where  $q_i(t)$  denotes the  $q$ -th percentile of the distribution of process  $i$  and  $q$  is the quantile function of the normal distribution. The above expressions are exact for a sum of independent Gaussian distributions. For the sea level rise problem, the approximate relation (3.6) produces results within 5 cm of the direct estimate from the distribution itself.

### 3.2.5 Scenarios for the 21st century

Scenarios have been obtained for the global-averaged sea-level and for two subdomains. In addition, the scenarios are determined locally (i.e., at the grid-scale of 1×1 degree). The following subsections describe the results. Note that in the following the contribution termed “Oceans” involves ocean expansion due to thermo- and halosteric changes, as well as the dynamic changes.

#### **Target sight years**

Table 3.3 displays the scenarios for the two key sight years 2050 and 2085 and the two scenarios (low and high) and for three spatial scales: 1) Global, 2) North East Atlantic (25W-10E,40-65N) and 3) North Sea (3.5W-7.5E,51-60N). The motivation for creating scenarios for both NE-Atlantic and the North Sea, is that the former served as a basis for the KNMI'06 scenarios (Van den Hurk et al. 2007). Note that the ranges do not include natural variability on time-scales of less than 30-years.

The scenario ranges for the North Sea area in 2085 are very similar to those of the global scale. However, the relative importance of the components differ, with the “Oceans” (expansion + dynamics) contribution being larger than the global average in the North Sea basin, and the Greenland Ice sheet contributions being smaller. This is in agreement with the results presented in IPCC 5AR and Slangen et al. (2014).

To better appreciate the change of overlap and uncertainty with time we have also constructed timeseries for the sea level scenarios for all years between 1995 and 2100. These are discussed in the following subsections.

#### **Global response**

Figure 3.23 displays the KNMI scenarios for global mean sea level. Observed 30-year running average sea-level from 1890 to 2002 is also included (Church and White 2011), as well as the 5-year running averages (dots). Also shown are the 5-year running average observations from satellite altimetry (Nerem et al. 2010). Satellite data has become available since 1993, and for this reason the reference period was set to 1993-1998, around the central year 1995. To show that the scenarios attach smoothly to the observations, the scenario shading

includes natural variability on a 5-year time-scale. As with the observations, this term is estimated here from the variance of the 5-year running average deviations from the 30-year running mean (climatologies), and is assumed to be constant during the 21st century. It is also included in the figures by means of the vertical bars. Estimated ranges without natural variability are indicated in the colored legends for a few key sight years. In addition, the right margin displays the ranges of the contributing processes in 2100.

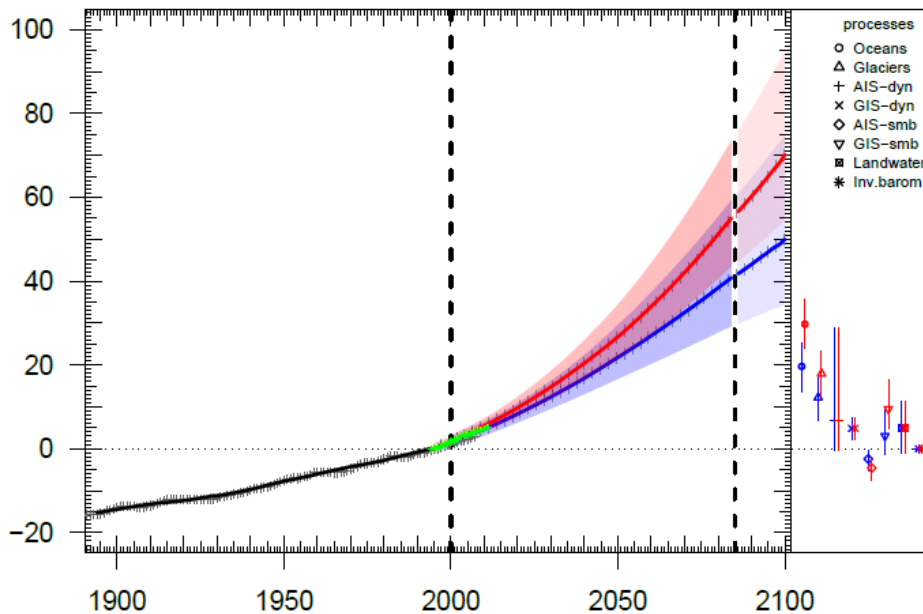


Figure 3.23: KNMI'14 scenarios for global mean sea-level rise and its likely range (shading), relative to 1986-2005 mean. The vertical axis denotes the 30-year running mean sea-level change in cm, while the horizontal axis denotes time. For years before 2000 and beyond 2085 (vertical dashed line), the mean was taken over a smaller window and is therefore drawn in a different shading. Natural variability at 5-year time-scale is included in the range and also shown as vertical bars. The black line denotes the 30-year running mean through the observations (1890-2009), symbols denote the 5-year running means. The green symbols indicate the 5-year running mean obtained from satellite altimetry (1993-2013) with respect to a reference period 1993-1998. The right margin of the plot shows the ranges from the different processes in 2100. Observational data: PSMSL database (Church and White 2011).

The quadratic-like shape reveals that the rate of sea-level change is estimated to increase with time in both scenarios. The largest contribution is from the ocean expansion. Second in line are the glaciers and small ice-caps. Especially near the end of the 21st century, however, the likely range strongly widens in both scenarios. This widening is caused partly by the relatively large model-uncertainty in the ocean component, but also by the very large range of the rapid dynamic component of the Antarctic Ice-Sheet (AIS-dyn), as can be seen from the process contributions in the right margin. This component is strongly asymmetric around the median (symbol), reflecting the large uncertainty in the upper-bound. The only negative contribution to global sea-level relates to the surface mass balance changes of Antarctica. Precipitation increase and hence increasing accumulation is the main driver behind this. Note that even at 5-year time-scale there is considerable variability in the observed global-mean sea level. This variability is well captured by the scenarios in the sense that the observed fluctuations fall within the initial width of the (overlapping) scenario ranges.

Table 3.3 and the right margin in Figure 3.23 show that all components have considerable associated uncertainties. Therefore, it is instructive to compare them for total rises near the lower and upper limit of the estimated ranges. Figure 3.24 shows such a comparison. It displays for sight year 2085 the process contributions for a high W-scenario (values within 2.5cm of the upper limit of the estimated range of the "High" distribution) and a low G-scenario (values within 2.5cm of the lower limit of the estimated range of the "Low" distribution). The low "Low" scenario has markedly smaller contributions from all components. However, the largest difference between these two extremes comes from the AIS-dyn component, reflecting the very large uncertainty in this component.

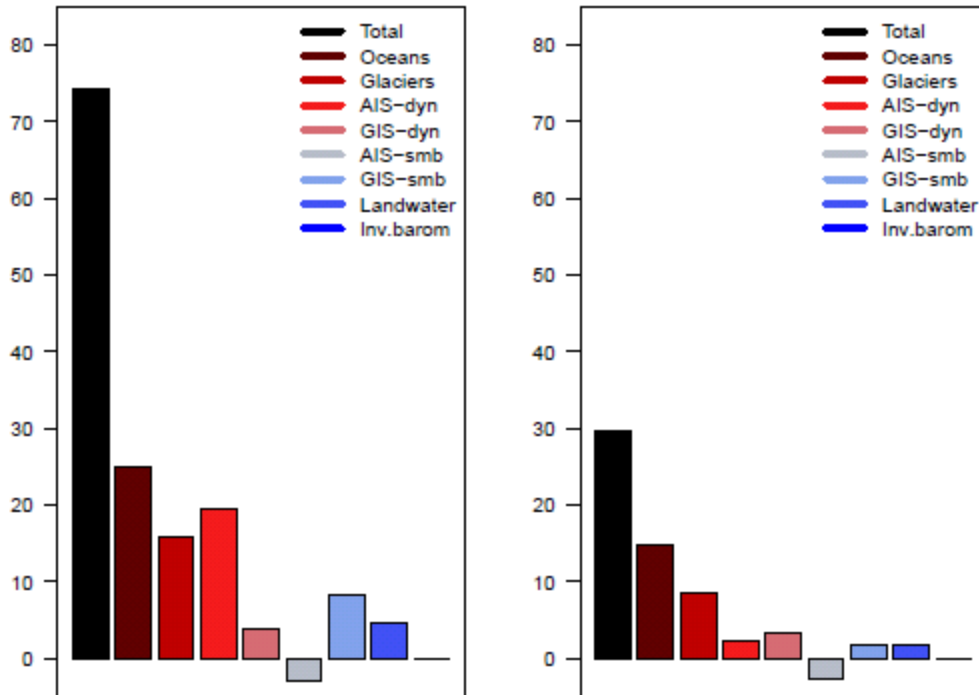


Figure 3.24: Extremes in the KNMI scenarios for global mean sea-level rise. Mean contribution in 2085 from the different components for (left) high “High” scenario (values within 2.5cm of the upper limit of the estimated range) and (right) the low “Low” scenario (values within 2.5cm of the lower limit of the estimated range).

### Regional response

#### North-East Atlantic Ocean

Figure 3.25 shows the scenarios for the North East Atlantic. The scenario ranges now are lower than for the global mean (Figure 3.23), and by comparing the right margins, one can notice that although the ocean contribution and that of the AIS-dyn are somewhat larger than in case of the global mean, the other terms are smaller, with three components yielding negative central estimates. Since these terms all have been parameterized using global mean temperature, the differences are a direct consequence of the mass-redistribution, and the associated fingerprint fields (Figure 3.21 and Figure 3.22). Observations of 6 stations along the Dutch coast are also included, as well as the observations from satellite altimetry of the North Atlantic.

#### North Sea

Figure 3.26 finally shows the result for the North Sea region (defined as the sea within the rectangular box bounded by 3.5°W–7.5°E and 51°–60°N). The natural variability simulated by the scenarios on the 5-year timescale (vertical dashes) now fits well with the amplitude of the natural variability in the observational record. The 30-year running-averages also attach smoothly to the scenarios. While the possible and uncertain contribution from Antarctica is large, changes in the GIS result in marginal sea-level changes for the North Sea.

As with the global scenarios it is useful to compare the extremes. Figure 3.27 shows for sight year 2085 the process contributions for a high W-scenario (within 2.5cm of the upper limit of the estimated range of the “High” distribution) and a low G-scenario (within 2.5cm of the lower limit of the estimated range of the “Low” distribution). As in the global case (Figure 3.24), the largest difference between these two extremes come from the AIS-dyn component, but also the ocean contribution is much higher in the high scenario, reflecting both the difference in scenario temperatures and the relatively large model uncertainty in this area.

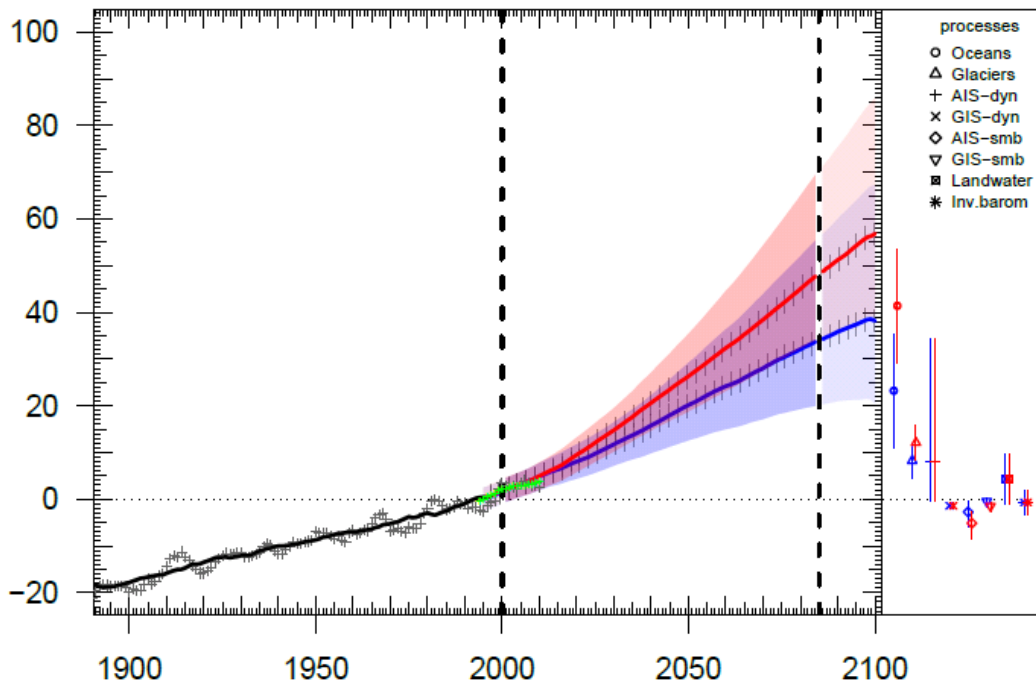


Figure 3.25: As Figure 3.23 but for the North East Atlantic (25W-10E,40-65N). The green symbols indicate the 5-year running means obtained from satellite altimetry (1993-2013) over the North Atlantic, with respect to 1993-1998. As there is no North East Atlantic estimate available, observational data (black) consists of the average of 6 stations in The Netherlands (source observations: Permanent Service for Mean Sea Level, <http://www.psmsl.org>).

### Gridded response

In addition to the time-series for the specific target areas, scenarios have been constructed for each geographical location separately. This has been done only for the target sight years of 2050 and 2085 and using a smaller sample-size. The results then assume the form of gridded maps, which can be used to examine the spatial robustness of the local scenarios discussed previously. Note that for fields that have been created using the fingerprinting technique, the sign of a local quantile response may differ from the global value (cf., Figure 3.22). One therefore has to be cautious in trying to explain geographical differences of the gridded maps by common physical causes, especially of the terms that have been determined using fingerprinting (and therefore also of the “total”).

Figure 3.28 shows the lower-bound (P05) and upper-bound (P95) for the “Low” and “High” scenario in 2085 for the North Atlantic. One can notice a clear South-east to North-west gradient in the scenario values, mostly related to the fingerprint of Greenland. This gradient in the scenario patterns is a motivation to indeed use the North Sea scenario values as the ones most relevant to the Netherlands. However, despite the better agreement with the observations, there are reasons to be cautious in zooming in too strongly in to a particular region of the globe, such as the North Sea. Perhaps the most important caveat is the regional pattern of expansion related to changes in ocean dynamics. At present the confidence in the ability of climate models to simulate these changes correctly is low, due to their coarse resolution. Well known biases in ocean circulation in the northeast Atlantic are a too zonal North Atlantic Current, which in the observations is steered by the Mid Atlantic ridge, a feature only simulated by ocean models at  $0.25^\circ$  resolution or higher. This bias causes the subpolar gyre to extend too far to the east, resulting in too large sea-surface height (SSH) gradients in the north eastern basin. This may affect the simulated dynamical response when the subpolar gyre is projected to weaken. Also, the connection between shelf sea (North Sea) and deep ocean is not well resolved in climate models. Gradients in SSH between shelf sea and deep ocean may exist and can be associated with slope currents, but these features are absent in coarse resolution climate models.

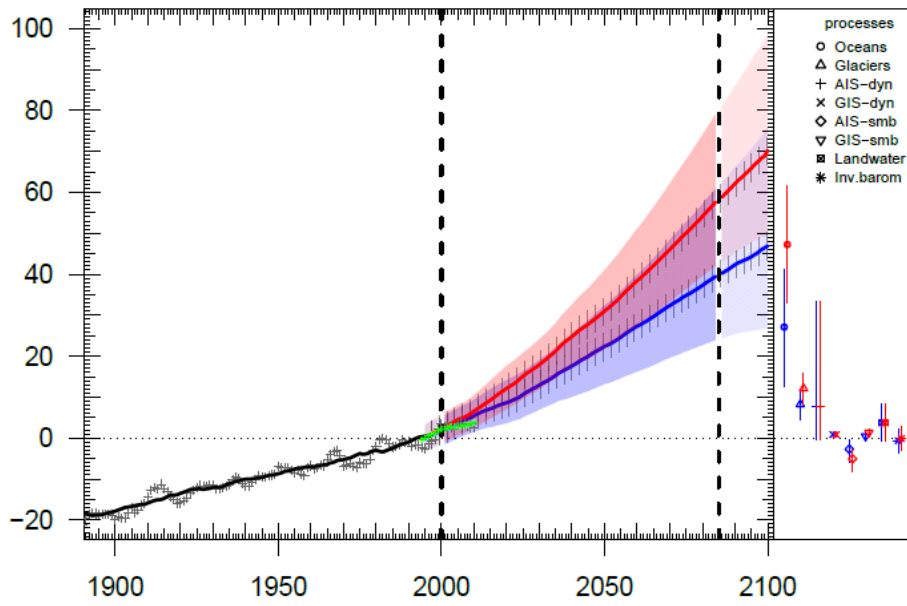


Figure 3.26: As in Figure 3.23 but for the North Sea area. Observational data consists of the average of 6 stations in The Netherlands. The green symbols indicate the 5-year running means obtained from satellite altimetry (1993-2013) over the North Atlantic, with respect to 1993-1998. (source observations: Permanent Service for Mean Sea Level, <http://www.psmsl.org>).

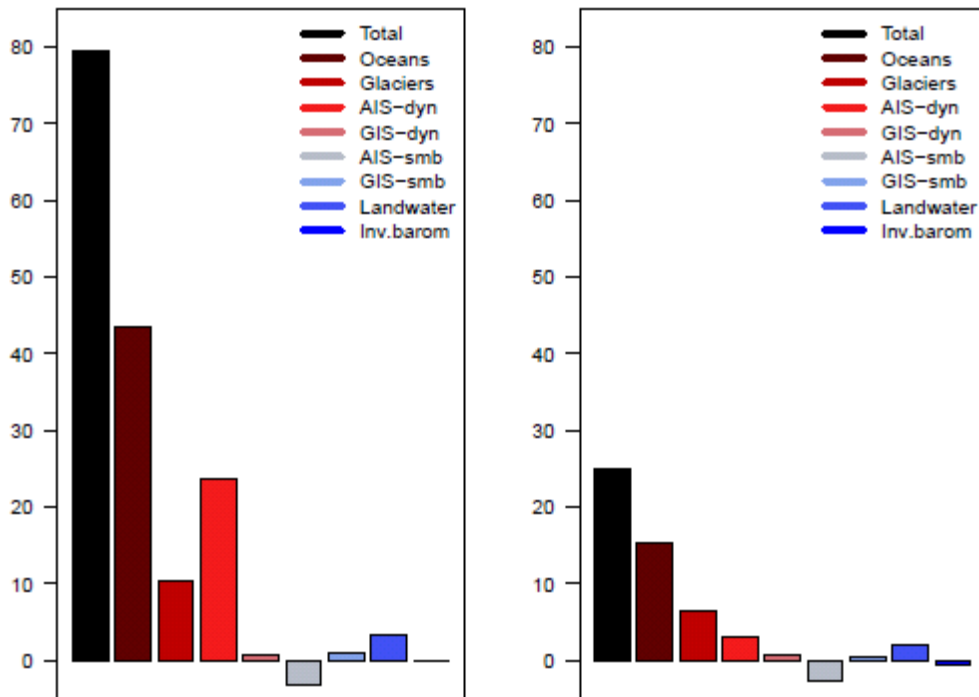


Figure 3.27: Extremes in the KNMI scenarios for sea-level rise in the North Sea. Mean contribution in 2085 from the different components for (left) high “High” scenario (values within 2.5cm of the upper limit of the estimated range) and (right) the low “Low” scenario (values within 2.5cm of the lower limit of the estimated range).

### 3.2.6 Conclusion and discussion

In this chapter a set of KNMI sea-level scenarios has been developed for the North Sea. They have been constructed using global temperature as the main steering variable. Two scenarios are proposed (“Low” and “High”). Uncertainty in each of the scenarios is included by expressing the scenario values as likely ranges. Each likely range is set as the 5-95% percentile ranges obtained from a distribution of sea-level projections for the 21st century. This distribution is formed by combining many physical processes that contribute to sea-level rise. The scenario values are listed in Table 3.2 (rounded to 5cm precision), and in Table 3.3 with contributions from separate processes.

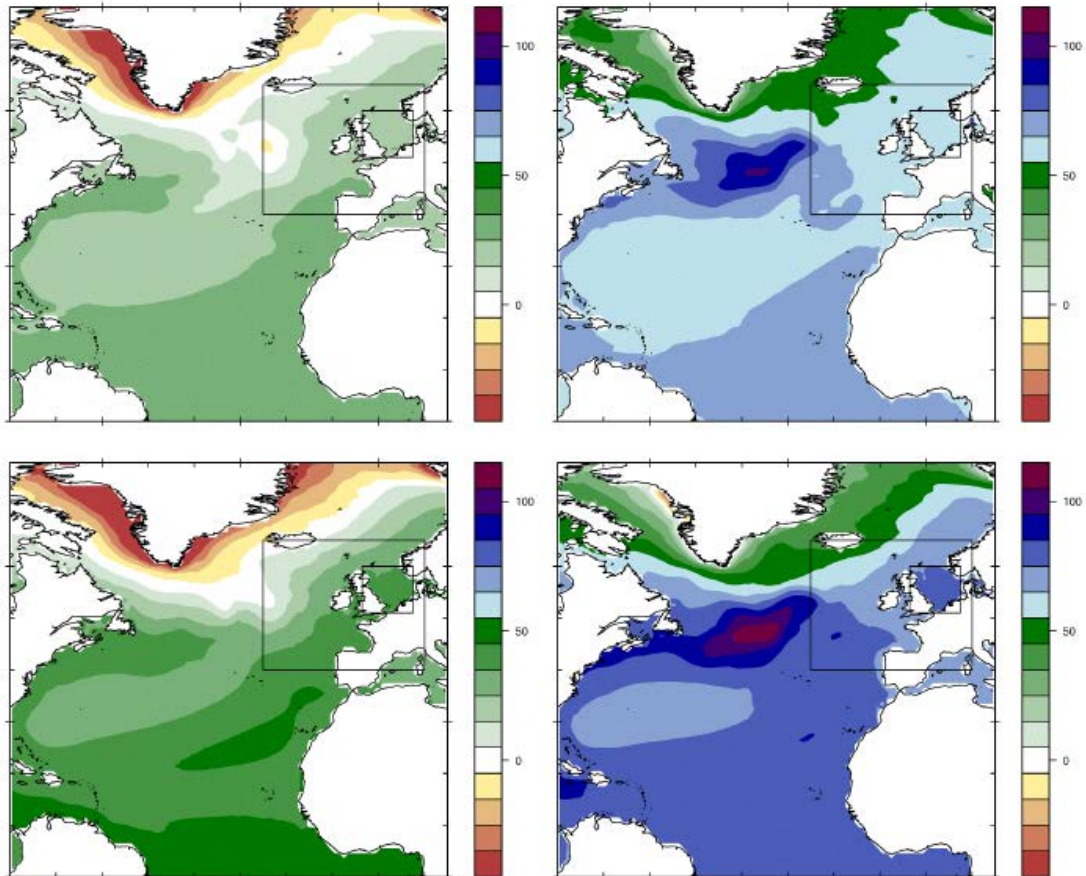


Figure 3.28: (top) Lower bound (P05) and Upper bound (P95) for “Low” scenario in 2085. (bottom) Same but for “High” scenario.

Results can be compared to the previous scenarios (KNMI'06, Van den Hurk et al. 2007). Comparing sight year 2050, the upper-bound of KNMI'14 is about 5cm higher than KNMI'06. Part of this difference can be accounted for by the different range definitions (KNMI'06 used 10-90% of the model-based range, whereas KNMI'14 uses 5-95% range for consistency with IPCC AR5). Also, the AIS-DYN component is significantly larger in the new scenarios (see section 3.2.4). Finally, the “Oceans” (expansion + dynamics) contribution is larger in the new scenarios. We have already noticed that this component is larger for the North Sea than for the North-East Atlantic on which KNMI'06 was based.

However, it is clear that the new scenarios result in higher values in 2100 than the estimations in KNMI'06. In fact, the KNMI'06 2100 results are similar to the new scenario results in 2085. The differences can be accounted for partly by the different range-definitions, but even the 10-90% range of KNMI'14 is still about 5cm higher in 2100 (not shown). The mean glacier contribution is higher in KNMI'14, as well as the Landwater contribution. Furthermore, both the North Sea and the North East Atlantic have a higher estimated contribution from the “Oceans” than in the KNMI'06 scenarios. A further systematic difference with respect to the KNMI'06 is related to the way the effects from Antarctica and Greenland are taken into account in KNMI'14. In KNMI'06 no fingerprinting technique was used, and only the global-mean estimates were taken.

### 3.3 Extreme wind

#### 3.3.1 Introduction: scope and model quality assessment.

This chapter describes projected changes in large-scale winds over the Netherlands and the North Sea. Possible changes of small-scale wind events associated with strong convection (thunderstorms) are treated in section 3.5.

Traditionally, analyses of wind climate are restricted to near-surface winds (typically  $U_{10}$ , the wind at a height of 10 m), and particular attention is paid to high wind speeds that may cause damage, either directly, or indirectly by causing high waves on the sea and storm surges. The proliferation of wind turbines makes it necessary to widen the analysis to winds at higher vertical levels and to low winds. The typical hub height of modern wind turbines is 100 m, with a rotor diameter of the same order. For their operation the wind in the lower 150 m or so of the troposphere is relevant. The typical threshold wind speed below which no electricity is produced is 5 m/s. If periods with such low-wind conditions were to increase the turbine would produce less energy than it was designed for, reducing their revenues and posing a risk to energy supply.

As for any climate variable, projections of wind are based on the results of climate models. It is therefore important to know to what extent these models are capable of reproducing the current wind climate. Van Ulden and van Oldenborgh (2006) investigated the ability of CMIP3 models to reproduce the monthly-mean large-scale flow over Europe. Out of the 23 models investigated, only five represented the flow over Central Europe reasonably, while the others produced too zonal a flow, with westerlies dominating too much. This dominance of westerly winds still holds for the CMIP5 models as recently shown by Brands et al. (2013), Lee et al. (2013) and (Zappa et al. 2013b). However, these papers show that the zonal flow is underestimated over Northern Europe, and that in most models the boundary between over- and under-estimation runs across the North Sea, so that the model bias has a minimum in the region considered here. For one particular model (ECHAM5/MPI-OM) Sterl et al. (2009) showed that the overrepresentation of westerly winds also holds for extreme winds (here winds exceeding 8 Bf or 17 m/s), at least in the southern part of the basin. For the same model they showed that pressure fields over the North Sea area, especially those leading to very high wind speeds, are realistically simulated, and that a surge model driven by the model winds reproduces realistic water levels along the southern coast of the North Sea. De Winter et al. (2013) investigated extreme wind cases as simulated by 12 CMIP5 models by fitting a Gumbel distribution to the annual maxima of daily-mean wind speed ( $U_{10}^{\text{amx}(dm)}$ ). Values for the location parameters and associated 100-year return values ( $U_{100}$ ) differ by several m/s between the models (see Figure 3.29a and Table 3.5). Interestingly, there is no relation between the models' horizontal resolution and their simulated maximum wind speeds (Table 3.5). For example, the two models with the lowest resolution (CanESM2 and MIROC-ESM-CHEM) produce respectively the highest and second to lowest  $U_{100}$  values.

Compared to ERA-Interim (Dee et al. 2011) some models overestimate high wind speeds, while others underestimate them. De Winter et al. (2013) also investigate the directional distribution of strong winds. They find a shift from northerly to westerly directions as compared to ERA-Interim (see Figure 3.30) that is comparable to that of Sterl et al. (2009).

A substantial part of the conclusions in this report relies on results from the EC-Earth climate model. For this model Hazeleger et al. (2012) show that differences of sea level pressure with ERA-40 are smaller than 2 hPa, making EC-Earth better than any CMIP3 model in this respect. Especially the dominant pressure pattern over the North Atlantic (the NAO) is reproduced well, albeit with too low variability. Figure 3.29a and Table 3.5 show that the characteristics of high wind speeds compare well with those of ERA-Interim. The analysis of Zappa et al. (2013) shows that the characteristics of extra-tropical cyclones in EC-Earth are very close to those of several reanalyses. This success in simulating a realistic wind climate over the North Sea region makes us confident that EC-Earth is a good model to investigate global-warming induced changes of the wind climate in the North Sea region.

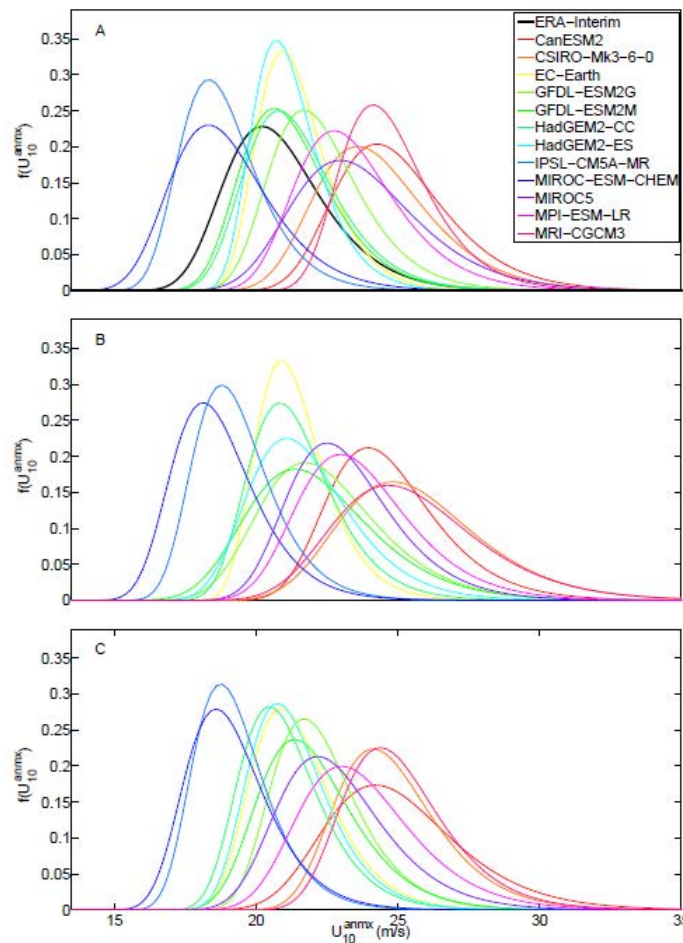


Figure 3.29: Gumbel distributions of  $U_{10}^{amax(dm)}$  for each of the CMIP5 models. The maxima over a box covering the southern North Sea (53 - 57°N, 1 - 7°E) are used. The fit has actually been done to  $(U_{10}^{amax(dm)})^2$  to speed up convergence and transformed to be linear in  $U_{10}^{amax(dm)}$ . The three panels are for the present climate and the RCP4.5 and RCP8.5 projections, respectively. The corresponding fit for ERA-Interim is given as a reference in panel (a) (from De Winter et al. 2013).

### Regionalization

Winds at the coast are higher than those land-inward, where the winds slow down due to the much higher surface roughness over land. However, this does not mean that trends or changes of wind speeds should vary over the country. We here deal with winds produced by large scale pressure systems, systems that are much larger than the Netherlands. It is therefore hard to see why trends in wind speed should be different in different parts of the country. This argumentation is backed by model results. As Figure 3.32 (to be discussed later) shows, projected trends of annual-maximum winds do not show large variations over the Netherlands. Furthermore, the trends are small and mostly insignificant, so that any detected differences in trends is meaningless. Similar results are obtained from daily-mean or monthly-mean wind speeds.

As discussed below, increasing land surface roughness has had an impact on wind speeds over land. If future land surface roughness changes are inhomogeneously distributed over the country, this may lead to regional differences in trends. It is, however, beyond the scope of this report to assess the development of land surface roughness. Taking these arguments together, we conclude that it is neither necessary nor possible to assess regional differences in the future development of wind speeds.

### 3.3.2 Observations - past changes

#### In the North Sea

Storminess (climate of high winds) and windiness (climate of mean wind) in the North-East Atlantic Ocean and the North Sea have shown large, highly correlated variations during the 20<sup>th</sup> century. The driving force for these

low-frequency variations is not fully understood. Any projected future changes must be compared with these natural fluctuations.

Table 3.4: Models used in the study of investigated by De Winter et al. (2013), their horizontal resolution and an indication of their performance a high winds. The corresponding values for ERA-Interim are given as a reference.  $\lambda$  and  $\varphi$  are the increments in longitudinal and meridional direction, respectively, in degrees. The increments in latitudinal direction are averages as some models use non-constant (e.g., Gaussian) latitudes. The last two columns display the location parameter ( $\mu$ ) of a Gumbel fit to annual-maximum daily-mean wind speeds ( $U^{amx(dm)}_{10}$ ) and the corresponding 100-year return values ( $U_{100}$ ) for the historical period 1951-2000 over the southern North Sea (53 - 57°N, 1 - 7°E) (both in m/s).

Model	longitude		latitude		$\mu$	$U_{100}$
	#pts	$\Delta\lambda$	#pts	$\Delta\varphi$		
ERA-Int		0.7		0.7	20.1	26.5
CanESM2	128	2.8125	64	2.8125	24.1	31.5
CSIRO-Mk3-6-0	192	1.875	96	1.875	23.4	30.8
EC-Earth	320	1.125	160	1.125	20.9	25.5
GFDL-ESM2G	144	2.5	90	2.0	21.6	27.5
GFDL-ESM2M	144	2.5	90	2.0	20.5	26.4
HadGEM2-CC	192	1.875	144	1.25	20.7	26.6
HadGEM2-ES	192	1.875	144	1.25	20.7	25.1
IPSL-CM5A-MR	144	2.5	143	1.25	18.2	23.3
MIROC5	256	1.41	128	1.41	22.8	30.8
MIROC-ESM-CHEM	128	2.8125	64	2.8125	18.2	24.5
MPI-ESM-LR	192	1.875	96	1.875	22.6	29.3
MRI-CGCM3	320	1.125	160	1.125	24.0	29.9

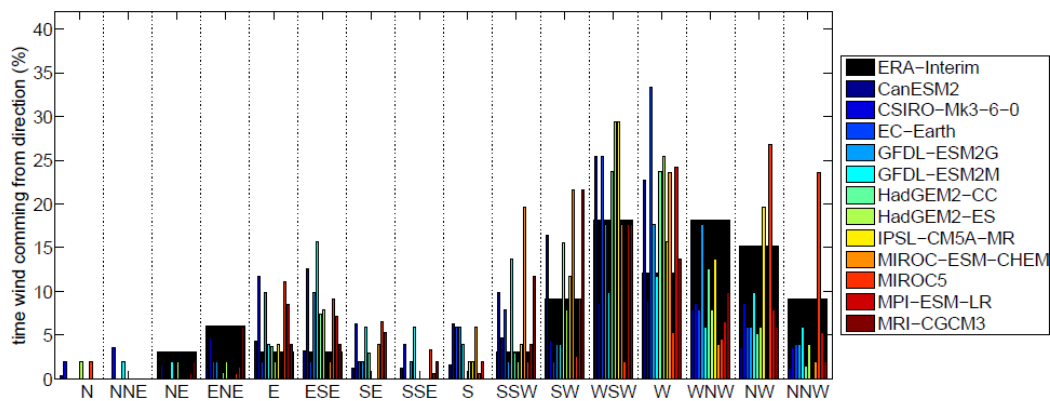


Figure 3.30: Percentage of time for  $U^{amx(dm)}_{10}$  to come from the indicated directions. The values for ERA-Interim are given by the thick black bars, and for the historical runs by the thin coloured ones. Values are for the area 53 - 57°N, 1 - 7°E in the southern North Sea (from De Winter et al. 2013).

Long-term direct wind observations are sparse, prone to errors and not available over the open sea. An indirect measure of storminess can be obtained by calculating the average geostrophic wind within a triangle from surface pressure measurements at the corner points. Pressure has been measured for a long time with great precision at several locations. Following earlier work by Alexandersson et al. (2000) and Wang et al. (2009), who investigated the whole north-east Atlantic, Bakker and Hurk (2012) investigated several pressure triangles covering the North Sea. Confirming results from the earlier work they find large interannual variations superimposed on a low-frequency evolution with higher values at the beginning and end of the 20<sup>th</sup> century and lower values at mid-century (Figure 3.31). Since the 1950s, storminess and windiness rose until the beginning of the 1990s, when a maximum was reached, which, however, was not exceptional when compared to the late 19th century. Since then both wind indicators are sharply declining over the North Sea. There is no discernible trend over the whole period of 140 years.

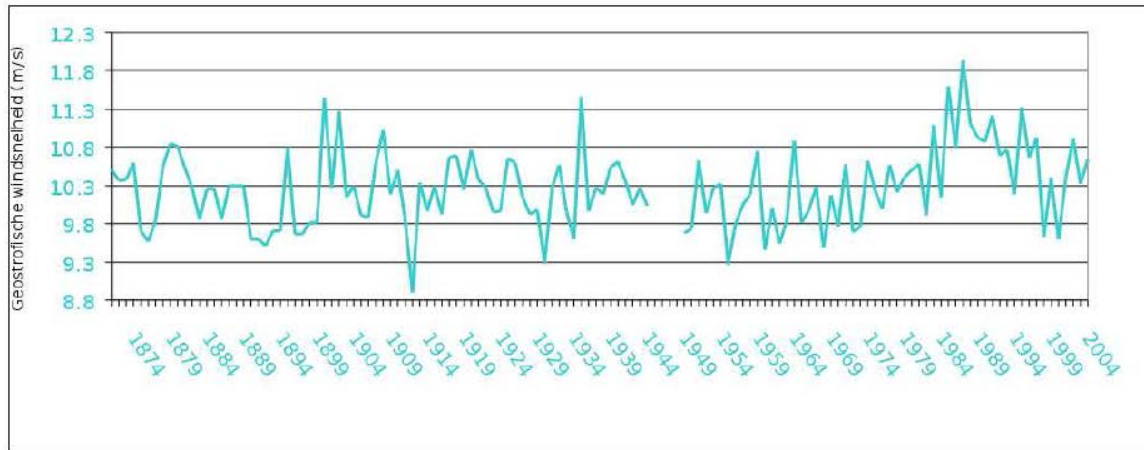


Figure 3.31: Annual-mean geostrophic wind (as a measure of windiness) for the pressure triangle Aberdeen-Tyboron-De Bilt, which covers the whole southern North Sea.

### Over land

Smits et al. (2005) notice that surface winds (10 m height) over land in the Netherlands exhibit a decreasing trend between 1962 and 2002, while geostrophic winds based on a pressure triangle covering the country show no trend. Vautard et al. (2010) show that this decrease is not limited to the Netherlands, but a widespread phenomenon of the Northern Hemisphere. They ascribe between 25% and 60% of the decrease between 1979 and 2008 to increased surface roughness over land. For the Netherlands, Wever (2012) estimates that surface roughness increase accounts for up to 70% of the observed wind speed reduction over the 1981-2009 period. He finds negative trends in annual-mean winds of typically 0.25 m/s per decade for inland stations, but no significant trends for coastal ones. Bakker et al. (2013) investigated several indices related to wind-power production over the period 1988-2010 and found that they were decreasing. However, they found no convincing evidence for surface roughness changes being a major cause. This difference with the results of Vautard et al. (2010) and Wever (2012) can partly be explained by the different periods used. It is important to note that Vautard et al. (2010) find no or even a positive wind speed trend away from the surface where the influence of the surface is small. This has implications for wind energy generation as modern wind turbines have a hub height of about 100 m. However, Bakker et al. (2013) show that also indices based on actual wind power generation show a decreasing trend.

Cusack (2013) analysed 101 years (1910-2010) of wind measurements at five stations in the Netherlands. He focuses on potentially damaging storms which he defines as storms in which the daily maximum wind speed,  $U_{10}^{dmx}$ , exceeds its climatological 99%-ile. Both the number of potentially damaging storms per year and their loss index, which is proportional to  $(U_{10}^{dmx})^3$ , show high inter-annual variability and decadal-scale variations, but no long-term trend. Both variables reach their highest values at the beginning and the end of the 20th century, showing that the low-frequency variations found in the pressure triangle results (Figure 3.31) over sea extend onto land. The number of potentially damaging storms reaches an additional maximum in the middle of the century, which is mainly due to relatively weak storms, and an absolute minimum at the beginning of the 21st century.

### 3.3.3 Projections for the future

#### KNMI'06, CMIP3, AR4, and the Delta Committee

The KNMI'06 wind scenario was derived from CMIP3 model output. The main result was that "the wind scenarios give small changes compared to the typical interannual variability of the scenario variable" (p 49 in Van den Hurk et al. 2006). A similar conclusion was reached by IPCC's Fourth Assessment Report (AR4). Sterl et al. (2009) presented a literature survey (which originally was performed for the Delta Committee (Katsman et al. 2011)), in which they reinforce the earlier conclusions: Modelled wind speed changes in the North Sea differ between models and are usually small when compared to natural variability.

These results are mainly based on the output of Global Climate Models (GCMs) with a typical horizontal resolution of 150 km or more. To investigate the impact of climate change on smaller spatial scales, the output of such models is used to drive a Regional Climate Model (RCM) which covers a limited area of the Earth (typically Europe) at a higher resolution. Using output from an ensemble of RCMs, driven by various GCMs,

Nikulin et al. (2011) find no significant changes in the 20-year return wind speed over the North Sea, and Pryor et al. (2012) find no changes in the strength of winds gusts. Both studies back the results obtained using GCMs alone.

### CMIP5

Since the work of the Delta Committee a new generation of climate models has been developed and used to generate climate projections in the CMIP5 project (Taylor et al. 2011). Using output from these models several authors have investigated changes in the frequency and intensity of storms. Harvey et al. (2012) and Chang et al. (2012) conclude that wind speed changes over western Europe are smaller than natural variability. Instead of studying wind speed, Mizuta (2012) uses the CMIP5 models to investigate extra-tropical cyclone numbers and cyclone growth rates. He finds that changes in these variables are small in the North Atlantic, and that they differ between models. Eichler et al. (2013) find a decrease of storm frequency, but an increase of storm intensity in the North Atlantic, which, however, does not extend into the North Sea region. Zappa et al. (2013) analyse storm tracks in 22 CMIP5 models. While they find decreasing trends in cyclone number and frequency in most of the North Atlantic and Europe, they find a small region over the British Isles and the southern North Sea with an increasing trend. Although the signal is small (less than 1% in wind speed!), they find it to be significant as it is consistent among models.

Based on these and other papers the AR5 concludes (sec. 14.6.3) “There is high confidence that the global number of extra-tropical cyclones is unlikely to decrease by more than a few percent due to anthropogenic change. There is high confidence that a small poleward shift is likely in the Southern Hemisphere storm track, but the magnitude is model-dependent. There is medium confidence that a poleward shift in the N. Pacific storm track is more likely than not and that it is unlikely that the response of the N. Atlantic storm track is a simple poleward shift. There is low confidence in the magnitude of regional storm track changes, and the impact of such changes on regional surface climate.”

Concluding, papers published so far suggest no significant changes of the wind climate in the north-east Atlantic under climate warming. Natural variability is large and dominant and remains so for the century to come. In the following sections we zoom in on the North Sea area to see whether this large-scale picture remains valid for our neighbourhood.

### The North Sea area in CMIP5 models

We are interested in possible changes of the most extreme wind speeds as these cause the largest damage. Naturally, wind speeds averaged over a short period can reach higher values than those averaged over a longer period. However, in order to have an appreciable impact on water level (surge height) or wave height, such winds have to last for at least several hours. Therefore, De Winter et al. (2013) analysed daily-mean wind output (10-m wind,  $U_{10}$ ) from twelve CMIP5 models (Table 3.5). For some of the models several runs were available. They assess differences between the two 50-year periods 2051-2100 and 1951-2000 for two forcing scenarios (RCP4.5 and RCP8.5). Figure 3.32 shows the differences in the average annual-maximum daily-mean wind speed ( $U_{10}^{\text{amx(dm)}}$ ) for each of the twelve models for the RCP8.5 scenario. These differences appear to differ widely between models, but in all cases the changes are small. In general, they are not significant in the open North Sea. Over land some models show statistically significant changes, but without agreeing on their sign.

The annual-maxima from a large box in the southern North Sea have been fitted to a Gumbel distribution. The resulting fits are shown in Figure 3.29, and their location parameters and the corresponding 100-year return values are given in Table 3.5. A fit using ERA-Interim (Dee et al. 2011) is plotted as reference in the upper panel. The models show a wide spread around the semi-observational ERA-Interim, reflecting the large sensitivity of annual maxima to model formulation, e.g., parametrizations. Comparison between the three panels shows only small differences. Differences between the models are much larger than projected changes. This is reflected in the return values (not shown), for which changes usually fall within the 95% confidence intervals of the present distribution. These results are a direct consequence of the fact that changes in annual maxima are not significant (see above).

De Winter et al. (2013) find indications for maximum winds coming more often from westerly directions and less often from northerly ones (see Figure 3.32), confirming the results of Van den Hurk et al. (2006) and Sterl et al. (2009). Winds from westerly directions are less dangerous for the Dutch coast as their fetch is shorter, resulting in smaller storm surges.

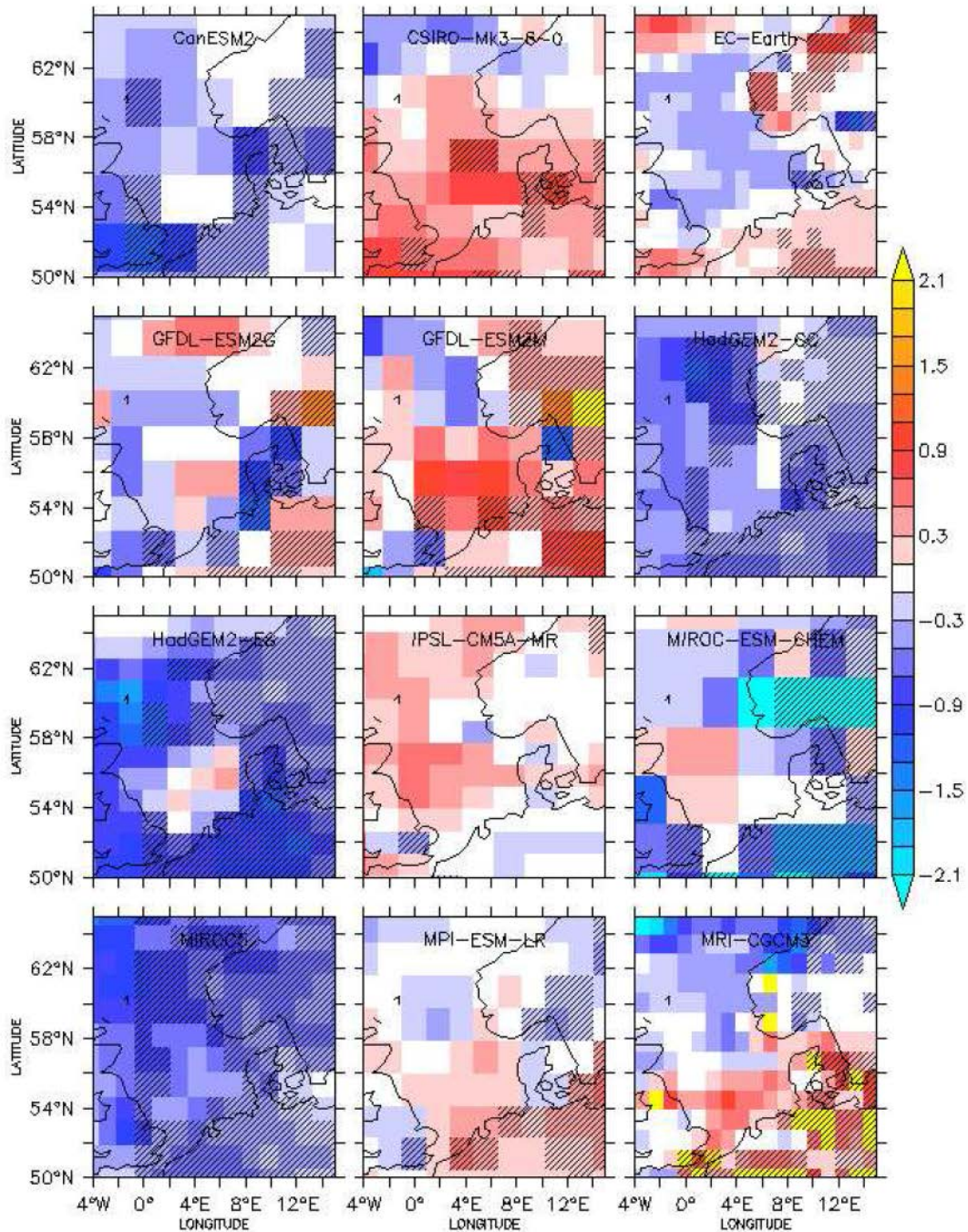


Figure 3.32: Difference in  $U^{amx(dm)}_{10}$  (in m/s) between 2050-2100 in RCP8.5 and 1950-2000 for each of the twelve CMIP5 models investigated. Hatching denotes grid points where the changes are significant at the 95% level (from De Winter et al. 2013).

Figure 3.34 shows the *annual-mean wind speed change* (2071-2100 relative to 1976-2005) from the KNMI EC-Earth runs. Note that the data for the period 1976-2005 are from the historic EC-Earth run, not from observations. The changes are all negative, but non-significant. Splitting the results into months (not shown) reveals that the mean wind speed decreases in almost all months. Only in late summer and early autumn (Sept./Oct.) some increases do appear. However, neither the positive nor the negative changes are significant at the 95% level for any month.

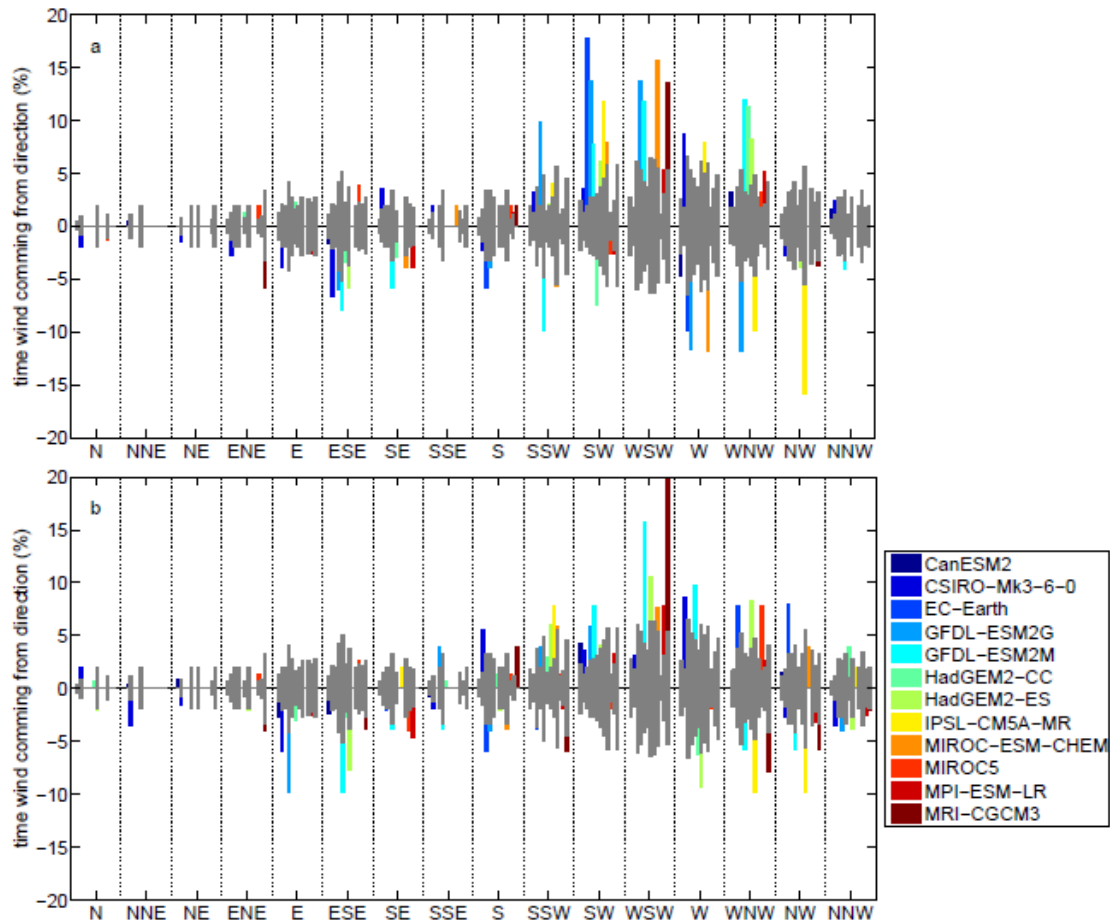


Figure 3.33: Changes in the percentage of time that  $U_{10}^{anmx(dm)}$  is projected to come from a certain direction (a) RCP4.5 - historical, (b) RCP8.5 - historical. In gray, the standard deviation of the historical run is depicted as an indication of the statistical uncertainty. Values are for the box 53 - 57°N, 1 - 7°E in the southern North Sea (from De Winter et al. 2013).

Prolonged periods of *low wind* can be a problem for the wind energy sector. We here present an assessment of possible changes of the frequency of low-wind events. We define a low wind day as a day with a mean  $U_{10}$  of less than 5 m/s. Recall that at wind speeds lower than 5 m/s a turbine would produce no electricity. Figure 3.35 shows the number of such days for a location in the southern North Sea as derived from the EC-Earth scenario runs. The frequency of low-wind days varies around 6 per month, with large inter-annual and inter-decadal variations, but no long-term trend. The two future scenarios show no signs of a systematic difference between each other or with the historical period. Repeating the same analysis for a threshold of 3 m/s or a land point gives a similar picture. Of course, the mean frequency changes ( 1.4 d/mon for the sea point and 9 d/mon for the land point (5°E, 51°N), both for a 3 m/s threshold), but the variability remains large and no long-term trend can be discerned. We therefore conclude that systematic changes in the frequency of low-wind days are not to be expected.

### Downscaling

To obtain information on smaller scales than resolved by GCMs we use RACMO (Van Meijgaard et al. 2008) to dynamically downscale results from EC-Earth. Due to their higher resolution RCMs can generate higher extremes, as extremes are usually confined to small spatial areas. Eight EC-Earth runs have been downscaled, and from these runs conditions that best comply with the four scenarios (W/W+ and G/G+) have been selected (see section 3.1.2). As differences between the resampled runs are not significant, only results from the basic downscaled runs are shown here.

### EC–Earth: wind (ann. mean)

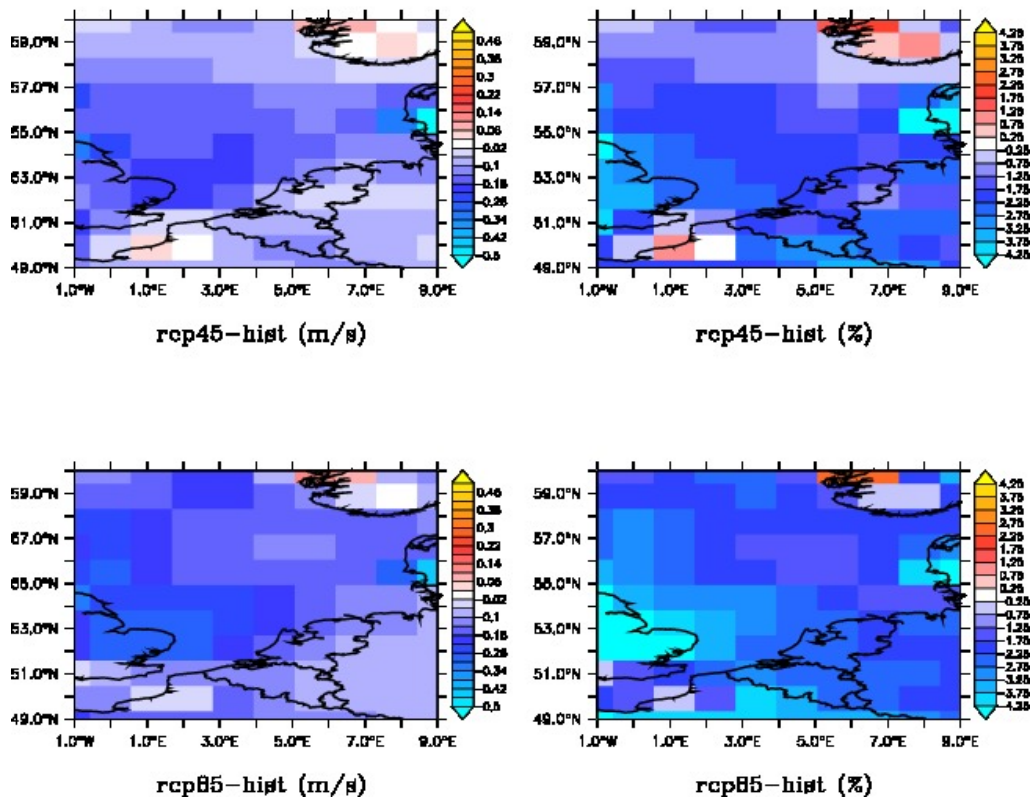


Figure 3.34: Differences in annual-mean wind speed between 2071-2100 and 1976-2005 from the EC-Earth runs (one run for the historical period, one for each of the two scenarios). The upper (lower) row is for RCP4.5 (RCP8.5). The left (right) column gives absolute (relative) differences.

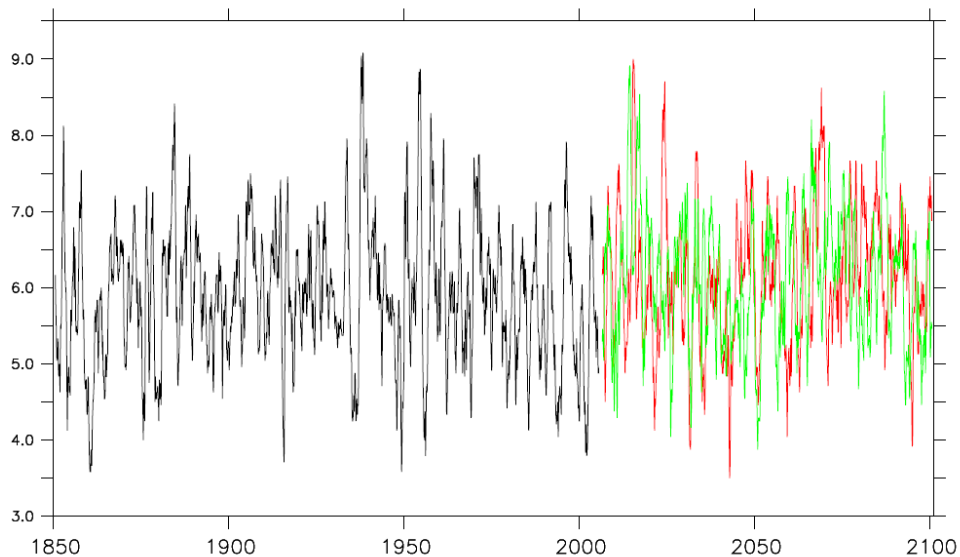


Figure 3.35: Number of low-wind days (daily-mean  $U_{10} < 5$  m/s) per month according to EC-Earth historic (black), RCP4.5 (red) and RCP8.5 (green) scenario runs for the point (4 °E, 54 °N) on the North Sea. A 12 month running-mean filter has been applied to the data to enhance visibility.

In Figure 3.36 we present 100-year return values ( $U_{100}$ ) for wind speed as derived from the downscaled RACMO data. The 100-year return values were determined from a Gumbel fit to the annual-maxima of daily-maximum 10-m wind speeds. Note that this is different from De Winter et al. (2013) who used annual-maxima of daily means. Therefore, the 100-year return values from RACMO shown in Figure 8 are higher than those

from CMIP5 as given in Figure 3.29. However, daily-mean and daily-max values show the same trends in EC-Earth (not shown). Panels (a) and (b) show  $U_{100}$  values for respectively the historical period (1981-2010) and the end of this century (2071-2100), and panel (c) their difference. The difference pattern is noisy and consists of patches of increasing or decreasing  $U_{100}$ , suggesting that the changes are probably not significant. To formally estimate the significance of these changes we divide the differences by an estimate of the uncertainty of the difference in panel (d). The following uncertainty measure is used. For each of the two periods we generate

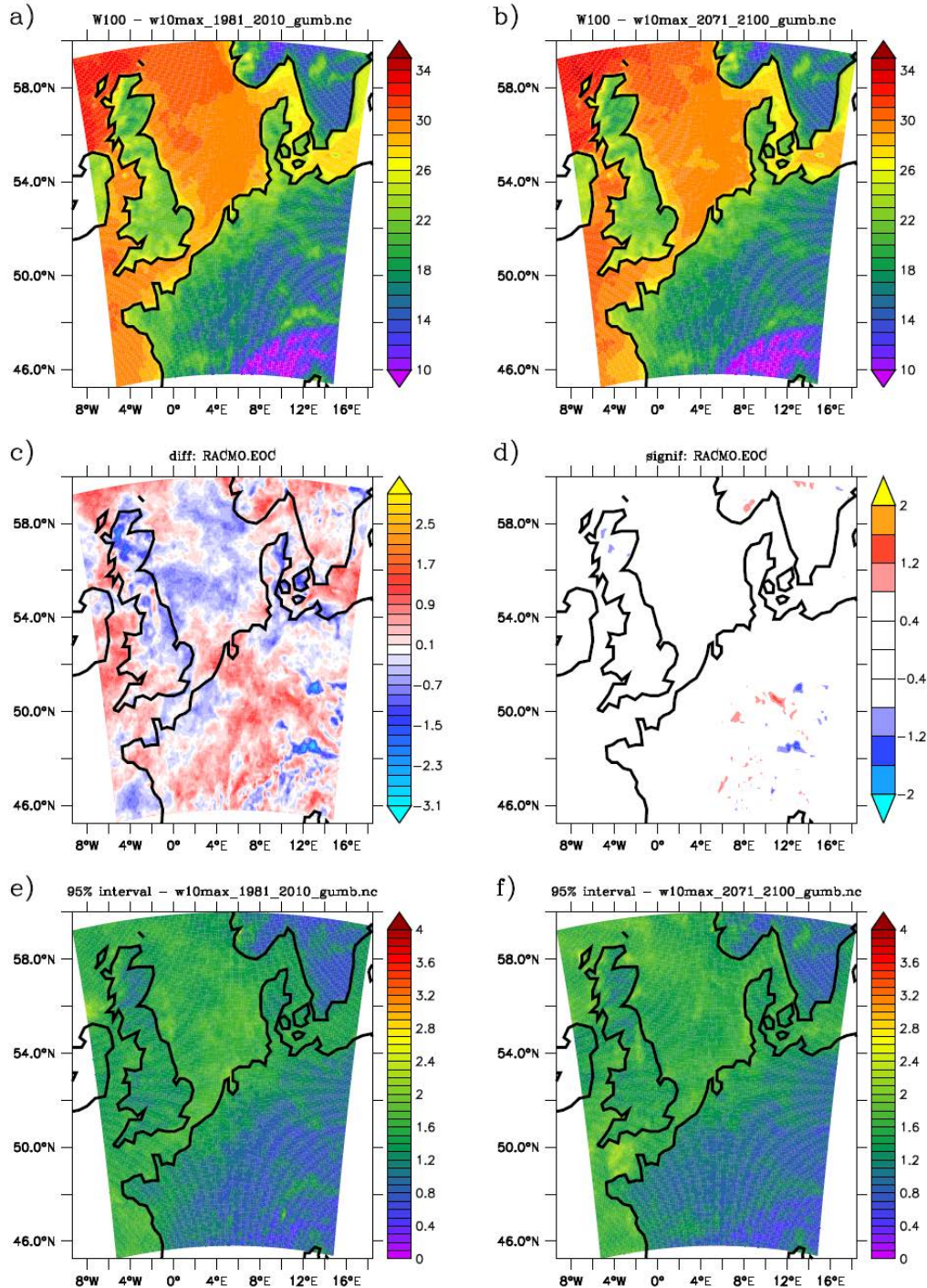


Figure 3.36: 100-year return values of daily-maximum wind speed as obtained from a Gumbel fit to the RACMO output for (a) the historical period (1981-2010) and (b) the last 30 years of the 21st century (2071-2100). Their difference is given in (c), and (d) shows the difference divided by the spread  $\sigma_{95}^{tot}$  of  $U_{100}$  values as obtained from bootstrapping the data 1000 times. Panels (e) and (f) show the spreads ( $\sigma_{95}$ ) for the two periods.

1000  $U_{100}$  values by bootstrapping and take the 95% interval of these 1000 values,  $\sigma_{95}$ . The final uncertainty measure is obtained by quadratically adding the  $\sigma_{95}$  values for the two periods. Panels (e) and (f) show that the uncertainty (spread of bootstrapped values) is the same for the two periods, indicating that the variability does not change. Panel (d) is mainly white, indicating that the simulated differences in  $U_{100}$  are smaller than their uncertainty. In other words, the changes are not significant.

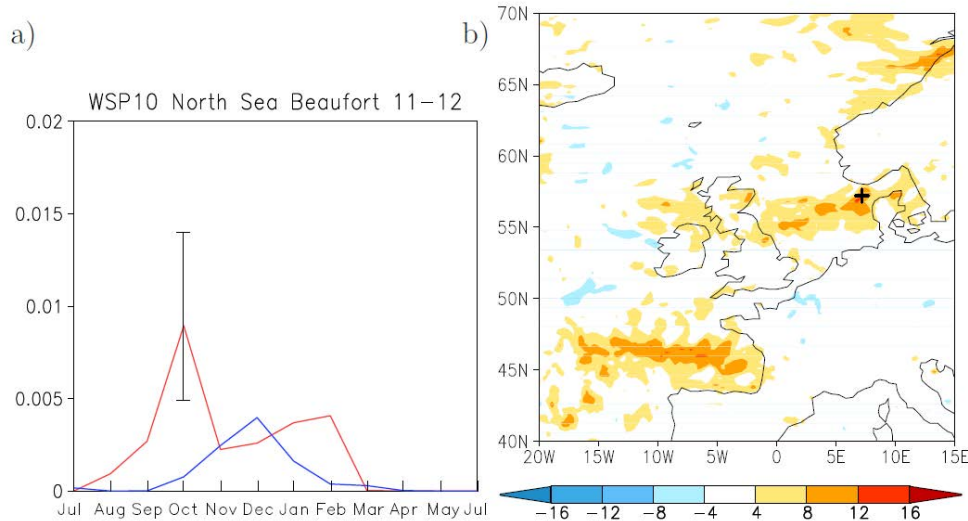


Figure 3.37: Wind speed changes over the 21st century in the North Sea region in the high resolution run. (a) Frequency distribution of the area-averaged 3-hourly 10 m wind speed ( $U_{10}$ ) for Beaufort 11-12 ( $U_{10} > 28.4$  m/s) for present (blue) and future (red) conditions. The frequency is multiplied by 102. The 95% significance interval based on a Poisson distribution for the future peak in October is indicated by a vertical bar. (b) Wind speed change (m/s) for the period August-October between future and present conditions. Results are significant at 95% confidence level (from Haarsma et al. 2013b).

### High-resolution global modelling

Regional climate models get their lateral boundary conditions from a global model. Therefore, their mean conditions cannot deviate much from that of the driving GCM. Especially, events not resolved by the GCM that occur outside of the area covered by the RCM cannot influence the course of events inside that area. To allow small-scale events that happen far away from Europe to influence European weather a model has to be used that has a high resolution everywhere. Running a fully coupled climate model at such a resolution is still not feasible due to computational constraints. In an attempt to circumvent this constraint Haarsma et al. (2013) have run a high-resolution version of the atmospheric component of EC-Earth driven by prescribed SSTs taken from coarse-resolution climate model runs. This approach avoids running an ocean model at high resolution. Nevertheless, computational costs were still so high that only two 30-year time slices (present and future, represented by 2004 and 2096, respectively) could be run. For the North Sea region the runs project an increasing number of severe storms (Bf 11 and higher) and an earlier onset of the storm season (Figure 3.37). This is caused by tropical cyclones (hurricanes) being able to reach Europe more easily in a warmer climate. This has two reasons. Tropical cyclones can only be generated over regions where SST exceeds  $27^{\circ}\text{C}$ . In a warmer climate this region is larger, extending further eastward than at present. Therefore, the hurricanes can be generated further eastward in the subtropical Atlantic, i.e., closer to Europe. Furthermore, their path to Europe leads over warmer water, keeping them strong. Although they are formally no longer tropical storms when arriving in Europe as they have undergone a transition to an extratropical storm, they are still extraordinarily strong and change the storm climatology significantly. In the relatively coarse state-of-the-art climate models like EC-Earth this mechanism cannot be simulated because tropical cyclones cannot develop properly.

The results of Haarsma et al. (2013b) are based on only one model. They obviously need confirmation by other models run in a similar set-up. Furthermore, it cannot be excluded that the missing interaction between the atmosphere and the ocean that is caused by prescribing SST prevents the cyclones from weakening on their way to Europe. However, if other models confirm the possibility of tropical cyclones to reach Europe more research is needed to investigate the consequences. Storms earlier in the year can cause more damage than

the same storm in winter because trees still have their leaves and provide more drag, and because more outdoor activities take place. Furthermore, the heavy rains that accompany the formerly tropical storms may cause problems, too. As the storms move west-east across the North Sea their fetch is relatively short, so that their effect on wave heights and storm surges is probably modest.

### 3.3.4 Construction of the wind scenarios

As shown above, neither the CMIP5 runs nor the downscaling RACMO runs do suggest a change in wind climate that systematically exceeds the large natural variability. However, the RACMO runs have been re-sampled to take into account possible systematic changes in the large-scale atmospheric circulation that are not captured by EC-Earth, the model driving RACMO. Four different scenarios were thus created (section 2.3). These resampled runs constitute the basis for the scenarios numbers given in the tables in section 4. The numbers for wind are based on daily-mean output at grid point 4.74°E, 52.96°N, the sea-point closest to Den Helder.

The two thirty-year intervals 2036-2065 and 2071-2100 were considered representative of mid-century and end-century conditions, respectively. Reference values were calculated from the period 1981-2010. Given that there are eight resampled runs for each of the four scenarios, this choice results in 240 years of data for each of the periods and each of the scenarios.

For each of the three periods (reference plus two future) and each of the four scenarios, several statistics were calculated, among them the mean wind, certain percentiles, and the number of days with wind speed above certain thresholds, as well as directional distributions. Changes were then calculated as the relative (percentage) difference between the future and the reference period.

The directional distribution was calculated for 30°-sectors, with the first sector centred on North. For the category *number of days between south and west* the four sectors spanning 165°-285° were lumped together. The final results can be found in Table 4.2 and Table 4.3.

### 3.3.5 Conclusions

- The storm climate in and around the North Sea is very variable. Observations show decadal-scale variations, but no long-term trend over the past 130+ years.
- Results from recent state-of-the-art climate models as well as RCM studies suggest no changes in the wind climate. This is true for mean wind conditions, low wind conditions and extreme wind speeds. Modelled changes are statistically insignificant. *Confirms KNMI'06*
- The climate models point to an increasing frequency of extremes coming from westerly directions. *Confirms KNMI'06*
- Results from a high-resolution atmosphere-only model run suggest that in a warmer climate tropical cyclones can reach the North Sea. They do so before the classical storm season, leading to very high wind speeds (Bf 11 and more) already in September. These results need confirmation from other models, and their impact has to be investigated. *New result since KNMI'06.*

## 3.4 Relative humidity, solar radiation, evaporation and drought

### 3.4.1 Observed trends

The **annual sum of solar radiation** is calculated for the De Bilt 1958-2013. The trend line is calculated for the 1981-2013 period only (disregarding the earlier data) to make the trend estimate comparable with those presented in IPCC-AR5 report (IPCC 2013c; p.184), where widespread brightening after 1980 is mentioned.

Figure 3.38 shows the annual sum of solar radiation in De Bilt and the linear trend line for the 1981-2013 period. The values on the trend line in 1981 and 2013 equal 339.6 and 369.7 kJ/cm<sup>2</sup>, respectively. The total increase between 1981 and 2013 equals 30.1 kJ/cm<sup>2</sup> (8.9%). When we consider the whole 1958-2013 period (not shown), the increase equals 6.7%.

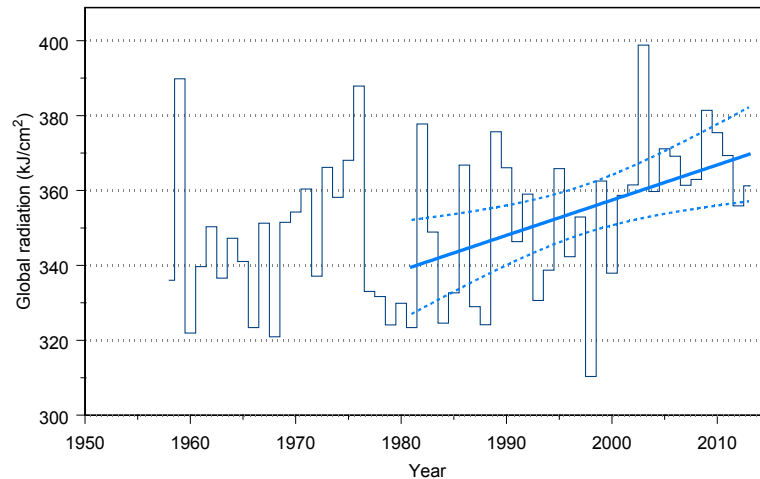


Figure 3.38: Annual sum of solar radiation for the De Bilt 1958-2013. The straight line represent a linear regression fit for the 1981-2013 period. The dashed lines give the 95% confidence bounds.

**Potential evaporation** is the evaporation occurring when there are no limitations in water supply, i.e. the soil moisture content does not restrict plant growth and evaporation directly from the soil. Here we consider the total potential evaporation for De Bilt in the growing season (1 April – 30 September) as calculated with the formula of Makkink (see section 2.4.1).

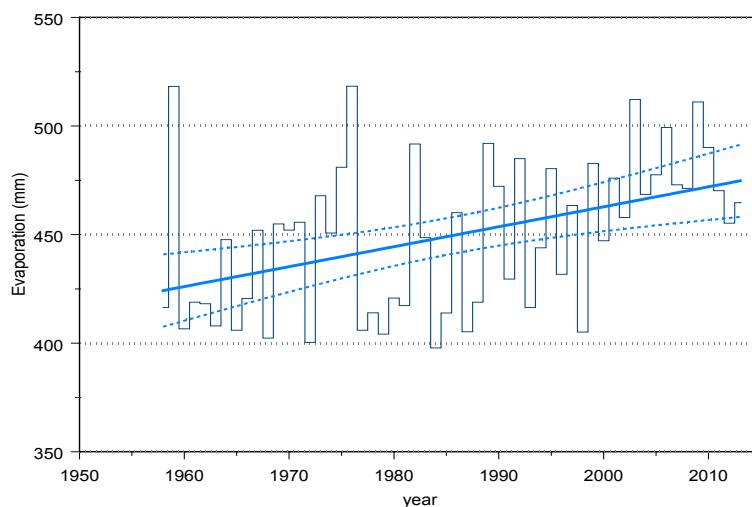


Figure 3.39: Sum of potential evaporation in the growing season (1 April – 30 September) for the De Bilt 1958-2013. The straight line represent a linear regression fit. The dashed lines give the 95% confidence bounds.

Figure 3.39 shows the linear trend line for the cumulative growing season potential evaporation in De Bilt. The values on the trend line in 1958 and 2013 equal 424.2 and 474.7 mm, respectively. The total increase between 1958 and 2013 equals 50.5 mm (11.9%).

### 3.4.2 Seasonal and monthly responses

#### **Relative humidity**

Changes in the seasonal mean relative humidity are taken directly from the RACMO2 re-samples for region MON (see Figure 3.9).

#### **Solar radiation**

Changes in the seasonal and monthly mean solar radiation  $Q$  are taken directly from the RACMO2 re-samples for region MON (see section 3.1.4 and Figure 3.9). The monthly mean changes are used for the transformation of the daily solar radiation time series for the period 1981 – 2010 (similar to the procedure for temperature

described in section 3.1.5). Apart from the constraint that the surface downwelling radiation should not exceed 70% of the Top of Atmosphere (TOA) incoming radiation flux, a linear transformation is applied:

$$Q^f = \min(a_i Q^c, 0.7Q_{TOA}) \quad (3.7)$$

where, as before, superscripts *c* and *f* refer to reference and future time series, and *a<sub>i</sub>* is a monthly varying transformation coefficient derived from the model output.

The transformed solar radiation time series is used (together with the transformed temperature time series) to determine the evaporation scenario's (see below).

### Potential Evaporation

Evaporation is calculated from daily solar radiation and daily temperature according to the Makkink formula for potential evaporation (section 2.4.1). To determine the change in the (Makkink) evaporation the Makkink formula is applied to the transformed daily temperature (see section 3.1.5) and transformed daily solar radiation time series for the period 1981 – 2010 (see above). The difference in seasonal/monthly Makkink evaporation from the original 1981 – 2010 temperature and solar radiation series and the transformed 1981 – 2010 temperature and solar radiation series gives the scenario change values for evaporation presented in chapter 4.

### Drought and precipitation deficit

Similar to the Makkink evaporation the scenario change values of the mean maximum and one in 10-year precipitation deficit are obtained from the difference between the transformed precipitation deficit time series for 1981 – 2010 and the original transformed precipitation deficit time series for that period. The 'transformed precipitation deficit' time series is easily obtained from the transformed precipitation time series (see section 3.1.5) and the transformed (Makkink) evaporation time series (see previous paragraph). The statistics of the precipitation deficit in the transformed time series are calculated in exactly the same way as those in the original time series. The scenario change values for the change in the once in 10 year precipitation deficit correspond to the average changes of the driest three years (1995, 2003 and 1989) in the 1981 – 2010 period based on the 'transformed' precipitation deficit series.

## 3.5 Extreme weather

Direct output from global climate models (i.e EC-Earth) and even of Regional Climate Models (RACMO) give limited information on the occurrence of extreme events such as extreme precipitation, thunderstorms and fog. This is partly due to their limited numerical resolution but even more so due to the fact that the essential dynamical and physical processes are missing. Non-hydrostatic effects play a key role in the mesoscale organisation of deep moist convection leading to squall lines, cold pools, super cells etc, and hazardous weather often occurs in the presence of these mesoscale organisation. Since EC-Earth and RACMO are hydrostatic models they are not well capable of representing such phenomena, let alone, trends of such events in a perturbed climate. The use of a high resolution non-hydrostatic model (such as HARMONIE) is not feasible for the coming 5~10 years as the computer resources do not allow climate integrations beyond a period of a few years at the most. For fog and visibility there are similar problems. One of the key ingredients for the formation and occurrence of fog and low visibilities is the presence of cloud condensation nuclei (CCN) and the condensation processes of moisture on these CCN. As the influence of CCN concentrations on cloud condensation processes are not represented in the current climate and weather models (i.e. EC-Earth, RACMO and HARMONIE), the model output can not be used directly to make statements on the trends of fog, haze and visibility in the current and future climate.

For the KNMI'14 scenarios model output is used that correlates well with the extreme events of interest. This model output is used either as direct predictors for trends of these events or as input in off-line models that do represent these events in a physically sound way. In addition use is made of conceptual models that further support and elucidate the physical mechanisms behind these correlations in order to build up physical evidence for the reliability of the detected trends of the extreme events of interest.

For extreme precipitation the approach is described in section 3.1.6. For thunderstorms and hail events observed relationships of the occurrence of such events with CAPE and deep shear are used. For fog and visibility an offline model is used that determines the trends of visibility in present and future climate as a function of aerosol concentrations and modelled trends in near surface relative humidity.

### 3.5.1 Hail and Thunderstorms.

#### Methodology

Thunderstorms and their associated phenomena such as hail and wind gusts are increasingly recognized as an important hazard to life and property in the Netherlands. However little is known about the effects of climate change on occurrence of these phenomena. Direct climate model output is of limited value since these phenomena are poorly resolved. Indirect climate model output that are well known to correlate well with the occurrence of thunderstorms are the vertical stability of the atmosphere such as measured by the convective available potential energy (CAPE) and the vertical wind shear as measured by the Deep Layer Shear (DLS) defined as the maximum wind difference in the lowest 6 km of the atmosphere. High values of both these quantities support the occurrence of severe weather conditions.

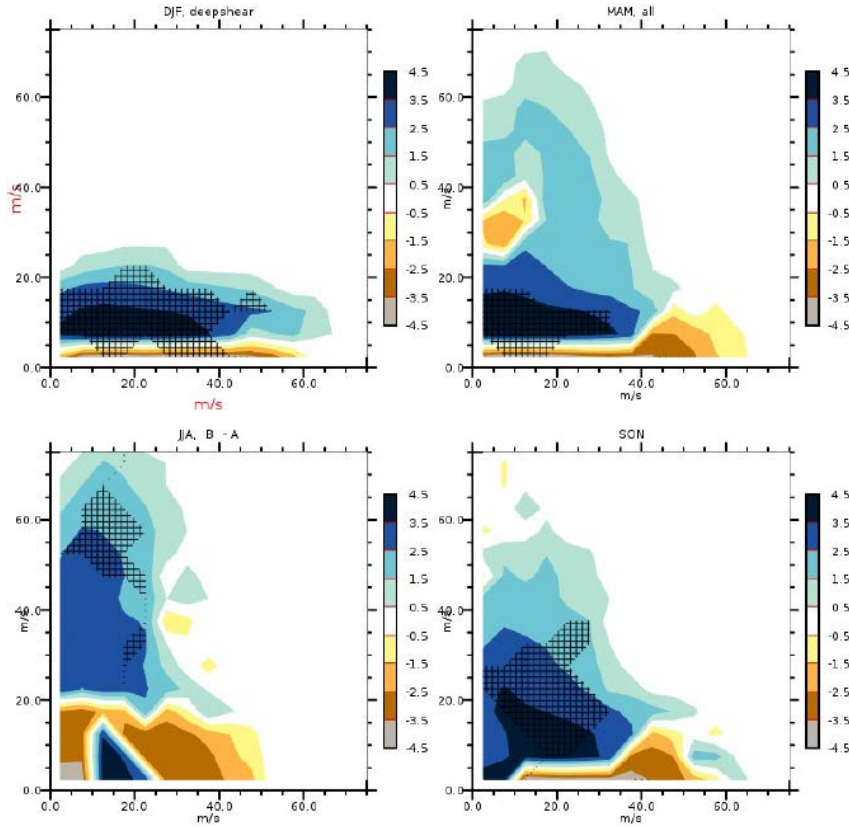


Figure 3.40: Change of frequency for Deep Layer Shear (DLS) on the horizontal axis and the square root of CAPE on the vertical axis for Winter (upper panel left), Spring (upper panel right), Summer (lower panel left) and Autumn (lower panel right) for 17 representative grid points in the Netherlands

This notion can be made more precise if we define  $P$  as the probability of occurrence of severe weather events as a function of CAPE and DLS, and  $f$  as the frequency of occurrence of these parameters or “proxies”. The number of severe weather events  $N$  can then be obtained by the product of the probability of occurrence of these events ( $P$ ) and the frequency of occurrence of the proxies, integrated over all values of the proxies CAPE (denoted by  $x_{CAPE}$ ) and DLS denoted by  $x_{DLS}$  as:

$$N = \iint P f dx_{CAPE} dx_{DLS} \quad (3.8)$$

It should be noted that the probability of occurrence of extreme events is large for high numbers of these proxies while the frequency of occurrence is large for small numbers of these proxies (see figure 1). So it is a priori difficult to estimate for which values of the integrand  $P \cdot f$  will peak, even in our present climate.

In our changing climate we are interested in the change  $\Delta N$  of the number of extreme weather events which can be written down to first order as

$$\Delta N = \iint \Delta P \cdot f dx_{CAPE} dx_{DLS} + \iint P \Delta f dx_{CAPE} dx_{DLS} \quad (3.9)$$

The first term describes the change in probability of extreme events, *given* certain values of CAPE and DLS. Such a change can occur if for instance the triggering probability of deep convection changes, for instance due to changes in the large scale vertical wind, a quantity that is known to influence the triggering of convection. This term is likely to be affected by large scale conditions and we will refer to it as *the large scale circulation term*. The second term describes the changes in frequency of occurrence of the local stability and shear and we will therefore refer to this term as the *thermodynamics term*. The large scale circulation term is difficult to estimate as the precise mechanisms of triggering are uncertain and not well represented in climate models; even in short term weather prediction there is uncertainty in estimating  $P$  in the presence of high CAPE and DLS. Making reliable statements on the change in  $P$  in a warming climate is not (yet) possible. For lack of better knowledge we will assume this term to be zero to first order. The thermodynamics term, on the other hand, can be obtained from climate model output through diagnosing the changes of frequencies in those areas in the phase space where the probability of occurrence is significantly larger than zero. The threshold values for which beyond severe weather can be expected has a wide range of uncertainty but should be around

$$CAPE \approx 1000 \sim 2000 \text{ m}^2 \text{ s}^{-2} \quad DLS \approx 10 \sim 15 \text{ ms}^{-1} \quad (3.10)$$

We will therefore assess, understand and quantify changes in the frequency of occurrence of CAPE and DLS and use these results to draw conclusions on the change of occurrence of thunderstorms.

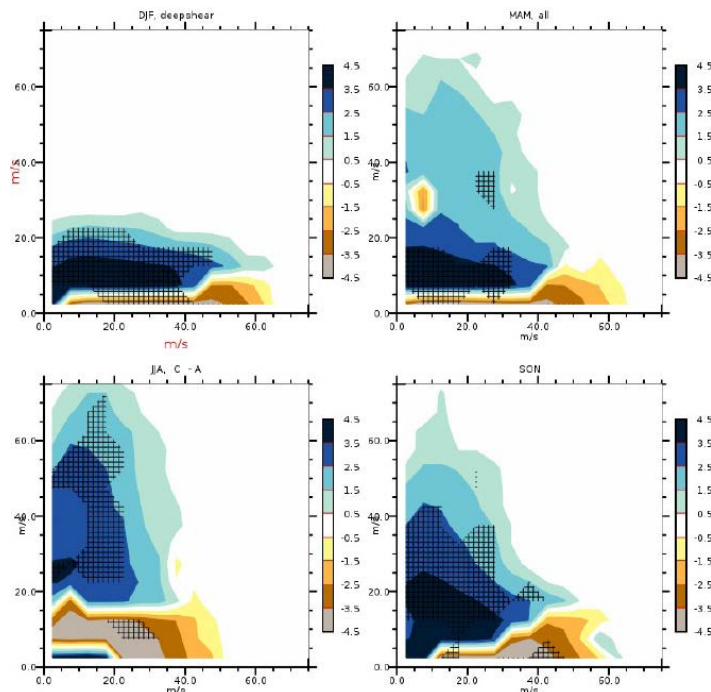


Figure 3.41: As Figure 3.40 but now the frequency difference plots are shown for the end of the century (2064-2095).

## Results

An 8-member ensemble future climate run (RCP8.5) of EC-Earth has been downscaled with RACMO. High frequency model results for 17 representative locations in the Netherlands have been retrieved. From this model output, joint frequency distributions  $f$  of  $\sqrt{CAPE}$  and DLS have been made for the periods 1981-2010 representing present climate, 2046-2075 representing near future climate and 2065-2094 representing end of the century climate. The frequency difference distribution  $\Delta f$  with respect to the present climate has been determined for both the near future climate and for the end of the century climate. Figure 3.40 shows the change in frequency for the near future per season, while Figure 3.41 shows similar results for the end of the century. From these figures we can conclude that an increase in especially CAPE can be observed for all seasons but increase in the that area of high values of CAPE and DLS exceeding the thresholds of Eq (3.10) is only expected in summer and, to a lesser extend in Autumn and Spring. Comparing Figure 3.40 and Figure 3.41 also shows that most of the increase in CAPE occurs in the near future with a relative less significant increase toward the end of the 21<sup>st</sup> century.

These results can be made more quantitative by concentrating on trends in the occurrence of high CAPE values. Figure 3.42a shows the trend of the change in the probability of exceedance (POE) of CAPE for the summer period (JJA). It shows that especially the frequency of occurrence for the large CAPE values are strongly increasing with time. In line with these results the trends of the 99, 99,9 and the 99,99 percentiles (Figure 3.42b) show an increasing trend with time as well although a flattening of trend can be observed toward the end of the century.

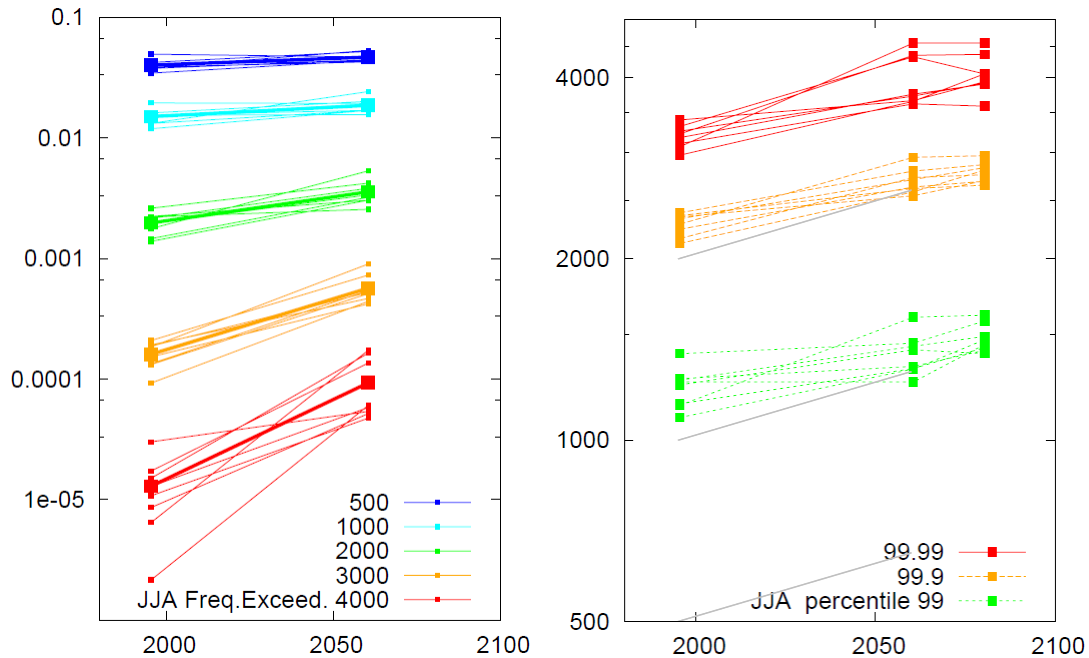


Figure 3.42: a) Probability of exceedance of CAPE as a function of time for a range of CAPE values and b) the trend of the high percentiles of CAPE.

The increasing trend in CAPE can be explained through the fact that the atmospheric warming in the midlatitudes is rather uniform with height (see Figure 3.18). This has to be contrasted with the tropics where the warming profile of the atmosphere follows the moist adiabat leading to an increasing warming with height. As shown by Loriaux et al. 2013), warming under a constant relative humidity following the moist adiabat, results in an invariant CAPE while a uniform warming with height leads to increase of CAPE of around 15% per K, consistent with the trends observed in Figure 3.42.

The levelling off of this trend in the second half of the century is probably due to the relative drying of the boundary layer in terms of the relative humidity. The decrease of the boundary layer relative humidity is a feature that is due to the fact that the increasing surface evaporation cannot keep up with the atmospheric warming as to maintain a constant relative humidity. Lower relative humidity leads to higher cloud base height and to lower CAPE values than in the case of constant relative humidity.

The effect of change in the probability distribution (the circulation term) has not been included in the analysis

### Conclusions

An assessment of trends in thunderstorms has been made using a trend analysis of CAPE and DLS in a warming climate over the Netherlands. A significant increasing trend of the large CAPE values (> 1000~2000 J/kg) can be obtained from all downscaled ensemble members of the rcp8.5 CMIP5 scenario's during the summer season. This increase can be attributed to the magnitude and the shape of the tropospheric warming profile which is to first order uniform with height leading to a stronger conditional instability as quantified by the CAPE. The high percentiles of summertime CAPE values show an increase of around 15%/K, a value that can be understood from idealized uniform warming under constant relative humidity conditions.

The levelling off in the latter half of the century may be attributed to the fact that the constant relative humidity is not maintained in the boundary layer leading to a smaller increase of CAPE. Lower boundary layer RH might also contribute in the change in the probability distribution (the circulation term) but this effect has not been taken into account.

In conclusion and based on the numerical and physical arguments sketched above, it is likely that both frequency and intensity of summertime thunderstorm will increase. It is difficult to give numbers but assuming the circulation term remains constant the results suggest at least a doubling of the frequency severe summertime thunderstorms for a 2K warming scenario. The levelling off the CAPE increase in the second half of the century suggests that the results will not scale linearly with temperature warming.

### 3.5.2 Visibility

In western Europe, fogs (i.e. visibility less than 1 km) have been on the decline for more than 30 years which has been attributed to a reduction in aerosol emissions (van Oldenborgh et al. 2010; Vautard et al. 2010). However, here it is shown that changes in hygroscopicity also play an important role in visibility trends. Observations of visibility in the period 1956 – 2010 are combined with scenarios of visibility in the period 2010 – 2100. Visibility observations were obtained from the five main climate stations in the Netherlands. Scenario calculations were based on aerosol composition scenarios obtained from global (TM5) and regional (LOTOS-EUROS) aerosol emission computations that were fed into RACMO-runs regionally downscaled from 9 members of EC-EARTH CMIP5-climate model runs. Using the shape of aerosol size spectra obtained from the EUCAARI-extended period (Kulmala et al. 2011; Asmi et al. 2011) at the climate station of Cabauw (2008-2011), and under the assumption that the shapes will not change in the next 90 years the mass scenarios were converted to yearly aerosol size spectra.

#### **Aerosol Mass Model and Hygroscopicity**

The aerosol masses were redistributed into insoluble black carbon [BC1], soluble black carbon [BC2], insoluble organic aerosol [OA1], soluble organic carbon [OA2], soluble oceanic organic aerosols [OAS], sulphuric acid anion sulphate [SO4], ammonium [NH3] and nitrogen acid anion, nitrate [NO3], sodium cation [Na-mixed], chloride anion [Cl-mixed], mineral dust [DUS] and externally mixed sodium chloride [NaCl-unmixed]. The time series from 1955 – 2100 of the twelve species are shown in Figure 3.43.

There is a strong reduction in BC and OA aerosols in the period 1955 – 1990. In the same period SO4 peaks around 1980 and then decreases, while the masses of NH3 and NO3 both increase. When observing the relative proportions of the various species it is apparent that the water chemistry in the Netherlands is undergoing a transition from a sulphur-based chemistry as was the case in 1960- 1980 to a nitrogen-based chemistry from present day onwards until 2100. Overall there is a decrease in aerosol mass throughout the entire period of 145 years. Half of this decrease takes place in the first 55 years, the other half in the last 90 years. The naturally occurring aerosol masses of Na, Cl, OAS and DUS are kept constant over the entire period as there is no reason to believe that any of these is subject to a systematic change.

A separation was made between the aerosol group of [BC1, BC2, OA1, OA2, OAS, DUS] and the group of inorganic aerosols [SO4, NH3, NO3, Na, CL]. The hygroscopicities (often designated by a factor  $k$ ) of individual species in the first group were simply assigned values according to what has been reported in the literature [0.0,0.4,0.0,0.4,0.4,0.1]. For the group of the inorganic soluble aerosols no hygroscopicity can be assigned to individual cations or anions and they are assumed to interact. The interaction is simulated by means of the water chemistry model ISORROPIA (Nenes et al. 1998). From the given composition a volume-weighted hygroscopicity of the inorganic mixture was calculated to be ranging from  $k = 0.65 - 0.75$ . It should be noted that most uncertainty in the aerosol mass assignment in the period 1956 – 2010 is in the specification of the BC and OA types as there is little or no information about their exact value.

#### **Conversion of aerosol mass to number concentration and optical calculations**

Here we use two premises from which the size distribution are reconstructed 1) The distributions conform to the lognormal shape of distribution as observed during the EUCAARI – extended period (2008 – 2011) at the climate station of Cabauw (Asmi et al. 2011), and 2) The shapes of the distributions do not change over time, only the total aerosol concentration. Under these two assumptions the mass per species can be calculated from the third moment of the lognormal distribution or vice versa. At Cabauw there is significant year-to-year variation in aerosol concentration. For the years 2008 – 2010, the mean aerosol concentrations in the range up to a radius of 0.5  $\mu\text{m}$  were respectively 8394,7388, and 6948  $\text{cm}^{-3}$ . In contrast, there was not much change in the shape of the aerosol distribution suggesting that the shape is region-dependent, and may indeed be less changeable over time. Next, Mie-calculations were performed and tables of optical extinction values were constructed using the species-dependent hygroscopicity and complex index of refraction.

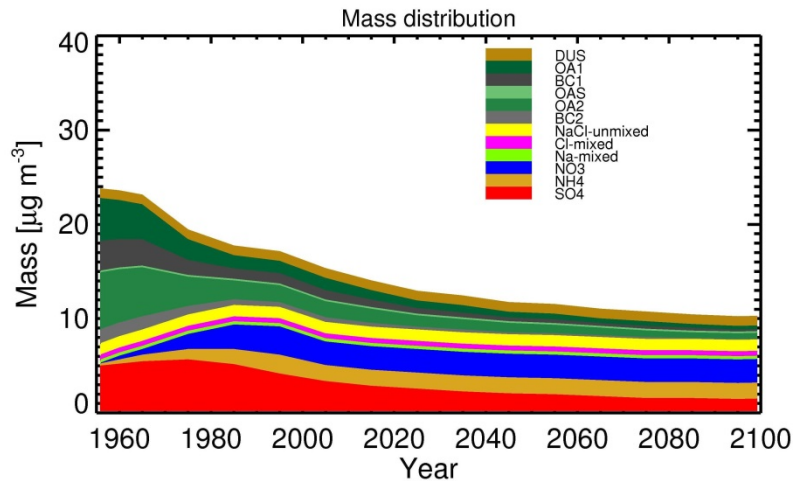


Figure 3.43: Near surface aerosol mass and composition, [re]constructed using a combination of model output modified and adjusted in part by observations. Aerosol masses are distributed into insoluble black carbon [BC1], soluble black carbon [BC2], insoluble organic aerosol [OA1], soluble organic aerosol [OA2], soluble oceanic organic aerosol [OAS], sulphuric acid anion sulphate [SO4], ammonium [NH3] and nitrogen acid anion, nitrate [NO3], sodium cation [Na-mixed], chloride anion [Cl-mixed], dust [DUS] and unmixed sodium chloride [NaCl-unmixed]. The boundary between insoluble and soluble aerosols is given by the light green line.

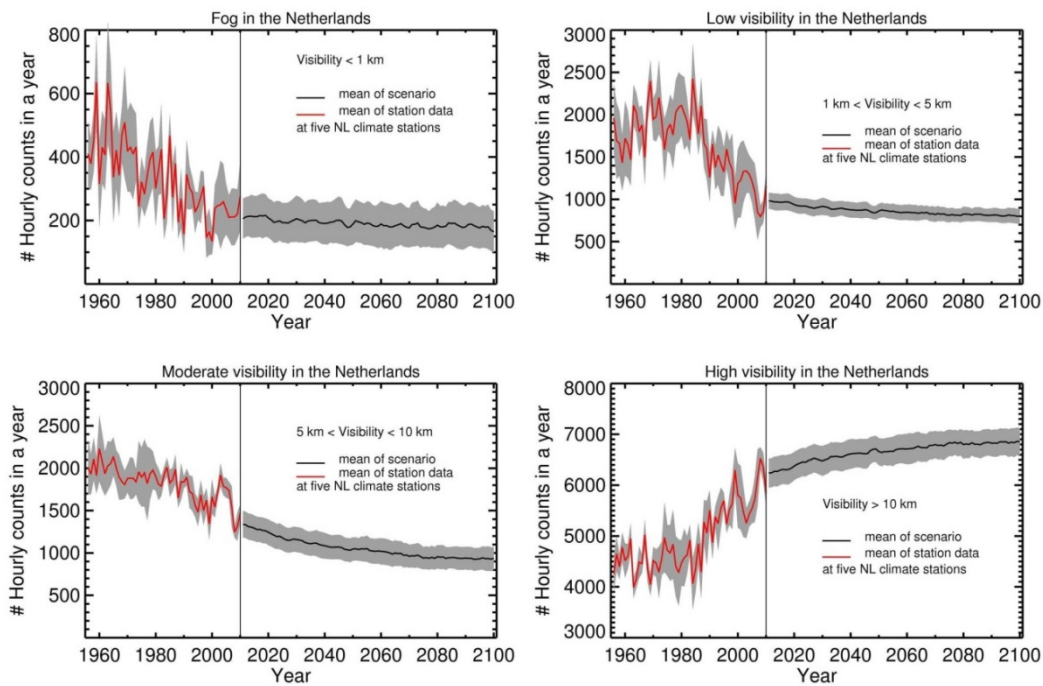


Figure 3.44: Hourly counts of visibility in four visibility classes. From 1956 – 2010, numbers are based on station data (grey area is standard deviation around the mean in red), from 2011 to 2100 they are based on aerosol mass scenarios. The separation between data and scenario is indicated by the vertical line.

**Visibility from NL climate stations**

In the Netherlands weather and climate observations are recorded at 42 stations. The majority of these station date back to the 1970 – 1980s. However, a number of stations have a longer history. For this study we are particularly interested in long continuous records of visibility. Five stations were chosen, consisting of the five main climate stations (De Kooy, Vlissingen, De Bilt, Eelde and Maastricht) (Figure 3.9). Together they form a good representation of the region. Records of visibility date back to the early 1950s on a patchy basis but here we will use the uninterrupted data set from 1956 onwards. Initially, visibility was recorded hourly by an

observer from known landmarks. In the 1960s and 1970s transmissometers were introduced at some stations, while a transition to fully automatic visibility detection with a Väisälä Present Weather Sensor (PWS) took place in the period 1998 - 2000.

Here, four visibility classes are defined. The first class is fog, which is defined as a visibility of less than 1 km. This is the traditional definition and no further differentiation into moderate and dense fog is used. The second class is 'low visibility' with visibility restricted between 1 and 5 km. The third class is 'moderate visibility' with visibility between 5 and 10 km. Finally, the fourth class is 'high visibility' and applies to situations with a visibility greater than 10 km.

The results for the five stations in the Netherlands are plotted in four panels in Figure 3.44. Here we focus initially only on the period 1956 – 2010, which is the period comprising the entire set of observations without the application of scenario computations that will be shown later. For each of these classes, the number of hours occurring in the class were counted and the mean value (red) and standard deviation (grey region) over the five stations. No smoothing was applied. The scenario calculations (period 2010 – 2100) will be discussed later.

Even though there is considerable year – to – year variation, a consistent signature in all four plots is the improving visibility. However, the signatures in the individual plots demonstrates the complexity involved in interpreting the visibility data. After 1970, there is a uniform decrease in the number of hours in the fog class except for the last five years of the period. The fog visibility class is the only one in which a fraction of the aerosol particles will activate to cloud droplets and the data presented here indicates that the number of hours this class has been reduced by 50% in the last 40 years. Yet, the class of low visibility shows an initial increase in the number of hours from 1956 onwards reaching a plateau between 1970 and 1985 after which it decreased again. Additionally, there has been a 25% reduction in the number of hours in the class of moderate visibility, and, since the 1980's more than 1500 hours per year have been added to the class of high visibility. This amounts to 15% of the total of 8760 hours available in a year of 365 days.

To determine the overall change, a linear trend line was fitted to the annual mean number of hours with fog in the Netherlands between 1956 and 2002. The values on the trend line in 1956 and 2002 equal 485 and 205 hours, respectively. The total decrease between 1956 and 2002 equals 280 hours.

### Visibility calculations and scenarios

During the scenario calculations the Mie-tables were used to determine the time-dependent behaviour of the visibility. Visibility is proportional to the inverse of the sum of the optical extinction based on all aerosol species. So the procedure called for a species-dependent conversion of the scenario aerosol masses to concentration and hygroscopicity which in turn were used to calculate visible extinction. The sum of species extinction is then inverted to obtain visibility on an hourly basis. Then, for each year, the number of hours assigned to each of the four visibility classes is counted to produce the time series. One problem arose because the calculated extinction in the period 1956 – 2010 is considerably lower than the actually observed visible extinction, the latter of which can be directly inferred from the station visibility observations. This means that the presumed aerosol mass in the scenario of the period 1956 - 2010 may be too small, which is likely caused by our uncertainty in specifying the aerosol mass in the black carbon and organic aerosol species. This means that the scenario visibility calculated from 2010 onwards extends the actual visibility record from the period 1956 – 2010 in a discontinuous manner. However, when the mass scenario from 2010 onwards is inspected, it appears that only a small tendency with time is foreseen in the future, whatever the correct mass values of BC and OA may be. Given the assumption of a fixed shape of the aerosol size spectra this means that the actual change in visibility between 2010 and 2100 will not be large. Therefore an ad hoc correction was applied to the hour counts in each visibility class so as to join the hour counts based on the station observed visibility (1956 – 2010) to the hour counts based on aerosol scenario in a continuous manner. The corrections applied are +20 hours in the fog class, + 480 hours in the low visibility class, + 300 hours in the medium visibility class and -800 hours in the high visibility class. Even though these count values seem high, it should be realized that the inverse relationship of visibility and optical extinction implies that the assignment of individual hours to one or the other visibility class is highly sensitivity to changes in the optical extinction, which in the case at hand is caused by changing / adjusting the aerosol concentration.

The corrected hour counts of visibility appear in Figure 3.44 as the solid lines extending from 2010 onwards. The single most important conclusion that can be drawn from this figure is that in a general sense the largest changes in visibility as a result from change in aerosol mass are already behind us. Although the improvement in visibility will continue in the next 90 years, the changes will not be as significant as those occurring in the last 60 years.

## Discussion and conclusions

When examining the figures and depending on the visibility class in which one is interested, different conclusions will emerge on when the upward trends in visibility have started. If one is interested in extreme conditions such as fog, the situation has continually been improving since the 1960's. Yet, the low visibility class exhibits a marked peak around 1980, while the higher classes indicates the onset of improved visibility well after 1980. Even though the most significant driver for the improvement seems to be the continued decrease in (foreseen) aerosol emissions, two important additional factors should be taken into account, namely the changing hygroscopicity and the activation of fog droplets. As the proportion of the hydrophobic BC and OA ( $0 < k < 0.4$ ) has decreased over the last 60 years and will continue to do so in comparison to the hydrophilic inorganic anthropogenic species ( $0.65 < k < 0.75$ ) the hygroscopicity of the entire mixture has continually been increasing, ranging from  $k \approx 0.4$  around 1956 to  $k \approx 0.5$  at present with a foreseen value of  $k \approx 0.60$  in 2100. Leaving all other conditions the same this implies a relative increase in optical extinction over the same years which partly compensates the relative decrease in optical extinction as a result of decreased numbers of aerosols.

Despite the year-to-year fluctuations there is a uniform downward tendency in the number of fog hours over the years and this trend is clearly different from the other three visibility classes. The fog visibility class is the only one in which aerosols will activate to small cloud droplets as this class is the only one where the relative humidity  $RH = 100\%$ . Activation of aerosol particles in fog is quite different from activation of aerosol particles in an air parcel subject to vertical movements. It is straightforward to show that the typical cooling rates at night in an atmospheric layer susceptible to fog formation is more than an order of magnitude smaller than that of a typical air parcel rising near cloud base. Calculations of the activation process indicate that under these very weak cooling conditions the total aerosol concentration is by far the controlling factor in determining the formation of fog [and hence the number of fog hours per year] when compared to the hygroscopicity of the aerosol mixture. In other words the overall downward trend in fog hours in the 1956 – 2010 period can tentatively be seen as a proxy for the overall decrease in aerosol concentration (but not for its composition and / or hygroscopicity).

Although it could be argued that changes in relative humidity over the years could also impact changes in visibility, this factor can be ruled out. None of the 5 climate station shows any evidence of overall changes in relative humidity in the past 60 year, although some multi-year variability is present. Furthermore, the scenario calculations suggest a reduction in relative humidity over the entire 150 year period of less than 1%, and this is not enough to explain the improvement in visibility.

Table 3.6 summarizes the results.

*Table 3.5: Summary of the visibility results based on observations and model results for the period 1956-2100. Because of the year-to-year fluctuations in the hour counts, the reported numbers of hour counts in the respective visibility classes are rounded and should be viewed as indications of the trends only.*

	Aerosol mass [ $\mu\text{g m}^{-3}$ ]	Hygroscopicity	Vis < 1km [hours]	1 < Vis < 5km [hours]	5 < Vis < 10km [hours]	Vis > 10km [hours]
1956	24	0.4	500	1750	2100	4600
2013	15	0.5	250	1000	1400	6300
2100	10	0.6	175	800	900	6900

### 3.5.3 Summary of changes in extreme weather

#### Extreme Precipitation:

- The intensity of summertime heavy precipitation on a sub-hourly timescale will likely increase with near surface dew point temperature as 9~14% per K.
- For longer timescales (order one day) an lower increase of around 7% per K in summertime is to expected
- These results are based on observations, simulations, and conceptual models. The level of confidence is therefore large.
- These results will be translated to the 4 KNMI scenarios by linking it to the trends to near surface dew point temperature.

**Hail and Thunderstorms**

- Climate models show a consistent increase in vertical atmospheric stability for summertime conditions as measured by the Conditional Available Potential Energy (CAPE) of 15% per K
- This robust change in stability will favour an increase of summertime thunderstorms and hail events.
- Based on this trend a doubling of the number of weather alarms related to thunderstorms in summertime is well possible

**Fog**

- Over the Netherlands visibility has improved in the last 50 years adding 1700 extra hours in the class of high visibility. The trend will continue in the future albeit not at the rate as we have seen over the last 50 years.
- The occurrence of fog, defined as the visibility below 1 km has gone down from 500 hours in 1956 to 250 hours in 2013. It will keep decreasing, though at a lower rate to 175 hours in 2100.
- The main reason for the increased visibility and the associated decrease of the frequency of occurrence of fog is the decrease in near surface aerosol concentrations.
- The improvement in visibility caused by the overall reduction in aerosol concentration is dampened by a concurrent increase in optical extinction due to the increased relative proportion of hydrophilic aerosols in the aerosol mixture.

## 4. The KNMI'14 scenarios table: key figures

The final scenario values, obtained as described in the previous sections, are given in Table 4.1 and Table 4.2 for the scenario periods 2030, 2050 and 2085 respectively. Table 4.4 gives an overview of the methodology used to derive the scenario variables and the related observational reference.

Table 4.1: Scenario variables for the period around 2030, including an estimate of the natural variability of 30-year mean climate variables

Season <sup>A)</sup>	Variable	Indicator	Climate <sup>B)</sup> 1981-2010 = reference period	Central estimate of change value for 2030 <sup>C)</sup> (2016-2045)	Natural variations averaged over 30 years <sup>D)</sup>
Year	Sea level at North Sea coast	absolute level <sup>E)</sup>	3 cm above NADP	+10 tot +25 cm	±1.4 cm
		rate of change	2.0 mm/year	+1 to +6 mm/year	±1.4 mm/year
	Temperature	mean	10.1 °C	+1.0 °C	±0.16 °C
	Precipitation	mean amount	851 mm	+5%	±4.2%
	Solar radiation	solar radiation	354 kJ/cm <sup>2</sup>	+0.2%	±1.6%
	Evaporation	potential evaporation (Makkink)	559 mm	+2.5%	±1.9%
	Fog	number of hours with visibility < 1 km	300 hour <sup>G)</sup>	-100 hour	±39 hour
Winter	Temperature	mean	3.4 °C	+1.2 °C	±0.48 °C
	Precipitation	mean amount	211 mm	+8.5%	±8.3%
		10-day amount exceeded once in 10 years <sup>I)</sup>	89 mm	+9%	±11%
		number of wet days (≥ 0.1 mm)	55 days	+1.5%	±4.7%
	Wind	mean wind speed	6.9 m/s	+0.5%	±3.6%
		highest daily mean wind speed per year	15 m/s	-1.0%	±3.9%
number of days between south and west		49 days	+2.5%	±6.4%	
Spring	Temperature	mean	9.5 °C	+0.8 °C	±0.24 °C
	Precipitation	mean amount	173 mm	+5.5%	±8.0%
Summer	Temperature	mean	17.0 °C	+0.9 °C	±0.25 °C
	Precipitation	mean amount	224 mm	+0.2%	±9.2%
		daily amount exceeded once in 10 years <sup>I)</sup>	44 mm	+1.7 tot +10%	±15%
		maximum hourly intensity per year	15.1 mm/hour	+5.5 tot +11%	±14%
		number of wet days (≥ 0.1mm)	43 days	+0.5%	±6.4%
	Solar radiation	solar radiation	153 kJ/cm <sup>2</sup>	+1.9%	±2.4%
	Humidity	relative humidity	77%	-0.6%	±0.86%
	Evaporation	potential evaporation (Makkink)	266 mm	+3.5%	±2.8%
Drought	mean highest precipitation deficit during growing season <sup>I)</sup>	144 mm	+4%	±13%	
Autumn	Temperature	mean	10.6 °C	+1.0 °C	±0.27 °C
	Precipitation	mean amount	245 mm	+5.5%	±9.0%

A) winter = December, January, February; spring = March, April, May; summer = June, July, August; autumn = September, October, November; information on all indicators for all seasons is available at [www.climatecenarios.nl](http://www.climatecenarios.nl)

B) averages for the Netherlands; for temperature only observations taken at De Bilt have been used, and for wind only Den Helder / De Kooy; for precipitation the number of stations for which 60 years of data is available is less than in the climate atlas; the difference between the averages for 1951-1980 and for the reference period 1981-2010 roughly corresponds to a 30 year trend

C) scenario values have been rounded taking into account the magnitude of the change and the differences between the four scenarios

D) 30-year averages fall in the given range with 90% probability

E) the absolute increase, without land subsidence, falls in the given range with 90% probability

F) the time series for solar radiation observations, which is also used for potential evaporation and precipitation deficit, starts in 1958

G) the reference climate is 1971-2000 because the time series for visual fog observations ended in 2002

- H) annual means fall in the given range with 90% probability
- I) for these indicators, 30-year periods are actually too short to determine the values accurately
- J) growing season runs from 1 April until 30 September

*Table 4.2: Overview of the climate change values according to the different KNMI'14 scenarios for the period 2036 – 2065 and the period 2071 – 2100.*

see table on next page

Season <sup>A)</sup>	Variable	Indicator	Climate <sup>B)</sup> 1951-1980	Climate <sup>B)</sup> 1981-2010 = reference period
Global temperature rise:				
Change in air circulation pattern:				
Year	Sea level at North Sea coast	absolute level <sup>E)</sup>	4 cm below NAP	3 cm above NAP
		rate of change	1.2 mm/year	2.0 mm/year
	Temperature	mean	9.2 °C	10.1 °C
	Precipitation	mean amount	774 mm	851 mm
	Solar radiation	solar radiation	346 kJ/cm <sup>2F)</sup>	354 kJ/cm <sup>2</sup>
	Evaporation	potential evaporation (Makkink)	534 mm <sup>F)</sup>	559 mm
	Fog	number of hours with visibility < 1 km	412 hours	300 hours <sup>G)</sup>
Winter	Temperature	mean	2.4 °C	3.4 °C
		year-to-year variation <sup>H)</sup>	-	± 2.6 °C
		daily maximum	5.1 °C	6.1 °C
		daily minimum	-0.3 °C	0.5 °C
		coldest winter day per year	-7.5 °C	-5.9 °C
		mildest winter day per year	10.3 °C	11.1 °C
		number of frost days (min temp < 0°C)	42 days	38 days
	Precipitation	number of ice days (max temp < 0°C)	11 days	7.2 days
		mean amount	188 mm	211 mm
		year-to-year variation <sup>H)</sup>	-	± 96 mm
		10-day amount exceeded once in 10 years <sup>I)</sup>	80 mm	89 mm
		number of wet days (≥ 0.1 mm)	56 days	55 days
	Wind	number of days ≥ 10 mm	4.1 days	5.3 days
		mean wind speed	-	6.9 m/s
highest daily mean wind speed per year		-	15 m/s	
Spring	number of days between south and west	44 days	49 days	
	Temperature	mean	8.3 °C	9.5 °C
	Precipitation	mean amount	148 mm	173 mm
Summer	Temperature	mean	16.1 °C	17.0 °C
		year-to-year variation <sup>H)</sup>	-	± 1.4 °C
		daily maximum	20.7 °C	21.9 °C
		daily minimum	11.2 °C	11.9 °C
		coolest summer day per year	10.3 °C	11.1 °C
		warmest summer day per year	23.2 °C	24.7 °C
		number of summer days (max temp ≥ 25°C)	13 days	21 days
		number of tropical nights (min temp ≥ 20°C)	< 0.1 days	0.1 days
	Precipitation	mean amount	224 mm	224 mm
		year-to-year variation <sup>H)</sup>	-	± 113 mm
		daily amount exceeded once in 10 years <sup>I)</sup>	44 mm	44 mm
		maximum hourly intensity per year	14.9 mm/hour	15.1 mm/hour
		number of wet days (≥ 0.1mm)	45 days	43 days
		number of days ≥ 20 mm	1.6 days	1.7 days
	Solar radiation	solar radiation	149 kJ/cm <sup>2F)</sup>	153 kJ/cm <sup>2</sup>
	Humidity	relative humidity	78%	77%
	Evaporation	potential evaporation (Makkink)	253 mm <sup>F)</sup>	266 mm
Drought	mean highest precipitation deficit during growing season <sup>J)</sup>	140 mm	144 mm	
	highest precipitation deficit exceeded once in 10 years <sup>I)</sup>	-	230 mm	
Autumn	Temperature	mean	10.0 °C	10.6 °C
	Precipitation	mean amount	214 mm	245 mm

Scenario change values for the climate around <b>2050<sup>(c)</sup></b> (2036-2065)				Scenario change values for the climate around <b>2085<sup>(c)</sup></b> (2071-2100)				Natural variations averaged over 30 years <sup>(d)</sup>
<b>G<sub>L</sub></b>	<b>G<sub>H</sub></b>	<b>W<sub>L</sub></b>	<b>W<sub>H</sub></b>	<b>G<sub>L</sub></b>	<b>G<sub>H</sub></b>	<b>W<sub>L</sub></b>	<b>W<sub>H</sub></b>	
+1 °C	+1 °C	+2 °C	+2 °C	+1.5 °C	+1.5 °C	+3.5 °C	+3.5 °C	
Low value	High value	Low value	High value	Low value	High value	Low value	High value	
+15 to +30 cm	+15 to +30 cm	+20 to +40 cm	+20 to +40 cm	+25 to +60 cm	+25 to +60 cm	+45 to +80 cm	+45 to +80 cm	± 1.4 cm
+1 to +5.5 mm/year	+1 to +5.5 mm/year	+3.5 to +7.5 mm/year	+3.5 to +7.5 mm/year	+1 to +7.5 mm/year	+1 to +7.5 mm/year	+4 to +10.5 mm/year	+4 to +10.5 mm/year	± 1.4 mm/year
+1.0 °C	+1.4 °C	+2.0 °C	+2.3 °C	+1.3 °C	+1.7 °C	+2.8 °C	+3.7 °C	± 0.16 °C
+4%	+2.5%	+5.5%	+5%	+5%	+5%	+6%	+7 %	± 4.2%
+0.6%	+1.6%	-0.8%	+1.2%	-0.5%	+1.1%	-0.8%	+1.4 %	± 1.6%
+3%	+5%	+4%	+7%	+2.5%	+5.5%	+6%	+10 %	± 1.9%
-110 hours	-110 hours	-110 hours	-110 hours	-120 hours	-120 hours	-120 hours	-120 hours	± 39 hours
+1.1 °C	+1.6 °C	+2.1 °C	+2.7 °C	+1.3 °C	+2.0 °C	+2.8 °C	+4.1 °C	± 0.48 °C
-8%	-16%	-13%	-20%	-10%	-17%	-13%	-24%	-
+1.0 °C	+1.6 °C	+2.0 °C	+2.5 °C	+1.2 °C	+2.0 °C	+2.7 °C	+3.8 °C	± 0.46 °C
+1.1 °C	+1.7 °C	+2.2 °C	+2.8 °C	+1.4 °C	+2.1 °C	+3.0 °C	+4.4 °C	± 0.51 °C
+2.0 °C	+3.6 °C	+3.9 °C	+5.1 °C	+2.7 °C	+4.1 °C	+4.8 °C	+7.3 °C	± 0.91 °C
+0.6 °C	+0.9 °C	+1.7 °C	+1.7 °C	+1.0 °C	+1.2 °C	+2.4 °C	+3.1 °C	± 0.42 °C
-30%	-45%	-50%	-60%	-35%	-50%	-60%	-80%	± 9.5%
-50%	-70%	-70%	-90%	-60%	-80%	-80%	< -90%	± 31%
+3%	+8%	+8%	+17%	+4.5%	+12%	+11%	+30%	± 8.3%
+4.5%	+9%	+10%	+17%	+6.5%	+12%	+14%	+30%	-
+6%	+10%	+12%	+17%	+8%	+12%	+16%	+25%	± 11%
-0.3%	+1.4%	-0.4%	+2.4%	+0.3%	+1.0%	-0.9%	+3%	± 4.7%
+9.5%	+19%	+20%	+35%	+14%	+24%	+30%	+60%	± 14%
-1.1%	+0.5%	-2.5%	+0.9%	-2.0%	+0.5%	-2.5%	+2.2%	± 3.6%
-3%	-1.4%	-3%	0.0%	-2.0%	-0.9%	-1.8%	+2.0%	± 3.9%
-1.4%	+3%	-1.7%	+4.5%	-1.6%	+6.5%	-6.5%	+4%	± 6.4%
+0.9 °C	+1.1 °C	+1.8 °C	+2.1 °C	+1.2 °C	+1.5 °C	+2.4 °C	+3.1 °C	± 0.24 °C
+4.5%	+2.3%	+11%	+9%	+8%	+7.5%	+13%	+12%	± 8.0%
+1.0 °C	+1.4 °C	+1.7 °C	+2.3 °C	+1.2 °C	+1.7 °C	+2.7 °C	+3.7 °C	± 0.25 °C
+3.5%	+7.5%	+4%	+9.5%	+5%	+9%	+6.5%	+14%	-
+0.9 °C	+1.4 °C	+1.5 °C	+2.3 °C	+1.0 °C	+1.7 °C	+2.6 °C	+3.8 °C	± 0.35 °C
+1.1 °C	+1.3 °C	+1.9 °C	+2.2 °C	+1.4 °C	+1.7 °C	+2.9 °C	+3.7 °C	± 0.18 °C
+0.9 °C	+1.1 °C	+1.6 °C	+2.0 °C	+1.0 °C	+1.4 °C	+2.3 °C	+3.1 °C	± 0.43 °C
+1.4 °C	+1.9 °C	+2.3 °C	+3.3 °C	+2.0 °C	+2.6 °C	+3.6 °C	+4.9 °C	± 0.52 °C
+22%	+35%	+40%	+70%	+30%	+50%	+90%	+130%	± 13%
+0.5%	+0.6%	+1.4%	+2.2%	+0.9%	+1.2%	+4.5%	+7.5%	-
+1.2%	-8%	+1.4%	-13%	+1.0%	-8%	-4.5%	-23 %	± 9.2%
+2.1 to +5%	-2.5 to +1.0%	+1.4 to +7%	-4 to +2.2%	+1.2 to +5.5%	-2.5 to +1.9%	-0.6 to +9%	-8.5 to +2.3%	-
+1.7 to +10%	+2.0 to +13%	+3 to +21%	+2.5 to +22%	+2.5 to +15%	+2.5 to +17%	+5 to +35%	+5 to +40%	± 15%
+5.5 to +11%	+7 to +14%	+12 to +23%	+13 to +25%	+8 to +16%	+9 to +19%	+19 to +40%	+22 to +45%	± 14%
+0.5%	-5.5%	+0.7%	-10%	+2.1%	-5.5%	+4%	-16%	± 6.4%
+4.5 to +18%	-4.5 to +10%	+6 to +30%	-8.5 to +14%	+5 to +23%	-3.5 to +14%	+2.5 to +35%	-15 to +14%	± 24%
+2.1%	+5%	+1.0%	+6.5%	+0.9%	+5.5%	+3%	+9.5%	± 2.4%
-0.6%	-2.0%	+0.1%	-2.5%	0.0%	-2.0%	-0.6%	-3%	± 0.86%
+4%	+7%	+4%	+11%	+3.5%	+8.5%	+8%	+15%	± 2.8%
+4.5%	+20%	+0.7%	+30%	+1.0%	+19%	+13%	+50%	± 13%
+5%	+17%	+4.5%	+25%	+3.5%	+17%	+14%	+40%	-
+1.1 °C	+1.3 °C	+2.2 °C	+2.3 °C	+1.6 °C	+1.6 °C	+3.3 °C	+3.8 °C	± 0.27 °C
+7%	+8%	+3%	+7.5%	+7.5%	+9%	+5.5%	+12%	± 9.0%



Table 4.3: Guidance table providing methodological cross-references of the scenario values, shown in Table 4.1 and Table 4.2.

Variable	Observations	Climate normals and Natural Variability (NV)	Scenarios (2030, 2050 and 2085)
<b>Sea level (rise):</b> Absolute level (cm)	6 stations along the Dutch coast (Delfzijl, Den Helder, Harlingen, Hoek van Holland, IJmuiden and Vlissingen; 1901-2012). See section 2.4.1.	NV of absolute level estimated from standard deviation of successive difference series and corrected for serial correlation (~0.26) of annual mean sea level. See section 2.4.2.	Combining several physical processes which depend on global temperature change and that contribute to sea level rise at the Dutch coast. See section 3.2.
Rate of change (mm/yr)		Normals for rate of change are determined from the annual sea levels series averaged over the 6 gauging stations and 30-year regressions on that series for respectively 1951-1980 and 1981-2010. NV of rate of change from all overlapping 30-year regressions in the 1901 – 2012 series for each of the 6 stations. NV averaged over the 6 stations. See section 2.4.2.	Scenario changes for the rate of change are obtained as the derivatives of the curves presented in Figure 3.26 (see section 3.2).
<b>Temperature:</b>	Station De Bilt (1901 – 2013). See section 2.4.1.	NV estimated from standard deviation of successive difference series. Necessity of correction of NV for serial correlation (~0.20) in the annual and some seasonal means doubtful. Therefore no correction applied for the NV estimates in the scenario tables. However, corrected NV values presented in section 2.4.2.	Changes in means directly taken from RACMO2 re-samples for region MON (see section 3.1.4). Changes in all other temperature indices after Time series transformation of the De Bilt series for 1981 – 2010 (see section 3.1.5).
<b>Precipitation:</b> mean amount, number of wet days ( $\geq$ 0.1mm), number of days $\geq$ 10 or 20 mm;	102 homogenized pr102 homogenized precipitation stations (1910 – 2013). See section 2.4.1.	102 selected precipitation stations. Normal values are averages over all 102 stations. NV estimated from standard deviation of successive difference series (no serial correlation). NV calculated for all 102 stations and then averaged.	Changes in means directly taken from the RACMO2 re-samples for region NLD (see section 3.1.4). Changes in all other precipitation indices after time series transformation of the 102 station series for 1981-2010 (see sections 3.1.5 and 3.1.6). ---
once in 10 year precipitation (10-day in winter and 1-day in summer);	240 homogenized precipitation stations (1981 – 2010). See section 2.4.1.	GEV distributions fitted to 240 precipitation stations. Shape parameter $\kappa$ fixed. Normal values are averages of return levels from all 240 fitted distributions (see section 2.4.2). NV of return levels from the expected Fisher information	GEV distributions fitted to transformed 1981-2010 times series for 240 precipitation stations using TP. Change in return level from change in average return level.
hourly intensity	Station De Bilt (1906 – 2013). See section 2.4.1.	NV estimated from standard deviation of successive difference series (no serial correlation). See section 2.4.2.	Scenario changes are based on Table 3.1. The ranges of change of the hourly precipitation intensity per °C in that table are multiplied by the scenario changes in the dew point temperature (see section 3.1.6).
<b>Wind:</b> wind speed wind direction	Station Den Helder. (wind dir.: 1906-2012; wind speed 1981-2012). See section 2.4.1.	For wind speed use is made of the so-called potential wind (see section 2.4.1). The wind directions indicated as 'between south and west' corresponds to directions between 165 and 285 degrees. This 120 degree range is obtained by combining four of the 12 ordinary 30 degree sectors. NV estimated from standard deviation of successive difference series (no serial correlation). See section 2.4.2.	Changes directly from changes in daily-mean wind speed and wind direction from the RACMO2 re-samples for the grid point 4.74 E, 52.96 N, representing Den Helder (see sections 3.3.3 and 3.3.4).

<b>Variable</b>	<b>Observations</b>	<b>Climate normals and Natural Variability (NV)</b>	<b>Scenarios (2030, 2050 and 2085)</b>
<b>Relative humidity</b>	Station De Bilt (1951-2013). See section 2.4.1.	NV estimated from standard deviation of successive difference series (no serial correlation). See section 2.4.2.	Changes directly taken from the RACMO2 re-samples for region MON (see section 3.4.2).
<b>Solar radiation</b>	Station De Bilt (1958-2013). See section 2.4.1.	The solar radiation starts in 1958 (see section 2.4.1). NV estimated from standard deviation of successive difference series (no serial correlation). See section 2.4.2.	Changes directly taken from the RACMO2 re-samples for region MON (see section 3.4.2)
<b>Evaporation</b>	Station De Bilt (1958-2013). Makkink evaporation calculated from daily solar radiation and temperature. See section 2.4.1.	Evaporation is based on solar radiation and therefore starts in 1958 (see section 2.4.1). NV estimated from standard deviation of successive difference series (no serial correlation). See section 2.4.2.	Changes based on 'transformed' 1981-2010 daily temperature and solar radiation time series using the Makkink formula for potential evaporation (see sections 2.4.1 and 3.4.2).
<b>Precipitation deficit: average highest precipitation deficit during the growing season;</b>	Station De Bilt (1951 – 2010). See section 2.4.1.	Precipitation deficit available from 1951 onwards (see section 2.4.1). NV from standard deviation of original series (see section 2.4.2).	Changes based on changes in evaporation (i.e. changes in mean temperature and solar radiation) and changes in precipitation, from 'transformed' 1981-2010 daily precipitation and evaporation time series (see section 3.4.2).
once in 10 year precipitation deficit during the growing season		For the once in 10-year precipitation deficit the 2003 precipitation deficit is used (see section 2.4.2) and no NV estimate is presented.	Change in once in 10 year precipitation deficit based on the 'transformed' precipitation deficit series (see section 3.4.2).
<b>Fog</b>	5 stations (Beek, De Bilt, De Kooy, Eelde and Vlissingen; 1956 – 2010). See section 2.4.1.	Fog visual measurements start in 1956 and stop in 2002. Therefore 'adapted' normal (see section 2.4.2). NV estimated from standard deviation of successive difference series (no serial correlation) for the years 1956 to 2010 (see section 2.4.2).	Changes based on emission scenarios (see section 3.5.2).

## 5. Guidance for use

### 5.1 Difference with earlier scenarios

In many aspects the new climate change scenarios are different from the previous generation (KNMI'06). Table 5.1 compares the new KNMI'14 climate scenarios with the previous scenarios of 2006.

Table 5.1: Overview of differences between KNMI'06 and KNMI'14

KNMI'06	KNMI'14
Four scenarios for future climate change in the Netherlands	Four scenarios for future climate change in the Netherlands
Up to 35 cm sea level rise in 2050 and up to 85 cm sea level rise in 2100 (=95 cm when corrected for the different definition of the upper value than in KNMI'14)	Up to 40 cm sea level rise in 2050, 80 cm in 2085 and 100 cm in 2100
Severe summer warming and drying in the G+ and W+ scenarios with changes in air circulation	Less summer warming and drying in the GH and WH scenarios with changes in air circulation
Coastal precipitation effect added in 2009 (Klein Tank and Lenderink 2009)	Coastal precipitation effect judged too uncertain to be included
No information on hourly precipitation change	Estimate of maximum hourly precipitation intensity
Based on SRES-A1b emission and land use scenarios	Based on RCP4.5, RCP6.0 and RCP8.5 emission and land use scenarios
Based on 5 GCMs and 10 RCMs	Based on EC-Earth and RACMO2 incorporating the projected changes from 250 GCM calculations
Time horizons 2050 (2036-2065) and 2100 (twice the changes of 2050, except for sea level)	Time horizons 2030 (2016-2045), 2050 (2036-2065) and 2085 (2071-2100, the maximum possible time horizon because GCM calculations run to 2100)
Reference period 1976-2005	Reference period 1981-2010 (= climate atlas period; KNMI 2011)
Set of 5 climate variables and 10 climate indicators	Set of 12 climate variables and 22 climate indicators, including fog, clouds, solar radiation, and evaporation
No information on natural variations	Natural variation estimates included for the 30-year period of the scenarios
No regional differentiation	Regional differentiation for robust changes such as mean temperature
User involvement mainly after scenario development	User involvement during each stage of scenario development
Time series transformation tool provided	Time series transformation tool and option for tailored future weather calculations provided
Few examples of user applications	Main risks and opportunities of climate change for the Netherlands summarized on the basis of more examples of user applications and literature

A quantitative comparison between KNMI'06 and KNMI'14 is shown in Table 5.2 and Table 5.3. The reference numbers (norms) have been based on the average of 102 stations for precipitation, and the De Bilt station for temperature and potential evaporation. For wind a coastal station has been used.

For KNMI'06 the period 1976–2005 was used as reference, whereas for KNMI'14 this is 1981–2010. These reference periods are characterized by different climatological values, which can be a result of natural variability, a systematic trend, or a combination. This difference can be accounted for in three different ways:

1. Linear interpolation/extrapolation: in order to translate the KNMI'06 numbers for 2050 into the KNMI'14 framework the differences in KNMI'06 need to be multiplied by  $(2050-1995)/(2050-1990)$ .
2. subtract/add the difference between the two reference periods to the changes reported: for instance, a difference of 0.2°C between 1976-2005 and 1981-2010 must be subtracted from the KNMI'06 changes

3. extrapolate the observed trend from e.g. 1951 to estimate the difference between the reference periods.

For the results for 2050 (Table 5.2) the 1<sup>st</sup> method is used, while for 2085 (Table 5.3) a linear extrapolation from 2050 to 2085 is applied (2<sup>nd</sup> method) for all quantities except sea level rise. Since for extreme precipitation and extreme wind a systematic difference is not detectable, no such correction has been applied for this quantity.

*Table 5.2: Quantitative comparison between KNMI'06 and KNMI'14 for the 2050 target period and the 2081-2010 reference period. Differences due to shifting reference periods are accounted for by adding/subtracting the climatological mean in these periods (method 1; see text).*

	norm	norm	KNMI'	KNMI'	KNMI'	KNMI'	KNMI'	KNMI'	KNMI'	KNMI'
	1976-	1981-	06	14	06	14	06	14	06	14
	2005	2010	G	G <sub>L</sub>	G+	G <sub>H</sub>	W	W <sub>L</sub>	W+	W <sub>H</sub>
<b>Annual</b>										
Mean temperature (°C)	9.9	10.1	0.7	1.0	1.0	1.4	1.6	2	2.4	2.3
Mean precipitation (mm, %)	826.5	851	0	4	-4	3	3	6	-5	5
Reference evaporation (mm, %)	552.5	559	1	3	4	5	4	4	8	7
<b>Winter</b>										
Mean temperature (°C)	3.2	3.4	0.7	1.1	0.9	1.6	1.6	2.1	2.1	2.7
Coldest winter day (°C)	-6.3	-5.9	0.6	2.0	1.1	3.6	1.7	3.9	2.5	5.1
Warmest winter day (°C)	11.1	11.1	0.8	0.6	0.9	0.9	1.6	1.7	1.7	1.7
Mean precipitation (mm, %)	209.7	211	3	3	6	8	6	8	13	17
Wet day fraction (%)	54.3	54.6	-1	0	0	1	-1	0	1	2
10-daily precipitation sum, exceeded 1/10yrs (mm, %)	89	89	4	6	6	10	8	12	12	17
Annual maximum daily mean wind speed (%)	15	15	0	-3	2	-1	-1	-3	4	0
<b>Spring</b>										
Mean temperature (°C)	9.2	9.5	0.6	0.9	0.9	1.1	1.5	1.8	2.3	2.1
Mean precipitation (mm, %)	168.4	173	0	5	-2	2	3	11	0	9
<b>Summer</b>										
Mean temperature (°C)	16.8	17	0.7	1	1.2	1.4	1.5	1.7	2.6	2.3
Coldest summer day (°C)	11	11.1	0.8	0.9	1.0	1.1	1.6	1.6	2.2	2
Warmest summer day (°C)	24.5	24.7	0.8	1.4	1.7	1.9	1.9	2.3	3.6	3.3
Mean precipitation (mm, %)	210.1	224	-3	1	-16	-8	-1	1	-24	-13
Wet day fraction (%)	42.7	43.2	-3	1	-11	-6	-4	1	-20	-10
range low				2		2		3		3
daily precipitation sum, exceeded 1/10yrs (mm, %)	44	44	13		5		27		10	
range high				10		13		21		22
Reference evaporation (%)	262.6	265.6	2	4	7	7	6	4	14	11
<b>Autums</b>										
Mean temperature (°C)	10.5	10.6	0.8	1.1	1.2	1.3	1.7	2.2	2.6	2.3
Mean precipitation (mm, %)	237.3	245	0	7	-6	8	3	3	-9	8

## 5.2 Scenarios in neighbouring countries

Most countries in Europe produce climate scenarios or projections for their own country, often using the same basic information (RCM projections) from large European projects such as PRUDENCE and ENSEMBLES, but all with their own methods to construct climate scenarios, which does not allow a straightforward comparison or combination. Table 5.4 presents regional climate scenarios of various European countries. Table 5.5 gives some characteristics of the various sets of climate scenarios.

Table 5.3: As Table 5.2 for the 2085 target period

	norm	norm	KNMI'	KNMI'	KNMI'	KNMI'	KNMI'	KNMI'	KNMI'	KNMI'
	1976-2005	1981-2010	06	14	06	14	06	14	06	14
			G	G <sub>L</sub>	G+	G <sub>H</sub>	W	W <sub>L</sub>	W+	W <sub>H</sub>
<b>Annual</b>										
Mean temperature (°C)	9.9	10.1	1.3	1.3	1.9	1.7	2.8	2.8	4.2	3.7
Mean precipitation (mm, %)	826.5	851	2	5	-5	5	8	6	-6	7
Reference evaporation (mm, %)	552.5	559	4	3	9	6	9	6	18	10
<b>Winter</b>										
Mean temperature (°C)	3.2	3.4	1.3	1.3	1.7	2	2.9	2.8	3.7	4.1
Coldest winter day (°C)	-6.3	-5.9	1.4	2.7	2.1	4.1	3.2	4.8	4.5	7.3
Warmest winter day (°C)	11.1	11.1	1.4	1	1.5	1.2	2.7	2.4	2.9	3.1
Mean precipitation (mm, %)	209.7	211	5	5	11	12	11	11	23	30
Wet day fraction (%)	54.3	54.6	-1	0	1	1	-1	-1	3	3
10-daily precipitation sum, exceeded 1/10yrs (mm, %)	89	89	7	8	10	12	14	16	20	25
Annual maximum daily mean wind speed (%)	15	15	-1	-2	3	-1	-2	-2	7	2
<b>Spring</b>										
Mean temperature (°C)	9.2	9.5	1.2	1.2	1.7	1.5	2.8	2.4	4.1	3.1
Mean precipitation (mm, %)	168.4	173	2	8	-1	8	7	13	2	12
<b>Summer</b>										
Mean temperature (°C)	16.8	17	1.3	1.2	2.2	1.7	2.7	2.7	4.6	3.7
Coldest summer day (°C)	11	11.1	1.4	1	1.8	1.4	2.8	2.3	3.8	3.1
Warmest summer day (°C)	24.5	24.7	1.6	2	3.0	2.6	3.4	3.6	6.3	4.9
Mean precipitation (mm, %)	210.1	224	-1	1	-22	-8	4	-5	-37	-23
Wet day fraction (%)	42.7	43.2	-4	2	-17	-6	-6	4	-33	-16
range low				3		3		5		5
daily precipitation sum, exceeded 1/10yrs (mm, %)	44	44	23		9		46		17	
range high				15		17		35		40
Reference evaporation (%)	262.6	265.6	5	4	12	9	11	8	24	15
<b>Autums</b>										
Mean temperature (°C)	10.5	10.6	1.4	1.6	2.1	1.6	3.0	3.3	4.5	3.8
Mean precipitation (mm, %)	237.3	245	2	8	-8	9	7	6	-13	12

Table 5.5 shows that none of the countries uses the same regional scenarios. Therefore, the projections for the future, and the range of the possible futures spanned may differ per country. Figure 5.1 gives an example of the differences in ranges for future temperature and precipitation changes that are spanned by some of the above climate scenario sets. The ranges are rather difficult to compare, since the reference periods and time horizons also differ between countries (Dalelane, 2014).

Table 5.4: Regional climate scenarios/projections and their names in various European countries: links to the websites (source: a.o. Dalelane, 2014; links last checked March 30, 2014).

Country	Website with regional climate scenarios
Austria	<a href="http://klimawandelanpassung.at/ms/klimawandelanpassung/de/klimawandelinoe/kwa_zukunftsszenarien/">klimawandelanpassung.at/ms/klimawandelanpassung/de/klimawandelinoe/kwa_zukunftsszenarien/</a>
Belgium	CCI-HYDR for Flanders: <a href="http://www.kuleuven.be/hydr/CCI-HYDR.htm">www.kuleuven.be/hydr/CCI-HYDR.htm</a>
Denmark	<a href="http://en.klimatilpasning.dk/knowledge/climate/denmarksfutureclimate.aspx">en.klimatilpasning.dk/knowledge/climate/denmarksfutureclimate.aspx</a> <a href="http://www.dmi.dk/klima/fremtidens-klima/klimascenarier/">www.dmi.dk/klima/fremtidens-klima/klimascenarier/</a> <a href="http://www.dmi.dk/klima/fremtidens-klima/danmark/">www.dmi.dk/klima/fremtidens-klima/danmark/</a> <a href="http://www.dmi.dk/fileadmin/Rapporter/DKC/dkc12-04.pdf">www.dmi.dk/fileadmin/Rapporter/DKC/dkc12-04.pdf</a>
France	DRIAS: <a href="http://www.gip-ecofor.org/gicc">www.gip-ecofor.org/gicc</a> , <a href="http://www.drias-climat.fr/">www.drias-climat.fr/</a> <a href="http://www.meteofrance.fr/climat-passe-et-futur/changement-climatique/projections-">www.meteofrance.fr/climat-passe-et-futur/changement-climatique/projections-</a>

Country	Website with regional climate scenarios
Finland	climatiques/les-projections-climatiques-regionalisees ilmasto-opas.fi/en/ilmastonmuutos/suomen-muuttuva-ilmasto/-/artikkeli/74b167fc-384b-44ae-84aa-c585ec218b41/ennustettu-ilmastonmuutos-suomessa.html; ilmasto-opas.fi/en/datat/mennyt-ja-tuleva-ilmasto#DoubleMapTimelinePlace:vertailu
Germany	DWD Klimaatlas: www.dwd.de/klimaatlas/ KLIWAS: www.kliwas.de/ WettReg2010: www.cec-potsdam.de/Produkte/Klima/WettReg/wettreg.html CSC Klimasignalkarten: www.climate-service-center.de/031443/index_0031443.html.de
Ireland	www.epa.ie/pubs/reports/research/climate/STRIVE_48_Fealy_ClimateModelling_web.pdf
Nether-lands	KNMI'06 and KNMI'14: www.knmi.nl/climatescenarios/
Norway	met.no/Forskning/Klimaforskning/Klimascenarier/ www.senorge.no/index.html?p=klima
Portugal	www.ipma.pt/pt/oclima/servicos.clima/index.jsp?page=cenarios21.clima.xml siam.fc.ul.pt/
Spain	www.aemet.es/es/elclima/cambio_climat/escenarios
Sweden	www.smhi.se/klimatdata/Framtidens-klimat/Klimatscenarier/2.2252/2.2264 www.mistra-swecia.se/ (phase II to be completed in 2015)
Switzerland	CH2011: www.ch2011.ch/
UK	UKCP09: ukclimateprojections.defra.gov.uk/

Table 5.5: Regional climate scenarios/projections in various European countries: some characteristics (source: Dalelane, 2014).

Country	Scenarios	Reference period	Time horizons	Ensemble	Basic information source	Regional differentiation
Belgium CCI-HYDR	High, mean, low	1961-1990	2071-2100	Multi-model, multi-emissions	PRUDENCE	Only for precipitation 50*50 km
France: simulateur climatique	A2 and B2	1960-1990	2050-2100	Multi-emissions, one model	ARPEGE-model	Administrative regions, zones
Germany, KLIWAS	8 runs (RCMs)	1961-1990	2000-2100	Multi-model, A1B	ENSEMBLES	25*25 km and river basins
Germany, DWD Klimaatlas	15 <sup>th</sup> , 50 <sup>th</sup> and 85 <sup>th</sup> percentile	1961-1990	2021-2050	Multi-model, A1B	ENSEMBLES + German RCM	25*25 km
Netherlands KNMI'06	4 scenarios, driving variables: global temperature and circulation	1976-2005	2050, 2100	Multi-model, multi-emissions	AR4, PRUDENCE	no
Netherlands KNMI'14	4 scenarios, driving variables: global temperature and circulation	1981-2010	2050, 2085	Multi-model, multi-emissions	CMIP5 + ensemble of EC-EARTH and RACMO	Only for temperature
Switzerland CH2011	A1B, A2, and RCP3PD	1980-2009	2020-2049	Multi-model (RCM's), multi-emissions (GCM)	ENSEMBLES	Averages over 3 regions

Country	Scenarios	Reference period	Time horizons	Ensemble	Basic information source	Regional differentiation
UK	B1, A1B and A1FI	1961–1990	2020s, 2050s & 2080s	Perturbed physics ensemble, multi-emissions, one model	Model Hadley Centre	25*25 km, administrative regions, river basins

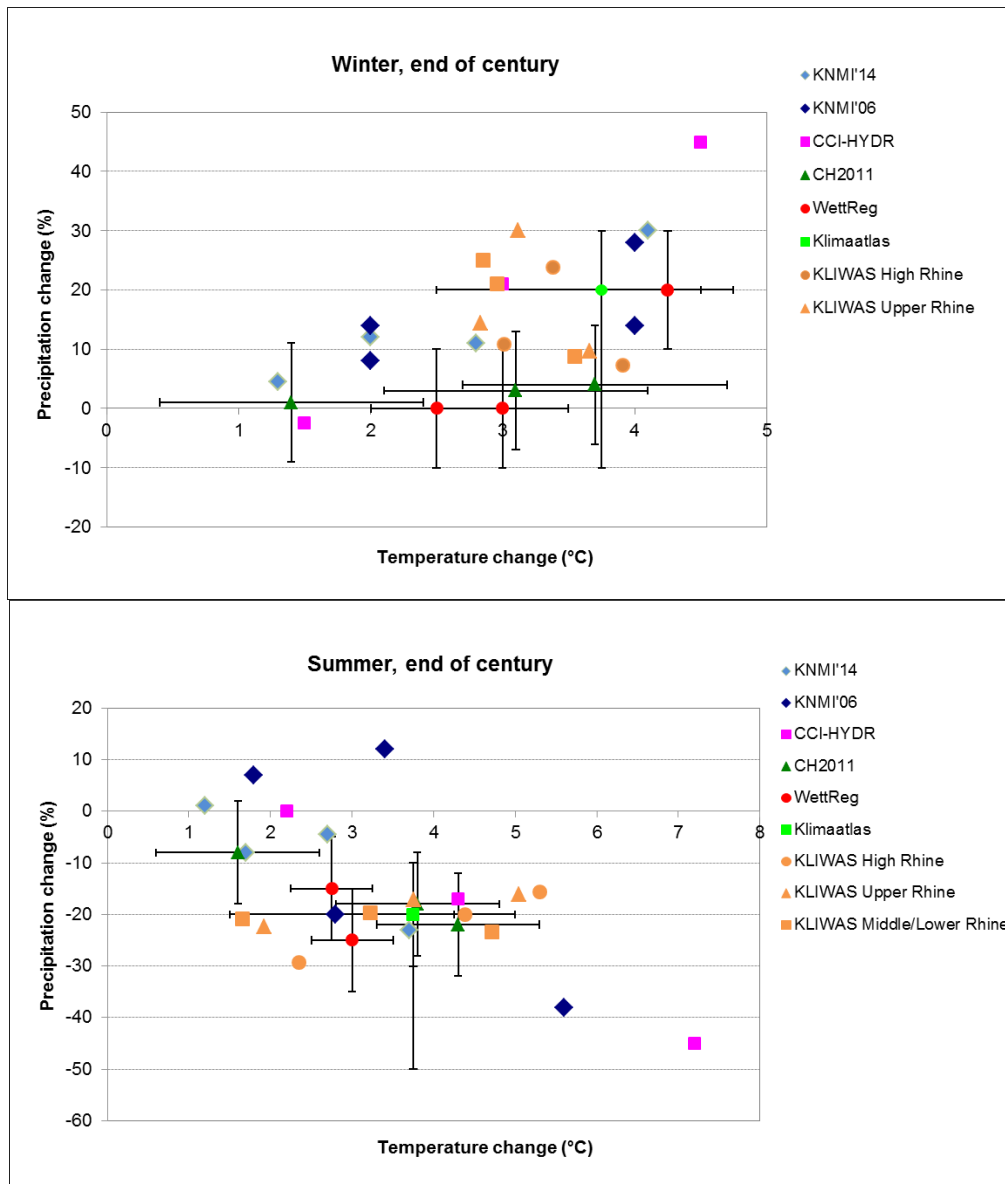


Figure 5.1: Graphical comparison of various sets of regional climate change scenarios in Europe: changes in average temperature and average precipitation in winter (upper panel) and summer (lower panel) for the end of the 21st century. Source: Dalelane (2014).

## Acknowledgements

Sections of this report have been commented by Roderik van de Wal and Gerbrand Komen, which is highly appreciated.

## References

- Alexandersson, H., H. Tuomenvirta, T. Schmidh, and K. Iden, 2000: Trends of storms in NW Europe derived from an updated pressure data set. *Clim. Res.*, 71–73.
- Arendt, A., T. Bolch, J. Cogley, and et al, 2012: Randolph Glacier Inventory [v2.0]: A Dataset of Global Glacier 491 Outlines. [http://www.glims.org/RGIRGI Tech Report V2.0.pdf](http://www.glims.org/RGIRGI_Tech_Report_V2.0.pdf).
- Asmi, A., and Coauthors, 2011: Number size distributions and seasonality of submicron particles in Europe 2008–2009. *Atmospheric Chem. Phys.*, **11**, 5505–5538, doi:10.5194/acp-11-5505-2011.
- Attema, J. J., and G. Lenderink, 2014: The influence of the North Sea on coastal precipitation in the Netherlands in the present-day and future climate. *Clim. Dyn.*, **42**, 505–519, doi:10.1007/s00382-013-1665-4.
- , J. M. Loriaux, and G. Lenderink, 2014: Extreme precipitation response to climate perturbations in an atmospheric mesoscale model. *Environ. Res. Lett.*, 14003, doi:10.1088/1748-9326/9/1/014003.
- Baas, P., S. Roode, and G. Lenderink, 2008: The Scaling Behaviour of a Turbulent Kinetic Energy Closure Model for Stably Stratified Conditions. *Bound.-Layer Meteorol.*, **127**, 17–36, doi:10.1007/s10546-007-9253-y.
- Bakker, A., and J. Bessembinder, 2012: *Time series transformation tool: description of the program to generate time series consistent with the KNMI'06 climate scenarios*. KNMI, De Bilt, Netherlands, 75 pp.
- Bakker, A. M. R., B. J. J. M. Van den Hurk, and J. P. Coelingh, 2013: Decomposition of the windiness index in the Netherlands for the assessment of future long-term wind supply. *Wind Energy*, **16**, 927–938, doi:10.1002/we.1534.
- Bakker, A. R., and B. J. M. Van den Hurk, 2012: Estimation of persistence and trends in geostrophic wind speed for the assessment of wind energy yields in Northwest Europe. *Clim. Dyn.*, **39**, 767–782, doi:10.1007/s00382-011-1248-1.
- Bamber, J. L., and W. P. Aspinall, 2013: An expert judgement assessment of future sea level rise from the ice sheets. *Nat. Clim Change*, **3**, 424–427, doi:10.1038/nclimate1778.
- Beersma, J.J. en T.A. Buishand, 2002: Droog, droger, droogst; bijdrage van het KNMI aan de eerste fase van de Droogtestudie Nederland. KNMI-publicatie 199-I, KNMI, De Bilt, 42 pp.
- Berkhout, F., B. Van den Hurk, J. Bessembinder, J. De Boer, B. Bregman, and M. Van Drunen, 2013: Framing climate uncertainty: socio-economic and climate scenarios in vulnerability and adaptation assessments. *Reg. Environ. Change*, doi:10.1007/s10113-013-0519-2.
- Bessembinder, J., A. M. R. Bakker, R. Leander, and A. Feijt, 2011a: *Time series transformation tool: development and use in CCsP projects*. KvK,.
- , B. Overbeek, and G. Verver, 2011b: Inventarisatie van gebruikerswensen voor klimaatinformatie - KNMI. [www.knmi.nl/bibliotheek/knmipubTR/TR317.pdf](http://www.knmi.nl/bibliotheek/knmipubTR/TR317.pdf).
- Brands, S., S. Herrera, J. Fernández, and J. M. Gutiérrez, 2013: How well do CMIP5 Earth System Models simulate present climate conditions in Europe and Africa? *Clim. Dyn.*, **41**, 803–817, doi:10.1007/s00382-013-1742-8.

- Brandsma, T., R. Jilderda, and R. Sluijter, 2013: *Standardization of data and methods for calculating daily Tmean, Tn and Tx in the Netherlands for the 1901-1970 period*. KNMI, De Bilt, Netherlands,.
- Bray, D., and H. von Storch, 2009: "Prediction" or "Projection"? The Nomenclature of Climate Science. *Sci. Commun.*, **30**, 534–543.
- Bruggeman, W., and Coauthors, 2013: Deltascenario's voor 2050 en 2100 - Nadere uitwerking 2012-2013. <http://www.pbl.nl/sites/default/files/cms/publicaties/Deltascenario%27s%20voor%202050%20en%202100.pdf>.
- De Bruin, H. A. R., 1981: *The determination of (reference crop) evapotranspiration from routine weather data*. Comm. Hydrol. Research TNO, The Hague, 25-37 pp.
- Buishand, T. A., G. De Martino, J. N. Spreeuw, and T. Brandsma, 2013: Homogeneity of precipitation series in the Netherlands and their trends in the past century. *Int. J. Climatol.*, **33**, 815–833, doi:10.1002/joc.3471.
- Cash, D. W., W. C. Clark, F. Alcock, N. M. Dickson, N. Eckley, D. H. Guston, J. Jäger, and R. B. Mitchell, 2003: Knowledge systems for sustainable development. *Proc. Natl. Acad. Sci.*, **100**, 8086–8091, doi:10.1073/pnas.1231332100.
- Chang, E. K. M., Y. Guo, and X. Xia, 2012: CMIP5 multimodel ensemble projection of storm track change under global warming. *J. Geophys. Res. Atmospheres*, **117**, D23118, doi:10.1029/2012JD018578.
- CHO (Commissie voor Hydrologisch Onderzoek TNO), 1988: Van Penman naar Makkink; Een nieuwe berekeningswijze voor de klimatologische verdampingsgetallen. Rapporten en nota's No. 19, CHO TNO, 's-Gravenhage.
- Christensen, J., and O. Christensen, 2007: A summary of the PRUDENCE model projections of changes in European climate by the end of this century. *Clim. Change*, **81**, 7–30, doi:10.1007/s10584-006-9210-7.
- Church, J., and N. White, 2011: Sea-Level Rise from the Late 19th to the Early 21st Century. *Surv. Geophys.*, **32**, 585–602, doi:10.1007/s10712-011-9119-1.
- Church, J. A., and Coauthors, 2010: Sea-Level Rise and Variability: Synthesis and Outlook for the Future. *Understanding Sea-Level Rise and Variability*, Wiley-Blackwell, 402–419 <http://dx.doi.org/10.1002/9781444323276.ch13>.
- , and Coauthors, 2011: Revisiting the Earth's sea-level and energy budgets from 1961 to 2008. *Geophys. Res. Lett.*, **38**, L18601, doi:10.1029/2011GL048794.
- Cusack, S., 2013: A 101 year record of windstorms in the Netherlands. *Clim. Change*, **116**, 693–704, doi:10.1007/s10584-012-0527-0.
- Dee, D. P., and Coauthors, 2011: The ERA-Interim reanalysis: configuration and performance of the data assimilation system. *Q. J. R. Meteorol. Soc.*, **137**, 553–597, doi:10.1002/qj.828.
- Eichler, T. P., N. Gaggini, and Z. Pan, 2013: Impacts of global warming on Northern Hemisphere winter storm tracks in the CMIP5 model suite. *J. Geophys. Res. Atmospheres*, **118**, 3919–3932, doi:10.1002/jgrd.50286.
- Enserink, B., J. H. Kwakkel, and S. Veenman, 2013: Coping with uncertainty in climate policy making: (Mis)understanding scenario studies. *Futures*, **53**, 1–12, doi:10.1016/j.futures.2013.09.006.
- Fettweis, X., B. Franco, M. Tedesco, J. H. van Angelen, J. T. M. Lenaerts, M. R. van den Broeke, and H. Gallée, 2013: Estimating the Greenland ice sheet surface mass balance contribution to future sea level rise

- using the regional atmospheric climate model MAR. *The Cryosphere*, **7**, 469–489, doi:10.5194/tc-7-469-2013.
- Giorgi, F., 2005: Climate Change Prediction. *Clim. Change*, **73**, 239–265, doi:10.1007/s10584-005-6857-4.
- Giorgi, F., C. Jones, and G. Asrar, 2009: Addressing climate information needs at the regional level: the CORDEX framework. *WMO Bull.*, **58**, 175–183.
- Grinsted, A., 2013: An estimate of global glacier volume. *The Cryosphere*, **7**, 141–151, doi:10.5194/tc-7-141-2013.
- Haarsma, R., F. Selten, and G. Oldenborgh, 2013a: Anthropogenic changes of the thermal and zonal flow structure over Western Europe and Eastern North Atlantic in CMIP3 and CMIP5 models. *Clim. Dyn.*, **41**, 2577–2588, doi:10.1007/s00382-013-1734-8.
- Haarsma, R. J., F. Selten, B. vd Hurk, W. Hazeleger, and X. Wang, 2009: Drier Mediterranean soils due to greenhouse warming bring easterly winds over summertime central Europe. *Geophys. Res. Lett.*, **36**, L04705, doi:10.1029/2008GL036617.
- , W. Hazeleger, C. Severijns, H. de Vries, A. Sterl, R. Bintanja, G. J. van Oldenborgh, and H. W. van den Brink, 2013b: More hurricanes to hit western Europe due to global warming. *Geophys. Res. Lett.*, **40**, 1783–1788, doi:10.1002/grl.50360.
- Van Haren, R., G. Oldenborgh, G. Lenderink, M. Collins, and W. Hazeleger, 2013: SST and circulation trend biases cause an underestimation of European precipitation trends. *Clim. Dyn.*, **40**, 1–20, doi:10.1007/s00382-012-1401-5.
- Harvey, B. J., L. C. Shaffrey, T. J. Woollings, G. Zappa, and K. I. Hodges, 2012: How large are projected 21st century storm track changes? *Geophys. Res. Lett.*, **39**, L18707, doi:10.1029/2012GL052873.
- Hazeleger, W., 2012: *Verhalen van Weer in de Toekomst / Story telling of future weather*. Wageningen University, Wageningen, 21 pp.
- , and Coauthors, 2012: EC-Earth V2.2: description and validation of a new seamless earth system prediction model. *Clim. Dyn.*, **39**, 2611–2629, doi:10.1007/s00382-011-1228-5.
- , V. Guemas, B. Wouters, S. Corti, I. Andreu-Burillo, F. J. Doblas-Reyes, K. Wyser, and M. Caian, 2013: Multiyear climate predictions using two initialization strategies. *Geophys. Res. Lett.*, **40**, 1794–1798, doi:10.1002/grl.50355.
- Hohenegger, C., P. Brockhaus, C. S. Bretherton, and C. Schär, 2009: The Soil Moisture–Precipitation Feedback in Simulations with Explicit and Parameterized Convection. *J. Clim.*, **22**, 5003–5020, doi:10.1175/2009JCLI2604.1.
- Hulme, M., and S. Dessai, 2008: Predicting, deciding, learning: can one evaluate the “success” of national climate scenarios? *Environ. Res. Lett.*, **3**, doi:10.1088/1748-9326/3/4/045013.
- Van den Hurk, B., and Coauthors, 2006: *KNMI Climate Change Scenarios 2006 for the Netherlands*. KNMI, De Bilt, <http://www.knmi.nl/bibliotheek/knmipubWR/WR2006-01.pdf>.
- , and Coauthors, 2007: New climate change scenarios for the Netherlands. *Water Sci. Technol.*, **56**, 27–33, doi:10.2166/wst.2007.533.
- , A. Klein Tank, C. Katsman, G. Lenderink, and A. te Linde, 2013: Vulnerability Assessments in the Netherlands Using Climate Scenarios. *Climate Vulnerability*, R.A. Pielke, Ed., Academic Press, Oxford, 257–266 <http://www.sciencedirect.com/science/article/pii/B9780123847034005384>.

- Van den Hurk, B., G. Van Oldenborgh, G. Lenderink, W. Hazeleger, R. Haarsma, and H. De Vries, 2014: Drivers of mean climate change around the Netherlands derived from CMIP5. *Clim. Dyn.*, **42**, 1683–1697, doi:10.1007/s00382-013-1707-y.
- Huss, M., and D. Farinotti, 2012: Distributed ice thickness and volume of all glaciers around the globe. *J. Geophys. Res. Earth Surf.*, **117**, F04010, doi:10.1029/2012JF002523.
- IPCC, 2013a: Annex I: Atlas of Global and Regional Climate Projections. *Climate Change 2013: The Physical Science Basis. Contribution of Working Group I to the Fifth Assessment Report of the Intergovernmental Panel on Climate Change*, G.J. Van Oldenborgh, M. Collins, J. Arblaster, J.H. Christensen, J. Marotzke, S.B. Power, M. Rummukainen, and T. Zhou, Eds., Cambridge University Press, Cambridge, United Kingdom and New York, NY, USA.
- , 2013b: *Climate Change 2013: The Physical Science Basis. Contribution of Working Group I to the Fifth Assessment Report of the Intergovernmental Panel on Climate Change*. Stocker, T. et al., Eds. Cambridge University Press, Cambridge, United Kingdom and New York, NY, USA.,.
- , 2013c: Annex III: Glossary. *Climate Change 2013: The Physical Science Basis. Contribution of Working Group I to the Fifth Assessment Report of the Intergovernmental Panel on Climate Change*, Planton, S., Ed., Cambridge University Press, Cambridge, United Kingdom and New York, NY, USA.
- , 2013d: Chapter 13, Sea Level Change. *Climate Change 2013: The Physical Science Basis. Contribution of Working Group I to the Fifth Assessment Report of the Intergovernmental Panel on Climate Change*, J.A. Church, and Clark, Eds., Cambridge University Press, Cambridge, United Kingdom and New York, NY, USA.
- , 2013e: Observations: Atmosphere and Surface. *Climate Change 2013: The Physical Science Basis. Contribution of Working Group I to the Fifth Assessment Report of the Intergovernmental Panel on Climate Change*, D.L. Hartmann et al., Eds., Cambridge University Press, Cambridge, United Kingdom and New York, NY, USA.
- Katsman, C., and Coauthors, 2011: Exploring high-end scenarios for local sea level rise to develop flood protection strategies for a low-lying delta—the Netherlands as an example. *Clim. Change*, **109**, 617–645, doi:10.1007/s10584-011-0037-5.
- Kirschke, S., and Coauthors, 2013: Three decades of global methane sources and sinks. *Nat. Geosci.*, **6**, 813–823.
- Klein Tank, A., and G. Lenderink, eds., 2009: *2009: Climate change in the Netherlands; Supplements to the KNMI'06 scenarios*. KNMI, De Bilt, Netherlands, [www.knmi.nl/knmi-library/climatereport/supplementsto06scenarios.pdf](http://www.knmi.nl/knmi-library/climatereport/supplementsto06scenarios.pdf).
- KNMI, 2011: *De Bosatlas van het Klimaat*. Noordhoff Uitgevers, Groningen, 112 pp. [www.klimaatatlas.nl](http://www.klimaatatlas.nl).
- , 2014: The KNMI'14 climate scenarios for the Netherlands; A guide for professionals in climate adaptation.
- Können, G., 2001: Climate Scenarios for impact studies in the Netherlands. [s3.amazonaws.com/gunther-konnen/documents/109/2001\\_ClimateScenarios.pdf?1292779623](http://s3.amazonaws.com/gunther-konnen/documents/109/2001_ClimateScenarios.pdf?1292779623).
- Kulmala, M., and Coauthors, 2011: General overview: European Integrated project on Aerosol Cloud Climate and Air Quality interactions (EUCAARI) &ndash; integrating aerosol research from nano to global scales. *Atmospheric Chem. Phys.*, **11**, 13061–13143, doi:10.5194/acp-11-13061-2011.
- Leander, R., and T. A. Buishand, 2007: Resampling of regional climate model output for the simulation of extreme river flows. *J. Hydrol.*, **332**, 487–496, doi:10.1016/j.jhydrol.2006.08.006.

- Lee, T., D. E. Waliser, J.-L. F. Li, F. W. Landerer, and M. M. Gierach, 2013: Evaluation of CMIP3 and CMIP5 Wind Stress Climatology Using Satellite Measurements and Atmospheric Reanalysis Products. *J. Clim.*, **26**, 5810–5826, doi:10.1175/JCLI-D-12-00591.1.
- Lenderink, G., and A. A. M. Holtslag, 2004: An updated length-scale formulation for turbulent mixing in clear and cloudy boundary layers. *Q. J. R. Meteorol. Soc.*, **130**, 3405–3427, doi:10.1256/qj.03.117.
- Lenderink, G., and E. van Meijgaard, 2010: Linking increases in hourly precipitation extremes to atmospheric temperature and moisture changes. *Environ. Res. Lett.*, **5**, 025208, doi:10.1088/1748-9326/5/2/025208.
- Lenderink, G., A. Ulden, B. Hurk, and F. Keller, 2007: A study on combining global and regional climate model results for generating climate scenarios of temperature and precipitation for the Netherlands. *Clim. Dyn.*, **29**, 157–176, doi:10.1007/s00382-007-0227-z.
- Te Linde, A. H., J. C. J. H. Aerts, A. M. R. Bakker, and J. C. J. Kwadijk, 2010: Simulating low-probability peak discharges for the Rhine basin using resampled climate modeling data. *Water Resour. Res.*, **46**, W03512, doi:10.1029/2009WR007707.
- Van der Linden, P., and J. F. B. Mitchell, 2009: *ENSEMBLES: Climate Change and its Impacts: Summary of research and results from the ENSEMBLES project*. Met Office Hadley Centre, FitzRoy Road, Exeter EX1 3PB, 160 pp. [http://ensembles-eu.metoffice.com/docs/Ensembles\\_final\\_report\\_Nov09.pdf](http://ensembles-eu.metoffice.com/docs/Ensembles_final_report_Nov09.pdf).
- Loriaux, J. M., G. Lenderink, S. R. De Roode, and A. P. Siebesma, 2013: Understanding Convective Extreme Precipitation Scaling Using Observations and an Entraining Plume Model. *J. Atmospheric Sci.*, **70**, 3641–3655, doi:10.1175/JAS-D-12-0317.1.
- Marzeion, B., A. H. Jarosch, and M. Hofer, 2012: Past and future sea-level change from the surface mass balance of glaciers. *The Cryosphere*, **6**, 1295–1322, doi:10.5194/tc-6-1295-2012.
- McKenzie-Hedger, M., M. Cornell, and P. Bramwell, 2006: Bridging the gap: empowering decision-making for adaptation through the UK Climate Impacts Programme. *Clim. Policy*, **6**, 201–215.
- Meehl, G. A., C. Covey, K. E. Taylor, T. Delworth, R. J. Stouffer, M. Latif, B. McAvaney, and J. F. B. Mitchell, 2007: THE WCRP CMIP3 Multimodel Dataset: A New Era in Climate Change Research. *Bull. Am. Meteorol. Soc.*, **88**, 1383–1394, doi:10.1175/BAMS-88-9-1383.
- Van Meijgaard, E., L. H. Van Ulft, W. J. Van de Berg, F. C. Bosveld, B. J. J. M. Van den Hurk, G. Lenderink, and A. P. Siebesma, 2008: *The KNMI regional atmospheric climate model RACMO, version 2.1*. KNMI, [http://www.knmi.nl/publications/fulltexts/tr302\\_racmo2v1.pdf](http://www.knmi.nl/publications/fulltexts/tr302_racmo2v1.pdf).
- , —, G. Lenderink, S. R. De Roode, L. Wipfler, R. Boers, and R. Timmermans, 2012: Refinement and application of a regional atmospheric model for climate scenario calculations of Western Europe.
- Milne, G. A., W. R. Gehrels, C. W. Hughes, and M. E. Tamisiea, 2009: Identifying the causes of sea-level change. *Nat. Geosci.*, **2**, 471–478, doi:10.1038/ngeo544.
- Min, E., W. Hazeleger, G. Van Oldenborgh, and A. Sterl, 2013: Evaluation of trends in high temperature extremes in north-western Europe in regional climate models. *Environ. Res. Lett.*, 014011, doi:10.1088/1748-9326/8/1/014011.
- Mitrovica, J. X., M. E. Tamisiea, J. L. Davis, and G. A. Milne, 2001: Recent mass balance of polar ice sheets inferred from patterns of global sea-level change. *Nature*, **409**, 1026–1029, doi:10.1038/35059054.
- Mizuta, R., 2012: Intensification of extratropical cyclones associated with the polar jet change in the CMIP5 global warming projections. *Geophys. Res. Lett.*, **39**, L19707, doi:10.1029/2012GL053032.

- Nenes, A., S. Pandis, and C. Pilinis, 1998: ISORROPIA: A New Thermodynamic Equilibrium Model for Multiphase Multicomponent Inorganic Aerosols. *Aquat. Geochem.*, **4**, 123–152, doi:10.1023/A:1009604003981.
- Nerem, R. S., D. P. Chambers, C. Choe, and G. T. Mitchum, 2010: Estimating Mean Sea Level Change from the TOPEX and Jason Altimeter Missions. *Mar. Geod.*, **33**, 435–446, doi:10.1080/01490419.2010.491031.
- Nikulin, G., E. KJELLSTRÖM, U. HANSSON, G. STRANDBERG, and A. ULLERSTIG, 2011: Evaluation and future projections of temperature, precipitation and wind extremes over Europe in an ensemble of regional climate simulations. *Tellus A*, **63**, 41–55, doi:10.1111/j.1600-0870.2010.00466.x.
- Oldenborgh, G., F. Doblas-Reyes, B. Wouters, and W. Hazeleger, 2012: Decadal prediction skill in a multi-model ensemble. *Clim. Dyn.*, **38**, 1263–1280, doi:10.1007/s00382-012-1313-4.
- Van Oldenborgh, G. J., P. Yiou, and R. Vautard, 2010: On the roles of circulation and aerosols in the decline of mist and dense fog in Europe over the last 30 years. *Atmospheric Chem. Phys.*, **10**, 4597–4609, doi:10.5194/acp-10-4597-2010.
- Van Oldenborgh, G. J., S. Drijfhout, A. van Ulden, R. Haarsma, A. Sterl, C. Severijns, W. Hazeleger, and H. Dijkstra, 2009: Western Europe is warming much faster than expected. *Clim Past*, **5**, 1–12, doi:10.5194/cp-5-1-2009.
- Orrell, D., and P. McSharry, 2009: System economics: Overcoming the pitfalls of forecasting models via a multidisciplinary approach. *Spec. Sect. Decis. Mak. Plan. Low Levels Predict.*, **25**, 734–743, doi:10.1016/j.ijforecast.2009.05.002.
- Prescott, P. and Walden, A. T., 1980: Maximum likelihood estimation of the parameters of the generalized extreme-value distribution. *Biometrika*, **67**, 723–724.
- Pryor, S. C., R. J. Barthelmie, N. E. Clausen, M. Drews, N. MacKellar, and E. Kjellström, 2012: Analyses of possible changes in intense and extreme wind speeds over northern Europe under climate change scenarios. *Clim. Dyn.*, **38**, 189–208, doi:10.1007/s00382-010-0955-3.
- Radić, V., A. Bliss, A. C. Beedlow, R. Hock, E. Miles, and J. G. Cogley, 2014: Regional and global projections of twenty-first century glacier mass changes in response to climate scenarios from global climate models. *Clim. Dyn.*, **42**, 37–58, doi:10.1007/s00382-013-1719-7.
- Sanderson, B. M., and R. Knutti, 2012: On the interpretation of constrained climate model ensembles. *Geophys. Res. Lett.*, **39**, L16708, doi:10.1029/2012GL052665.
- Slangen, A., and et al., 2014: Projecting 21st century regional sea level changes. *Clim. Change Submitt.*,
- Slangen, A. B. A., and R. S. W. Van de Wal, 2011: An assessment of uncertainties in using volume-area modelling for computing the twenty-first century glacier contribution to sea-level change. *The Cryosphere*, **5**, 673–686, doi:10.5194/tc-5-673-2011.
- Slangen, A. B. A., C. A. Katsman, R. S. W. Wal, L. L. A. Vermeersen, and R. E. M. Riva, 2012: Towards regional projections of twenty-first century sea-level change based on IPCC SRES scenarios. *Clim. Dyn.*, **38**, 1191–1209, doi:10.1007/s00382-011-1057-6.
- Smith, L. A., 2002: What might we learn from climate forecasts? *Proc. Natl. Acad. Sci.*, **99**, 2487–2492, doi:10.1073/pnas.012580599.
- Smits, A., A. M. G. Klein Tank, and G. P. Können, 2005: Trends in storminess over the Netherlands, 1962–2002. *Int. J. Climatol.*, **25**, 1331–1344, doi:10.1002/joc.1195.

- Sterl, A., H. van den Brink, H. de Vries, R. Haarsma, and E. van Meijgaard, 2009: An ensemble study of extreme storm surge related water levels in the North Sea in a changing climate. *Ocean Sci*, **5**, 369–378, doi:10.5194/os-5-369-2009.
- Von Storch, H., Gonnert, G., and Meine, M., 2008: Storm surges - an option for Hamburg, Germany, to mitigate expected future aggravation of risk. *Environ. Sci. Policy*, **8**, 735–742.
- Tang, S., and S. Dessai, 2012: Usable Science? The U.K. Climate Projections 2009 and Decision Support for Adaptation Planning. *Weather Clim. Soc.*, **4**, 300–313, doi:10.1175/WCAS-D-12-00028.1.
- Taylor, K. E., R. J. Stouffer, and G. A. Meehl, 2011: An Overview of CMIP5 and the Experiment Design. *Bull. Am. Meteorol. Soc.*, **93**, 485–498, doi:10.1175/BAMS-D-11-00094.1.
- Van Ulden, A. P., and G. J. van Oldenborgh, 2006: Large-scale atmospheric circulation biases and changes in global climate model simulations and their importance for climate change in Central Europe. *Atmos Chem Phys*, **6**, 863–881, doi:10.5194/acp-6-863-2006.
- Vautard, R., J. Cattiaux, P. Yiou, J.-N. Thepaut, and P. Ciais, 2010: Northern Hemisphere atmospheric stilling partly attributed to an increase in surface roughness. *Nat. Geosci*, **3**, 756–761, doi:10.1038/ngeo979.
- Van Vuuren, D., and Coauthors, 2011: The representative concentration pathways: an overview. *Clim. Change*, **109**, 5–31, doi:10.1007/s10584-011-0148-z.
- Van de Wal, R. S. W., and M. Wild, 2001: Modelling the response of glaciers to climate change by applying volume-area scaling in combination with a high resolution GCM. *Clim. Dyn.*, **18**, 359–366, doi:10.1007/s003820100184.
- Wang, X., F. Zwiers, V. Swail, and Y. Feng, 2009: Trends and variability of storminess in the Northeast Atlantic region, 1874–2007. *Clim. Dyn.*, **33**, 1179–1195, doi:10.1007/s00382-008-0504-5.
- Wever, N., 2012: Quantifying trends in surface roughness and the effect on surface wind speed observations. *J. Geophys. Res. Atmospheres*, **117**, D11104, doi:10.1029/2011JD017118.
- De Winter, R. C., A. Sterl, and B. G. Ruessink, 2013: Wind extremes in the North Sea Basin under climate change: An ensemble study of 12 CMIP5 GCMs. *J. Geophys. Res. Atmospheres*, **118**, 1601–1612, doi:10.1002/jgrd.50147.
- Zappa, G., L. C. Shaffrey, and K. I. Hodges, 2013a: The Ability of CMIP5 Models to Simulate North Atlantic Extratropical Cyclones\*. *J. Clim.*, **26**, 5379–5396, doi:10.1175/JCLI-D-12-00501.1.
- , —, —, P. G. Sansom, and D. B. Stephenson, 2013b: A Multimodel Assessment of Future Projections of North Atlantic and European Extratropical Cyclones in the CMIP5 Climate Models\*. *J. Clim.*, **26**, 5846–5862, doi:10.1175/JCLI-D-12-00573.1.
- Zhang, J., and J. S. Reid, 2010: A decadal regional and global trend analysis of the aerosol optical depth using a data-assimilation grade over-water MODIS and Level 2 MISR aerosol products. *Atmospheric Chem. Phys.*, **10**, 10949–10963, doi:10.5194/acp-10-10949-2010.

## 6. Annexes

### 6.1 List of GCMs

Table 6.1: overview of all CMIP5 simulations used. Indicated are the model label used in the figures, and number of models and ensemble members per RCP.

Label	name	RCP2.6	RCP4.5	RCP6.0	RCP8.5
	nr of models	n=24	n=36	n=16	n=34
01	ACCESS1-0		1		1
02	ACCESS1-3		1		1
03	BNU-ESM	1	1		1
04	bcc-csm1-1	1	1		1
05	CanESM2	5	5		5
06	CCSM4	5	5	5	5
07	CESM1-BGC		1		1
08	CESM1-CAM5	3	3	3	3
09	CMCC-CM		1		1
10	CMCC-CMS		1		1
11	CNRM-CM5	1	1		5
12	CSIRO-Mk3-6-0	10	10	10	10
13	EC-EARTH		7		8
14	EC-EARTH_r				8
15	FGOALS-g2		1		1
16	GFDL-CM3	1	1	1	1
17	GFDL-ESM2G	1	1	1	1
18	GFDL-ESM2M	1	1	1	1
19	GISS-E2-H-CC_p1		1		
20	GISS-E2-R-CC_p1		1		
21	GISS-E2-R_p1	1	5	1	1
22	GISS-E2-R_p2	1	5	1	1
23	GISS-E2-R_p3	1	5	1	1
24	HadGEM2-AO	1	1	1	1
25	HadGEM2-CC		1		1
26	HadGEM2-ES	4	4	3	4
27	inmcm4		1		1
28	IPSL-CM5A-LR	3	4	1	4
29	IPSL-CM5A-MR	1	1		1
30	MIROC5	1	1	1	1
31	MIROC-ESM	1	1	1	1
32	MIROC-ESM-CHEM	1	1	1	1
33	MPI-ESM-LR	3	3		3
34	MPI-ESM-MR	1	3		1
35	MRI-CGCM3	1	1		1
36	NorESM1-M	1	1	1	1
37	NorESM1-ME		1		
<b>Total (n=245)</b>		<b>50</b>	<b>83</b>	<b>33</b>	<b>79</b>

## **6.2 Appendix to the KNMI'14 sea-level scenarios**

See following pages

# Appendix to the KNMI'14 Sea-Level Scenarios

May 22, 2014

**This appendix contains details on the data and methods regarding the construction of the KNMI'14 sea-level scenarios. Much of what is described below is based on IPCC AR5 (Chapter 13) and De Vries and Katsman (in preparation).**

## A Data and sampling

### A.1 Data

Climate model data that has been used in this study is obtained from the CMIP5 database [Taylor et al., 2012]. The data that has been used comprises of surface pressure, 2m air temperature, precipitation, global mean thermosteric sea-level rise and the regional sea surface height. In total output from 42 AOGCMs has been used (21 for both RCP4.5 and RCP8.5). The data was provided to KNMI on the original ocean grids. This data has subsequently been interpolated to a regular 1x1 degree grid. The same models stand at the base of IPCC AR5. If we compare these CMIP5 models to the previous generation of climate models, CMIP3, which has been used in IPCC AR4, their representation of current-climate has improved [Yin et al., 2010, Yin, 2012].

### A.2 Sampling approach

A sampling approach is used to estimate the distribution of possible sea-level changes. Such a sampling method is convenient if one does not know the exact underlying distribution [von Storch and Zwiers, 2003]. In the case of the sea-level rise problem, the distribution is formed using input from many models, and many processes. In addition methodological uncertainty is included in some processes in the form of (stochastic) noise-factors, making a sampling approach the only viable way to determine the approximate shape of the distribution. In the sampling, we draw  $N_{MC} = 10^4$  times a random member from the 42 model Tglobal time-series (drawing with replacement). The sample-member id's are retained and will be used also to select the  $N_{MC}$  accompanying ocean and ibe (inverse barometer) sample fields. Based on these  $N_{MC}$  samples and the other components (see below), we obtain an estimate of the distribution from which compute a central value and likely range for each component and the total. This process is repeated 100 times. We thus obtain a 100-member ensemble of central values, and likely ranges etc. The median of each is selected to be the final estimate. For the three areas and the current value of  $N_{MC}$  and the chosen likely range, we did find that the differences between the members generally stayed within 2cm. For the gridded responses, we use a different method. Because of computational limitations in this case we only once draw  $N_{MC}$  members (equivalent to obtaining one sample distribution). These figures should therefore be used to give a qualitative overview only. Below, the sampling method is referred to as the Monte-Carlo simulation.

## B Process contributions

In this section we discuss in more detail how the different contributions to the sea level problem have been estimated. Much of this can also be found in de Vries and Katsman (in preparation), and is based on Chapter 13 of IPCC 5AR.

### B.1 Ocean contributions

Data has been used from 42 AOGCMs that contributed to CMIP5 (21 for both RCP4.5 and RCP8.5). A drift correction has been applied by subtracting the linear trend in the time series of the accompanying pre-industrial control run [Gregory et al., 2001, Katsman et al., 2008]. The end product is a set of global, drift corrected thermosteric expansion fields, starting in 1850, and running (depending on the model) until 2100 (or even to 2300 for some simulations). How temperature-dependent scenario contributions are estimated from the 42 model simulations, is explained below.

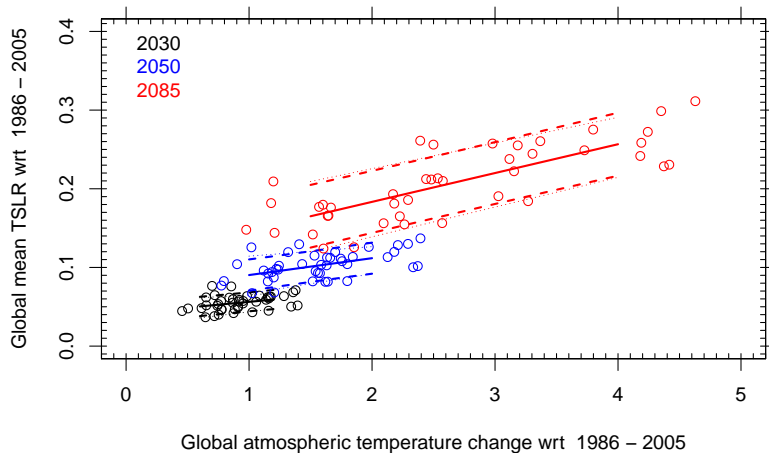


Figure B1: Illustration of the temperature regression approach. Ocean contribution to global temperature change, for three years (30 year windows are used). The symbols indicate 30-year averages from the AOGCMS. Linear regressions are drawn, and 10-90% confidence band is computed by treating the residuals as normally distributed.

#### B.1.1 Temperature-regression approach

Temperature-dependent scenarios for a specific year are constructed using a similar approach to that which has been used in previously published sea-level scenarios for the Dutch coast [van den Hurk et al., 2006]. The technique is illustrated here for the ocean steric / dynamic contribution, but is also used for the components that are parameterized in terms of global temperature change. The process is repeated for each year from 2000 to 2100 to yield time-evolving scenarios. The first step is to compute 30-year averages of the ocean contribution from each of the 42 models. This gives 42 change values. These values are regressed against 30-year averaged global temperature changes for the respective sight-year. The scenario values are then computed as the predicted values at the desired sight-year temperatures. The likely range (as well as any other quantile) is computed as the predicted value augmented with the 5-95% range of the residuals, assuming that the spread is independent of global temperature change. Figure B1 shows an example for the global mean ocean contribution (local

<b>Global Glacier Model</b>	f (mm K-1 yr-1)	p
Giesen and Oerlemans [2013]	3.02	0.733
Marzeion et al. [2012]	4.96	0.685
Radic et al. [2013]	5.45	0.676
Slangen and van de Wal [2011]	3.44	0.742

Table 3: Parameters for the fits to the global glacier models.

contributions are treated in the same way). In the Monte Carlo simulation  $N_{MC}$  members were drawn randomly from the 42 contributing models. Unless indicated otherwise, no additional methodological uncertainty is taken into account.

## B.2 Glaciers and Ice Caps (GIC)

A parameterization is used based on global temperature. Specifically, we use:

$$\Delta_{gic}(t) = fI(t)^p, \quad I(t) = \int_{2006}^t [T(t') - \bar{T}] dt'; \quad (\text{B1})$$

where  $\bar{T}$  is the global temperature of the reference period (1986-2005) and  $f$  and  $p$  are fitting parameters. The parameters  $f$  and  $p$  in this global scaling formula (with  $\Delta_{gic}$  in mm change with respect to 2006) are obtained by fitting<sup>1</sup>  $\log(I)$  to  $\log(\Delta)$  in the output of a global glacier model that takes into account local climate change and its effect on the surface mass balance and hypsometry of individual glaciers. As in IPCC AR5 we combine the output from 4 different glacier models (see Table 3) which give rise to slightly different values of  $f$  and  $p$ . An equal-weighted approach of the results for these 4 different models is used.

An additional 9.5mm is added to include the change from 1996 to 2005. For the period 1986-2005 we fit a quadratic polynomial, which passes through zero in 1996, and attaches smoothly to the result at 2006. Following IPCC AR5 and the cited literature, the spread around the predictions (standard deviation divided by the mean) is about 20%. This uncertainty is included as a normally distributed methodological error by multiplying the predictions by  $\mathcal{N}_{gic}$  with  $\mathcal{N}_{gic} = \mathcal{N}(\mu = 1, \sigma = 0.2)$ . In this way we obtain  $N_{MC}$  possible realizations of  $\Delta_{gic}(t)\mathcal{N}_{gic}$ . To obtain the KNMI scenario values and ranges from this distribution, we use the same temperature regression approach as with the ocean contributions (see sec B.1): regress 30-year averages against global temperature, and construct the quantiles from the residuals.

## B.3 Surface Mass Balance changes

### B.3.1 Greenland Ice Sheet SMB

For the surface mass balance (SMB) changes of the Greenland Ice Sheet, we closely follow IPCC AR5 and use the parameterization described in Fettweis et al. [2013]. This parameterization is expressed in global temperature change

$$SLR(t) \sim -71.5 \cdot \Delta T(t) - 20.4 \cdot (\Delta T(t))^2 - 2.8 \cdot (\Delta T(t))^3 \quad (\text{B2})$$

<sup>1</sup>Taking the logarithm of (B1) gives  $y = a + bx$ , with  $y = \log \Delta(t)$ ,  $x = \log(I(t))$ ,  $a = \log(f)$  and  $b = p$ . The constants  $a$  and  $b$  are determined by linear regression.

where  $\Delta T(t)$  is the global temperature difference with respect to 1980-1999 period. The resulting  $\Delta SMB$  is in units of Gigatonnes (GT) per year (water equivalent), i.e it is a sea-level tendency. To compute the actual sea-level rise at a specific time, therefore, we have to integrate the equation in time, after scaling with a factor  $-1E+12/(A_{oc}\rho_w) \sim -2.7245E-06$  (units  $m\ kg^{-1}$ ), containing ocean area  $A_{oc}=3.6704E+14\ m^2$  and density of water  $\rho_w=1E+3\ kg\ m^{-3}$ :

$$\Delta_{smb,gis}(t) = 2.7245 \cdot 10^{-6} \int_{t_0}^t SLR(t') dt' \quad (B3)$$

in units [m]. The parameterization has been developed with respect to the reference period 1980-1999 and appears to work reasonably well for global temperature changes up to 5-6 degrees. It is unknown whether the parameterization can be used also backward in time. In addition, because of the integrating character of sea-level rise, one has to define a start-date from which to integrate onward. This start date is set to  $t_0 = 2006$ . For dates before this date the tendencies are manually set to zero. However, an additional 2.91mm is added to include the contribution from 1995-2005. In this way one obtains a time-series for the sea-level rise contribution from each AOGCM. Two additional methodological model uncertainties are included. The first is motivated by the fact that different studies give rise to slightly different estimates of the SMB changes. This uncertainty is implemented as a log-normal distribution  $\mathcal{LN}$  with zero mean (i.e., giving an unbiased result) and a standard deviation of 0.4. The log-normal distribution is used because the various Greenland SMB models are positively skewed with respect to the projections obtained with (B2). None of the models includes the SMB change associated with the evolving ice-sheet surface topography, which gives a positive feedback. This feedback is included by using a randomly varying factor with a uniform probability  $\mathcal{U}$  between 1.00 and 1.15 (IPCC AR5).

Using repeated sampling we obtain  $N_{MC}$  samples from  $\mathcal{LN} \cdot \mathcal{U} \cdot \Delta_{smb,gis}(t)$ . To estimate the resulting values for the KNMI scenarios we have two options. Either we use the same approach as with the ocean data, i.e., take regressions against global temperature change for given eight years. Alternatively, we can use the equation above to compute the total sea-level rise given the time-path of the Tglob scenario. In the second approach, one relies strongly on the *exact* time-path of the hypothesized temperature scenario. As we consider this an unwanted feature, the first approach is used instead.

### B.3.2 Antarctic Ice Sheet SMB

In Antarctica the surface mass balance changes mostly arise from increased precipitation. AR5 states that the fractional precipitation increase is  $5.1 \pm 1.5\%$  per degree warming and the ratio of warming in Antarctica to Tglobal (South-polar amplification) is  $1.1 \pm 0.2$ . The uncertainties indicated are taken as independent normally distributed model-uncertainties  $\mathcal{N}_1$  and  $\mathcal{N}_2$ . Together with the AOGCM global temperature output, the reference surface mass balance of Antarctica ( $S_{ref} = 1983GT$ , AR5 section 4.4.2.2.1), and the ocean area ( $A_{oc}=3.6704E+14\ m^2$ ), this can be converted to a global sea-level change of

$$\Delta_{smb,ais}(t) = -\beta \mathcal{N}_1 \cdot \mathcal{N}_2 \int_{t_0}^t \Delta T(t') dt' \quad (B4)$$

where  $\beta = (0.01 \cdot S_{ref})/(\rho_w A_{oc})$ . The effect of the increased accumulation onto the dynamics is not taken into account in the above description. Scientific knowledge has not advanced far enough to completely resolve this issue and therefore an additional term is included. Following AR5, the

implementation is as follows. A rate  $-\mathcal{U}\Delta_{smb,ais}(t)$  is added to the above result, with  $\mathcal{U}$  a random factor drawn from a uniform distribution between 0.00 and 0.35. Thus on average the contribution from the increased dynamics is about 17.5% of the change predicted by accumulation changes only, but this may vary for different models and simulations.

In the sampling method,  $N_{MC}$  samples are drawn from  $(1 - \mathcal{U})\Delta_{smb,ais}(t)$ . For the KNMI scenarios we have again the choice to use the exact trajectory of Tglobal, or to use the Tglobal projections from the CMIP5 ensemble and take linear regressions for each sight-year. For the same reasons as before we decide for the latter.

#### B.4 Rapid Dynamical Ice Sheet changes

For the rapid dynamical changes of the Ice Sheets (dyn-ais and dyn-gis) we basically follow IPCC AR5, but modify the estimated upper-bound for the Antarctic contribution. In IPCC AR5, quadratic functions of time are fitted given constraints on the observed rates and the estimated final amount. Specifically, we solve  $a_{1,2}$  for each ice-sheet  $i$  from the equation

$$\Delta_{dyn,i}(t) = a_1(t - t_{2006}) + a_2(t - t_{2006})^2, \quad (B5)$$

$$SLR_{dyn,i}(t) = \frac{\partial \Delta_{dyn,i}(t)}{\partial t} = a_1 + 2a_2(t - t_{2006}) \quad (B6)$$

For Greenland the observed present-day tendency is taken as half the total observed tendency for the period 2005-2010, while for Antarctica we take all of the observed tendency. This gives  $SLR_{dyn,ais}(t_{2006}) = (0.20, 0.61)$  [mm/yr];  $\Delta_{dyn,ais}(t_{2100}) = (-3.4, 16.7)$  [cm];  $SLR_{dyn,gis}(t_{2006}) = 0.5 \cdot (0.43, 0.76)$  [mm/yr];  $\Delta_{dyn,gis}(t_{2100}) = (1.7, 7.4)$  [cm]. The approach above gives lower-bound and upper-bound AR5 values. For the Greenland Ice sheet, samples are created by combining the lower and upper bounds using using a uniform distribution  $\mathcal{U}(0, 1)$

$$\Delta_{dyn,gis}(t) = \left[ \mathcal{U}\Delta_{dyn,gis}^{AR5,hi}(t) + (1 - \mathcal{U})\Delta_{dyn,gis}^{AR5,lo}(t) \right] \quad (B7)$$

This approach is used also for the contribution from the Greenland Ice Sheet in the KNMI scenarios.

For the Antarctic Ice Sheet the possibility for a higher upper-bound is explicitly included. The main motivation for doing this is the fact that recent findings assess the distribution to be strongly positively skewed (e.g., Bamber and Aspinall [2013]). The lower and central values are taken from IPCC AR5, but the upper-bound is estimated to be 40 cm of rise with respect to the reference period in 2100. The latter value is regarded as the 98% percentile of a log-normal distribution. Note that this level is still below the extreme scenarios discussed in Katsman and et al. [2011]. This means that for Antarctica we estimate the contributions as:

$$\Delta_{dyn,ais}(t) = \tau_{dyn,ais}(t) + e^{\mu_{dyn,ais}(t) + \sigma_{dyn,ais}(t)\mathcal{N}(0,1)} \quad (B8)$$

with

$$\tau_{dyn,ais}(t) = \Delta_{dyn,ais}^{AR5,lo}(t), \quad (B9)$$

$$\mu_{dyn,ais}(t) = \ln \left[ \Delta_{dyn,ais}^{AR5,cen}(t) - \Delta_{dyn,ais}^{AR5,lo}(t) \right], \quad (B10)$$

$$\sigma_{dyn,ais}(t) = \frac{1}{\alpha_{98}} \ln \left[ \frac{\Delta_{dyn,ais}^{KNMI,hi}(t) - \Delta_{dyn,ais}^{AR5,lo}(t)}{\Delta_{dyn,ais}^{AR5,cen}(t) - \Delta_{dyn,ais}^{AR5,lo}(t)} \right], \quad (B11)$$

where  $\Delta_{dyn,ais}^{KNMI,hi}(t) = (0.40/0.16) \cdot \Delta_{dyn,ais}^{AR5,hi}(t)$ , 0.16 being the approximate value of  $\Delta_{dyn,ais}^{AR5,hi}(t)$  in 2100. For the Antarctic contribution we further assume that the higher values are positively correlated with the term in the surface mass balance associated with the altering dynamics due to enhanced accumulation. This means in practice that  $\mathcal{N}(0, 1)$  in equation (B8) is computed as  $\alpha[\mathcal{U}(0, 1)]$  with  $\alpha(q)$  the quantile function for a normal distribution and  $\mathcal{U}(0, 1)$  the same uniform distribution as the one used in the surface mass balance term of Antarctica.

## B.5 Landwater changes

To estimate the landwater changes, quadratic functions are fitted through observed rates and future estimates. Specifically we use:

$$\Delta_{grw}(t) = a_1(t - t_{2006}) + a_2(t - t_{2006})^2, \quad (\text{B12})$$

$$SLR_{grw}(t) = \frac{\partial \Delta_{grw}(t)}{\partial t} = a_1 + 2a_2(t - t_{2006}) \quad (\text{B13})$$

with constraints  $SLR_{grw}(t_{2006}) = (0.26, 0.49)$  [mm/yr] (5-95% range) and  $\Delta_{grw}(t_{2100}) = (-1, +9)$  [cm] (5-95% range). These ranges are determined by existing literature (e.g. [Wada et al., 2012]). A lower and upper fit are constructed which start at the minimum and upper initial rate and end at the minimum and maximal final amount respectively. A central estimate is obtained as mean of the two. Samples are computed as:

$$\Delta_{grw}(t) = \Delta_{grw}^{cen}(t) + \mathcal{N}(0, \sigma_{grw}(t)), \quad (\text{B14})$$

$$\sigma_{grw}(t) = \left[ \frac{\Delta_{grw}^{upper}(t) - \Delta_{grw}^{lower}(t)}{\alpha_{95} - \alpha_{05}} \right] \quad (\text{B15})$$

with  $\alpha_q$  the quantile function for a normal distribution. The current state of knowledge does not admit a separation of the above estimate for different temperature paths. For this reason the landwater contributions are taken to be the same in both KNMI scenarios.

## References

- A. Arendt, T. Bolch, J. G. Cogley, and et al. Randolph Glacier Inventory [v2.0]: A Dataset of Global Glacier Outlines, 2012. URL [http://www.glims.org/RGI/RGI\\_Tech\\_Report\\_V2.0.pdf](http://www.glims.org/RGI/RGI_Tech_Report_V2.0.pdf).
- J.L. Bamber and W.P. Aspinall. An expert judgment assessment of future sea level rise from the ice sheets. *Nature Climate Change*, in press:1–4, 2013. doi: 10.1038/NCLIMATE1778.
- J.A. Church and N.J. White. Sea-level rise from the late 19th to the early 21st century. *Surveys in Geophysics*, 32:585–602, 2011. doi: 10.1007/s10712-011-9119-1.
- J.A. Church, P.L. Woodworth, T. Aarup, and W.S. Wilson. *Understanding sea-level rise and variability*. Wiley-Blackwell, 2010.
- J.A. Church, P. U. Clark, and et al. *Chapter 13, Sea Level Change. In: Climate Change 2013: The scientific basis. Contribution of Working Group I to the Fifth Assessment Report of the Intergovernmental Panel on Climate Change.* www.ipcc.ch, 2013.

- N. J. Church, J.A. and White, L. F. Konikow, C. M. Domingues, J. G. Cogley, E. Rignot, J. M. Gregory, M. R. van den Broeke, A. J. Monaghan, and I. Velicogna. Revisiting the earth's sea-level and energy budgets from 1961 to 2008. *Geophysical Research Letters*, 38:L18601, 2011.
- X. Fettweis, B. Franco, M. Tedesco, J.H. van Angelen, J.T.M. Lenaerts, M.R. van den Broeke, and H. Galle. Estimating the greenland ice sheet surface mass balance contribution to future sea level rise using the regional atmospheric climate model mar. *The Cryosphere*, 7:469–489, 2013. doi: 10.5194/tc-7-469-2013.
- R.H. Giesen and J. Oerlemans. Climate-model induced differences in the 21st century global and regional glacier contributions to sea-level rise. *Clim. Dyn.*, 2013. doi: 10.1007/s00382-013-1743-7.
- J.M. Gregory, J.A. Church, G.J. Boer, K.W. Dixon, and et al. Comparison of results from several AOGCMs for global and regional sea level change 1900-2100. *Climate Dynamics*, 18:225–240, 2001.
- A. Grinsted. An estimate of global glacier volume. *The Cryosphere*, 7:141–151, 2013.
- M. Huss and D. Farinotti. Distributed ice thickness and volume of 180,000 glaciers around the globe. *Journal of Geophysical Research*, 117(F04010), 2012.
- C. A. Katsman and et al. Exploring high-end scenarios for local sea level rise to develop flood protection strategies for a low-lying delta - the netherlands as an example. *Climatic Change*, 109:617–645, 2011. doi: 10.1007/s10584-00037-5.
- C. A. Katsman, W. Hazeleger, S.S. Drijfhout, and et al. Climate scenarios of sea level rise for the northeast Atlantic Ocean: a study including the effects of ocean dynamics and gravity changes induced by ice melt. *Climatic Change*, 91:351–374, 2008.
- B. Marzeion, A.H. Jarosch, and M. Hofer. Past and future sea-level changes from the surface mass balance of glaciers. *The Cryosphere*, 6:1295–1322, 2012. doi: 10.5194/tc-6-1295-2012.
- Malte Meinshausen, S. Smith, K. Calvin, J. Daniel, M. Kainuma, J-F. Lamarque, K. Matsumoto, S. Montzka, S. Raper, K. Riahi, A. Thomson, G. Velders, and D.P. van Vuuren. The RCP greenhouse gas concentrations and their extensions from 1765 to 2300. *Climatic Change*, 109:213–241, 2011. ISSN 0165-0009. doi: 10.1007/s10584-011-0156-z. URL <http://dx.doi.org/10.1007/s10584-011-0156-z>.
- G.A. Milne, W.R. Gehrels, C.W. Hughes, and M.E. Tamisiea. Identifying the causes of sea-level change. *Nature Geoscience*, 2:471–478, 2009.
- R. S. Nerem, D. Chambers, C. Choe, and G. T. Mitchum. Estimating mean sea level change from the TOPEX and Jason altimeter missions. *Marine Geodesy*, 33:435, 2010.
- V. Radic, A. Bliss, and et al. Regional and global projections of the 21st century glacier mass changes in response to climate scenarios from global climate models. *Clim. Dyn.*, 2013. doi: 10.1007/s00382-013-1719-7.
- A. Slangen and et al. Projecting twenty-first century regional sea-level changes. *Climatic Change (submitted)*, 2013.

- A. Slangen, C. A. Katsman, R. S. van de Wal, L.L.A. Vermeersen, and R.E.M. Riva. Towards regional projections of twenty-first century sea-level change based on IPCC SRES scenarios. *Climate dynamics*, 38:1191–1209, 2012. doi: 10.1007/s00382-011-1057.
- A. B. A. Slangen and R.S.W. van de Wal. An assessment of uncertainties in using volume-area modelling for computing the twenty-first century glacier contribution to sea-level change. *The Cryosphere*, 5:673–686, 2011. doi: 10.5194/tc-5-673-2011.
- K. E. Taylor, R. J. Stouffer, and G. A. Meehl. An overview of cmip5 and the experiment design. *Bull. Amer. Meteor. Soc.*, 93:485–498, 2012. doi: 10.1175/BAMS-D-11-00094.1.
- R.S.W. van de Wal and M. Wild. Modelling the response of glaciers to climate change, applying volume-area scaling in combination with a high resolution gcm. *Climate Dynamics*, 18:359–366, 2001.
- B. van den Hurk, A. M. G. Klein Tank, G. Lenderink, and et al. KNMI Climate Change Scenarios 2006 for the Netherlands. Technical Report WR2006-01, Koninklijk Nederlands Meteorologisch Instituut (KNMI), 2006.
- H. von Storch and F. W. Zwiers. *Statistical Analysis in Climate Research*. Cambridge University Press, 1st edition, 2003.
- Y. Wada, L.P.H. van Beek, F.C. Sperna, B.F. Weiland, Y.-H. Wu Chao, and M.F.P. Bierkens. Past and future contribution of global groundwater depletion to sea-level rise. *Geophys. Res. Lett.*, 39 (L09402):1–6, 2012. doi: 10.1029/2012GL051230.
- J. Yin. Century to multi-century sea level rise projections from CMIP5 models. *Geophys. Res. Lett.*, 39, 2012. doi: 10.1029/2012GL052947.
- J. Yin, S.M. Griffies, and R.J. Stouffer. Spatial variability of sea-level rise in 21st century projections. *J. Clim.*, 23:4585–4607, 2010.

## **6.3 Meteorological scenarios translated to changes in air pollution levels**

See following pages

# Meteorological scenarios translated to changes in air pollution levels

19 May 2013

## **Introduction: Climate scenarios for future air pollution levels in the Netherlands**

Changes in climate will affect the future air quality in the Netherlands. The concentrations of pollutants like aerosols (particulate matter) increase during calm weather conditions, in particular close to sources. Ozone is sensitive to temperature and concentrations rapidly increase during heat waves. Pollution levels in the Netherlands are also enhanced under conditions of weak southerly or easterly winds, when import of pollutants from Belgium or Germany takes place. The average surface ozone and particulate matter (PM) levels in the Netherlands typically decrease from the southeast (Maastricht) to the northwest (Texel).

Here we present the results of a statistical analysis based on the approach developed by Lennard Jansen [2013]. Relationships are derived between observed meteorological conditions and the observed ozone and PM10 (particles smaller than 10 micron) levels in the Netherlands. These relationships are subsequently used to estimate the effects of future climate change on ozone and PM10 levels in the Netherlands based on the four KNMI'14 climate scenarios. This work is similar to e.g. the work of Varotsos et al. (2013), who estimated the number of exceedances of ozone in Europe above the limits set by the EU, based on future climate scenarios.

Another method to study the impact of climate change on future air quality is by using deterministic three-dimensional chemistry-transport models driven by a consistent set of future climate parameters (Langner et al., 2012, Manders et al., 2012). The model intercomparison study by Langner et al. (2012) suggests that state-of-the-art deterministic models provide a wide range of projections for surface ozone. This is partly because future changes in biogenic emissions in response to climate change are uncertain, even for a given climate scenario.

The projected temperature-driven increases in ozone during hot summer days could be prevented by policy measures on pollutant emissions and introduction of clean technologies. Such measures have not been taken into account in the numbers presented here, which purely account for the effects of climate change. The statistical analysis is based on observed relations between ozone and meteorology for present day and thus implicitly assumes no changes in pollutant emissions from industry, traffic, etc. Furthermore, a secondary climate-change driven increase in ozone levels in the Netherlands might be expected as a result of increased downward transport of ozone from the stratosphere, enhancing surface ozone concentrations at our latitudes. Finally, the development of pollutant emissions in other parts of the world, in particular in Asia and America, could have a significant influence on the future levels of ozone in the Netherlands. Such effects, although potentially significant, have not been accounted for in the analysis presented below.

## Approach

This report combines the statistical approach developed by Lennard Jansen [2013] with the newly developed KNMI scenarios and the corresponding climate model runs. The approach consists of two parts:

### 1. Regression of air pollution against weather parameters for the period 2003-2006.

This step consists of finding statistical relations between measured daily air pollution levels for ozone and PM10 as a function of the meteorological situation. The air quality parameters considered are the daily maximum hourly concentrations of ozone, and the daily mean PM10 concentrations. The period 2003-2006 was chosen because it includes two warm summers and two colder summers, which allow the regressions to explore the impact of heat waves on pollution levels.

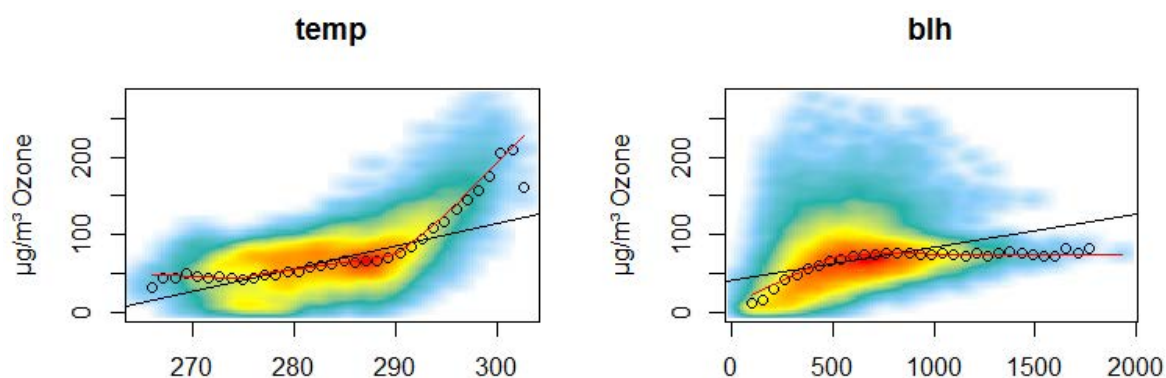


Fig. 1. Relation between the daily maximum ozone concentration and temperature (left) resp. boundary layer height (right). The figure also show a comparison of a linear regression (black) and univariate MARS (red) of the 2003-2006 ozone concentration. MARS shows a largely improved skill to describe the behaviour for the high ozone values relevant for exceedances.

The air quality observations (2003-2006) are obtained from the Landelijk Meetnet Luchtkwaliteit (LML) of the RIVM, <http://lml.rivm.nl>, e.g. Nguyen et al. [2012]. The regression is performed for six rural stations, see Fig. 2 of Jansen [2013]. The weather parameters are obtained from the ECMWF operational analyses for the period 2003-2006. Daily mean collocated surface or near-surface values of temperature, wind speed, wind direction, relative humidity, boundary layer height, rain and cloud cover are used.

The advanced MARS (multivariate adaptive regression splines) method is used. A cross-validation approach is applied in which three years are used to obtain the regression coefficients, and the fourth year is used to test the predictions. The weather parameters which provide most of the information are temperature in the case of ozone, and boundary layer height in the case of PM10. But information is obtained from many parameters, as described in table 6 and 7 of the report of Jansen. For ozone, the proportion of variability explained (in terms of  $R^2$ ) is 0.76. For PM10 this number is lower, 0.32.

An example of a MARS fit is given in Fig. 1, which shows the scatter density plot of ozone against temperature and boundary layer height. The benefit of the advanced fitting approach is that it much better describes the non-linear behaviour of ozone versus temperature as compared to a more conventional multivariate linear fit.

The result of these regressions is a "model" of ozone and PM10 as a function of the meteorological input parameters.

### 2. Use of the regression to estimate the impact of climate change on future air pollution.

In a second step we apply the model found in the first step to the daily mean meteorological parameters of the climate scenario model runs.

The results are based on the resampled RACMO/EC-Earth model runs that form the basis for the KNMI'14 scenarios. For each of the four scenarios there are two periods defined, mid of century (MOC) and end of century (EOC), as well as a reference period (1981-2010). In turn, each of these scenarios consists of eight members. In total, 64 resampled scenario runs over a period of 30 years have been processed, together with the corresponding 30-year reference runs, which amounts to about 4000 years of daily quantities.

As described in Jansen [2013], the climate model output fields are collocated to six locations in the Netherlands with a meteorological observation station. These locations are close to the six LML locations described above, and cover the Netherlands in an approximately uniform way.

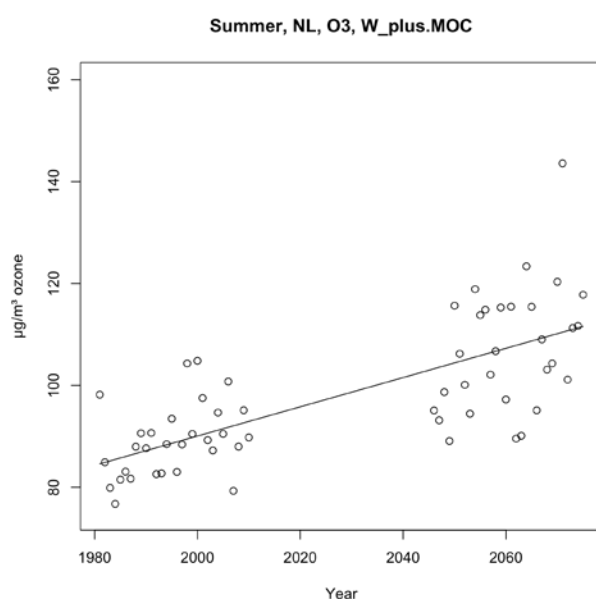


*Fig. 2. Trend in the summertime daily maximum ozone concentration in the  $W_H$  scenario, middle of century. The circles show the seasonal means, averaged over the six surface locations, for each of the 30 reference years and 30 scenario years for the first of the eight members (runs).*

Jansen found that the RACMO climate runs as compared to the ECMWF meteorological analyses shows significant differences in the distribution of the meteorological variables. In order to avoid biased results, he introduced a scaling factor and a shift for each of the meteorological parameters, demanding that the mean of the RACMO distribution and the width, averaged over the four-year period 2003-2006 (from the reference), becomes consistent with the mean and width of the corresponding ECMWF weather analyses. The same transformation was also applied to the KNMI'14 model runs. Both the RACMO present-day and future scenario variables are rescaled with the same scaling numbers.

Clear increasing trends in temperature and boundary layer height are observed in the  $W_H$  scenario, but also in the other scenarios, although less pronounced. Rain shows a decrease in summer, and increase in winter. See the other sections of this report for more details.

The MARS regressions, discussed above, are determined for each of the six stations separately, and are applied to each of the nearby meteorological locations introduced above. Thus, there is a spread in the results due to local differences in the regressions obtained from the 2003-2006 observations at the six LML stations. Furthermore, the RACMO runs show differences in trends for the different regions in the Netherlands.

The result for ozone is summarised in Fig. 2. For the summer season a consistent increase is obtained for all the runs, regressions and locations. This is somewhat different for wintertime PM10, which shows both decreasing and increasing trends for scenario  $W_H$  depending on the station.

### Summary of result - mean increase of air pollution

The results of applying the regressions to the KNMI' 14 scenarios are given in Table 1 for the middle of century. The number provided are the increase in pollutant concentrations between the scenario period and reference period, in  $\mu\text{g}/\text{m}^3$  averaged over the six stations, and averaged over the eight member runs in each scenario. The error bar provided (one standard deviation) is the spread of values obtained for the six stations and eight members.

MOC scenario	Ozone Summer	Ozone Winter	PM10 Summer	PM10 Winter
$G_L$	$7.6 \pm 2.3$ (92.7)	$1.8 \pm 0.8$ (49.5)	$1.5 \pm 0.5$ (24.3)	$0.0 \pm 0.6$ (29.3)
$G_H$	$11.0 \pm 3.3$ (91.1)	$3.1 \pm 1.3$ (48.8)	$2.1 \pm 0.7$ (24.0)	$-0.6 \pm 1.0$ (29.7)
$W_L$	$13.6 \pm 3.7$ (93.2)	$3.5 \pm 1.2$ (49.5)	$2.9 \pm 1.0$ (24.3)	$0.2 \pm 1.1$ (29.6)
$W_H$	$18.7 \pm 5.2$ (90.5)	$5.0 \pm 1.7$ (48.8)	$3.7 \pm 1.3$ (23.7)	$-0.7 \pm 1.5$ (29.5)

Table 1. Increase in daily maximum ozone and daily mean PM10, in summer and winter, for the four scenarios and for the middle of the 21st century (MOC). In brackets is shown the mean value in the reference period. Unit:  $\mu\text{g}/\text{m}^3$ .

The table shows a consistent picture. From  $G_L$  to  $W_H$  the concentration increases with roughly similar steps. For ozone, the high scenarios  $G_H$  and  $W_H$  show a stronger trend than the corresponding low scenarios. The spread in values is generally small compared to the mean trend. The exception to the overall increase is PM10 in wintertime, which shows an insignificant trend. These results shows that, despite changes in the local surroundings and sources of pollution, and despite the regional differences (coastal vs. inland), and differences in the regression coefficients, the stations show a good consistency in their description of the weather-driven response of air pollution concentrations. The main conclusions from the tables are:

- The strongest climate effect is seen for summertime ozone. This can be understood from the large sensitivity of the regional production of ozone on maximum temperatures. Drier summers and changes in circulation add to the effect. For  $W_H$  we find a large 20% increase for the middle of the century.
- The ozone trend in winter is found to be significant as well, but an understanding of this is more difficult because local production is small compared to summer, and long-range transport plays a major role. Note that wintertime ozone is low compared to summer, and is less important for human health and agricultural crop yields.
- PM10 shows a positive trend in summer. This may be related to changes in circulation and more frequent stagnant conditions.

- PM10 in winter shows a nearly zero trend. The high scenarios show a decrease, which may be related to wetter winters.
- The EOC scenarios show a good consistency with the MOC result (not shown), with an overall amplification of the MOC trends by about 40%.

### Ozone exceedances

For ozone the EU air quality directives prescribe a limit of  $180 \mu\text{g}/\text{m}^3$  above which citizens need to be informed. The impact of climate change on the number of ozone exceedances for this limit value has been estimated in two ways. First, the observed exceedance statistics in 2003-2006 can be combined with the mean increases in daily maximum concentrations due to climate change. Secondly, we can directly apply the regression to the future scenarios and count the exceedances. Both approaches give comparable results, summarised in Table 2.

One important finding is a large gradient in the number of exceedances over the country. In the North-West (e.g. IJmuiden) no exceedances are found, while in the South-East (e.g. Beek) an increase of up to 8 exceedances per year is found, starting from about 2 exceedances per year for present-day climate. So, with unchanged emissions of air pollutants, the four scenarios predict increases in the number of summertime ozone exceedances between 50% and 400%.

Exceedance days	G <sub>L</sub>	G <sub>H</sub>	W <sub>L</sub>	W <sub>H</sub>
Increase	3	4	5	8

*Table 2: Increase in the number of ozone exceedances ( $>180 \mu\text{g}/\text{m}^3$ ) per year in the South-East of the Netherlands, for the four mid-century scenarios (MOC). In other parts of the Netherlands the number of exceedances, as well as the future increase of this number, is less.*

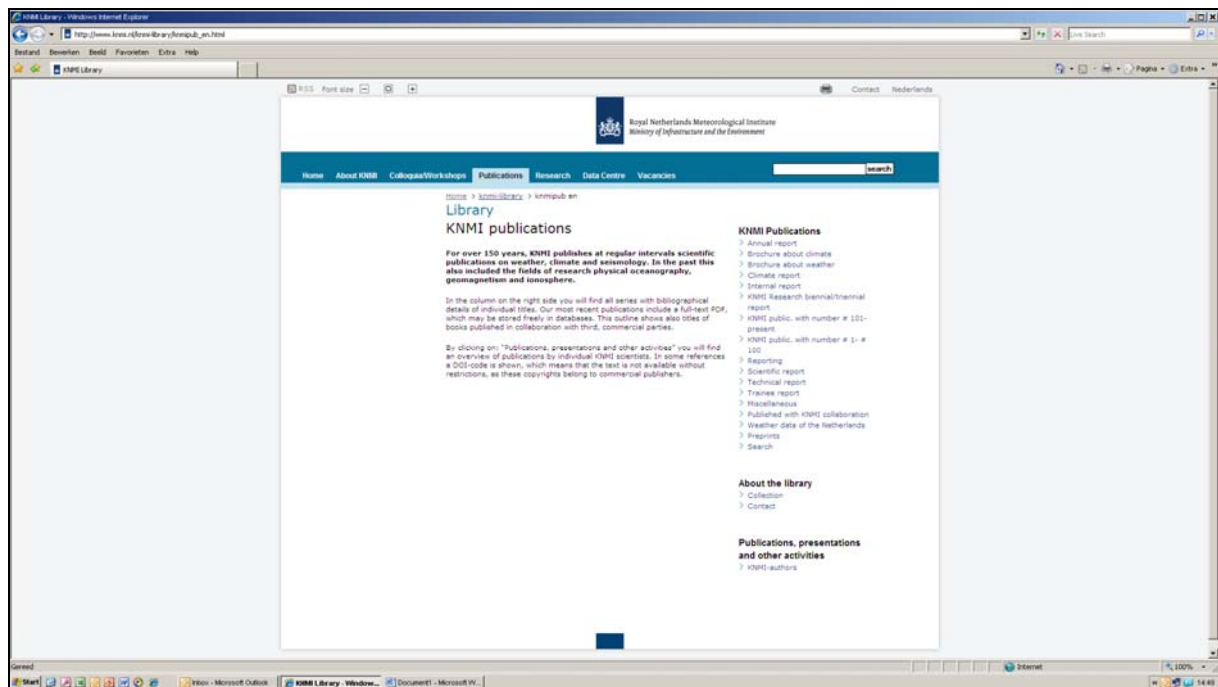
## References

- Jansen, L., The influence of climate change on air pollution in the Netherlands: Statistical analysis based on RACMO, Stageverslag 31-1-2013, KNMI wetenschappelijk rapport 2013/01, <http://www.knmi.nl/bibliotheek/knmipubWR/WR2013-01.pdf>.
- Langner, J., Engardt, M., Baklanov, A., Christensen, J. H., Gauss, M., Geels, C., Hedegaard, G. B., Nuterman, R., Simpson, D., Soares, J., Sofiev, M., Wind, P., and Zakey, A.: A multi-model study of impacts of climate change on surface ozone in Europe, *Atmos. Chem. Phys.*, 12, 10423-10440, doi:10.5194/acp-12-10423-2012, 2012.
- Manders, A., E. van Meijgaard, A. Mues, R. Kranenburg, L. van Ulft, and M. Schaap (2012), The impact of differences in large-scale circulation output from climate models on the regional modeling of ozone and PM, *Atmospheric Chemistry and Physics*, 12(20), 9441–9458. [online] Available from: <http://www.atmos-chem-phys.net/12/9441/2012/acp-12-9441-2012.html>
- Nguyen, P.L., G. Stefess, D. de Jonge, A. Snijder, P.M.J.A. Hermans, S. van Loon, R. Hoogerbrugge, RIVM, Evaluation of the representativeness of the Dutch air quality monitoring stations: The National, Amsterdam, Noord-Holland, Rijnmond-area, Limburg and Noord-Brabant networks, RIVM Report 680704021/2012.
- Varotsos, K. V., M. Tombrou, and C. Giannakopoulos (2013), Statistical estimations of the number of future ozone exceedances due to climate change in Europe, *Journal of Geophysical Research: Atmospheres*, 118, doi:10.1002/jgrd.50451. [online] Available from: <http://dx.doi.org/10.1002/jgrd.50451>



**A complete list of all KNMI -publications (1854 – present) can be found on our website**

[www.knmi.nl/knmi-library/knmipub\\_en.html](http://www.knmi.nl/knmi-library/knmipub_en.html)



**The most recent reports are available as a PDF on this site.**

